



UNIL | Université de Lausanne

Unicentre

CH-1015 Lausanne

<http://serval.unil.ch>

---

Year : 2018

## MORPHODYNAMICS AND SEDIMENT TRANSFER IN A HUMAN-IMPACTED ALPINE RIVER

Bakker Maarten

Bakker Maarten, 2018, MORPHODYNAMICS AND SEDIMENT TRANSFER IN A HUMAN-IMPACTED ALPINE RIVER

Originally published at : Thesis, University of Lausanne

Posted at the University of Lausanne Open Archive <http://serval.unil.ch>

Document URN : urn:nbn:ch:serval-BIB\_9B2F2721DB3D1

### **Droits d'auteur**

L'Université de Lausanne attire expressément l'attention des utilisateurs sur le fait que tous les documents publiés dans l'Archive SERVAL sont protégés par le droit d'auteur, conformément à la loi fédérale sur le droit d'auteur et les droits voisins (LDA). A ce titre, il est indispensable d'obtenir le consentement préalable de l'auteur et/ou de l'éditeur avant toute utilisation d'une oeuvre ou d'une partie d'une oeuvre ne relevant pas d'une utilisation à des fins personnelles au sens de la LDA (art. 19, al. 1 lettre a). A défaut, tout contrevenant s'expose aux sanctions prévues par cette loi. Nous déclinons toute responsabilité en la matière.

### **Copyright**

The University of Lausanne expressly draws the attention of users to the fact that all documents published in the SERVAL Archive are protected by copyright in accordance with federal law on copyright and similar rights (LDA). Accordingly it is indispensable to obtain prior consent from the author and/or publisher before any use of a work or part of a work for purposes other than personal use within the meaning of LDA (art. 19, para. 1 letter a). Failure to do so will expose offenders to the sanctions laid down by this law. We accept no liability in this respect.



University of Lausanne  
Faculty of Geosciences and Environment  
Institute of Earth Surface Dynamics

# **MORPHODYNAMICS AND SEDIMENT TRANSFER IN A HUMAN-IMPACTED ALPINE RIVER**

**Ph.D. thesis**

Presented at the  
Faculty of Geosciences and Environment, University of Lausanne  
by

**MAARTEN BAKKER**

M.Sc. University of Utrecht (The Netherlands)

**JURY**

Director:	Prof. Stuart Lane
Co-director:	Prof. Peter Molnar
Examiner :	Dr. Alexandre Badoux
Examiner :	Prof. Francesco Comiti
Examiner :	Prof. Grégoire Mariéthoz
President of the jury:	Prof. Michel Jaboyedoff

Lausanne, 2018



## IMPRIMATUR

Vu le rapport présenté par le jury d'examen, composé de

Président de la séance publique :	M. le Professeur Michel Jaboyedoff
Président du colloque :	M. le Professeur Michel Jaboyedoff
Directeur de thèse :	M. le Professeur Stuart Lane
Co-directeur de thèse :	M. le Professeur Peter Molnar
Expert interne :	M. le Professeur Grégoire Mariéthoz
Expert externe :	M. le Docteur Alexandre Badoux
Expert externe :	M. le Professeur Francesco Comiti

Le Doyen de la Faculté des géosciences et de l'environnement autorise l'impression de la thèse de

### **Monsieur Maarten BAKKER**

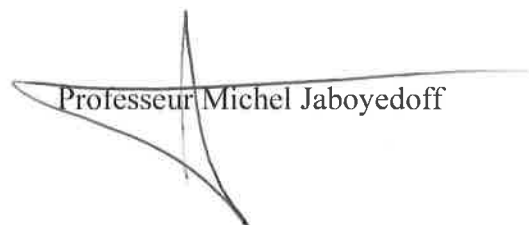
Titulaire d'un  
*Master in Physical Geography*  
*de l'Université d'Utrecht*

intitulée

### **Morphodynamics and sediment transfer in a human-impacted Alpine river**

Lausanne, le 28 août 2018

Pour le Doyen de la Faculté des géosciences et de  
l'environnement



Professeur Michel Jaboyedoff



## TABLE OF CONTENTS

TABLE OF CONTENTS .....	i
ACKNOWLEDGEMENTS .....	iii
ABSTRACT .....	v
RÉSUMÉ .....	vii
1. INTRODUCTION .....	1-1
1.1 Motivation .....	1-1
1.2 SEDFATE project .....	1-3
1.3 Thesis objectives.....	1-4
1.4 Approach and geographical focus of the research.....	1-5
1.5 Key contributions .....	1-8
1.6 Thesis structure .....	1-10
References.....	1-11
2. RESEARCH CONTEXT .....	2-13
2.1 Climate change in an Alpine setting.....	2-13
2.2 Hydropower flow abstraction .....	2-16
2.3 Braided river morphodynamics and sediment transfer .....	2-18
References.....	2-22
3. ARTICLE 1: ARCHIVAL PHOTOGRAMMETRIC ANALYSIS OF RIVER–FLOODPLAIN SYSTEMS USING STRUCTURE FROM MOTION (SfM) METHODS.....	3-33
3.1 Introduction.....	3-33
3.2 Methods .....	3-35
3.2.1 Overview.....	3-35
3.2.2 Case study: Borgne d'Arolla.....	3-35
3.2.3 Archival aerial photographs .....	3-36
3.2.4 Ground control .....	3-37
3.2.5 Photogrammetric analysis.....	3-37
3.2.6 Point cloud registration.....	3-40
3.2.7 DEM and DoD generation.....	3-40
3.3 Results .....	3-41
3.3.1 Quality of the SfM bundle adjustment.....	3-41
3.3.2 Exterior orientation and lens parameter estimation .....	3-42
3.3.3 Impact of image acquisition parameters.....	3-44
3.3.4 Systematic error minimization in SfM point clouds .....	3-45

3.4	Discussion .....	3-49
3.4.1	Bundle adjustment .....	3-49
3.4.2	Image properties and data quality .....	3-51
3.4.3	Systematic error minimization .....	3-52
3.5	Conclusions.....	3-53
	References.....	3-55
4.	ARTICLE 2: COMBINED FLOW ABSTRACTION AND CLIMATE CHANGE IMPACTS ON AN AGGRADING ALPINE RIVER.....	4-63
4.1	Introduction.....	4-64
4.2	Study Area .....	4-66
4.3	Methods .....	4-67
4.3.1	Overview.....	4-67
4.3.2	Morphologic Change Based on Photogrammetry .....	4-68
4.3.3	Discharge and Sediment Supply .....	4-70
4.3.4	Sediment Budget and Sediment Transfer .....	4-75
4.3.5	Sediment Transport Capacity and Supply Capacity Ratio .....	4-75
4.3.6	Climate Change.....	4-76
4.4	Results .....	4-78
4.4.1	Evolution of River Bed Aggradation and Sediment Transfer.....	4-78
4.4.2	Forcing of Sediment Supply and Transport Capacity .....	4-84
4.5	Discussion .....	4-88
4.5.1	Morphological Response to Sediment Supply and Transfer .....	4-88
4.5.2	Climate Forcing of Sediment Delivery .....	4-90
4.5.3	Human Forcing of System Sensitivity .....	4-91
4.6	Conclusions.....	4-93
	References.....	4-95
5.	ARTICLE 3: MORPHOLOGICAL RESPONSE OF AN ALPINE BRAIDED REACH TO SEDIMENT-LADEN FLOW EVENTS.....	5-103
5.1	Introduction.....	5-104
5.2	Study area.....	5-105
5.3	Methods .....	5-106
5.3.1	Overview.....	5-106
5.3.2	Flow events: upstream discharge and sediment supply .....	5-107
5.3.3	Morphological change .....	5-108
5.3.4	2D Sediment transport rates .....	5-110

5.3.5	Spatial forcing and response .....	5-113
5.4	Results .....	5-114
5.4.1	Sediment budget .....	5-114
5.4.2	Morphological change .....	5-116
5.4.3	Sediment transport .....	5-117
5.4.4	Morphological forcing of change.....	5-119
5.5	Discussion .....	5-123
5.5.1	Spatial and temporal morphodynamics .....	5-123
5.5.2	Upstream and local forcing of morphodynamics .....	5-124
5.5.3	System dynamics driving morphological evolution.....	5-126
5.6	Conclusions.....	5-127
	References.....	5-129
6.	CONCLUSIONS .....	6-135
6.1	Synthesis.....	6-135
6.1.1	Quantifying river morphodynamics at the decadal scale.....	6-135
6.1.2	External forcing of Alpine river evolution .....	6-136
6.1.3	Alpine river morphodynamics .....	6-139
6.2	Implications for sediment transfer from glacier to delta.....	6-140
6.3	Perspectives.....	6-145
	References.....	6-147
	APPENDICES.....	A-153
	A1: Orthoimages for reaches A-D, for the years 1959-2014.....	A-154
	A2: DEM local error estimation based on orthoimage texture.....	A-157
	A3: Grain size sampling and orthoimage semivariogram analysis .....	A-158
	A4: Sediment transport capacity calculation .....	A-159
	A5: Tsijiore Nouve water yield and sediment supply .....	A-161
	A6: Cross section evolution and effect on SCR.....	A-162
	References.....	A-164
	B1: Local uncertainty assessment based on lidar point density .....	B-165



## ACKNOWLEDGEMENTS

I am grateful to have worked with a lot of nice people from various backgrounds, who have directly or indirectly contributed to the results, analyses and ideas presented in this thesis.

First of all, I want to thank Stuart for his support during my PhD. You were always enthusiastic and supportive, gave me the guidance where I needed it and the freedom where I sought it.

Thanks to my SEDFATE collaborators at ETH Zürich, University of Bern and University of Geneva. I enjoyed working together on the larger basin-scale of the study and learnt a lot from the different disciplines involved.

Thanks to the thesis committee members for your reading/commenting/evaluating this thesis.

At UNIL, I would like to thank my colleagues for both the scientific and non-scientific discussions. A particular thanks to my room mates over the years, Nico, Natan, Chrystelle, Gilles, Pascal, and the rest of 'group Lane', Annegret, François, Romain, Gelare and Gustavo. Also thanks to all the students I have worked with over the years and those who have supported me in the field, Marie, Jean-Noël and Pascal. Furthermore, thank you to the people of the Val d'Hérens and Arolla, the Bornatici family in particular, for the warm welcome I got during my stays in the field.

I am also very happy and grateful for the support and the visits from the Netherlands, in particular my parents/parents in law. Lastly, thanks a lot to my lovely family Renske, Lise and Espen! I hope to experience many more adventures and nice moments together and I am excited to move on to our next destination.

MERCI!

*This thesis was written within the context of the SEDFATE project funded by the SNSF Sinergia grant CRSII2\_147689. I would like to thank the SNSF for their financial support. In addition thanks goes out to the SAV for providing an additional research subsidy.*



## ABSTRACT

In the Anthropocene, river basins have been affected by human impact both indirectly, e.g. through changes in climate and land-use, and directly, e.g. through river engineering and flow management. The Swiss Rhône basin is a notable example, where its Alpine tributaries are heavily impacted upon by climate warming and hydro-electric power exploitation (hydropower). Upstream, the Rhône's catchment is responding to the accelerated release of unconsolidated sediment associated with a history of glacial recession and ongoing climate change. In parallel, there is extensive abstraction of flow for hydropower, a common practice throughout the European Alps, which strongly reduces river sediment transport capacity whilst, contrary to classical reservoir dams, maintains sediment supply to streams. Combined, these impacts affect the morphodynamics and sediment storage of Alpine streams and hence the downstream transfer of sediment to the main rivers such as the Rhône.

In this thesis, the morphodynamics and sediment transfer of a left bank tributary of the Rhône, the Borgne d'Arolla, are studied in response to the combined effects of climate change and flow abstraction. The river has a strongly regulated flow with c. 90% of water abstracted at intakes. The intakes have to be flushed of sediment and most flow then occurs as a result of this short duration (typically 30 minutes to 2 hours) flushing. Additional flow can occur if the upstream water transfer tunnels are full and the intake has to be opened for longer duration. The result is that the stream bed is dry for most of the time, but perturbed by flushing events. This makes the field site well adapted for the quantification of morphological change, through the remote sensing of the dry braided river bed at timescales from the daily to the decadal. It also allows provides high quality flow records at the intakes, which also record flushing, and so allow reconstruction of sediment supply rates from the 1970s. The river bed level evolution since the onset of flow abstraction in the early 1960s was analysed through the development of Structure from Motion (SfM) photogrammetric techniques for application to archival imagery. This partly automated methodology allows for the generation of detailed and accurate historical Digital Elevation Models (DEMs), although it requires the careful consideration of photogrammetric principles, particularly in low-relief environments such as braided rivers. Over shorter timescales (daily) the river morphodynamics were monitored using a long-range terrestrial laser scanner.

The reaches just below the main intake show considerable aggradation (up to 5 meters) since the onset of flow abstraction. Widespread aggradation however did not commence until the onset of glacier retreat in the late 1980s and the dry and notably warm years of the early 1990s which intake records suggest led to an increase in upstream sediment supply. Surprisingly, most of the supplied sediment (c. 75%) was transferred through the studied reaches despite flow abstraction reducing

transport capacity by an order of magnitude. This was because the natural transport capacity was substantially greater than sediment supply rates such that the reduction in capacity due to abstraction still allowed significant sediment flux. However, abstraction rendered the system more sensitive to internal and external forcing, whether 'natural' or human-induced.

The spatial and temporal distribution of sediment transport and morphological change within the reaches varies strongly between events with similar levels of forcing (imposed flow and sediment supply). This stresses the importance of antecedent conditions, i.e. river bed topography and sediment stored, and internal morphological feedbacks on sediment transport rates and challenges simplistic notions regarding the equilibrium morphology in these systems. The system sensitivity also leads to the rapid response of the river to climate-driven hydrological variability and climate induced changes in sediment delivery rates and intake system functioning. The flow abstraction itself was designed under different climatic conditions such that the transfer tunnels are no longer sufficient to transport all glacial melt under extreme summer temperatures. This led to a strong increase in non-regulated flood events when the intake is opened for longer durations of time. The onset of these events has had a major impact on the downstream export of sediment from the reaches. In the wider river basin, the climate driven increases in sediment supply are conveyed downstream and reflected in: (1) temporal trends in sediment mining in the tributary basin; (2) the abundance of headwater sediments in the river bed sediment composition near the tributary outlet; and (3) increasing suspended load at the outlet of the Rhône in Lake Geneva.

## RÉSUMÉ

Au cours de l'Anthropocène, les bassins versants alpins ont été affectés par les activités humaines de manière indirecte, via les changements climatiques et l'évolution des usages du sol, et directement à travers l'ingénierie des cours d'eau et la régulation des débits. Le bassin du Rhône suisse est un exemple notoire, ses tributaires alpins étant significativement impacté par le réchauffement climatique et l'exploitation hydroélectrique. Les environnements alpins s'adaptent en réponse à l'accélération du taux de livraison de sédiments non-consolidés depuis l'amont en lien avec la récession glaciaire récente et les changements climatiques en cours. Parallèlement, beaucoup de bassins versants alpins sont affectés par des prélèvements d'eau pour l'exploitation hydroélectrique. Cette pratique, commune à travers la chaîne alpine, réduit drastiquement la capacité de transport des cours d'eau tout en laissant dans le lit l'entier de la masse sédimentaire, contrairement aux lacs de barrage qui tendent à stocker les matériaux et produire des déficits sédimentaires à l'aval. Combinés, les impacts des changements climatiques et des prélèvements d'eau affectent ainsi la dynamique morphologique, la capacité de stockage et la capacité de transfert des tributaires alpins vers les émissaires principaux, le Rhône dans ce cas précis.

Dans ce travail de thèse, ce sont la dynamique morphologique et les transferts sédimentaires de la Borgne d'Arolla, tributaire du Rhône, qui ont été étudiés en réponse aux effets combinés des changements climatiques et des prélèvements d'eau pour la production hydroélectrique. Le caractère intermittent et hautement régulé des écoulements permet la quantification précise des changements morphologiques à travers la télédétection du lit pendant les périodes sèches où le débit est nul, et la reconstruction du taux de livraison sédimentaire depuis les années 1970 est rendue possible par les données de purge des captages. L'évolution du lit de la Borgne depuis le début de l'exploitation hydroélectrique au début des années 1960 a été étudié à travers l'application de méthodes photogrammétriques 'Structure from Motion' à des images aériennes historiques. Cette méthode semi-automatique permet la production de modèles numériques de terrain historiques à haute résolution (MNTs), où la faible amplitude altitudinale des plaines alluviales alpines requière un contrôle consciencieux des résultats photogrammétriques.

Les résultats de l'étude montrent que le tronçon situé directement en aval du captage principal a subi une aggradation considérable (jusqu'à 5 mètres) depuis le début des prélèvements d'eau. L'aggradation du lit à plus large échelle n'a toutefois pas débuté jusqu'à l'initiation du retrait glaciaire à la fin des années 1980 et au cours des années particulièrement chaudes du début des années 1990 qui ont conduit à une augmentation dans le taux de livraison sédimentaire depuis l'amont. Malgré cela, les données montrent que la majeure partie des sédiments (environ 75%) ont pu être transférés

à travers le tronçon d'étude. En effet, si les prélèvements d'eau ont significativement réduit la capacité de transport de la Borgne, il apparaît que la capacité de transport résiduelle reste proche du taux de livraison depuis l'amont. Cet équilibre rend le système hautement sensible aux forçages internes et externes, qu'ils soient 'naturels' ou anthropiques. La distribution spatiale et temporelle du transport sédimentaire et les changements morphologiques au sein des tronçons étudiés varient significativement entre des séquences intermittentes d'écoulement qui correspondent à des 'purges sédimentaires' des captages d'eau. Ceci souligne l'importance des conditions antérieures à la purge à l'aval du captage, notamment la morphologie des chenaux de la plaine alluviale et le stockage des sédiments en leur sein, ainsi que leurs rétroactions sur les taux de transport, pour la compréhension de l'équilibre morphologique de ces systèmes. La sensibilité du système conduit également à des réponses rapides face aux forçages externes liés aux changements climatiques et hydrologiques dans le bassin versant, notamment l'évolution des taux de livraison sédimentaire et la fréquence des purges des captages d'eau qui avait été dimensionnés par le passé sur la base de conditions climatiques plus froides. Ceci conduit à une forte augmentation de la fréquence des crues non régulées en raison de la surcharge du système de captage et de transfert des eaux, ce qui impacte significativement l'export de sédiment vers l'aval. Dans le bassin versant à plus large échelle, l'augmentation du taux de livraison sédimentaire dû aux changements climatiques et sa propagation peuvent être perçus: (1) dans la variabilité temporelle des prélèvements de matériaux dans les carrières du bassin versant; (2) dans le volume des cônes de déjection à la confluence des tributaires avec les émissaires principaux; et (3) dans l'augmentation de la charge en suspension dans le delta du Rhône sur le lac Léman.

# 1. INTRODUCTION

## 1.1 Motivation

Mountain streams lie at the interface between Alpine environments and larger piedmont river systems. They not only transfer water, but may also large amounts of sediment. The high sediment transfer follows from high rates of Alpine erosion (Hinderer *et al.* 2013) and the relatively steep and narrow river beds which may result in high sediment transport capacity. Following from high energy availability and sediment load, these rivers may be dynamic, as a function of flow and sediment supply. Where the valley bottom allows (i.e. lateral accommodation space, lower slope), this may lead to local deposition and the development of braided reaches (Church 2006; Wheaton *et al.* 2013), changing local riparian habitat and impacting human settlements and infrastructure (Figure 1-1). These impacts may extend some way downstream (Syvitski *et al.* 2005; Costa *et al.* 2017), with consequences for wider river management and exploitation.



*Figure 1-1 (left) Sediment deposition and subsequent channel expansion and flooding in Canmore Creek (Canada) in 2013; image taken from Jonathan Hayward/Canadian Press; (right); riparian trees that are covered by sediment and subsequently dying off in the study area of this thesis, the Borgne d’Arolla, Switzerland.*

Whilst Alpine streams are intrinsically dynamic, they are also influenced by external drivers. Four need particular mention:

- Climate change: Increasing amounts of sediment may be exposed and susceptible to erosion in Alpine catchments due to climate driven glacial retreat and permafrost degradation, and may subsequently easily be mobilized and transferred to river channels (Church and Ryder 1972; Ballantyne 2002). Associated changes in discharge regime may enhance the already high levels of sediment transport capacity of Alpine rivers (e.g. Lane *et al.* 2017). At lower elevations, vegetation and land-cover changes due to climate and human management will have an impact (Gimmi *et al.* 2010).
- Hydroelectric power generation: The high energy of Alpine rivers is extensively exploited by hydroelectric power generation (hereafter “hydropower”) installations (Zimmermann 2001). Exploitation may directly affect river discharge and discharge regime (Petts and Gurnell 2005) and river sediment load, which may be trapped in reservoirs (e.g. Anselmetti *et al.* 2007) or transported at lower rates due to flow impacts (Gabbud and Lane 2016). These impacts eventually force changes in downstream river bed morphology (Williams and Wolman 1984).
- Sediment extraction: Sediment may be extracted from Alpine streams, typically for building material (Kündig 1997), which lead to local and downstream changes in river bed morphology (e.g. Kondolf 1997)
- River engineering: Local engineering has developed to protect human infrastructure, e.g. roads, and to limit the river width (through e.g. dikes) for land-use purposes, e.g. pastures and settlements.

Although there is a general understanding of the impacts that these drivers may have on Alpine river geomorphology, it is not clear how their combined effects will affect sediment fluxes on a larger, source-to-sink scale. For example, increases in sediment fluxes due to climate change may be (partly) counteracted by decreased sediment transfer rates due to hydropower exploitation. Thus, what is the net effect? If we are to understand depositional records in the Anthropocene and contemporary basin-wide sediment transfer, there is the need to understand the fundamental processes through which external drivers impact fluvial systems and how these respond to the combined forcing. This is the aim of the interdisciplinary project SEDFATE: SEDiment FATE in a changing watershed during the Anthropocene.

## 1.2 SEDFATE project

In the SEDFATE project we explored the effects of human impact on erosion and sediment transfer in the Swiss Upper Rhône drainage basin in the context of declining sedimentation rates in Lake Geneva since the 1950s (Figure 1-2; Loizeau and Dominik, 2000). This observation coincided with a strong increase in installed reservoir capacity in upstream tributaries (Figure 1-3; Loizeau and Dominik, 2000). Although some of this decline could be accounted for by sediment storage in reservoirs, large amounts are expected to remain within the river corridor. The main questions that arise are where does the sediment reside and for how long? To answer this, we need to consider changes in sediment production and transfer rates against a background of climate change (Hinderer *et al.* 2013). Whilst the fate of sediment in the wider catchment was addressed in the overall project, this thesis aims to provide physical explanations of the coupled evolution of fluvial morphodynamics with human and climate forcing.

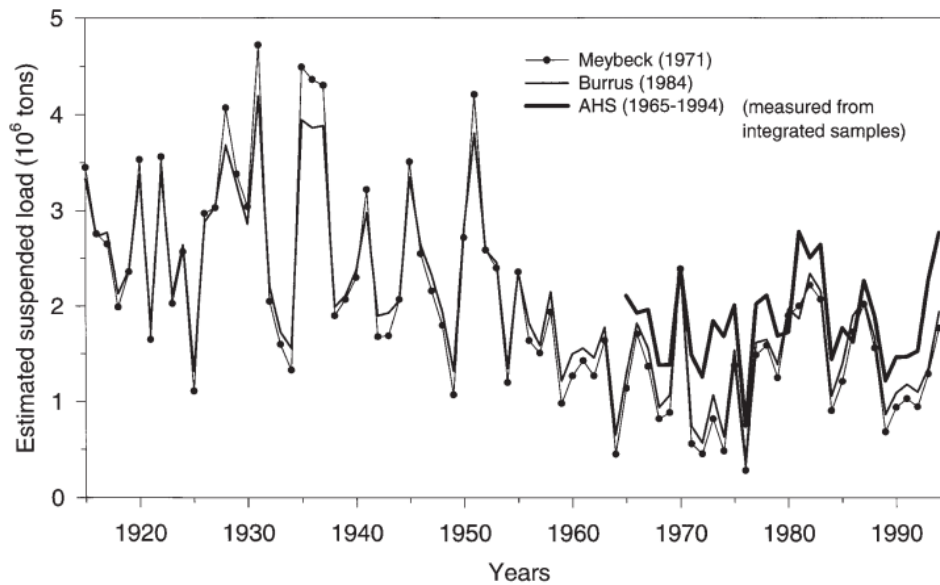


Figure 1-2 Modelled and measured (AHS) suspended sediment input to Lake Geneva from the Rhone River; taken from Loizeau and Dominik (2000).

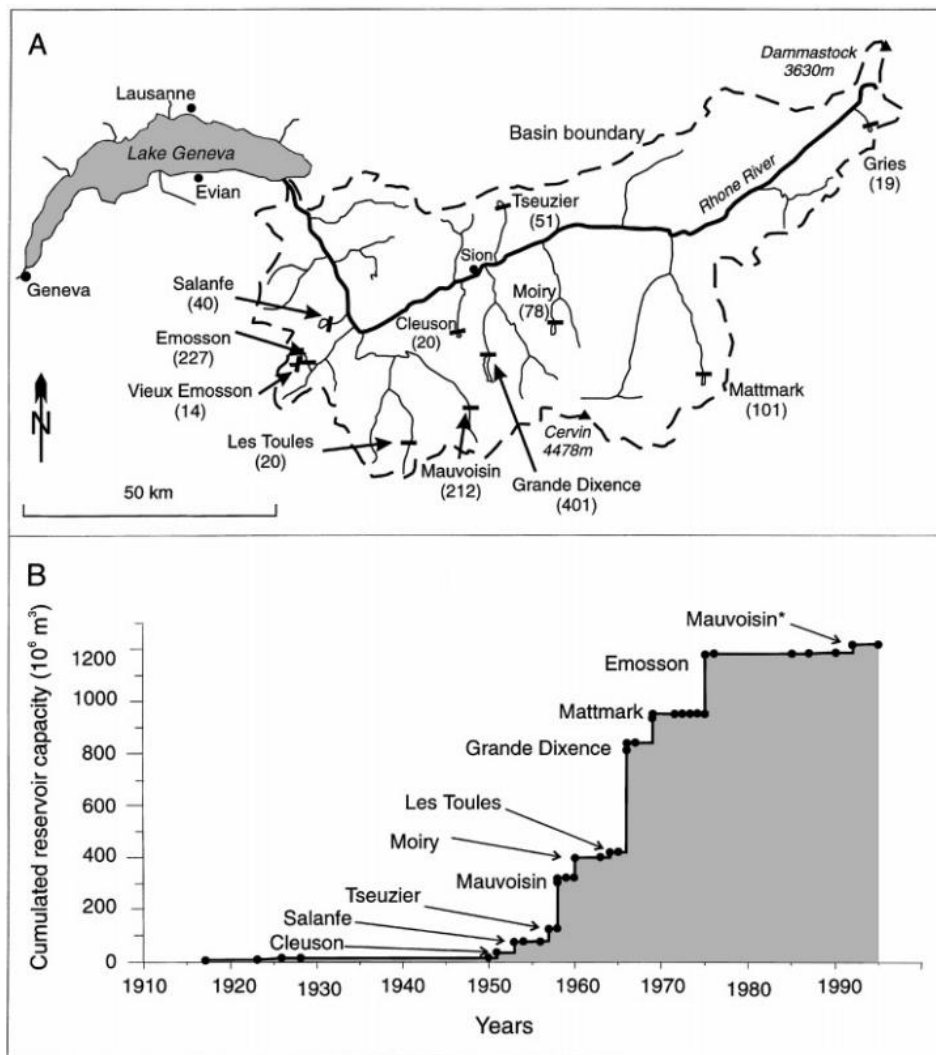


Figure 1-3 Overview of the major hydropower reservoirs in the Swiss Rhône basin (top) and the evolution of reservoir capacity in the 20<sup>th</sup> century (bottom); taken from Loizeau and Dominik (2000).

### 1.3 Thesis objectives

As noted above, the general aim of this thesis is to quantify and to explain the processes operating in a headwater Alpine catchment that might explain observations made in terms of sediment loading to the River Rhône and sedimentation rates in Lake Geneva, including how these processes are responding to internal and external forcing mechanisms. The thesis has two primary objectives which we address with following research questions:

1. Can the effects of climate change and flow abstraction be distinguished from 'natural' river bed evolution and what are their relative contributions to river morphological evolution and sediment transfer?
2. How do the morphodynamics of proglacial streams and associated sediment transport regulate these drivers?

In order to achieve primary objective 1, a third, methodological objective was necessary, namely the development of Structure from Motion photogrammetry for application to archival imagery so as to reconstruct historical reach-based sediment budgets.

### 1.4 Approach and geographical focus of the research

The thesis uses a case study approach to address the two primary objectives of the work, the Borgne d’Arolla in south-west Switzerland, on a time-scale that extends from days through to decades. The reaches investigated in this thesis are fed primarily by the retreating Bas Glacier d’Arolla, whose terminus lies c. 1 km further upstream, and indirectly by the Haut Glacier d’Arolla, which has been extensively investigated (Lane *et al.* 2017). However, most of the meltwater is intercepted by an intake (altitude 2110 m above sea level) that is part of the Grande Dixence hydropower scheme (Park 1980) and that transfers water to the Lac de Dix reservoir (Figure 1-4). At the intake, sediment is trapped and intermittently flushed down the investigated braided reaches in sediment laden “pulses”. Where this is a common practice in Switzerland and throughout the Alps, the Borgne is an exponent of a much wider class of human-impacted Alpine environments.

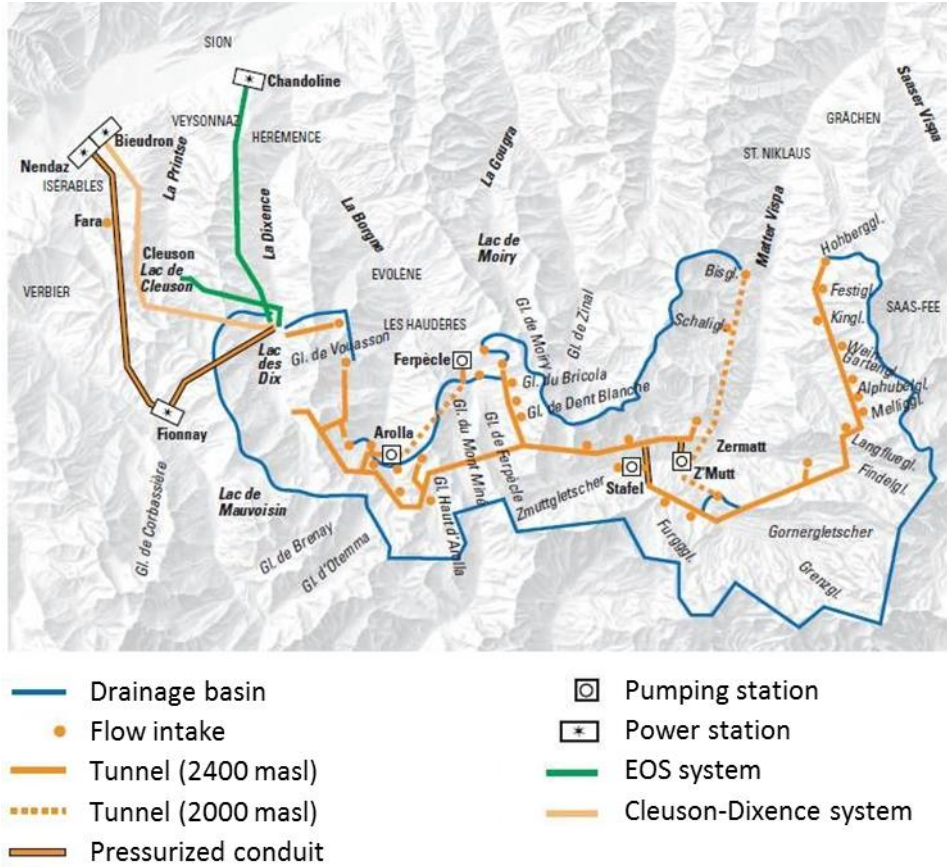


Figure 1-4 Overview of the Grande Dixence scheme; taken from EnergyForum Valais.

This setting is particularly suitable for a study of this type for two primary reasons:

- Quantification of river bed morphodynamics: due to the general abstraction of flow, the more or less dry river bed (Figure 1-5) was readily monitored using historical aerial images (Chapter 3) and terrestrial laser surveys from a vantage point on the valley slope (Chapter 5);
- Historical data on river flow and sediment supply: due to hydropower system operation and intake flow records (Figure 1-6), event-based river discharge and sediment fluxes could be inferred based on (Bezinge *et al.* 1989) and described in detail in Chapter 4 (Section 4.3.3). The latter provides a relatively unique record of sediment flux in terms of its length and its accuracy.

These two characteristics allow for the investigation of river morphodynamics at the scales that correspond to the two primary research objectives (Section 1.3). First, both the historical imagery and the flow/sediment data have been collected over a sufficiently long period that includes the onset of external forcing mechanisms and the registered response: historical aerial images date from 1959, where flow abstraction commenced in 1962; sediment flux records date from 1977, whereas the major increase in temperatures took place in the late 1980s. Second, the frequent occurrence of regulated flushing events whose impact on the river can be readily monitored with a terrestrial laser scanner, allowed the analysis of river morphodynamics at a higher temporal frequency (daily).



*Figure 1-5 Drone image of the uppermost studied reach without flow (flow direction from bottom to top) illustrating the braided spatial configuration (the road in the left bottom provides a scale indication).*

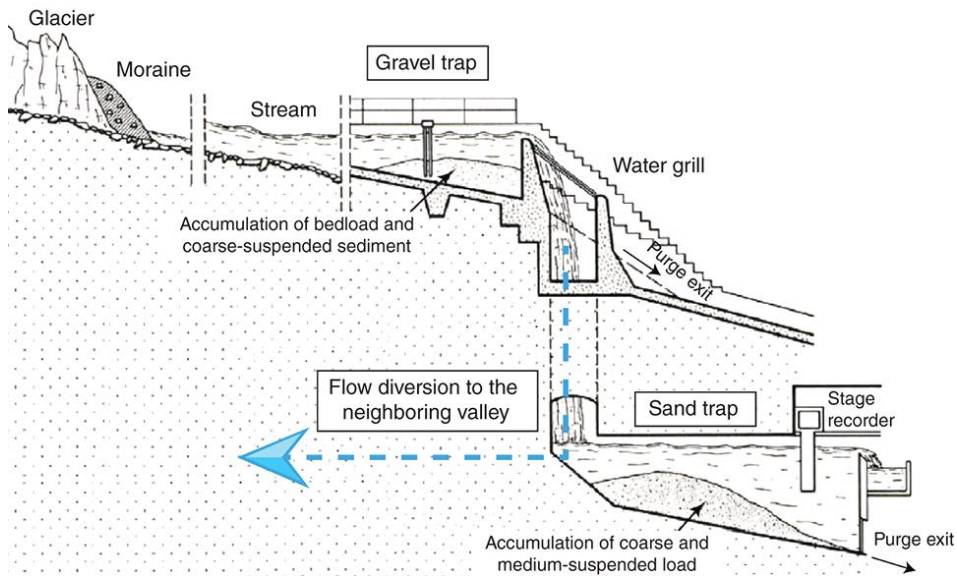


Figure 1-6 Lower Bertol intake sediment trap(s) and water intake; photograph (top) and cross section (bottom); image taken from (Gabbud and Lane 2016).

## 1.5 Key contributions

The core of this PhD thesis is based on the two primary objectives and the methodological objective identified in Section 1.3. The article addressing the methodological objective has been published and is included unmodified as Chapter 3. The article addressing the first primary objective has been published and is included unmodified as Chapter 4. The second primary objective has been addressed through a third manuscript that was submitted in July 2018 and which is included in this thesis as Chapter 5. Note here that this manuscript will still undergo a review process before publication.

### Chapter 3, methodological objective:

Bakker M. and Lane, S.N. (2017): Archival photogrammetric analysis of river–floodplain systems using Structure from Motion (SfM) methods. *Earth Surface Processes and Landforms* 42(8): 1274-1286.

### Chapter 4, primary objective 1:

Bakker, M., Costa, A., Silva, T.A., Stutenbecker, L., Girardclos, S., Loizeau J.-L., Molnar, P., Schlunegger, F., and Lane, S.N. (2018): Combined Flow Abstraction and Climate Change Impacts on an Aggrading Alpine River. *Water Resources Research*: 54(1): 223-242.

### Chapter 5, primary objective 2:

Bakker M., Antoniazza, G., Odermatt, E. and Lane, S.N.: Morphological Response of an Alpine Braided Reach to Sediment-laden Flow Events. Submitted to *Journal of Geophysical Research – Earth Surface*.

Where the scope of the research and the project was multidisciplinary, I also contributed to a number of published articles as co-author. The following articles provide (additional) insight in upstream climate forcing of glacially derived sediment export and proglacial sediment connectivity and feedback processes:

Lane, S.N., Bakker, M., Balin, D., Antoniazza, G. and Regamey, B. (2014): Climate forcing of sediment flux in mountain river systems. *River Flow 2014*. In A. J. Schleiss, G. de Cesare, M. J. Franca and M. Pfister (Eds.): 7-15.

Lane, S.N., Bakker, M., Gabbud, C., Micheletti, N. and Saugy, J.-N. (2017): Sediment export, transient landscape response and catchment-scale connectivity following rapid climate warming and Alpine glacier recession. *Geomorphology* 277: 210-227.

Further, the following articles contribute to the wider understanding of the implications of climate change and direct human impact in the river, hydropower exploitation, river regulation and sediment mining, on sediment production and transfer in the Swiss Rhône basin:

Costa, A., Molnar, P., Stutenbecker, L., Bakker, M., Silva, T.A., Schlunegger, F., Lane, S.N., Loizeau, J.-L. and Girardclos, S. (2017): Temperature signal in suspended sediment export from an Alpine catchment. *Hydrol. Earth Syst. Sci. Discuss*: 1-30.

Stutenbecker, L., Delunel, R., Schlunegger, F., Silva, T.A., Šegvić, B., Girardclos, S., Bakker, M., Costa, A., Lane, S.N., Loizeau J.-L., Molnar, P., Akçar, N., Christl, M. (2017): Reduced sediment supply in a fast eroding landscape? A multi-proxy sediment budget of the upper Rhône basin, Central Alps. *Sedimentary Geology*.

The key results and insights of these co-author articles will be included in the synthesis of this PhD thesis in Chapter 6, together with relevant ongoing work in which I am involved and that has been submitted or is in preparation.

## 1.6 Thesis structure

The thesis is structured as follows:

Chapter 2, research context: This chapter provides a background to climate change and hydropower exploitation in the Alpine river basins with a focus on Switzerland, and the key questions regarding their impact on fluvial morphodynamics which is investigated in Chapter 4. A very brief review of the functioning and dynamic nature of braided rivers is provided, which is investigated in Chapter 5.

Chapter 3, methodological objective: To explore human impacts on evolution, we first established the river bed evolution of the Borgne at a decadal time-scale. High spatial resolution topographic data were required to detect temporal changes in bed level height and assess evolution within and between reaches. We accomplished this through developing an archival Structure from Motion (SfM) based photogrammetric methodology that was used to quantify river bed topographic change as precisely as possible from historical aerial images from 1959 onwards, given their spatial resolution.

Chapter 4, primary objective 1: The historical bed level change was combined with a long term sediment flux record, derived from hydropower intake data, to set up a sediment budget for the upstream reaches of the Borgne. We then explored the impacts of flow abstraction, climate change and the combined impacts of hydropower management in response to climate change.

Chapter 5, primary objective 2: Following the long term analysis of system behaviour and response in Chapter 4, we observed detailed daily morphological change of the uppermost braided reach of the Borgne during the summer of 2015. This gives the opportunity to investigate braided sediment transport and morphodynamics in response to flushing sequences and unregulated floods.

Chapter 6, conclusions: This chapter integrates the results and insights of Chapters 3, 4 and 5, and puts these in the broader perspective of the SEDFATE project. A short outlook is given considering the issues that need to be addressed for further research.

## References

- Anselmetti, F. S., Bühler, R., Finger, D., Girardclos, S., Lancini, A., Rellstab, C., Sturm, M. 2007. Effects of Alpine hydropower dams on particle transport and lacustrine sedimentation. *Aquatic Sciences* 69(2): 179-198. DOI: 10.1007/s00027-007-0875-4.
- Ballantyne, C. K. 2002. A general model of paraglacial landscape response. *The Holocene* 12(3): 371-376. DOI: 10.1191/0959683602h1553fa.
- Bezinge, A., Clark, M., Gurnell, A., Warburton, J. 1989. The management of sediment transported by glacial melt-water streams and its significance for the estimation of sediment yield. *Annals of Glaciology* 13: 1-5.
- Church, M. 2006. Bed material transport and the morphology of alluvial river channels. *Annu. Rev. Earth Planet. Sci.* 34: 325-354.
- Church, M., Ryder, J. M. 1972. Paraglacial sedimentation: a consideration of fluvial processes conditioned by glaciation. *Geological Society of America Bulletin* 83(10): 3059-3072.
- Costa, A., Molnar, P., Stutenbecker, L., Bakker, M., Silva, T. A., Schlunegger, F., Lane, S. N., Loizeau, J. L., Girardclos, S. 2017. Temperature signal in suspended sediment export from an Alpine catchment. *Hydrol. Earth Syst. Sci. Discuss.* 2017: 1-30. DOI: 10.5194/hess-2017-2.
- Gabbud, C., Lane, S. N. 2016. Ecosystem impacts of Alpine water intakes for hydropower: the challenge of sediment management. *Wiley Interdisciplinary Reviews: Water* 3(1): 41-61. DOI: 10.1002/wat2.1124.
- Gimmi, U., Wohlgemuth, T., Rigling, A., Hoffmann, C. W., Bürgi, M. 2010. Land-use and climate change effects in forest compositional trajectories in a dry Central-Alpine valley. *Annals of Forest Science* 67(7): 701.
- Hinderer, M., Kastowski, M., Kamelger, A., Bartolini, C., Schlunegger, F. 2013. River loads and modern denudation of the Alps — A review. *Earth-Science Reviews* 118(0): 11-44. DOI: 10.1016/j.earscirev.2013.01.001.
- Kondolf, G. M. 1997. PROFILE: Hungry Water: Effects of Dams and Gravel Mining on River Channels. *Environmental Management* 21(4): 533-551. DOI: 10.1007/s002679900048.
- Kündig, R. 1997. Die mineralischen Rohstoffe der Schweiz, Schweizerische Geotechnische Kommission.
- Lane, S. N., Bakker, M., Gabbud, C., Micheletti, N., Saugy, J.-N. 2017. Sediment export, transient landscape response and catchment-scale connectivity following rapid climate warming and Alpine glacier recession. *Geomorphology* 277: 210-227. DOI: 10.1016/j.geomorph.2016.02.015.

- Loizeau, J.-L., Dominik, J. 2000. Evolution of the Upper Rhone River discharge and suspended sediment load during the last 80 years and some implications for Lake Geneva. *Aquatic Sciences* 62(1): 54-67. DOI: 10.1007/s000270050075.
- Park, C. 1980. The Grande Dixence hydro-electric scheme, Switzerland. *Geography*: 317-320.
- Petts, G. E., Gurnell, A. M. 2005. Dams and geomorphology: research progress and future directions. *Geomorphology* 71(1): 27-47.
- Syvitski, J. P., Vörösmarty, C. J., Kettner, A. J., Green, P. 2005. Impact of humans on the flux of terrestrial sediment to the global coastal ocean. *Science* 308(5720): 376-380.
- Wheaton, J. M., Brasington, J., Darby, S. E., Kasprak, A., Sear, D., Vericat, D. 2013. Morphodynamic signatures of braiding mechanisms as expressed through change in sediment storage in a gravel-bed river. *Journal of Geophysical Research: Earth Surface* 118(2): 759-779. DOI: 10.1002/jgrf.20060.
- Williams, G. P., Wolman, M. G. 1984. Downstream effects of dams on alluvial rivers, US Government Printing Office Washington, DC.
- Zimmermann, M. 2001. Energy situation and policy in Switzerland. *International journal of ambient energy* 22(1): 29-34.

## 2. RESEARCH CONTEXT

The aim of this Chapter is to provide the context for the key scientific questions addressed in Chapters 3, 4 and 5. Sediment transfer in Alpine rivers is forced by means of two important exogenic variables, climate change and hydropower exploitation, and through river morphodynamic response by means of autogenic processes. Hence the three corresponding sections that are addressed in this Chapter. Section 2.1 gives an overview of long term climate change and associated impacts in Alpine catchments. Section 2.2 discusses the geomorphological impacts of hydropower flow abstraction and how in turn this may be impacted upon by climate change. Section 2.3 discusses the internal processes and mechanisms that drive braided river dynamics, and their role in the storage and downstream transfer of sediment.

### 2.1 Climate change in an Alpine setting

Global climatic variability has played an important role in the geomorphological evolution of the landscape. This was particularly prominent during the last c. 2.5 million years (Dansgaard *et al.* 1993; Petit *et al.* 1999), when cycles of extensive glaciation caused accelerated mountain erosion and subsequent increases in global sediment fluxes (Herman *et al.* 2013). After the retreat of ice sheets in Europe some 12,000 years ago, there have been periods of both Alpine glacial expansion and retreat related to climatic oscillations (Holzhauser *et al.* 2005). The last phase, the Little Ice Age c. 1850 AD, is still clearly preserved in the terrain in, for example, the form of steep moraine deposits (Lambiel *et al.* 2016).

Since the middle to late 19<sup>th</sup> century, human impact appears to have started to play a significant role in global climate warming, most notably through the increasing effects of the emission of greenhouse gasses, in what is referred to as the beginning of the 'Anthropocene' (Crutzen 2006). In the 20<sup>th</sup> century, global mean surface temperature increased worldwide by nearly 1°C (IPCC: Stocker 2013; Figure 2-1). This increase was particularly pronounced in the Northern Hemisphere (Friedman *et al.* 2013). Mean annual temperatures in Switzerland (Figure 2-1; Begert *et al.* 2013) show a steady increase in the first half of the 20<sup>th</sup> century, then stabilized in the relatively cool and wet period in the 1960s and 1970s, before rapidly increasing again in the late 1980s. The accelerated increase in temperature was greater in the Alps (Rangwala and Miller 2012) and has had a clear impact on glacial extent in the Alps (Figure 2-2; Haeberli *et al.* 2007; Fischer *et al.* 2014) where rates of retreat in the last c. 50 years were a factor 7 times larger than those in the preceding c. 150 years (Paul *et al.* 2007). An acceleration in glacial retreat also occurred around the same time in North America (Moore *et al.* 2008), slightly earlier (c. 10 years) in the Andes (Rabatel *et al.* 2013) and slightly later (5-10 years) in

the Himalaya with the exception of the Karakoram where there are indications of glacier expansion (Bolch *et al.* 2012). Although a clear global trend in recession may be observed, changes in glacial cover and dynamics are variable and strongly dependent on local conditions (hypsometry) and regional climate (e.g. Barry 2003; Hoelzle *et al.* 2003).). At the same time, there is widespread permafrost degradation, although this is more difficult to observe directly, long-term records (boreholes) are sparse (e.g. Haeberli and Beniston 1998) and the spatial distribution of permafrost may be highly variable both in time and space (Beniston *et al.* 2018).

The spatial and temporal distribution in temperature and precipitation have also shown important changes. Temperature increases are highest at higher elevations, worldwide (Rangwala and Miller 2012; Pepin *et al.* 2015) and in Switzerland (Beniston *et al.* 1997; Giorgi *et al.* 1997). Various feedback mechanisms may play a role in this trend (Rangwala and Miller 2012; Mountain Research Initiative 2015), a.o. reduced albedo due to reduced snow cover duration. These processes may also lead to a large interannual variability (Beniston *et al.* 1997). Seasonal trends show the greatest temperature increases in summer and to a lesser extent spring (Rebetez and Reinhard 2008; Ceppi *et al.* 2012). More frequently occurring extremes have been reported, including heatwaves (Schar *et al.* 2004) and enhanced summer convective rainfall (Giorgi *et al.* 2016). Precipitation trends in the 19<sup>th</sup> century are not very strong, although increases in winter precipitation have been established throughout Switzerland (Widmann and Schär 1998). More significantly, warming leads to a clear reduction in precipitation that falls as snow and in the duration of snow cover (Serquet 2011; Klein 2016). This has important consequences for the seasonal hydrology of Alpine basins (Birsan *et al.* 2005; Molnar *et al.* 2011) and consequently also for the river capacity to transport sediment (Lane *et al.* 2014). In Section 6.2, the implications of these effects will be discussed further, including the longer term spatial and temporal hydro-climatic impacts on sediment fluxes in the Rhône catchment (Costa *et al.* 2017).

In the future, climate warming is projected to continue in Alpine regions, at rates higher than that recorded during the 20th century (Nogués-Bravo *et al.* 2007; Gobiet *et al.* 2014), and lead to a general increase in the frequency, intensity and duration of heat waves and precipitation events (Beniston *et al.* 2007; Beniston *et al.* 2011).

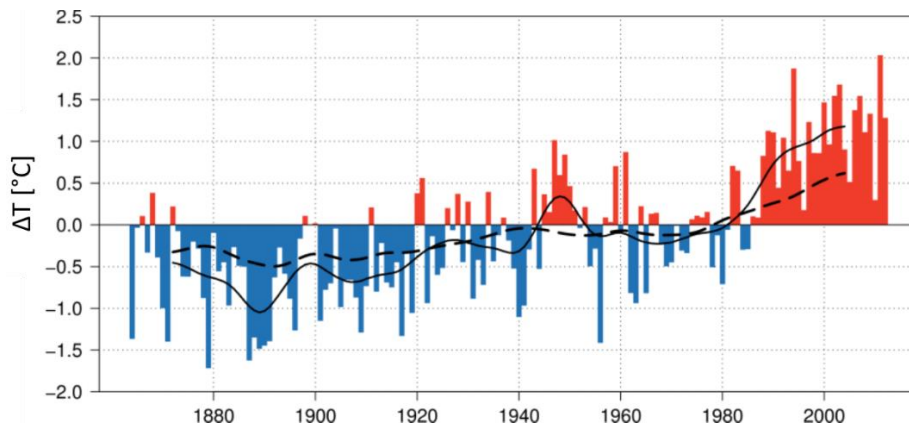


Figure 2-1 Mean temperature record of Switzerland with respect to the 1961-1990 average (red and blue bars, 10 year running mean in black) and with respect to the global mean land air temperature (dashed black line); taken from Begert et al. (2013).

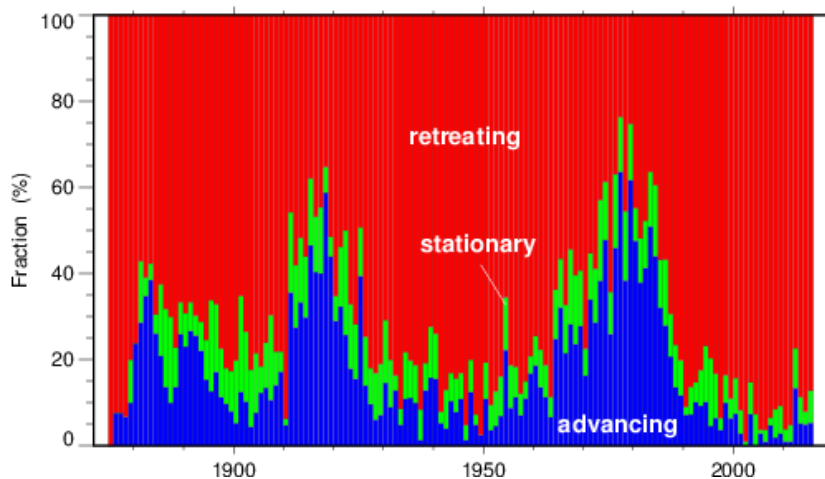


Figure 2-2 Variation in glacier length of c. 100 glaciers in the Swiss Alps; taken from Glaciological reports (1881-2017).

The effects of current climate change on sediment fluxes is poorly understood in general, despite the large impacts it may have on river dynamics and management (Knight and Harrison 2013). This uncertainty is amplified in Alpine environments because of the legacy of past climatic change. Alpine landscapes are largely in disequilibrium with the climate because the current distribution of sediment that may be mobilized does not reflect current climate, but rather this history of glacial advance and retreat. In order to explore the impacts of these changes on Alpine geomorphology, we need to investigate past records of change and understand the present day functioning in response to this (cumulative) change (e.g. Knight and Harrison 2014).

Glaciated basins in the Alps have sediment yields which are on average 5 to 10 times higher than in non-glaciated basins (Hinderer et al. 2013). Holocene sediment records from pro-glacial lake deposits have been related to phases of glacial change, where higher sedimentation rates are found in periods

with colder (summer) temperatures and greater glacial extent (Karlén 1976; Leemann and Niessen 1994). Leonard (1997), however, associated highest sedimentation rates with transitional periods before and after maximum ice retreat. During glacial retreat, large amounts of exposed and readily mobilized sediment becomes available from over-steepened slopes and unconsolidated deposits, due to degrading permafrost on slopes, and unreworked sediment that emerges from under the glacier (e.g. Lane *et al.* 2017). These sources may provide a large contribution to the total sediment flux that is supplied to the expanding proglacial outwash plain that modulates the downstream flux (Harbor and Warburton, 1993). On the long time-scale of decades to millennia, these amounts of sediment are expected to be exported according to an exponential decay curve as described in the paraglacial model (Church and Ryder 1972; Ballantyne 2002). However, the question is how do these systems respond and interact to accelerated climatic change over very short timescales? To answer this question, it is necessary to identify sediment sources and study decadal time-scale erosion and deposition (Schwab 2008; Micheletti *et al.* 2015) and sediment transfer rates (Micheletti and Lane 2016; Lane *et al.* 2017) in proglacial areas and braided river systems. Here, glacial, periglacial and hillslope and fluvial processes interact to regulate both the local river morphodynamics and how these flux sediment through the system. Key processes, mechanisms and feedbacks that act in the pro-glacial area and affect sediment storage and connectivity will be discussed in Section 6.1 (Lane *et al.* 2017).

## **2.2 Hydropower flow abstraction**

To understand the impacts of climate change and glacier recession on changes in Alpine sediment yield at the scale of recent decades, it is also necessary to consider and account for human impacts and notably hydropower. Syvitski *et al.* (2005) estimated that 60% of sediment delivery to the coastal zone is derived from basins draining high mountains (altitude >3000 m) whilst another 26% that could be potentially transferred is trapped in reservoirs most commonly found in these basins.

Hydropower is an important source of energy, contributing approximately 16% to the global electricity production and accounting for approximately 60% of the production of renewable energy (Spänhoff 2014; REN21 2018). In Alpine countries, hydropower may provide for more than half of the total production, e.g. 65% in Austria (Wagner *et al.* 2015) and 59% in Switzerland. For the latter, hydropower is expected to become even more important in the next decades, when the Swiss government is to phase out nuclear power, which contributes 34% of the total production (<http://www.world-nuclear.org>). Hydropower development rapidly expanded in the period 1950-1980, associated with worldwide growth in population and energy consumption (Chen *et al.* 2016), and it was in this period that the current hydropower capacity was largely put in place throughout

the Alps; in Austria (Wagner *et al.* 2015), France (Dalmasso 2008) and Switzerland (Margot *et al.* 1992; Zimmermann 2001; Figure 1-3). In the late 1950s, the Grande Dixence scheme was expanded to create the largest hydropower system in Switzerland (Park 1980; Figure 1-4), which impacts the Borgne tributary and Rhône River which are studied in this thesis.

Hydropower exploitation is typically classified as reservoir or run-of-the-river systems (e.g. by the International Hydropower Association). However, hydropower schemes often form a hybrid between these end-members, where flow may be abstracted and transferred (within or between basins) to a reservoir. Although flow abstraction schemes are rarely recognized (Halleraker *et al.* 2016) and much less frequently studied than the end-member systems, they are prominent in the Alps; in Austria (Tschada and Hofer 1990; Turowski and Rickenmann 2009), France (Marnezy 2008) and Switzerland (Bezinge *et al.* 1989; Raymond Pralong *et al.* 2015; Gabbud and Lane 2016), but also in Norway (Wold and Østrem 1979; Fergus 1997). In fact, in Switzerland the area affected by flow abstraction is greater than that affected by dams (Figure 2-3).

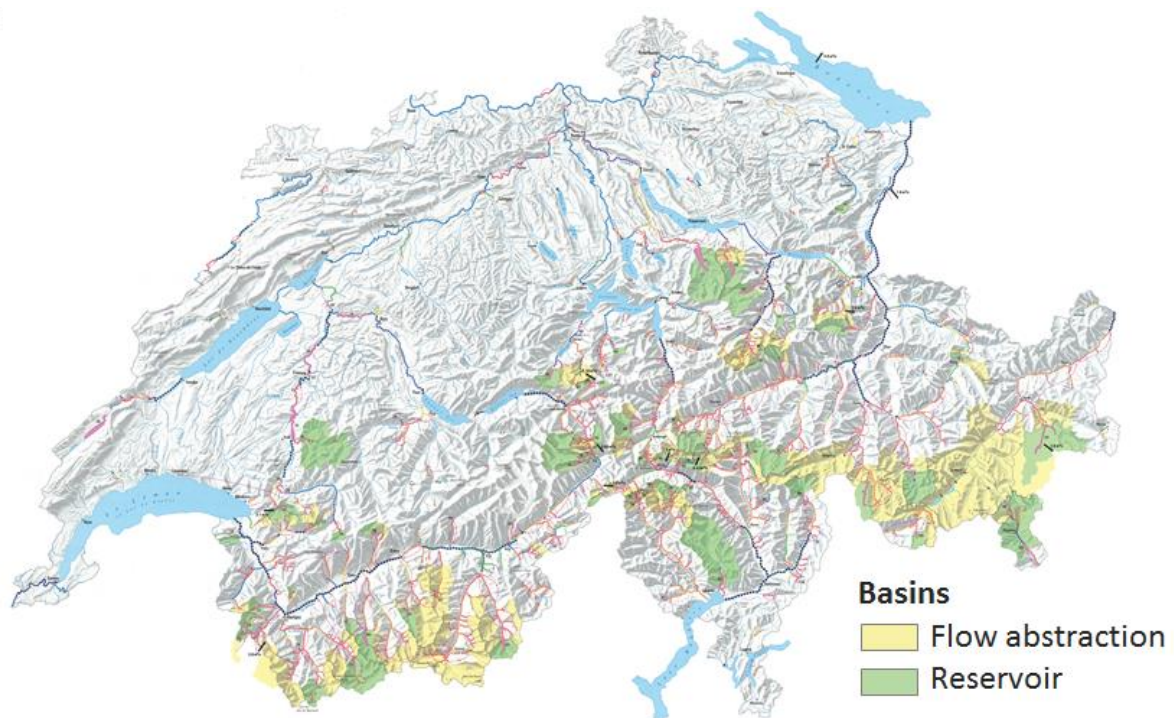


Figure 2-3 Overview of basins in Switzerland affected by flow abstraction and reservoir dams; adapted from (Margot *et al.* 1992).

Although hydropower is considered a renewable energy source, it can have considerable environmental impacts on downstream on sediment transfer (e.g. Williams and Wolman 1984; Petts and Gurnell 2005). The effects of reservoir dams and flow abstraction streams are however distinctly different. Dams commonly impede sediment flux and store sediment in their reservoirs for extended

periods of time; they may be designed to allow the occasional flushing of sediment, although this is rare in Swiss Alpine streams. Intakes are small scale structures that are designed to frequently flush sediment downstream in 'purges' and so they can maintain significant sediment connection in the impacted rivers. The question follows as to whether the reduced sediment transport capacity of these rivers due to flow intake remains sufficient to transfer supplied further sediment downstream (e.g. Gurnell 1983) or whether it is not and sediment is deposited. This practice of flow abstraction will have important consequences for the downstream bed evolution and river ecosystems (Petts and Bickerton 1994; Gabbud and Lane 2016). It is surprising that despite the widespread prevalence of these systems in the Alps, their effects have received so little attention.

The exploitation of hydropower is strongly linked to climatic conditions and how they impact the associated catchments, and so is likely to be affected by climate change. Water yield varies with seasonal changes in catchment precipitation and the net change in water storage, primarily through snow and ice melt (e.g. Finger *et al.* 2012). Over the short term, increasing temperatures will lead to glacier recession and an increase in water yield and sediment supply (e.g. Raymond Pralong *et al.* 2015; Lane *et al.* 2017). This will directly impact on the frequency of flushing at headwater flow intakes and hence the rate of delivery of sediment downstream. It is less clear how long such a change might be sustained. This will depend on glacial cover and catchment hypsometry (e.g. Farinotti *et al.* 2011), and how this decrease may be affected by feedback mechanisms such as debris cover insulation of glacial melt processes (Reznichenko *et al.* 2010; Pellicciotti *et al.* 2014). Over the long term, the contribution of glacial melt will decrease, a transition from glacial and glacio-nival regime will take place, and total flow will decrease (Bavay *et al.* 2013; Braun *et al.* 2017). In fact, in various mountain ranges around the world and at lower elevations, decreased run-off is already observed (Casassa *et al.* 2008; Huss and Hock 2018). The timing of maximum yield, will vary from catchment to catchment but is expected to occur before 2050 for a range of Swiss high-alpine catchments (Farinotti *et al.* 2011). In the second half of the 21<sup>st</sup> century, these changes may lead to a substantial decrease in hydropower production (Schaefli *et al.* 2007; Finger *et al.* 2012). This will also change flushing at flow intakes, but in a complex way, where the rate of delivery depends not only on water availability for transport but also on transfer dynamics and connectivity within the proglacial margin (Lane *et al.* 2017).

### **2.3 Braided river morphodynamics and sediment transfer**

Whilst climate change and hydropower represent key drivers in many Alpine hydrological and geomorphological systems, understanding their impact also needs to consider how the river corridor itself influences the propagation of the affected flow and sediment supply. Along the river course,

decreases in valley slope and/or increases in lateral accommodation space typically lead to reduced transport capacity, deposition and hence changes in river channel pattern. Where upstream forced changes in flow and sediment supply influence channel pattern, these may also feedback into sediment transport capacity as channel pattern affects (the distribution in) energy losses; transport capacity generally increases if channels tend towards single thread but decreases if they tend towards multiple thread. The understanding of depositional environments within Alpine rivers is therefore critical, whether natural or induced by climate change and/or hydropower changes in transport capacity and sediment delivery. For this reason, a major focus of this thesis is braided river morphodynamics, given evidence that suggests that climate change and hydropower impacts do lead to significant sediment deposition (Chapter 4) whilst still maintaining substantial downstream sediment flux (Chapter 5).

Braided rivers have been characterized based on their planform patterns of multiple channels and bars (Lane 1957; Leopold and Wolman 1957). These rivers typically have laterally unconfined river beds and high bed load transport rates (Ferguson 1987; Murray and Paola 1994), which lead to a high river bed morphodynamics. Braided reaches are common in Alpine environments, may occupy wide, glacially shaped, valley bottoms where the ice has recently retreated and vegetation has only sparsely established, limiting bank stabilising effects of vegetation encroachment (Tal and Paola 2010; Murray and Paola 1997). Here, bed load transport is driven by the high stream power (high channel gradients) and high sediment supply rates (with varying grain size), from glacial melt (Lane *et al.* 1996). The combination of a wide active channel, that can store and release large amounts of sediment, and the dynamics of braiding processes, that rework the river bed, allow Alpine braided reaches to play a key role in downstream sediment transfer and dynamics.

Various processes have been described by which braided rivers modify their river bed morphology, most notably central bar development, chute cut-off, lobe dissection and transverse bar conversion (Ashmore 1982, 1991a; Bridge 1993; Ferguson 1993; Wheaton *et al.* 2013). In essence, these all originate from a local instability causing bed aggradation (often by stalling of bed-load sheets) and associated lateral flow expansion (Ashmore 1991a). This leads to adjusted flow and sediment partitioning which propagates downstream through channels and bars that respond correspondingly through morphological adjustments (Ashworth and Ferguson 1986; Goff and Ashmore 1994). Continuous temporal variations in bed load transport (Gomez *et al.* 1989; Ashmore 1991b) and spatial variability in sediment storage takes place on different scales (Hoey 1992), resulting in recurring channel and bar patterns (Hundey and Ashmore 2009) that define braided river morphology. These changes in turn drive the spatio-temporal variation in bedload transport (Ashworth and Ferguson 1986). To understand the internal functioning of these streams, it is critical

to understand how, when, where and at what rates bed load material is transported, and how this feeds back into stream morphology. These questions are explored in Chapter 4.

Bed load transport is typically described by formulas where critical shear stress and grain effects reflect generalised, average conditions. At a smaller scale, the physical processes are much more complicated and not fully understood. Einstein (1937) was one of the first to recognize this and described the transport of individual grains as a probabilistic process. Indeed, due to the inherent interaction of bed load transport with the river bed, grain-scale changes affect flow resistance and turbulence which in turn will affect the critical shear stress to entrain sediment (Kirchner *et al.* 1990). Further, grains in transport also interact amongst each other in terms of grain dislodgement and sustaining transport, particularly in steep channels and sediment-laden flows (Ancy *et al.* 2008, Heyman *et al.* 2013). Various time-dependent feedback mechanisms or 'memory' effects, may originate from sediment deposition and organization at the surface of the river bed which may affect subsequent entrainment. Bed surface stabilization may occur due to erosion (pavement) or even during prolonged periods of inactivity at low flow conditions (Reid *et al.* 1985). This then requires subsequent destabilization before mobilization (Mao *et al.* 2017). Hysteresis effects have been found in flow hydrographs, where reduced mobility of sediments lead to reduced sediment transport rates during the falling limb (Mao 2012). Deposition sequences of graded sediment during the falling limb may also lead to a decrease in bed roughness and critical shear stress (Ferguson *et al.* 1989; Venditti *et al.* 2010) affecting sediment entrainment in a subsequent (high) flow event.

The variability in bed load processes and feedback mechanisms play a key role in forcing and maintaining braided river dynamics. Braiding processes may be maintained under steady state flow and sediment supply conditions (Ashmore 1982, 1991b). Braiding rivers do not necessarily aggrade, although net sediment input to a reach does promote braiding channel reworking (Germanoski and Schumm 1993; Ashworth *et al.* 2004). Cycles of longer term river bed aggradation and degradation have been reported, where phases of deposition involved the agglomeration of bars and an increase in braiding intensity and phases of channel incision led to a decrease braiding intensity and more efficient sediment transfer (Ashmore 1988, 1991b; Hoey and Sutherland, 1991; Lane *et al.* 1996). However, most studies have addressed braiding processes under (simplified) steady-state conditions, rather than looking at how unsteady flow and sediment supply impact upon these processes. Very little is known on how autogenic braiding processes interact with upstream forcing of flow and sediment to drive river bed evolution over the course of decades (e.g. Lane 2009; Zanoni *et al.* 2008). Important questions that remain concern the morphological effects of variations in discharge regime and flood events (Bertoldi *et al.* 2009, 2010), variability and changes in sediment supply (Harvey

1991; Macklin and Lewin 1989; Lane *et al.* 1996) and associated grain size (Chew and Ashmore 2001) and the development of floodplain vegetation (Bertoldi *et al.* 2011; Tal and Paola, 2010; Bätz *et al.* 2016). In this thesis, the question is how flow intake management and changes therein, impact braided river morphodynamics. Flows result from repeated, sediment-laden flushing events and higher magnitude, longer duration floods that are occurring with increased frequency. This increase in frequency is directly related to climate change driven ice melt that lead to the (near) surcharge of hydropower transfer tunnels. Morphological change dynamics and feedback mechanisms on sediment flux associated with these characteristic human-impacted flows are addressed in Chapter 5, providing further insight in the braiding processes that impact longer-term change (Chapter 4).

For the integrated assessment of braided dynamics, techniques and approaches are required that address both the temporal and spatial dynamics. This has been undertaken through controlled flume experiments in the past (e.g. Ashmore 1982), but remains a challenge in field settings due to the large scale and high detail of surveying and the difficulty of addressing the dynamics of specific processes and forcing mechanisms that operate simultaneously. The onset of remote sensing techniques, drone-base Structure from Motion (SfM) photogrammetry (Fonstad *et al.* 2013; Javernick *et al.* 2014) and laser scanning (Heritage and Hetherington 2007) has provided the opportunity to perform such topographic change monitoring. In Antoniazza *et al.* (in revision), we developed and applied a morphological budgeting approach (Ashmore and Church 1998) to determine minimum transport rates to account for spatial changes. We used a 2D sediment routing approach based on hydraulic model simulations and local slope to determine spatial bed load transport rates. Such a hybrid approach allows us to constrain the sediment fluxes based on measured changes as opposed to full 2D hydro-morphological modelling approaches that don't sufficiently capture system memory. This formed an important methodological development that allowed the investigation of braided sediment transport and morphodynamics in response to sequences of flushing events and unregulated floods in Chapter 5.

## References

- Alley, R. B., Cuffey, K. M., Evenson, E. B., Strasser, J. C., Lawson, D. E., Larson, G. J. 1997. How glaciers entrain and transport basal sediment: Physical constraints. *Quaternary Science Reviews* 16(9): 1017-1038. DOI: 10.1016/S0277-3791(97)00034-6.
- Ancey, C., Davison, A. C., Böhm, T., Jodeau, M., Frey, P. 2008. Entrainment and motion of coarse particles in a shallow water stream down a steep slope. *Journal of Fluid Mechanics* 595: 83-114. DOI: 10.1017/S0022112007008774.
- Antoniazza, G., Bakker, M., Lane, S. N. in revision. Revisiting the morphological method in two-dimensions to quantify bed material transport in braided rivers. *Earth Surface Processes and Landforms* Special edition.
- Ashmore, P. E. 1982. Laboratory modelling of gravel braided stream morphology. *Earth Surface Processes and Landforms* 7(3): 201-225.
- Ashmore, P. E. 1988. Bed load transport in braided gravel-bed stream models. *Earth Surface Processes and Landforms* 13(8): 677-695. DOI: 10.1002/esp.3290130803.
- Ashmore, P. E. 1991a. How do gravel-bed rivers braid? *Canadian Journal of Earth Sciences* 28(3): 326-341. DOI: 10.1139/e91-030.
- Ashmore, P. E. 1991b. Channel morphology and bed load pulses in braided, gravel-bed streams. *Geografiska Annaler. Series A. Physical Geography*: 37-52.
- Ashmore, P.E., Church, M. 1998. Sediment transport and river morphology: a paradigm for study. *Water Resources Publications LLC, Highlands Ranch, Colorado*: 115-148.
- Ashworth, P. J., Ferguson, R. I. 1986. Interrelationships of Channel Processes, Changes and Sediments in a Proglacial Braided River. *Geografiska Annaler. Series A, Physical Geography* 68(4): 361-371. DOI: 10.2307/521527.
- Ballantyne, C. K. 2002. A general model of paraglacial landscape response. *The Holocene* 12(3): 371-376. DOI: 10.1191/0959683602hl553fa.
- Barry, R. G. 2006. The status of research on glaciers and global glacier recession: a review. *Progress in Physical Geography: Earth and Environment* 30(3): 285-306. DOI: 10.1191/0309133306pp478ra.
- Bätz, N., Colombini, P., Cherubini, P., Lane, S. N. 2016. Groundwater controls on biogeomorphic succession and river channel morphodynamics. *Journal of Geophysical Research: Earth Surface* 121(10): 1763-1785. DOI: 10.1002/2016JF004009.
- Bavay, M., Grünewald, T., Lehning, M. 2013. Response of snow cover and runoff to climate change in high Alpine catchments of Eastern Switzerland. *Advances in Water Resources* 55: 4-16. DOI: 10.1016/j.advwatres.2012.12.009.

- Begert, M., Frei, C., Abbt, M. 2013. Einführung der Normperiode 1981-2010, MeteoSchweiz.
- Beniston, M., Diaz, H., Bradley, R. 1997. Climatic change at high elevation sites: an overview. *Climatic Change* 36(3-4): 233-251.
- Beniston, M., Farinotti, D., Stoffel, M., Andreassen, L. M., Coppola, E., Eckert, N., Fantini, A., Giacona, F., Hauck, C., Huss, M., Huwald, H., Lehning, M., López-Moreno, J.-I., Magnusson, J., Marty, C., Morán-Tejeda, E., Morin, S., Naaim, M., Provenzale, A., Vincent, C. 2018. The European mountain cryosphere: A review of its current state, trends, and future challenges. *The Cryosphere*. 12: 759-794.
- Beniston, M., Stephenson, D. B., Christensen, O. B., Ferro, C. A. T., Frei, C., Goyette, S., Halsnaes, K., Holt, T., Jylhä, K., Koffi, B., Palutikof, J., Schöll, R., Semmler, T., Woth, K. 2007. Future extreme events in European climate: an exploration of regional climate model projections. *Climatic Change* 81(1): 71-95. DOI: 10.1007/s10584-006-9226-z.
- Beniston, M., Stoffel, M., Hill, M. 2011. Impacts of climatic change on water and natural hazards in the Alps: Can current water governance cope with future challenges? Examples from the European "ACQWA" project. *Environmental Science & Policy* 14(7): 734-743. DOI: 10.1016/j.envsci.2010.12.009.
- Bertoldi, W., Gurnell, A. M., Drake, N. A. 2011. The topographic signature of vegetation development along a braided river: Results of a combined analysis of airborne lidar, color air photographs, and ground measurements. *Water Resources Research* 47(6). DOI: 10.1029/2010WR010319.
- Bertoldi, W., Zanoni, L., Tubino, M. 2009. Planform dynamics of braided streams. *Earth Surface Processes and Landforms* 34(4): 547-557. DOI: 10.1002/esp.1755.
- Bertoldi, W., Zanoni, L., Tubino, M. 2010. Assessment of morphological changes induced by flow and flood pulses in a gravel bed braided river: The Tagliamento River (Italy). *Geomorphology* 114(3): 348-360. DOI: 10.1016/j.geomorph.2009.07.017.
- Bezinge, A., Clark, M., Gurnell, A., & Warburton, J. (1989). The management of sediment transported by glacial melt-water streams and its significance for the estimation of sediment yield. *Annals of Glaciology*, 13, 1–5. DOI: 10.1017/S0260305500007527
- Birsan, M.-V., Molnar, P., Burlando, P., Pfaundler, M. 2005. Streamflow trends in Switzerland. *Journal of Hydrology* 314(1–4): 312-329. DOI: 10.1016/j.jhydrol.2005.06.008.
- Bolch, T., Kulkarni, A., Kääh, A., Huggel, C., Paul, F., Cogley, J. G., Frey, H., Kargel, J. S., Fujita, K., Scheel, M., Bajracharya, S., Stoffel, M. 2012. The State and Fate of Himalayan Glaciers. *Science* 336(6079): 310-314. DOI: 10.1126/science.1215828.
- Braun, L. N., Weber, M., Schulz, M. 2017. Consequences of climate change for runoff from Alpine regions. *Annals of Glaciology* 31: 19-25. DOI: 10.3189/172756400781820165.

- Bridge, J. S. 1993. The interaction between channel geometry, water flow, sediment transport and deposition in braided rivers. Geological Society, London, Special Publications 75(1): 13-71.
- Burki, V., Hansen, L., Fredin, O. L. A., Andersen Thorbjørn, A., Beylich Achim, A., Jaboyedoff, M., Larsen, E., Tønnesen, J.-F. 2010. Little Ice Age advance and retreat sediment budgets for an outlet glacier in western Norway. *Boreas* 39(3): 551-566. DOI: 10.1111/j.1502-3885.2009.00133.x.
- Casassa, G., López, P., Pouyaud, B., Escobar, F. 2008. *Processes* 23(1): 31-41. DOI: 10.1002/hyp.7194.
- Ceppi, P., Scherrer, S. C., Fischer, A. M., Appenzeller, C. 2012. Revisiting Swiss temperature trends 1959–2008. *International Journal of Climatology* 32(2): 203-213. DOI: 10.1002/joc.2260.
- Chen, J., Shi, H., Sivakumar, B., Peart, M. R. 2016. Population, water, food, energy and dams. *Renewable and Sustainable Energy Reviews* 56: 18-28. DOI: 10.1016/j.rser.2015.11.043.
- Church, M., Ryder, J. M. 1972. Paraglacial sedimentation: a consideration of fluvial processes conditioned by glaciation. *Geological Society of America Bulletin* 83(10): 3059-3072.
- Costa, A., Molnar, P., Stutenbecker, L., Bakker, M., Silva, T. A., Schlunegger, F., Lane, S. N., Loizeau, J. L., Girardclos, S. 2018. Temperature signal in suspended sediment export from an Alpine catchment. *Hydrol. Earth Syst. Sci. Discuss.* 2018: 1-30. DOI: 10.5194/hess-22-509-2018.
- Crutzen, P. J. 2006. *The “anthropocene”*, Springer.
- Cuffey, K., Alley, R. B. 1996. Is erosion by deforming subglacial sediments significant? (Toward till continuity). *Annals of Glaciology* 22: 17-24. DOI: 10.3189/1996AoG22-1-17-24.
- Dalmasso, A. 2008. Dams and Development in the French Alps in the Inter-war Period. *Journal of Alpine Research* 96(1): 55-66.
- Dansgaard, W., Johnsen, S., Clausen, H., Dahl-Jensen, D., Gundestrup, N., Hammer, C., Hvidberg, C., Steffensen, J., Sveinbjörnsdottir, A., Jouzel, J. 1993. Evidence for general instability of past climate from a 250-kyr ice-core record. *Nature* 364(6434): 218.
- Einstein, HA. 1937. Bedload transport as a probability problem. *Sedimentation* (reprinted in 1972). Water Resources Publications, Colorado: 105-108.
- Farinotti, D., Usselman, S., Huss, M., Bauder, A., Funk, M. 2011. Runoff evolution in the Swiss Alps: projections for selected high-alpine catchments based on ENSEMBLES scenarios. *Hydrological Processes* 26(13): 1909-1924. DOI: 10.1002/hyp.8276.
- Fergus, T. 1997. Geomorphological response of a river regulated for hydropower: River Fortun, Norway. *Regulated Rivers: Research & Management* 13(5): 449-461. DOI: 10.1002/(SICI)1099-1646(199709/10)13:5<449::AID-RRR468>3.0.CO;2-#.

- Ferguson, R. 1987. Hydraulic and sedimentary controls of channel pattern. *River channels: Environments and processes*: 129-158.
- Ferguson, R. I., Prestegard, K. L., Ashworth, P. J. 1989. Influence of sand on hydraulics and gravel transport in a braided gravel bed river. *Water Resources Research* 25(4): 635-643. DOI: 10.1029/WR025i004p00635.
- Finger, D., Heinrich, G., Gobiet, A., Bauder, A. 2012. Projections of future water resources and their uncertainty in a glacierized catchment in the Swiss Alps and the subsequent effects on hydropower production during the 21st century. *Water Resources Research* 48(2). DOI: 10.1029/2011WR010733.
- Fischer, M., Huss, M., Barboux, C., Hoelzle, M. 2014. The New Swiss Glacier Inventory SGI2010: Relevance of Using High-Resolution Source Data in Areas Dominated by Very Small Glaciers. *Arctic, Antarctic, and Alpine Research* 46(4): 933-945. DOI: 10.1657/1938-4246-46.4.933.
- Fonstad, M. A., Dietrich, J. T., Courville, B. C., Jensen, J. L., Carbonneau, P. E. 2013. Topographic structure from motion: a new development in photogrammetric measurement. *Earth Surface Processes and Landforms* 38(4): 421-430. DOI: 10.1002/esp.3366.
- Friedman, A. R., Hwang, Y.-T., Chiang, J. C. H., Frierson, D. M. W. 2013. Interhemispheric Temperature Asymmetry over the Twentieth Century and in Future Projections. *Journal of Climate* 26(15): 5419-5433. DOI: 10.1175/jcli-d-12-00525.1.
- Gabbud, C., Lane, S. N. 2016. Ecosystem impacts of Alpine water intakes for hydropower: the challenge of sediment management. *Wiley Interdisciplinary Reviews: Water* 3(1): 41-61. DOI: 10.1002/wat2.1124.
- Germanoski, D., Schumm, S. 1993. Changes in braided river morphology resulting from aggradation and degradation. *The Journal of Geology* 101(4): 451-466.
- Giorgi, F., Hurrell, J. W., Marinucci, M. R., Beniston, M. 1997. Elevation Dependency of the Surface Climate Change Signal: A Model Study. *Journal of Climate* 10(2): 288-296. DOI: 10.1175/1520-0442(1997)010<0288:EDOTSC>2.0.CO;2.
- Giorgi, F., Torma, C., Coppola, E., Ban, N., Schar, C., Somot, S. 2016. Enhanced summer convective rainfall at Alpine high elevations in response to climate warming. *Nature Geosci* advance online publication. DOI: 10.1038/ngeo2761
- Glaciological Reports. (1881-2017). "The Swiss Glaciers," Yearbooks of the Cryospheric Commission of the Swiss Academy of Sciences (SCNAT). Retrieved from <http://www.glamos.ch>
- Gobiet, A., Kotlarski, S., Beniston, M., Heinrich, G., Rajczak, J., Stoffel, M. 2014. 21st century climate change in the European Alps—A review. *Science of The Total Environment* 493: 1138-1151. DOI: 10.1016/j.scitotenv.2013.07.050.

- Goff, J. R., Ashmore, P. 1994. Gravel transport and morphological change in braided Sunwapta River, Alberta, Canada. *Earth Surface Processes and Landforms* 19(3): 195-212.
- Gomez, B., Naff, R. L., Hubbell, D. W. 1989. Temporal variations in bedload transport rates associated with the migration of bedforms. *Earth Surface Processes and Landforms* 14(2): 135-156.
- Gurnell, A. 1983. Downstream channel adjustments in response to water abstraction for hydro-electric power generation from alpine glacial melt-water streams. *The Geographical Journal* 149(3): 342-354. DOI: 10.2307/634009.
- Haeberli, W., Beniston, M. 1998. Climate change and its impacts on glaciers and permafrost in the Alps. *Ambio*: 258-265.
- Haeberli, W., Hoelzle, M., Paul, F., Zemp, M. 2007. Integrated monitoring of mountain glaciers as key indicators of global climate change: the European Alps. *Annals of Glaciology* 46(1): 150-160. DOI: 10.3189/172756407782871512.
- Halleraker, J., van de Bund, W., Bussettini, M., Gosling, R., Döbbelt-Grüne, S., Hensman, J., Kling, J., Koller-Kreimel, V., Pollard, P. 2016. Working Group ECOSTAT report on Common understanding of using mitigation measures for reaching Good Ecological Potential for heavily modified water bodies.
- Harbor, J., Warburton, J. 1993. Relative rates of glacial and nonglacial erosion in Alpine environments. *Arctic and Alpine Research*, 25(1), 1–7. DOI: 10.2307/1551473
- Harvey, A. M. 1991. The influence of sediment supply on the channel morphology of upland streams: Howgill Fells, Northwest England. *Earth Surface Processes and Landforms* 16(7): 675-684. DOI: 10.1002/esp.3290160711.
- Heritage, G., Hetherington, D. 2007. Towards a protocol for laser scanning in fluvial geomorphology. *Earth Surface Processes and Landforms* 32(1): 66-74. DOI: 10.1002/esp.1375.
- Herman, F., Seward, D., Valla, P. G., Carter, A., Kohn, B., Willett, S. D., Ehlers, T. A. 2013. Worldwide acceleration of mountain erosion under a cooling climate. *Nature* 504: 423. DOI: 10.1038/nature12877.
- Heyman, J., Mettra, F., Ma, H. B., Ancey, C. 2013. Statistics of bedload transport over steep slopes: Separation of time scales and collective motion. *Geophysical Research Letters* 40(1): 128-133. DOI: 10.1029/2012GL054280.
- Hinderer, M., Kastowski, M., Kamelger, A., Bartolini, C., Schlunegger, F. 2013. River loads and modern denudation of the Alps — A review. *Earth-Science Reviews* 118(0): 11-44. DOI: 10.1016/j.earscirev.2013.01.001.

- Hoelzle, M., Haeberli, W., Dischl, M., Peschke, W. 2003. Secular glacier mass balances derived from cumulative glacier length changes. *Global and Planetary Change* 36(4): 295-306. DOI: 10.1016/S0921-8181(02)00223-0.
- Hoey, T. 1992. Temporal variations in bedload transport rates and sediment storage in gravel-bed rivers. *Progress in Physical Geography: Earth and Environment* 16(3): 319-338. DOI: 10.1177/030913339201600303.
- Hoey, T. B., Sutherland, A. J. 1991. Channel morphology and bedload pulses in braided rivers: a laboratory study. *Earth Surface Processes and Landforms* 16(5): 447-462. DOI: 10.1002/esp.3290160506
- Holzhauser, H., Magny, M., Zumbuühl, H. J. 2005. Glacier and lake-level variations in west-central Europe over the last 3500 years. *The Holocene* 15(6): 789-801. DOI: 10.1191/0959683605hl853ra.
- Hundey, E. J., Ashmore, P. E. 2009. Length scale of braided river morphology. *Water Resources Research* 45(8). DOI: 10.1029/2008WR007521.
- Huss, M., Hock, R. 2018. Global-scale hydrological response to future glacier mass loss. *Nature Climate Change* 8(2): 135-140. DOI: 10.1038/s41558-017-0049-x.
- Javernick, L., Brasington, J., Caruso, B. 2014. Modeling the topography of shallow braided rivers using Structure-from-Motion photogrammetry. *Geomorphology* 213: 166-182. DOI: 10.1016/j.geomorph.2014.01.006.
- Karlén, W. 1976. Lacustrine Sediments and Tree-Limit Variations as Indicators of Holocene Climatic Fluctuations in Lappland, Northern Sweden. *Geografiska Annaler: Series A, Physical Geography* 58(1-2): 1-34. DOI: 10.1080/04353676.1976.11879921.
- Kirchner, J. W., Dietrich, W. E., Iseya, F., Ikeda, H. 1990. The variability of critical shear stress, friction angle, and grain protrusion in water-worked sediments. *Sedimentology* 37(4): 647-672. DOI: 10.1111/j.1365-3091.1990.tb00627.x.
- Knight, J., Harrison, S. 2013. The impacts of climate change on terrestrial Earth surface systems. *Nature Clim. Change* 3(1): 24-29.
- Knight, J., Harrison, S. 2014. Mountain glacial and paraglacial environments under global climate change: lessons from the past, future directions and policy implications. *Geografiska Annaler: Series A, Physical Geography* 96(3): 245-264. DOI: 10.1111/geoa.12051.
- Klein, G., Vitasse, Y., Rixen, C., Marty, C., Rebetez, M. 2016. Shorter snow cover duration since 1970 in the Swiss Alps due to earlier snowmelt more than to later snow onset. *Climatic Change* 139(3): 637-649. DOI: 10.1007/s10584-016-1806-y.

- Lambiel, C., Maillard, B., Kummert, M., Reynard, E. 2016. Geomorphology of the Hérens valley (Swiss Alps). *Journal of Maps* 12(1): 160-172.
- Lane, E. W. 1957. A study of the shape of channels formed by natural streams flowing in erodible material. MRD sediment series; no. 9.
- Lane, S. N. 2009. Approaching the system-scale understanding of braided river behaviour. In *Braided Rivers* (eds I. Jarvis, G. H. Sambrook Smith, J. L. Best, C. S. Bristow and G. E. Petts), Blackwell Publishing Ltd.: 107-135.
- Lane, S. N., Bakker, M., Balin, D., Lovis, B., Regamey, B. 2014. Climate and human forcing of Alpine river flow. In *River Flow 2014*. Schleiss, A. J., de Cesare, G., Franca, M. J., Pfister, M. (eds): 7-15.
- Lane, S. N., Bakker, M., Gabbud, C., Micheletti, N., Saugy, J.-N. 2017. Sediment export, transient landscape response and catchment-scale connectivity following rapid climate warming and Alpine glacier recession. *Geomorphology* 277: 210-227. DOI: 10.1016/j.geomorph.2016.02.015.
- Lane, S. N., Richards, K. S., Chandler, J. H. 1996. Discharge and sediment supply controls on erosion and deposition in a dynamic alluvial channel. *Geomorphology* 15(1): 1-15. DOI: 10.1016/0169-555X(95)00113-J.
- Leemann, A., Niessen, F. 1994. Holocene glacial activity and climatic variations in the Swiss Alps: reconstructing a continuous record from proglacial lake sediments. *The Holocene* 4(3): 259-268. DOI: 10.1177/095968369400400305.
- Leopold, L. B., Wolman, M. G. 1957. River channel patterns: Braided, meandering, and straight. Professional Paper. Washington, D.C.: 50.
- Macklin, M. G., Lewin, J. 1989. Sediment transfer and transformation of an alluvial valley floor: The river South Tyne, Northumbria, U.K. *Earth Surface Processes and Landforms* 14(3): 233-246. DOI: 10.1002/esp.3290140305.
- Mao, L. 2012. The effect of hydrographs on bed load transport and bed sediment spatial arrangement. *Journal of Geophysical Research: Earth Surface* 117(F3). DOI: 10.1029/2012JF002428.
- Mao, L., Dell'Agnese, A., Comiti, F. 2017. Sediment motion and velocity in a glacier-fed stream. *Geomorphology* 291: 69-79. DOI: 10.1016/j.geomorph.2016.09.008.
- Margot, A., Schädler, B., Sigg, R., Weingartner, R. 1992. Influence on rivers by water power stations (> 300 kW) and the lake control. *Hydrological Atlas of Switzerland*. Plate 5.
- Marnezy, A. 2008. Alpine dams. From hydroelectric power to artificial snow. *Journal of Alpine Research | Revue de Géographie Alpine* (96-1): 103-112.

- Micheletti, N., Lambiel, C., Lane, S. N. 2015. Investigating decadal-scale geomorphic dynamics in an alpine mountain setting. *Journal of Geophysical Research: Earth Surface* 120(10): 2155-2175. DOI: 10.1002/2015JF003656.
- Micheletti, N., Lane, S. N. 2016. Water yield and sediment export in small, partially glaciated Alpine watersheds in a warming climate. *Water Resources Research* 52(6): 4924-4943. DOI: 10.1002/2016WR018774.
- Molnar, P., Burlando, P., Pellicciotti, F. 2011. Streamflow trends in mountainous regions. *Encyclopedia of Snow, Ice and Glaciers*: 1084-1089.
- Moore, R. D., Fleming, S. W., Menounos, B., Wheate, R., Fountain, A., Stahl, K., Holm, K., Jakob, M. 2008. Glacier change in western North America: influences on hydrology, geomorphic hazards and water quality. *Hydrological Processes* 23(1): 42-61. DOI: 10.1002/hyp.7162.
- Mountain Research Initiative, E. D. W. W. G. 2015. Elevation-dependent warming in mountain regions of the world. *Nature Climate Change* 5: 424. DOI: 10.1038/nclimate2563
- Murray, A. B., Paola, C. 1994. A cellular model of braided rivers. *Nature* 371: 54. DOI: 10.1038/371054a0.
- Nicholas, A., Ashworth, P., Kirkby, M., Macklin, M., Murray, T. 1995. Sediment slugs: large-scale fluctuations in fluvial sediment transport rates and storage volumes. *Progress in physical geography* 19(4): 500-519.
- Nogués-Bravo, D., Araújo, M. B., Errea, M. P., Martínez-Rica, J. P. 2007. Exposure of global mountain systems to climate warming during the 21st Century. *Global Environmental Change* 17(3): 420-428. DOI: 10.1016/j.gloenvcha.2006.11.007.
- Park, C. (1980). The Grande Dixence hydro-electric scheme, Switzerland. *Geography*, 65, 317–320.
- Paul, F., Kääb, A., Haeberli, W. 2007. Recent glacier changes in the Alps observed by satellite: Consequences for future monitoring strategies. *Global and Planetary Change* 56(1): 111-122. DOI: 10.1016/j.gloplacha.2006.07.007.
- Pellicciotti, F., Carenzo, M., Bordoy, R., Stoffel, M. 2014. Changes in glaciers in the Swiss Alps and impact on basin hydrology: Current state of the art and future research. *Science of The Total Environment* 493: 1152-1170. DOI : 10.1016/j.scitotenv.2014.04.022.
- Pepin, N., Bradley, R., Diaz, H., Baraër, M., Caceres, E., Forsythe, N., Fowler, H., Greenwood, G., Hashmi, M., Liu, X. 2015. Elevation-dependent warming in mountain regions of the world. *Nature Climate Change* 5(5): 424.

- Petit, J.-R., Jouzel, J., Raynaud, D., Barkov, N. I., Barnola, J.-M., Basile, I., Bender, M., Chappellaz, J., Davis, M., Delaygue, G. 1999. Climate and atmospheric history of the past 420,000 years from the Vostok ice core, Antarctica. *Nature* 399(6735): 429.
- Petts, G. E., Bickerton, M. A. 1994. Influence of water abstraction on the macroinvertebrate community gradient within a glacial stream system: La Borgne d'Arolla, Valais, Switzerland. *Freshwater Biology* 32(2): 375-386. DOI: 10.1111/j.1365-2427.1994.tb01133.x.
- Petts, G. E., Gurnell, A. M. 2005. Dams and geomorphology: research progress and future directions. *Geomorphology* 71(1): 27-47.
- Rabatel, A., Francou, B., Soruco, A., Gomez, J., Cáceres, B., Ceballos, J. L., Basantes, R., Vuille, M., Sicart, J.-E., Huggel, C., Scheel, M., Lejeune, Y., Arnaud, Y., Collet, M., Condom, T., Consoli, G., Favier, V., Jomelli, V., Galarraga, R., Ginot, P., Maisincho, L., Mendoza, J., Menegoz, M., RAMÍREZ, E., Ribstein, P., Suarez, W., Villacis, M., Wagnon, P. 2013. Current state of glaciers in the tropical Andes: a multi-century perspective on glacier evolution and climate change. *The Cryosphere* 7(1): 81-102. DOI: 10.5194/tc-7-81-2013.
- Rangwala, I., Miller, J. R. 2012. Climate change in mountains: a review of elevation-dependent warming and its possible causes. *Climatic Change* 114(3): 527-547. DOI: 10.1007/s10584-012-0419-3.
- Raymond Pralong, M., Turowski, J. M., Rickenmann, D., Zappa, M. 2015. Climate change impacts on bedload transport in alpine drainage basins with hydropower exploitation. *Earth Surface Processes and Landforms* 40(12): 1587-1599. DOI: 10.1002/esp.3737.
- Rebetez, M., Reinhard, M. 2008. Monthly air temperature trends in Switzerland 1901–2000 and 1975–2004. *Theoretical and Applied Climatology* 91(1): 27-34. DOI: 10.1007/s00704-007-0296-2.
- Reid, I., Frostick, L. E., Layman, J. T. 1985. The incidence and nature of bedload transport during flood flows in coarse-grained alluvial channels. *Earth Surface Processes and Landforms* 10(1): 33-44. DOI: 10.1002/esp.3290100107.
- REN21 2018. Renewables 2018 Global Status Report. Retrieved July, 2018, from [http://www.ren21.net/wp-content/uploads/2018/06/17-8652\\_GSR2018\\_FullReport\\_web\\_final\\_.pdf](http://www.ren21.net/wp-content/uploads/2018/06/17-8652_GSR2018_FullReport_web_final_.pdf).
- Reznichenko, N., Davies, T., Shulmeister, J., McSaveney, M. 2010. Effects of debris on ice-surface melting rates: an experimental study. *Journal of Glaciology* 56(197): 384-394.
- Schaepli, B., Hingray, B., Musy, A. 2007. Climate change and hydropower production in the Swiss Alps: quantification of potential impacts and related modelling uncertainties. *Hydrology and Earth System Sciences Discussions* 11(3): 1191-1205.

- Schar, C., Vidale, P. L., Luthi, D., Frei, C., Haberli, C., Liniger, M. A., Appenzeller, C. 2004. The role of increasing temperature variability in European summer heatwaves. *Nature* 427(6972): 332-336.
- Serquet, G., Marty, C., Dulex, J. P., Rebetez, M. 2011. Seasonal trends and temperature dependence of the snowfall/precipitation-day ratio in Switzerland. *Geophysical research letters* 38(7).
- Spänhoff, B. 2014. Current status and future prospects of hydropower in Saxony (Germany) compared to trends in Germany, the European Union and the World. *Renewable and Sustainable Energy Reviews* 30: 518-525. DOI: 10.1016/j.rser.2013.10.035.
- Stocker, T. 2014. *Climate change 2013: the physical science basis: Working Group I contribution to the Fifth assessment report of the Intergovernmental Panel on Climate Change*, Cambridge University Press.
- Schwab, M., Rieke-Zapp, D., Schneider, H., Liniger, M., Schlunegger, F. 2008. Landsliding and sediment flux in the Central Swiss Alps: A photogrammetric study of the Schimbrig landslide, Entlebuch. *Geomorphology* 97(3-4): 392-406. DOI: 10.1016/j.geomorph.2007.08.019.
- Syvitski, J. P., Vörösmarty, C. J., Kettner, A. J., Green, P. 2005. Impact of humans on the flux of terrestrial sediment to the global coastal ocean. *Science* 308(5720): 376-380.
- Tal, M., Paola, C. 2010. Effects of vegetation on channel morphodynamics: results and insights from laboratory experiments. *Earth Surface Processes and Landforms* 35(9): 1014-1028. DOI:10.1002/esp.1908.
- Tschada, H., Hofer, B. 1990. Total solids load from the catchment area of the Kaunertal hydroelectric power station: the results of 25 years of operation.
- Turowski, J. M., Rickenmann, D. 2009. Tools and cover effects in bedload transport observations in the Pitzbach, Austria. *Earth Surface Processes and Landforms* 34(1): 26-37. DOI: 10.1002/esp.1686.
- Venditti, J. G., Dietrich, W. E., Nelson, P. A., Wyzga, M. A., Fadde, J., Sklar, L. 2010. Mobilization of coarse surface layers in gravel-bedded rivers by finer gravel bed load. *Water Resources Research* 46(7): W07506. DOI: 10.1029/2009WR008329.
- Wheaton, J. M., Brasington, J., Darby, S. E., Kasprak, A., Sear, D., Vericat, D. 2013. Morphodynamic signatures of braiding mechanisms as expressed through change in sediment storage in a gravel-bed river. *Journal of Geophysical Research: Earth Surface* 118(2): 759-779. DOI: 10.1002/jgrf.20060.
- Widmann, M., Schär, C. 1998. A principal component and long-term trend analysis of daily precipitation in Switzerland. *International Journal of Climatology* 17(12): 1333-1356. DOI: 10.1002/(SICI)1097-0088(199710)17:12<1333::AID-JOC108>3.0.CO;2-Q.

- Williams, G. P., Wolman, M. G. 1984. Downstream effects of dams on alluvial rivers, US Government Printing Office Washington, DC.
- Wold, B., & Østrem, G. (1979). Morphological activity of a diverted glacier stream in Western Norway. *GeoJournal*, 3(4), 345–349.
- Zanoni, L., Gurnell, A., Drake, N., Surian, N. 2008. Island dynamics in a braided river from analysis of historical maps and air photographs. *River Research and Applications* 24(8): 1141-1159. DOI: 10.1002/rra.1086.
- Zimmermann, M. 2001. Energy situation and policy in Switzerland. *International journal of ambient energy* 22(1): 29-34.

### **3. ARTICLE 1: ARCHIVAL PHOTOGRAMMETRIC ANALYSIS OF RIVER–FLOODPLAIN SYSTEMS USING STRUCTURE FROM MOTION (SfM) METHODS**

This chapter, by Bakker, M. and Lane, S.N., has been published in *Earth Surface Processes and Landforms* 42(8).

#### *Abstract*

In this study we evaluate the extent to which accurate topographic data can be obtained by applying Structure from Motion (SfM) photogrammetric methods to archival imagery. While SfM has proven valuable in photogrammetric applications using specially acquired imagery (e.g. from unmanned aerial vehicles), it also has the potential to improve the precision of topographic data and the ease with which can be produced from historical imagery. We evaluate the application of SfM to a relatively extreme case, one of low relative relief: a braided river–floodplain system. We compared the bundle adjustments of SfM and classical photogrammetric methods, applied to eight dates. The SfM approach resulted in data quality similar to the classical approach, although the lens parameter values (e.g. focal length) recovered in the SfM process were not necessarily the same as their calibrated equivalents. Analysis showed that image texture and image overlap/configuration were critical drivers in the tie-point generation which impacted bundle adjustment quality. Working with archival imagery also illustrated the general need for the thorough understanding and careful application of (commercial) SfM software packages. As with classical methods, the propagation of (random) error in the estimation of lens and exterior orientation parameters using SfM methods may lead to inherent systematic error in the derived point clouds. We have shown that linear errors may be accounted for by point cloud registration based on a reference dataset, which is vital for the further application in quantitative morphological analyses when using archival imagery.

#### **3.1 Introduction**

Photogrammetry is a well-established technique that has been used to quantify morphologic change for many decades (Chandler and Moore, 1989; Lane *et al.*, 1993, 2000). In river–floodplain systems it has been applied to the investigation and monitoring of morphological change and sediment transport (Heritage *et al.*, 1998; Chandler *et al.*, 2002; Brasington *et al.*, 2003; Lane *et al.*, 2010; Wheaton *et al.*, 2010, 2013), river bank erosion (Barker *et al.*, 1997; Pyle *et al.*, 1997; De Rose and Basher, 2011), flood risk assessment (Sanyal and Lu 2004; Saint-Geours *et al.*, 2015), river restoration and ecology (Gilvear *et al.*, 1995; Kondolf and Larson, 1995; Pasquale *et al.*, 2011; Dietrich, 2016), and archaeology (Pérez Álvarez *et al.*, 2013). For the investigation of morphological change, particularly in braided river systems, a thorough theoretical and practical basis has been developed,

including the assessment of error and uncertainties (Lane *et al.*, 2003, 2004; Westaway *et al.*, 2003; Wheaton *et al.*, 2010).

The application of archival photogrammetry for the investigation of historical river evolution has been limited to a few studies, typically at the annual scale (Lane *et al.*, 2010; Wheaton *et al.*, 2010, 2013). Critical for such application is the scale and frequency of available imagery which determine the potential for detecting and quantifying morphological change (Gilvear and Bryant, 2005). First, observed changes in river–floodplain systems are typically of the order of decimetres to meters, close to the limits of detection as predefined by image scale (Lane *et al.*, 2010). This makes error identification and correction particularly important (Lane *et al.*, 2004) and calls for cautious error propagation that is not overly conservative in terms of rejecting small magnitude but spatially coherent changes (Wheaton *et al.*, 2010). Second, as the time between available surveys increases, so does the probability of intervening erosion and deposition, which may significantly affect the cumulative volumes of change detected (Lane *et al.*, 1994).

Most recently, Structure from Motion (SfM) photogrammetry (Snavely, 2008; Westoby *et al.*, 2012; Smith *et al.*, 2015) has been advocated as allowing a more efficient generation of precise and high-density point cloud data as shown for river bed geomorphology (Fonstad *et al.*, 2013; Javernick *et al.*, 2014). SfM methods also have appeal because they use computer vision techniques to assist with the interior and exterior orientation of imagery: (a) substantially reducing the need for user involvement, and so further automating the photogrammetric process; and (b) using much more of the information contained within the imagery to aid the orientation process so, in theory, improving the quality of the analysis. This approach may therefore unlock large historical photogrammetric archives for morphologic analysis. However, the algorithms upon which the SfM software is based are often undisclosed, particularly in commercial packages, and vary in the ability of the user to assess and control the estimation of exterior orientation parameters compared with classical methods (Smith *et al.*, 2015; Eltner *et al.*, 2016), particularly concerning lens modelling (James and Robson, 2014; Eltner and Schneider, 2015). This is particularly relevant because Lane *et al.*, (2004) showed that random error in estimated exterior orientation parameters can propagate into systematic error in a DEM, which may be in the order of decimeters or more. Such errors become apparent for the DEMs of Differences (DoDs) of river–floodplain systems where detected changes are small and a tilt or banding effect may appear (Stojic *et al.*, 1998; Westaway *et al.*, 2003; Lane *et al.*, 2004). Systematic errors may be even larger when exterior orientation parameters are not reliably estimated due to poorly distributed Ground Control Points (GCPs) (James and Robson, 2012; Bertin *et al.*, 2015; Honkavaara *et al.*, 2016). Thus, systematic errors resulting from photogrammetric reconstruction

may have substantial impacts upon estimates of volume change and subsequent geomorphic interpretation.

The aim of this paper is to evaluate the application of SfM methods to archival imagery, specifically for the quantification of morphological change at the decadal scale in a river–floodplain system, so as to identify wider lessons for the application of these methods in geomorphic studies in general. We do this in three ways. First, we evaluate SfM bundle adjustment results and compare these with classical photogrammetric and camera calibration data. Second, we identify the controls on the (potential) quality of SfM results to assist in the identification of suitable archival imagery. Third, we address systematic errors that are inherent to both the classical and SfM photogrammetric approach and illustrate their potential impact on morphological interpretation if they are not adequately treated. This work is undertaken using a case-study: a braided river section of the Borgne d'Arolla in south-west Switzerland.

## **3.2 Methods**

### 3.2.1 Overview

The methodological approach is based on the application of SfM photogrammetry to archival river imagery and subsequent evaluation of the bundle adjustment parameters through comparison with classical photogrammetry and available camera calibration data. We used Pix4D, a commercially-available software package, for a ground control point (GCP) assisted bundle adjustment and georeferencing of scanned historical images. This resulted in eight topographic datasets spanning the period 1959–2005. The focus of the subsequent analysis was threefold. First, we evaluated the accuracy of the bundle adjustment and compared: (a) the SfM-estimated exterior orientation parameters with values derived using a classical photogrammetric approach; and (b) SfM-estimated lens parameters with the parameter values in the associated camera calibration certificates. Second, we assessed image acquisition properties (e.g. image texture, overlap) that affect the (potential) quality of the SfM bundle adjustment and the resulting point cloud precision and accuracy. Third, we considered the extent and nature of residual systematic errors in the photogrammetrically-generated point clouds and minimized these by means of registering stable zones to a reference dataset.

### 3.2.2 Case study: Borgne d'Arolla

The Borgne d'Arolla is a tributary of the Upper Rhône draining the Pennine Alps in south-west Switzerland. Under normal flow conditions, all water is abstracted by intakes at the tributary headwaters for the generation of hydropower (Gurnell, 1983; Bezinge *et al.*, 1989). This enables the application of photogrammetry on a more or less dry riverbed in the upstream reaches, without

requiring correction procedures associated with under water topography (Westaway *et al.*, 2001; Lane *et al.*, 2010). This study is motivated by the aim of using archival photogrammetry to study the morphological evolution of four braided river reaches (Figure 3-1; for the purpose here, we will refer to reaches C and D as the combined reach CD) since the onset of hydropower exploitation in the early 1960s.

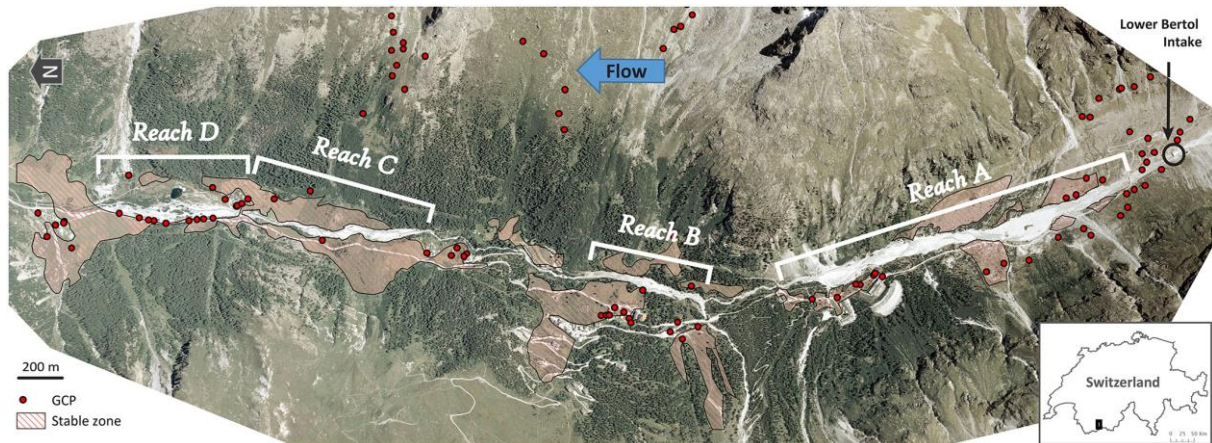


Figure 3-1 Orthoimage from 2005 giving an overview of the sedimentation reaches in the Borgne d'Arolla River, Switzerland. GCPs and stable zones used for referencing and registration are shown.

### 3.2.3 Archival aerial photographs

Historical aerial photographs were acquired from the Federal Office of Topography (SwissTopo) for the period 1959–2005 (Table 3-1). The images are black and white with the exception of 1999 and 2005 which are in colour. The image scale is in the range 1:19000 to 1:27000 and they were scanned at a resolution of 14 or 21  $\mu\text{m}$  by SwissTopo (original images were not available for higher resolution scanning). The images were acquired with large format photogrammetric cameras, which came with camera calibration certificates (available online: <http://www.swisstopo.admin.ch>), and camera position data was available for images from 1983, 1995, 1999 and 2005. In addition to these images, an aerial lidar-based 2 m resolution DEM (ALTI3D), filtered for vegetation and buildings, was available from SwissTopo for the year 2010.

As archival imagery can be of variable quality and can be acquired using different image configurations, we aimed to characterize these using two (derived) properties (Table 3-1). First, we determined the texture of the resulting orthoimage using an entropy measure:

$$e = \sum_{i=1}^I p(i) \log_2 p(i) \quad [1]$$

where  $I$  is the number of intensity levels on an 8 bit grey-scale image; and  $p(i)$  is the probability density function of the image intensity (Gonzalez *et al.*, 2003). The calculation of  $e$  was restricted to the river reaches and a 150 m buffer around them. Second, we determined the extent of image overlap as the fraction of the stereo-matched area (minimum of 2–3 overlapping images required) with respect to the total available image area. We assess the effects of these image acquisition properties on the bundle adjustment quality.

Year	Images	Scale [1 :x]	Resolution [ $\mu\text{m}$ ]	Texture (entropy)	Overlap [%]
1959	10	23200	21	3.39	15%
1965	6	21200	21	2.52	13%
1977	8	19600	14	3.47	30%
1983	12	19600	14	3.52	22%
1988	9	20900	14	3.59	19%
1995	8	26800	14	3.42	21%
1999	6	27000	14	3.27	17%
2005	3	24700	14	3.21	12%

Table 3-1 Overview and characteristics of historical aerial photographs.

### 3.2.4 Ground control

Ground control points (GCPs) of fixed objects, houses, boulders, etc. were surveyed with dGPS (Micheletti *et al.*, 2015) along the bottom and eastern side of the valley (Figure 3-1). Although they cover the region of interest, they are not ideally distributed over the extent of the photographs used. Owing to the difficulty in identifying stable points over the studied time period, GCPs are scarce in steeper terrain that is either heavily vegetated or unstable. As part of the methodology, additional zones were sought that were likely to be stable during the study period, i.e. without vegetation and human impacts (Figure 3-1). These were selected along the valley bottom and manually digitized based on orthoimages, where an optimal trade-off was sought between surface area, distribution and presumed stability.

### 3.2.5 Photogrammetric analysis

Photogrammetric data analysis of the sets of historical images (Table 3-1) drew upon two different sets of methods. As a starting point we use analyses conducted by Regamey (2013) with the classical photogrammetric ERDAS Imagine Leica Photogrammetry Suite (LPS) 2010. Classical airborne photogrammetry typically proceeds by: (1) image delineation and reconstituting lens parameters, aided by camera calibration certificates; (2) using initial estimates of (relative) camera position and orientation, GCPs and automatically generated tie-points between overlapping images to estimate the position and orientation of the camera during image acquisition: the bundle adjustment; and (3) applying stereo-matching to extract 3D point clouds. A detailed account on the application of this procedure in an Alpine landscape, including applied triangulation parameters/constraints and

automatic terrain extraction (ATE) correlation parameters, is given by (Micheletti *et al.*, 2015). We compare the bundle adjustment results with the SfM-based photogrammetric approach applied in this study.

SfM has become a well-established method in geomorphology that refers to a wide range of computer vision techniques, which have been applied to photogrammetry (see Smith *et al.*, 2015 for review). Here, we use the software Pix4D that has been previously been applied in geomorphological studies by Castillo *et al.* (2014) and Eltner *et al.* (2015). The basic difference with classical photogrammetry is that the analysis commences with the application of automatic stereo-matching algorithms using computer vision techniques to an unstructured set of images. This forms the basis for bundle adjustment, hence (largely) automating steps 1 and 2 in the classical photogrammetric approach described above. This process provides a large dataset of tie-points and this redundancy in theory eliminates the need and dependency on a priori specified: (a) image extent, in the form of fiducial marks; and (b) lens parameters, i.e. focal length, principle point of autocollimation and distortion (Vallet *et al.*, 2011; Aguilar *et al.*, 2013); in the determination of (c) exterior orientation parameters (Küng *et al.*, 2011). SfM typically doesn't require or even support the input of GCPs, although they may be used to aid the determination of exterior orientation parameters a priori, or to scale, to rotate and to translate the resulting point clouds a posteriori (Javernick *et al.*, 2014; Nebiker *et al.*, 2014). While early geomorphological application of SfM was hailed as freeing the user from the required expertise and time associated with classical photogrammetry (Fonstad *et al.*, 2013), subsequent research indicates that most if not all of the well-established photogrammetric controls on data quality remain. Among others, Wackrow *et al.* (2007), Wackrow and Chandler (2008) and James and Robson (2014) showed that non-linear systematic errors may occur where self-calibration algorithms, on which SfM applications rely, are limited in resolving lens distortion, particularly for near-nadir acquired imagery typical in archival photogrammetry. This may be minimized through the use of GCPs in the bundle adjustment (Eltner and Schneider, 2015), which is possible in Pix4D and for which purpose we used all GCPs in this study.

We used the original scanned aerial photographs in Pix4D v2.0 with large-frame extension. There was no need to downscale for processing time (Westoby *et al.*, 2012; Caduff and Rieke-Zapp, 2014) or to perform preliminary masking of the instrument strip and edges (Gomez *et al.*, 2015). Although Pix4D allows the a priori specification of interior orientation parameters, we chose to specify only the initial (calibrated) focal length and allowed the use of self-calibration for the optimization of the bundle adjustment (note that in some SfM packages camera parameters may not be specified and self-calibration is applied automatically). This reflects the often-expressed rationale of SfM (Fonstad *et al.*, 2013) that it facilitates the use of uncalibrated cameras or ones where lens parameters are not

known. Then, we assessed the potential limitations of SfM-based camera self-calibration with archival imagery by using the measured distortion in the calibration certificate and the statistical fit from ERDAS that was based on this. Lens distortion is typically modelled after Brown (1971):

$$\begin{pmatrix} \Delta x \\ \Delta y \end{pmatrix} = \begin{pmatrix} (1 + K_1 r^2 + K_2 r^4 + K_3 r^6)x + 2P_1 xy + P_2(r^2 + 2x^2) \\ (1 + K_1 r^2 + K_2 r^4 + K_3 r^6)y + 2P_2 xy + P_1(r^2 + 2y^2) \end{pmatrix} \quad [2]$$

where  $\Delta x, \Delta y$  are the deviations of coordinates  $x, y$  due to distortion,  $r^2 = x^2 + y^2$ ,  $K_1, K_2, K_3$  and  $P_1, P_2$  are the radial and tangential lens distortion parameters respectively. This forms the basis for both the ERDAS Imagine LPS and Pix4D models, where in ERDAS a linear  $K_0$  term is introduced (instead of the 1), which is not required in numerical applications (e.g. Luhmann et al. 2014), and  $K_3 = 0$  (ERDAS Imagine 2009). In Pix4D the distortion terms are presented in terms of  $R_x, T_x$  where  $R_x = K_x f^{2x+1}$  (Pix4D 2016).

During initial processing in Pix4D, a binary descriptor of the SIFT (Scale Invariant Feature Transform) algorithm (Lowe, 2004), similar to Strecha *et al.* (2012), is used to extract and then to match features from photographs (Küng *et al.*, 2011). Based on these and GCP data, Pix4D performs an iterative routine of camera self-calibration, automatic aerial triangulation (AAT) and block bundle adjustment (BBA) to determine and to optimize interior and exterior parameters. The exact sequence of processes and the optimization approach, i.e. cost functions used to assess the calculated reprojection errors (Triggs *et al.*, 1999) are proprietary and not disclosed. After initial processing, maximum point cloud densification is performed, based on multi-view stereo (MVS) algorithms (Seitz *et al.*, 2006), and orthoimages and DEMs are generated. We visually verified whether the automatically generated DEMs showed non-linear or dome-like systematic errors, using the 2010 ALTI3D as reference, before we used the densified point cloud for registration and final DEM generation.

We initially evaluate the bundle adjustment results using the typical performance indicators, average reprojection error and root mean square error (RMSE), which are based on the distance between the matched tie-point and/or marked GCP and its modelled position on the image. In addition, we compare the estimated exterior parameters, camera position X, Y, Z in the Swiss coordinate system CH1903, and orientation yaw ( $K$ ), pitch ( $\theta$ ) and roll ( $\Phi$ ), with values derived from classical photogrammetry (Regamey, 2013) and camera position data (SwissTopo). To facilitate comparison among the parameters, the values of the orientation parameters were translated to the potential error they may induce in planform position (in the case of  $K$ ) and elevation (in the case of  $\theta, \Phi$ ) for a 1 km reach with a mean error of zero. We also compared the SfM estimated radial distortion (based on Equation (2)) with camera calibration certificates and values derived using ERDAS Imagine LPS.

### 3.2.6 Point cloud registration

As has been shown that (random) error in exterior orientation parameters can propagate into systematic linear error in DEM surfaces (Lane *et al.*, 2004), we aimed to correct and to assess this effect through registering the photogrammetrically acquired point clouds to the 2010 lidar-based ALTI3D reference grid (SwissTopo). The potential of such an approach has already been demonstrated by Habib *et al.* (2004) and applied to archival photogrammetry by Miller *et al.* (2008) and Lane *et al.* (2016). Here, we used Riscan PRO software, which has its origin in the processing of terrestrial laser scanner point clouds (Heritage and Hetherington, 2007; Heritage *et al.*, 2009), and applied multi-station adjustment (Gabbud *et al.*, 2015) to the point cloud data from Pix4D and the reference grid.

The adjustment is based on so-called plane patches, which were derived from stable zones within the point clouds (Figure 3-1). In a filter routine, the planes are defined where a minimum of three points can be aligned within a 2 cm standard deviation (normal distance between points and plane). This is done for successively smaller grids ranging from 32.768 m to a minimum of 0.128 m (Riegler, 2015). A least-squares point matching algorithm (Zhang, 1994), was then used to iteratively identify the translation and rotation parameters (scaling was not applied) needed to minimize the error between the stable patches for different years with respect to the reference grid. For this a search radius of 2 m was used, equal to the size of the reference grid. We assessed the resulting reduction in (mean) error and compared the necessary adjustments among the reaches and with respect to the differences found in exterior orientation parameters between the SfM and classical approach.

### 3.2.7 DEM and DoD generation

To generate collocated 1 m resolution DEM grids, we applied a (default) linear point kriging variogram (slope and anisotropy equal to 1) to the resulting point clouds using Surfer 10 software (Heritage *et al.*, 2009). DEMs of Differences (DoDs) were determined for consecutive periods and clipped to the maximum extent of the active river bed which was manually digitized from the orthoimages, excluding areas where construction took place. This allowed us to assess the effect of the registration adjustment and its potential impact on morphological interpretation.

### 3.3 Results

#### 3.3.1 Quality of the SfM bundle adjustment

Table 3-2 shows the number of GCPs and the number of extracted and matched tie-points used in bundle adjustment. The reprojection error of these points is within 10 cm and the resulting mean RMSE values between  $\pm 0.20$  and  $\pm 0.45$  m, both of which are of the same order of magnitude as values derived using classical photogrammetric methods (Regamey 2013). Table 3-3 relates the control point RMSE, reflecting the precision of the bundle adjustment obtained, to the theoretical precision which may be estimated by the object space pixel size derived from the image scale and scanning resolution (Lane *et al.*, 2003). In general, the RMSE values are comparable, but when we resolve the mean and standard deviation of error in the SfM derived data, residual errors are revealed. Mean error over the whole study area is generally within the order of 5 cm, but higher values of up to 20 cm are found (Table 3-3). This suggests that there may be systematic error in the DEM surface, indicating the importance of subsequent point cloud registration.

Year	Number of GCPs	Tie-points per image	Reprojection error [m]	Mean RMSE [m]
1959	15 (14)	8387 (9)	0.08 (0.11)	$\pm 0.34$ ( $\pm 0.39$ )
1965	19 (17)	4254 (15)	0.06 (0.02)	$\pm 0.45$ ( $\pm 0.24$ )
1977	19 (41)	9563 (0)	0.04 (0.05)	$\pm 0.20$ ( $\pm 0.30$ )
1983	23 (25)	9692 (21)	0.04 (0.02)	$\pm 0.23$ ( $\pm 0.36$ )
1988	22 (18)	10505 (26)	0.04 (0.14)	$\pm 0.21$ ( $\pm 0.37$ )
1995	25	8387	0.05	$\pm 0.32$
1999	20	10261	0.06	$\pm 0.44$
2005	21 (30)	6240 (21)	0.08 (0.02)	$\pm 0.38$ ( $\pm 0.23$ )

Table 3-2 SfM block bundle adjustment results with classical photogrammetric reference values derived from Regamey (2013) shown in brackets.

Year	Theoretical precision [m]	Mean RMSE [m]	X [m]		Y [m]		Z [m]	
			ME   STDEV	ME   STDEV	ME   STDEV	ME   STDEV		
1959	$\pm 0.49$	$\pm 0.34$ ( $\pm 0.39$ )	0.01   0.30	0.08   0.39	0.00   0.33			
1965	$\pm 0.45$	$\pm 0.45$ ( $\pm 0.24$ )	-0.06   0.41	-0.10   0.57	-0.04   0.37			
1977	$\pm 0.27$	$\pm 0.20$ ( $\pm 0.30$ )	-0.01   0.18	-0.01   0.20	0.00   0.20			
1983	$\pm 0.27$	$\pm 0.23$ ( $\pm 0.36$ )	0.00   0.19	0.00   0.28	-0.01   0.21			
1988	$\pm 0.29$	$\pm 0.21$ ( $\pm 0.37$ )	-0.02   0.20	-0.01   0.22	-0.01   0.21			
1995	$\pm 0.38$	$\pm 0.32$	0.01   0.33	0.01   0.41	0.01   0.21			
1999	$\pm 0.38$	$\pm 0.44$	0.01   0.37	-0.20   0.57	-0.12   0.33			
2005	$\pm 0.35$	$\pm 0.38$ ( $\pm 0.23$ )	0.01   0.40	-0.01   0.53	0.02   0.21			

Table 3-3 Theoretical precision, mean RMSE and control point mean error (ME) and standard deviation of error (STDEV) in X, Y and Z direction. The RMSE values in brackets are derived from Regamey (2013) and determined by the authors (1977) and are given as a reference.

### 3.3.2 Exterior orientation and lens parameter estimation

In addition to the assessment of bundle adjustment quality, we compared the constituent exterior orientation parameters that were derived from SfM and classical bundle adjustment (Table 4-4). In general, there is a good agreement in the planar positioning of the images: with one exception these were all within 10 m. A slight systematic offset is detected in the X and to a lesser extent Y values.

Year	Position			Orientation		
	$\Delta X$ [m]	$\Delta Y$ [m]	$\Delta Z$ [m]	$\Delta K$ [°] ( $\Delta XY$ [m])	$\Delta \Theta$ [°] ( $\Delta Z$ [m])	$\Phi$ [°] ( $\Delta Z$ [m])
1959	-9.7	-0.9	-7.9	0.230 (2.01)	0.060 (0.52)	-0.062 (0.54)
1965	-2.2	2.6	-3.2	0.127 (1.11)	-0.005 (0.04)	-0.011 (0.10)
1977	1.1	2.3	-9.0	-0.322 (2.81)	-0.031 (0.27)	-0.065 (0.57)
1983	-2.9*	1.3*	-12.8	0.002 (0.02)	0.037 (0.32)	0.065 (0.57)
1988	-6.5	3.9	-0.3	-0.169 (1.47)	-0.016 (0.14)	0.001 (0.01)
1995	-3.2*	-1.6*				
1999	-2.8*	11.9*				
2005	-2.3*	-4.0*	28.0	-0.015 (0.13)	-0.373 (3.26)	-0.194 (1.69)
2005 fix	-3.5*	-4.5*	6.4	-0.056 (0.49)	0.024 (0.21)	-0.051 (0.45)

Table 3-4 Differences in exterior orientation parameters with respect to Regamey (2013) and Swisstopo\*. The maximum tilt adjustment (pitch or roll) has been translated to a potential error in meters. The 2005 fix row describes the 2005 bundle adjustment with fixed lens parameters.

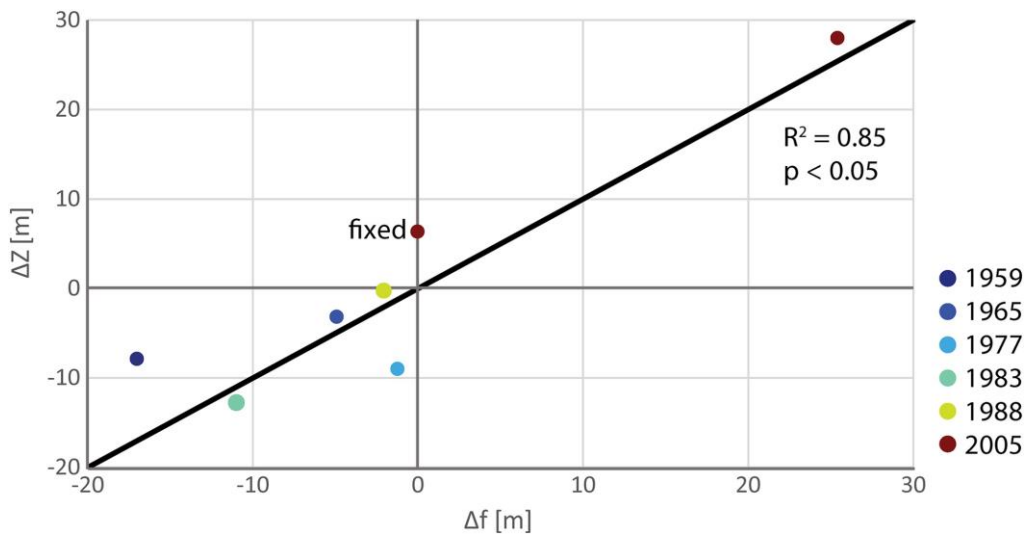


Figure 3-2 Relation between flying height difference ( $\Delta Z$ ) and the altitude difference that results from a change in focal length ( $\Delta f$ ) with respect to the calibrated value. Note that the line and statistics, Pearson's  $R^2$  and (significant)  $P$  value, follow a 1:1 relation and not a fitted regression line.

Larger differences are found in flying altitude, in the case of 2005 more than 25 m. However, these differences are largely attributable to the focal length adjustment that occurred during lens parameter optimization in SfM processing (significant relation in Figure 3-2). We verified this by fixing the lens parameters for 2005, which resulted in a marked reduction in altitude difference to about 6 m (last row Table 4-4). The resulting reprojection error and RMSE, however, increased to 0.20 and

$\pm 0.73$  m, respectively. Thus, there is evidence that the SfM approach, at least for a large part, compensates between estimates of exterior orientation parameters and those of lens parameters.

Regarding camera orientation, considerable differences in the yaw ( $K$ ) are found, which may be related to the distribution of GCPs and the limited number of tie-points in the classical approach (Table 4). Pitch ( $\theta$ ) and roll ( $\Phi$ ) values show good agreement with the values derived using classical photogrammetry provided that they are not required to ‘accommodate’ larger deviations in lens parameters. Note the decrease in difference when using a fixed focal length in 2005. The differences in orientation appear to compensate for the effects of the adjusted focal length, at least partially, but potentially also the lens distortion.

Figure 3-3 illustrates the results of camera self-calibration in Pix4D compared with the measured distortion from the camera calibration certificate and the statistical fit from ERDAS based on these measured values. It is clear that the polynomial form is not recovered, something which we find for other years in the dataset. However, the absolute lens distortion and the deviation from the calibrated distortion curve is very small, a few  $\mu\text{m}$ . The terrain displacement associated with this is less than 0.10 m and therefore much smaller than the pixel resolution of 0.35 m on which the self-calibration operates. For all years we found that the modelled absolute radial and tangential distortion did not exceed the measured distortion, which was maximally 8  $\mu\text{m}$ . Resulting differences will therefore have no major impact on the exterior orientation parameters (Table 3-4) or the quality of the bundle adjustment (Table 3-2).

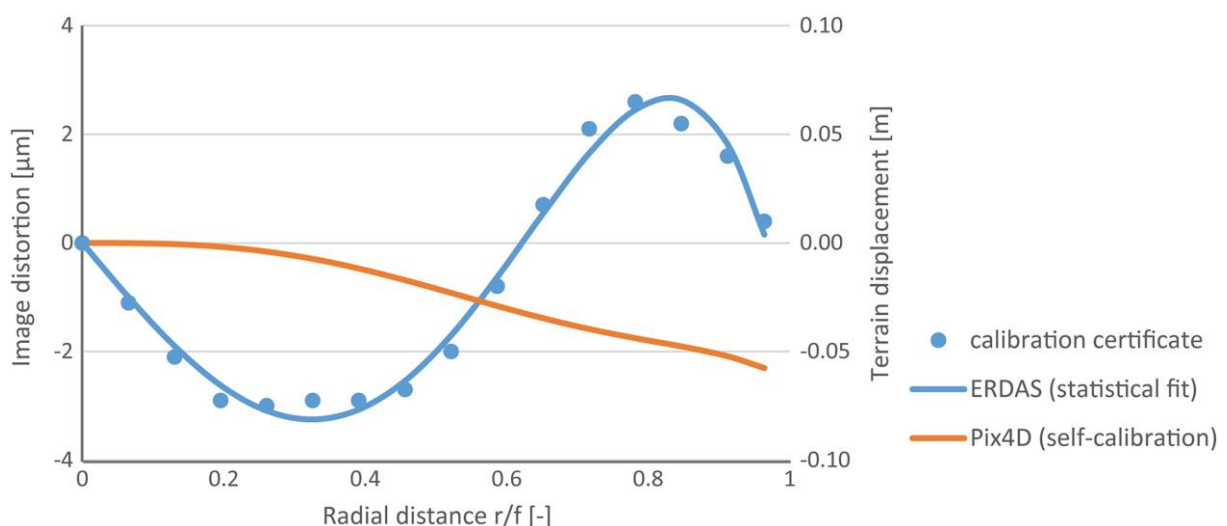


Figure 3-3 Radial distortion of the image and the related displacement in the terrain for the year with the largest calibrated distortion (2005). The ERDAS curve was statistically fitted using the measured deviations from the calibration certificate. The Pix4D curve was derived through self-calibration based on the images.

### 3.3.3 Impact of image acquisition parameters

Figure 3-4 shows the relationship between image acquisition properties and bundle adjustment quality. It should be mentioned that the bundle adjustment quality defines the best achievable or potential error, that is without additional errors associated with stereo-matching. The ability of SfM to extract and match tie-points is clearly related to entropy (the same may be expected for classical photogrammetric packages), emphasizing the importance of image texture. The extent of image overlap also appears to affect the ability to retrieve tie-points, but through a non-linear relation which may reflect a minimum threshold that is required for the successful matching of tie-points. The influences of image texture and overlap on the number of tie-points works through to the reprojection error and RMSE values, although it is slightly modulated (Figure 3-4). The low number of tie-points in 1965 and to a lesser extent 2005, has limited repercussions on the reprojection error and RMSE. This may indicate the importance of GCP's which are used in the bundle adjustment and ensure a base level quality – although marking these also requires sufficient texture.

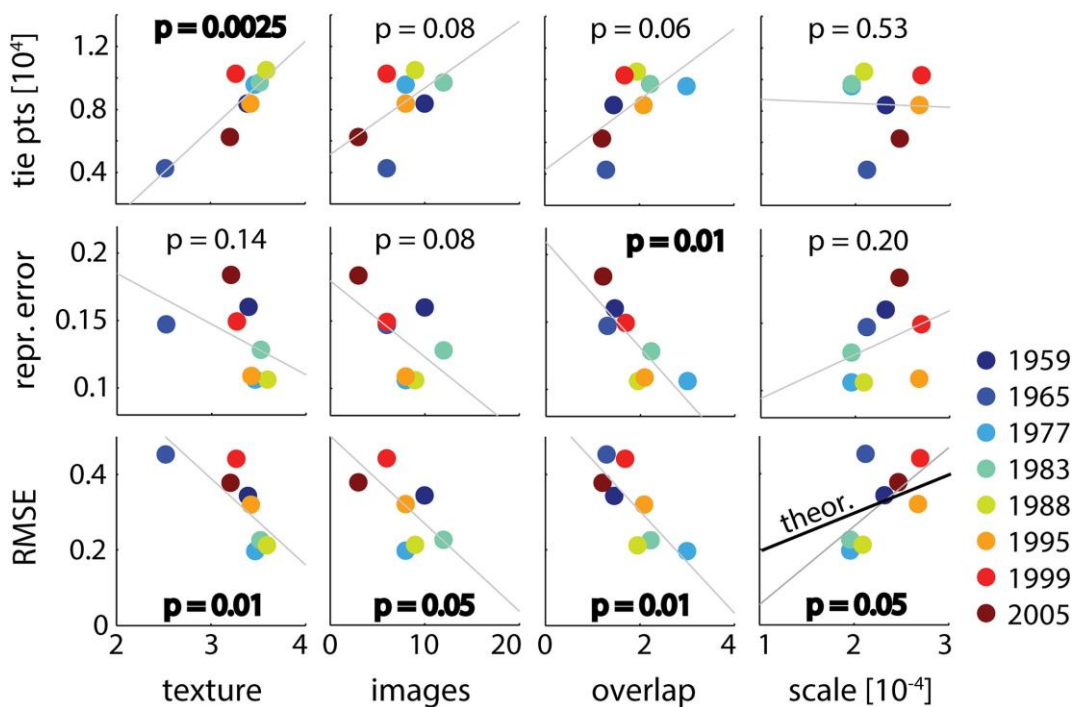


Figure 3-4 Scatter plots of image acquisition parameters, texture (entropy), images, image overlap and scale, vs. bundle adjustment parameters, tie-points, reprojection error and RMSE. Plots include P values for Pearson's R linear correlation. Theoretical precision as a function of scale is plotted based on a 14  $\mu\text{m}$  resolution (1959 and 1965 have a 21  $\mu\text{m}$  resolution and therefore plot above the theoretical precision).

The number of applied images alone is not of critical importance, but more their configuration and the resulting overlap. Whereas the overlap correlation values are highest and most significant, entropy may be of even larger importance when the 1965 outlier is disregarded, which results in less

scattered and markedly steeper (linear) relations. Finally, we find that the scale, with which we assessed the theoretical precision of the bundle adjustment, has no significant effect on the tie-point generation or reprojection error, but shows a significant increasing trend with the resulting RMSE (again 1965 is an outlier). It seems to limit the potential accuracy and precision that may be obtained, but does not directly control the bundle adjustment or is decisive for its quality, particularly in comparison with image texture and overlap.

### 3.3.4 Systematic error minimization in SfM point clouds

Where the mean error may average out to be more or less negligible at the scale of the entire study area, errors due to the incorrect DEM positioning or orientation may be large at the smaller reach scale. This is illustrated in the clear bias shown in the DoD in (Figure 3-5b), where the 2005 DEM lies systematically below the reference 2010 Alti3D. (Figure 3-5c) shows the same DoD where the DEM was registered based on the surrounding stable area (Figure 3-5a).

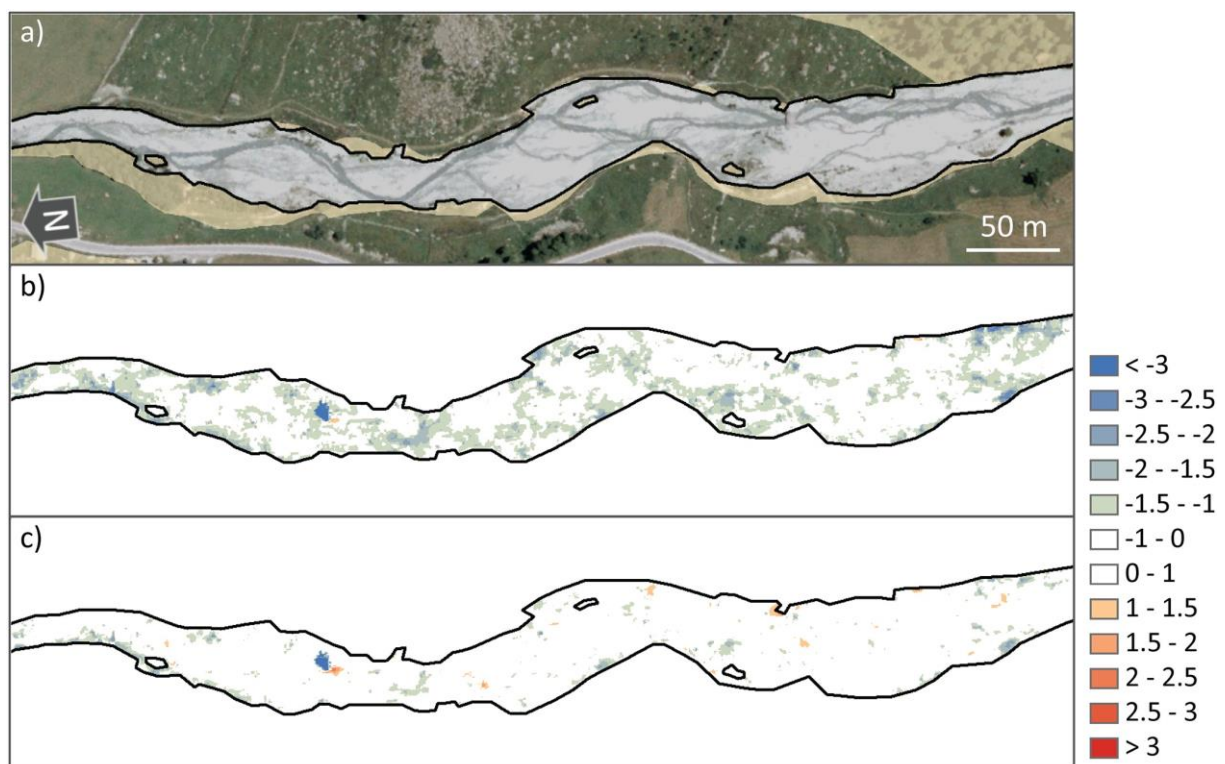


Figure 3-5 (a) 2005 Orthoimage of the main section of reach C and stable zones (non-stable river flood plain and forested areas are shaded), (b) 2005–2010 DoD before and (c) after point cloud registration (blue is erosion, red is deposition). Limit of detection (95% certainty) is  $\sim 1$  m.

Through applying registration, the bias is nearly completely removed, the absolute mean error decreases from 0.52 to 0.03 m and a nearly symmetric distribution of residuals is obtained (Figure 3-6). In addition, the standard deviation is slightly reduced from  $\pm 0.66$  m to  $\pm 0.56$  m, which will also allow a better limit of detection when analyzing morphological change. Note that these values are

not reflected in the mean error (0.02 m) and standard deviation ( $\pm 0.21$  m) of the entire study area as determined in the bundle adjustment (Table 3-3), emphasizing that the latter is not a sufficient indicator of the quality of derived DEMs which requires an independent reference dataset.

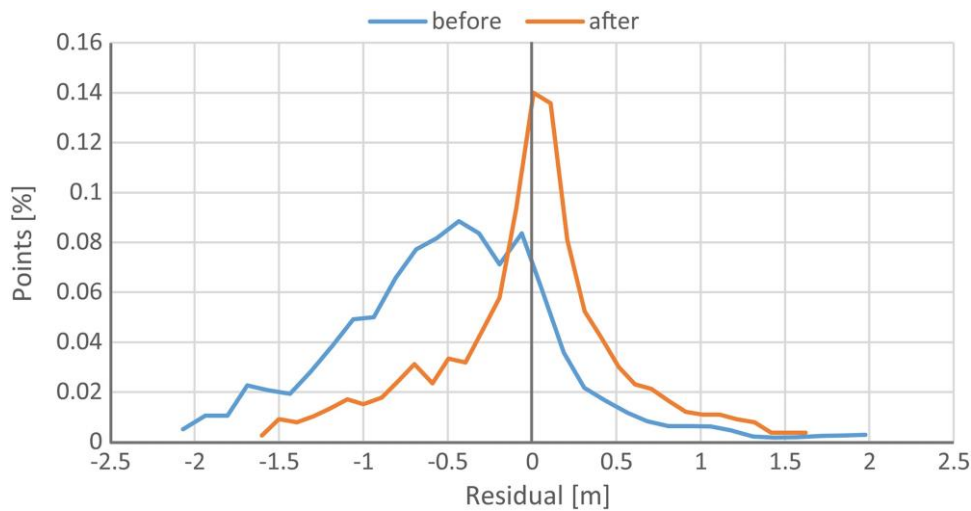


Figure 3-6 Normalized distribution of residual point distance between the stable zones in 2005 and 2010 for reach CD before and after registration.

Table 3-5 summarizes the mean error per reach before and after registration. On the whole, the decrease in absolute error is in the order of centimeters to tens of centimeters. Where there are consecutive and opposite errors such as 1959 and 1965 in reach B this can lead to an increased DoD error, 0.86 m as opposed to 0.08 m after error minimization. However, the adjustment is not always as effective (e.g. reaches B and CD in 1983) where the residual systematic error remains more or less intact. The improvement due to registration can also vary significantly between different reaches for the same year, e.g. 1959 and 1995 and between years, e.g. reach CD in 1977 and 1983. These indicate that, despite visual inspection, residual non-linear structural errors may still be present. However, with two exceptions all of the residual mean error values are within  $\pm 15$  cm.

Year	$\Delta Z$ Reach A [m]		$\Delta Z$ Reach B [m]		$\Delta Z$ Reach CD [m]	
	before	after (change)	before	after (change)	before	after (change)
1959	0.40	0.08 (0.32)	0.63	0.12 (0.51)	0.32	0.28 (0.04)
1965	0.05	0.04 (0.01)	-0.23	0.04 (0.19)	-0.06	0.05 (0.01)
1977	0.12	0.05 (0.07)	0.21	0.11 (0.10)	0.15	0.02 (0.13)
1983	-0.13	0.05 (0.08)	0.14	0.14 (0.00)	0.26	0.23 (0.03)
1988	0.24	0.04 (0.20)	0.12	0.08 (0.04)	0.32	0.14 (0.18)
1995	0.39	0.05 (0.34)	0.56	0.14 (0.42)	-0.10	0.09 (0.01)
1999	0.45	-0.01 (0.44)	-0.01	0.04 (-0.03)	0.17	0.06 (0.11)
2005	0.02	-0.01 (0.01)	0.53	0.09 (0.44)	0.52	0.03 (0.49)

Table 3-5 Stable-zone mean error (excluding outliers) values during multi-station adjustment. Improvements larger than 0.20 m are marked in green.

To gain insight into the nature of the registration we compare the reaches among each other and relate them to the differences found between SfM and classical photogrammetric bundle adjustment. The individual registration adjustments of the different reaches show a general level of consistency but may also vary significantly per year (Figure 3-7).

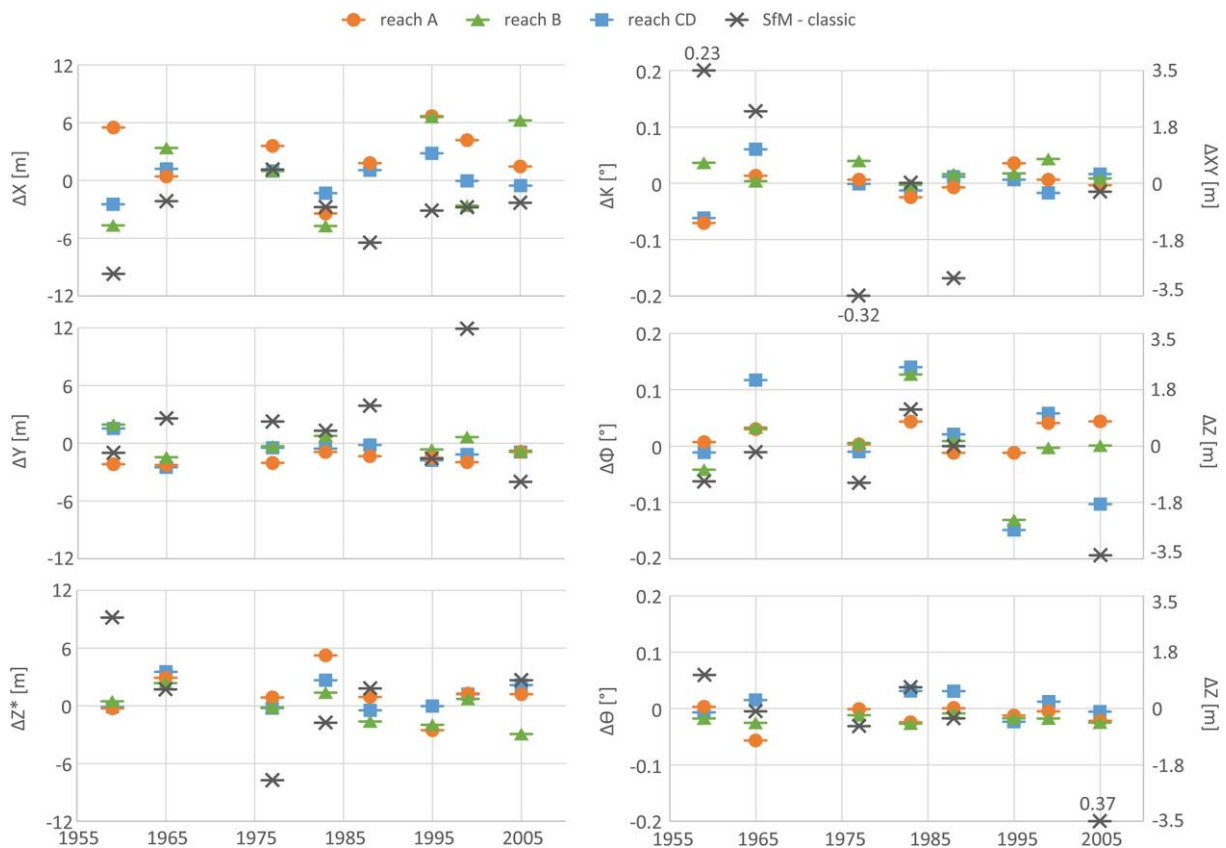


Figure 3-7 Adjustment of exterior parameters per reach with respect to deviation in bundle adjustment between SfM and classical photogrammetry (when they plot outside the y axis range, values are given – Table 3-2). For  $\Delta Z$  the values are corrected for focal length adjustment using the linear relation in Figure 3-2. The second y-axis for the orientation parameters gives the potential error in meters in a 1000 m reach.

The translational shifts in X and Y show a somewhat similar but opposite pattern to the difference between SfM and classical photogrammetry and could partially compensate for this. The changes in Z values are relatively consistent between the reaches and smaller than the residual difference found for the bundle adjustment, we corrected for height difference due to focal length using the relation in (Figure 3-2), giving us confidence in the quality of the SfM derived altitudes. The required adjustment in yaw (K) is small when compared with the bundle adjustment differences, which is supported by the notion that the large number of image-covering tie-points in SfM photogrammetry enable more accurate image alignment. Adjustments in roll ( $\Phi$ ) are considerable and show a similar behavior to the differences in bundle adjustment. Rather than diminishing these differences they appear correct for a common error. In this orientation, valley perpendicular, the bundle

adjustment is not well constrained by the GCPs, as opposed to the valley parallel orientation where differences in pitch ( $\theta$ ) adjustment are small. The magnitude of change in the exterior orientation parameters (Figure 3-7) with respect to the resulting decrease in error (Table 5) may give additional insight into the effectiveness of the registration and quality of the results. A relatively large decrease in error was achieved in reach B and CD in 2005 with a relatively limited adjustment in parameters; a shift in X and Z for reach B, and adjustment in roll ( $\Phi$ ) and to a lesser extent Z for reach CD. This gives confidence that a linear systematic error has been effectively corrected, moreover because little error is expected from potential instability of presumed stable areas with the reference year 2010. However, relatively large changes over a number of orientation parameters do not necessarily lead to significantly better results, for instance reaches B and CD in 1983, and these adjustments must be taken with caution. This may indicate an attempt to fit the data to non-linear or random error, potentially introducing (additional) systematic error.

Figure 3-8 shows the volumetric changes of the reaches through time, before and after registration adjustment, the latter including a correction for residual stable-zone mean error. Based on the available images and applied setting, we can conclude that volume changes due to systematic errors are of the same order of magnitude as actual morphological changes.

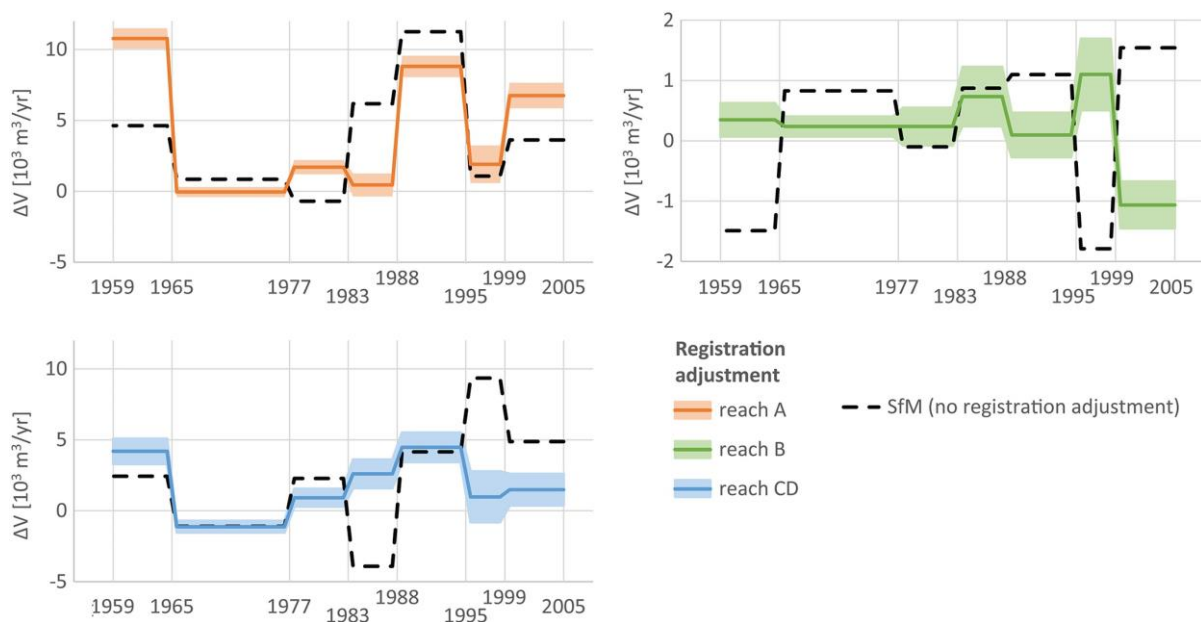


Figure 3-8 Average annual volume change per reach for periods between the available aerial photographs (specified on the x-axis). Change is displayed before registration adjustment (SfM) and after registration adjustment, including correction for residual stable-zone mean error (Table 3-5). The shaded uncertainty area for registration adjustment is based on a potential mean error in altitude values of  $\pm 0.05$  cm for reach A and  $\pm 0.10$  cm for reaches B and CD – these values were estimated based on Table 3-5.

Failing to acknowledge systematic errors in photogrammetric reconstruction can therefore lead to substantial errors in calculated volume changes, and the misinterpretation as to whether sedimentation or erosion has occurred (see also Figure 3-5). In addition, the correct interpretation of temporal trends in sedimentation is important for the understanding of sediment fluxes between the reaches and potentially the forcing mechanisms of these fluxes. Note that the responses of reaches A and CD largely coincide (the latter is slightly damped) whereas without the registration adjustment a significant delay in the signal between these reaches could have been identified.

### 3.4 Discussion

#### 3.4.1 Bundle adjustment

Comparison of SfM and classical photogrammetric approaches to archival images of braided river reaches showed that the two methods resulted in no clear preference for either method in terms of the reprojection error or the mean control point RMSE from the bundle adjustment (Table 3-2). Values obtained were comparable with the theoretically-expected precision. When considering mean error, the residuals did suggest the presence of systematic error (Table 3-3). Closer inspection of the exterior orientation parameters showed that, in general, SfM and classical photogrammetric values were comparable (Table 4-4). Differences were largely attributed to the interaction between exterior orientation and lens parameter optimization during the SfM photogrammetric process. The interaction was mainly revealed in counterbalancing adjustments, where changes in estimated focal length were largely compensated by changes in the estimated flying height (Figure 3-2). However, for this scaling relation to be completely valid the camera should be oriented vertically and the terrain horizontal (Gardner, 1939); whereas the former is more or less the case in archival aerial photography, the latter is not the case in this study.

Closer assessment of the self-calibrated lens distortion using camera calibration certificates revealed no indication of excessive distortion which may be introduced to compensate for potential errors in the estimation of external orientation parameters. Indeed, we did not find the dome-like errors which have been earlier found to result from insufficiently modelled lens distortion in SfM photogrammetry using non-metric cameras (Javernick *et al.*, 2014; Eltner and Schneider, 2015). The polynomial form of the radial distortion could not be resolved, but this is not surprising for archival imagery. First, the stereo geometry of archival imagery, based on near-nadir corridor/grid mapping, was not designed for camera self-calibration which works better with convergent/rotated image configurations (Remondino and Fraser, 2006; Wackrow and Chandler, 2008, 2011; James and Robson, 2014). Second, the metric cameras used in archival imagery have very little distortion, in

comparison with consumer-grade close-range cameras that are often used with SfM, but also in comparison with the pixel resolution on which the self-calibration operates. More generally, self-calibration in SfM applications needs to be assessed with care where it is subject to internal correlation between the K terms (Fraser, 1997), allowing for equifinal solutions (Carbonneau and Dietrich, 2016), and may be subject to residual systematic error and noise in the dataset. Lens parameters should be considered as model-specific and cannot be transferred to other applications or treated as universal values (Luhmann *et al.*, 2014).

Thus considering the combined bundle adjustment and camera self-calibration, similar levels of optimization (e.g. RMSE) can be achieved with different combinations of exterior orientation and lens parameters, and that simultaneous unsupervised self-calibration and bundle adjustment does not necessarily recover the 'correct' lens parameters and hence the correct exterior orientation. These findings are relevant when using archival imagery, for which camera calibration certificates may not always be available (Aguilar *et al.*, 2013), but the question remains whether it really matters for their application. Concerning focal length, others (Caduff and Rieke-Zapp, 2014) have identified the need for self-calibration in order to obtain a converged bundle adjustment. The fact that the changes in focal length and flying height with the SfM photogrammetric approach scaled linearly on one another (Figure 3-2) suggests that focal length optimization should not be a major concern unless it is attempting to correct for non-linear inaccuracies which may result from either measured (e.g. GCPs) or modelled parameters (e.g. lens distortion). Concerning lens distortion, we found no evidence for interaction with exterior parameters, although in this application with metric cameras there was also no real 'incentive' for such interaction. Fraser (1997) already established this coupling to be low. Error resulting from lens distortion in this type of archival application is only of secondary importance and of little influence on the overall error.

Bundle adjustment is a complex mathematical procedure, with a large number of degrees of freedom and many potential parameter correlations complicating the assessment of the influence of single parameters. In general, our findings emphasize the need for SfM applications to pay close attention to the bundle adjustment results, in relation to applied lens model optimization. They challenge the idea that SfM frees the user from the traditional concerns in photogrammetry and emphasize the importance of transparency in the algorithms used in SfM software packages (Smith *et al.*, 2015), as argued before in relation to early applications of automated digital photogrammetry (Chandler, 1999; Lane *et al.*, 2000).

### 3.4.2 Image properties and data quality

There was clear evidence that the success of a SfM approach was related to the way that image properties are exploited by computer vision techniques. The primary advantage with respect to the classical approach is the use of a much greater number of matched tie-points (Table 3-2) which are fully distributed over the images (not limited to the zone of interest), so, at least partly, overcoming the dependency on and limits imposed by GCP availability for archival purposes (James *et al.*, 2006; Walstra *et al.*, 2011). The addition of large amounts of automatically generated tie-points, where their accuracy is limited to simple outlier detection, to a small number of accurate, user-specified GCPs provides a good constraint for bundle adjustment. Not only are SfM methods efficient in the unsupervised automatic aligning of the photographs, we have also found that they lead to a more accurate alignment based on the limited required registration adjustment in the yaw ( $\kappa$ ) orientation (Figure 3-7).

Image texture, which can be effectively quantified using a simple measure of spectral entropy (Laliberte and Rango, 2009), directly affects the number of generated tie-points in bundle adjustment and subsequent reprojection error and RMSE (Figure 3-4). This is in line with the general notion that the texture is of critical importance for SfM feature extraction (Westoby *et al.*, 2012). Where the texture of archival images is predefined, the entropy may be used for quality screening of photographs. This however only indicates a potential, where spatial variability, in the form of surface cover and general morphology, is also required for feature extraction. For the successful matching of extracted features, high image overlap between photographs is also important (Figure 3-4; Westoby *et al.*, 2012). This enables the redundancy of tie-points and prevents potential difficulties in feature matching, due to dissimilarities between images that arise from perspective changes, which in turn allow for a reduced error in bundle adjustment. Here, a possible constraint on the application of SfM based archival photogrammetry arises where image acquisition in classical photogrammetry is designed with relatively limited overlap. This is, however, with reason, where from classical photogrammetry we know that the accuracy of elevation change actually increases with increasing perspective changes due to the parallax shift, which indicates a potential optimum in overlap/perspective change when applying SfM photogrammetry. Another difference arises where SfM algorithms extensively use tie-points and their automatic extraction and matching is scale invariant (Figure 3-4). SfM algorithms are therefore less dependent on image scale as compared to classical photogrammetry, which relies more strongly on GCP identification which is scale dependent.

Limitations in available image quality (texture), image overlap and image configuration (near-nadir imagery) in archival imagery, in combination with the interaction between bundle adjustment and

camera self-calibration demand the utmost insight and control in SfM photogrammetry. Where photogrammetric techniques will further develop and (hopefully) manifest themselves in SfM software, image acquisition properties are predefined and may be assessed for their SfM photogrammetric potential, just like the typically applied image scale. The ample use of GCPs may constrain the bundle adjustment and suppress errors (Eltner and Schneider, 2015). In archival applications these are likely to be limited, but in any case it is advisable to exploit these to the fullest in bundle adjustment control and preferably not as check points where error may also be estimated through subsequent registration or GCP sensitivity analysis. Despite the limitations we demonstrated that SfM methods do not only have the potential for the application in archival photogrammetry (Gomez *et al.*, 2015), they can be used for the accurate quantification of river–floodplain morphology. This is enhanced by the dense-matching/high resolution algorithms that these methods use which allow for higher precision and (associated) lower local error through interpolation in comparison with classical photogrammetry (Eltner *et al.*, 2016).

#### 3.4.3 Systematic error minimization

In all photogrammetric applications, regardless as to whether a SfM or classical approach is used, residual systematic errors may be expected which need to be independently verified both with other techniques or other datasets (Fonstad *et al.*, 2013; Eltner *et al.*, 2016). We have shown that this may not always be apparent from bundle adjustment quality parameters (mean error, Table 3-2), but may be revealed through registering the photogrammetrically derived point clouds to a reference grid, here based on lidar data (for example Figure 3-5). We found systematic errors on the reach scale that were typically of the order of decimeters (Table 5). After registration adjustment the residual error values were of the order of centimeters, and with two exceptions all values were within 15 cm. The effectiveness of the adjustment, in the form of the relative decrease in bias, varied somewhat among reaches and between years.

Closer inspection of the applied registration adjustment, orientation and magnitude, revealed both consistencies among the reaches, giving confidence in the adjustment to correct for systematic error, as well as considerable differences, which may indicate that errors are complex/non-linear and potentially noise dominated (Figure 3-7). The effectiveness of the registration also varied with the magnitude of the required change in orientation parameters, where it must be noted that the adjustment may also, theoretically, introduce an additional error. The required reduction in the (linear) systematic error was of the same order of magnitude or smaller than the differences we found between SfM and classical approaches. From this we can conclude that potential limitations associated with the application of SfM algorithms in the form of linear error (e.g. through focal

length modelling) may be overcome through subsequent registration. Indeed, registration adjustments are relevant for all photogrammetric applications, SfM or classical, where systematic linear errors may originate from the propagation of random error in the external orientation parameters (Westaway *et al.*, 2003; Lane *et al.*, 2004).

Failing to acknowledge systematic errors in photogrammetrically derived point clouds will allow them to translate and potentially amplify when determining morphological change. As we have shown in (Figure 3-8), this may lead to the misinterpretation of the occurrence of erosion/sedimentation, the absolute quantities of change and morphologic variability in time (in our case the decadal scale) and space (in our case between reaches). The application of archival photogrammetry in low relief environments such as river–floodplain systems is particularly sensitive to such errors (Heritage *et al.*, 1998; Lane *et al.*, 2010). Note that when no independent, high resolution reference dataset is available, a photogrammetrically derived DEM (typically the most recent) may be sufficient for the analysis of (relative) morphological change. Registration not only provides a means for minimizing linear structural errors, but also provides an uncertainty estimation for residual non-linear structural and random error (this may be conservative where particularly on the longer term zones may not be entirely stable due to slope processes, vegetation growth) for the assessment of detection limits and error propagation in elevational and volumetric changes (Lane *et al.*, 2004). Finally the registration procedure provides general insight into the quality of the photogrammetric reconstruction.

### **3.5 Conclusions**

In this study we applied computer vision based SfM methods to archival imagery for the quantification of river and floodplain morphology. Besides the widely recognized efficiency and precision, we found the resulting quality may be comparable with that obtained with classical methods. We showed that this application requires the careful consideration of photogrammetric principles to avoid and to mitigate structural error in DEMs. These may strongly affect the interpretation of morphological change, particularly for the application of archival photogrammetry in low relief river–floodplain environments. The results from this study may be summarized along three phases of the photogrammetric process, namely image acquisition, bundle adjustment and point cloud registration:

The potential of the application of SfM photogrammetric methods to archival imagery can be evaluated by reference to: (1) the temporal frequency and scale of images in relation to the relief that is to be measured and the magnitude of expected changes; in this sense SfM does not differ from the classical application; (2) image texture, which can be quantified using entropy, controls the

extent to which computer vision techniques can detect and match tie-points; (3) image overlap and configuration, which enables the redundancy of tie-points and enhances their accuracy (less mismatching). These last two points specifically apply to SfM photogrammetry where the tie-points largely control bundle adjustment precision, particularly with respect to the alignment of images; and (4) GCPs are ideally included in bundle adjustment as a basis on which the SfM computer vision techniques can enhance the dataset on which bundle adjustment is based and thereby its potential quality.

Despite non-ideal archival image acquisition, near-nadir and limited overlap which affect camera self-calibration and bundle adjustment, the bundle adjustment quality we acquired with SfM was similar to that which was acquired using classical photogrammetry. In both cases the quality of the photogrammetric reconstruction requires SfM software to provide insight and control over bundle adjustment parameters. Interaction between lens modelling parameters and exterior orientation parameters needs to be assessed in relation to one another. We found (linear) interaction between focal length and flying altitude, but these largely compensated each other. We did not find any indication that non-linear or dome-like errors were introduced through camera self-calibration, neither in the DEMs nor in the modelled distortion.

Registration adjustment provides a means for addressing linear systematic error in point clouds that remains, even with reliable bundle adjustment results, through: (1) systematic error detection which may be the result of (random) error propagation in classical or SfM photogrammetry; (2) error minimization through registration, which was able to compensate the potential (additional) error associated with the application of SfM photogrammetry, preventing error propagation into volume changes; and (3) quality assessment of the bundle adjustment and point cloud, which was possible through quantifying the residual error and analyzing the required rotation/translation.

#### *Acknowledgments*

Maarten Bakker is supported by the Swiss National Science Foundation, Synergia grant CRSII2\_147689, awarded to Fritz Schlunegger, Stéphanie Girardclos, Stuart Lane, Jean-Luc Loizeau and Peter Molnar. SwissTopo provided the scanned aerial photographs and Natan Micheletti provided the GCP data used in the study. Additional support came from the Canton Valais, the Fondation Herbette and the Commune of Evolène. We would like to thank Anette Eltner, an anonymous reviewer and Editor Mike Kirkby for their detailed and constructive comments which have led to the improvement of this manuscript.

## References

- Aguilar MA, Aguilar FJ, Fernández I, Mills JP. 2013. Accuracy assessment of commercial self-calibrating bundle adjustment routines applied to archival aerial photography. *The Photogrammetric Record* 28(141): 96–114. DOI:10.1111/j.1477-9730.2012.00704.x.
- Barker R, Dixon L, Hooke J. 1997. Use of terrestrial photogrammetry for monitoring and measuring bank erosion. *Earth Surface Processes and Landforms* 22(13): 1217–1227. DOI:10.1002/(SICI)1096-9837(199724)22:13<1217::AID-ESP819>3.0.CO;2-U.
- Bertin S, Friedrich H, Delmas P, Chan E, Gimel'farb G. 2015. Digital stereo photogrammetry for grain-scale monitoring of fluvial surfaces: error evaluation and workflow optimisation. *ISPRS Journal of Photogrammetry and Remote Sensing* 101: 193–208. DOI:10.1016/j.isprsjprs.2014.12.019.
- Bezinge A, Clark M, Gurnell A, Warburton J. 1989. The management of sediment transported by glacial melt-water streams and its significance for the estimation of sediment yield. *Annals of Glaciology* 13: 1–5.
- Brasington J, Langham J, Rumsby B. 2003. Methodological sensitivity of morphometric estimates of coarse fluvial sediment transport. *Geomorphology* 53(3–4): 299–316. DOI:10.1016/S0169-555X(02)00320-3.
- Brown DC. 1971. Close-range camera calibration. *Photogrammetric Engineering* 37(8): 855–866.
- Caduff R, Rieke-Zapp D. 2014. Registration and visualisation of deformation maps from terrestrial radar interferometry using photogrammetry and Structure from Motion. *The Photogrammetric Record* 29(146): 167–186. DOI:10.1111/phor.12058.
- Carbonneau PE, Dietrich JT. 2016. Cost-effective non-metric photogrammetry from consumer-grade sUAS: implications for direct georeferencing of structure from motion photogrammetry. *Earth Surface Processes and Landforms*: n/a-n/a. DOI:10.1002/esp.4012.
- Castillo C, Taguas EV, Zarco-Tejada P, James MR, Gómez JA. 2014. The normalized topographic method: an automated procedure for gully mapping using GIS. *Earth Surface Processes and Landforms* 39(15): 2002–2015. DOI:10.1002/esp.3595.
- Chandler J. 1999. Effective application of automated digital photogrammetry for geomorphological research. *Earth Surface Processes and Landforms* 24(1): 51–64. DOI:10.1002/(SICI)1096-9837(199901)24:1<51::AID-ESP948>3.0.CO;2-H.
- Chandler J, Ashmore P, Paola C, Gooch M, Varkaris F. 2002. Monitoring river-channel change using terrestrial oblique digital imagery and automated digital photogrammetry. *Annals of the Association of American Geographers* 92(4): 631–644.

- Chandler J, Moore R. 1989. Analytical photogrammetry: a method for monitoring slope instability. *Quarterly Journal of Engineering Geology and Hydrogeology* 22(2): 97–110.
- De Rose RC, Basher LR. 2011. Measurement of river bank and cliff erosion from sequential LIDAR and historical aerial photography. *Geomorphology* 126(132): –147.  
DOI:10.1016/j.geomorph.2010.10.037.
- Dietrich JT. 2016. Riverscape mapping with helicopter-based Structure-from-Motion photogrammetry. *Geomorphology* 252: 144–157. DOI:10.1016/j.geomorph.2015.05.008.
- Eltner A, Baumgart P, Maas H-G, Faust D. 2015. Multi-temporal UAV data for automatic measurement of rill and interrill erosion on loess soil. *Earth Surface Processes and Landforms* 40(6): 741–755. DOI:10.1002/esp.3673.
- Eltner A, Kaiser A, Carlos C, Rock G, Neugirg F, Abellan A. 2016. Image-based surface reconstruction in geomorphometry – merits, limits and developments of a promising tool for geoscientists. *Earth Surface Dynamics Discussions* 3: 359–389. DOI:10.5194/esurf-4-359-2016.
- Eltner A, Schneider D. 2015. Analysis of different methods for 3D reconstruction of natural surfaces from parallel-axes uav images. *The Photogrammetric Record* 30(151): 279–299.  
DOI:10.1111/phor.12115.
- ERDAS Imagine. 2009. LPS Project Manager User's Guide: 454.
- Fonstad MA, Dietrich JT, Courville BC, Jensen JL, Carbonneau PE. 2013. Topographic structure from motion: a new development in photogrammetric measurement. *Earth Surface Processes and Landforms* 38(4): 421–430. DOI:10.1002/esp.3366.
- Fraser CS. 1997. Digital camera self-calibration. *ISPRS Journal of Photogrammetry and Remote Sensing* 52(4): 149–159. DOI:10.1016/S0924-2716(97)00005-1.
- Gabbud C, Micheletti N, Lane SN. 2015. Lidar measurement of surface melt for a temperate Alpine glacier at the seasonal and hourly scales. *Journal of Glaciology* 61(229): 963–974.  
DOI:10.3189/2015JoG14J226.
- Gardner IC. 1939. Relation of camera error to photogrammetric mapping. *Journal of Research of the National Bureau of Standards* 22(RP1177): 209–238.
- Gilvear D, Bryant R. 2005. Analysis of aerial photography and other remotely sensed data. In *Tools in Fluvial Geomorphology*, Kondolf GM, Piégay H (eds). John Wiley & Sons, Ltd: Chichester, UK; 135–170.
- Gilvear DJ, Waters TM, Milner AM. 1995. Image analysis of aerial photography to quantify changes in channel morphology and instream habitat following placer mining in interior Alaska. *Freshwater Biology* 34(2): 389–398. DOI:10.1111/j.1365-2427.1995.tb00897.x.

- Gomez C, Hayakawa Y, Obanawa H. 2015. A study of Japanese landscapes using structure from motion derived DSMs and DEMs based on historical aerial photographs: new opportunities for vegetation monitoring and diachronic geomorphology. *Geomorphology* 242: 11–20. DOI:10.1016/j.geomorph.2015.02.021.
- Gonzalez RC, Woods RE, Eddins SL. 2003. *Digital image processing using MATLAB*. Prentice Hall: New Jersey.
- Gurnell A. 1983. Downstream channel adjustments in response to water abstraction for hydro-electric power generation from alpine glacial melt-water streams. *The Geographical Journal* 149(3): 342–354. DOI:10.2307/634009.
- Habib A, Ghanma M, Kima C, Mitishita E. 2004. Alternative approaches for utilizing lidar data as a source of control information for photogrammetric models. *International Archives of Photogrammetry, Remote Sensing and Spatial Information Sciences* 35(Part B1): 193–198.
- Heritage G, Hetherington D. 2007. Towards a protocol for laser scanning in fluvial geomorphology. *Earth Surface Processes and Landforms* 32(1): 66–74. DOI:10.1002/esp.1375.
- Heritage GL, Fuller IC, Charlton ME, Brewer PA, Passmore DP. 1998. CDW photogrammetry of low relief fluvial features: accuracy and implications for reach-scale sediment budgeting. *Earth Surface Processes and Landforms* 23(13): 1219–1233. DOI:10.1002/(SICI)1096-9837(199812)23:13<1219::AID-ESP927>3.0.CO;2-R.
- Heritage GL, Milan DJ, Large ARG, Fuller IC. 2009. Influence of survey strategy and interpolation model on DEM quality. *Geomorphology* 112(344): 334. DOI:10.1016/j.geomorph.2009.06.024.
- Honkavaara E, Eskelinen MA, Pölönen I, Saari H, Ojanen H, Mannila R, Holmlund C, Hakala T, Litkey P, Rosnell T, Viljanen N, Pulkkanen M. 2016. Remote sensing of 3D geometry and surface moisture of a peat production area using hyperspectral frame cameras in visible to short-wave infrared spectral ranges onboard a small unmanned airborne vehicle (UAV). *IEEE Transactions on Geoscience and Remote Sensing* 54(9): 5440–5454. DOI:10.1109/TGRS.2016.2565471.
- James MR, Robson S. 2012. Straightforward reconstruction of 3D surfaces and topography with a camera: accuracy and geoscience application. *Journal of Geophysical Research. Earth Surface* 117(F3). DOI:10.1029/2011JF002289.
- James MR, Robson S. 2014. Mitigating systematic error in topographic models derived from UAV and ground-based image networks. *Earth Surface Processes and Landforms* 39(10): 1413–1420. DOI:10.1002/esp.3609.
- James TD, Murray T, Barrand NE, Barr SL. 2006. Extracting photogrammetric ground control from lidar DEMs for change detection. *The Photogrammetric Record* 21(116): 312–328. DOI:10.1111/j.1477-9730.2006.00397.x.

- Javernick L, Brasington J, Caruso B. 2014. Modeling the topography of shallow braided rivers using Structure-from-Motion photogrammetry. *Geomorphology* 213: 166–182.  
DOI:10.1016/j.geomorph.2014.01.006.
- Kondolf GM, Larson M. 1995. Historical channel analysis and its application to riparian and aquatic habitat restoration. *Aquatic Conservation: Marine and Freshwater Ecosystems* 5(2): 109–126.  
DOI:10.1002/aqc.3270050204.
- Küng O, Strecha C, Beyeler A, Zufferey J-C, Floreano D, Fua P, Gervais F. 2011. The accuracy of automatic photogrammetric techniques on ultra-light UAV imagery. *UAV-g 2011-Unmanned Aerial Vehicle in Geomatics*.
- Laliberte AS, Rango A. 2009. Texture and scale in object-based analysis of subdecimeter resolution unmanned aerial vehicle (UAV) imagery. *Geoscience and Remote Sensing, IEEE Transactions on Geoscience and Remote Sensing* 47(3): 761–770. DOI:10.1109/TGRS.2008.2009355.
- Lane SN, Bakker M, Gabbud C, Micheletti N, Saugy J-N. 2016. Sediment export, transient landscape response and catchment-scale connectivity following rapid climate warming and Alpine glacier recession. *Geomorphology*. DOI:10.1016/j.geomorph.2016.02.015.
- Lane SN, James T, Crowell M. 2000. Application of digital photogrammetry to complex topography for geomorphological research. *The Photogrammetric Record* 16(95): 793–821. DOI:10.1111/0031-868X.00152.
- Lane SN, Reid SC, Westaway RM, Hicks DM. 2004. Remotely sensed topographic data for river channel research: the identification, explanation and management of error. In *Spatial Modelling of the Terrestrial Environment*, Kelly REJ, Drake NA, Barr SL (eds). John Wiley & Sons, Ltd: Chichester, UK; 113–136.
- Lane SN, Richards KS, Chandler JH. 1993. Developments in photogrammetry; the geomorphological potential. *Progress in Physical Geography* 17(3): 306–328.
- Lane SN, Richards KS, Chandler JH. 1994. Developments in monitoring and modelling small-scale river bed topography. *Earth Surface Processes and Landforms* 19(4): 349–368.  
DOI:10.1002/esp.3290190406.
- Lane SN, Westaway RM, Murray HD. 2003. Estimation of erosion and deposition volumes in a large, gravel-bed, braided river using synoptic remote sensing. *Earth Surface Processes and Landforms* 28(3): 249–271. DOI:10.1002/esp.483.
- Lane SN, Widdison PE, Thomas RE, Ashworth PJ, Best JL, Lunt IA, Sambrook Smith GH, Simpson CJ. 2010. Quantification of braided river channel change using archival digital image analysis. *Earth Surface Processes and Landforms* 35(8): 971–985. DOI:10.1002/esp.2015.

- Lowe DG. 2004. Distinctive image features from scale-invariant keypoints. *International Journal of Computer Vision* 60(2): 91–110. DOI:10.1023/B:VISI.0000029664.99615.94.
- Luhmann T, Robson S, Kyle S, Boehm J. 2014. *Close-Range Photogrammetry and 3D Imaging*, 2nd edn. De Gruyter: Berlin, Germany, 683.
- Micheletti N, Lane SN, Chandler JH. 2015. Application of archival aerial photogrammetry to quantify climate forcing of alpine landscapes. *The Photogrammetric Record* 30(150): 143–165. DOI:10.1111/phor.12099.
- Miller P, Mills J, Edwards S, Bryan P, Marsh S, Mitchell H, Hobbs P. 2008. A robust surface matching technique for coastal geohazard assessment and management. *ISPRS Journal of Photogrammetry and Remote Sensing* 63(5): 529–542. DOI:10.1016/j.isprsjprs.2008.02.003.
- Nebiker S, Lack N, Deuber M. 2014. Building change detection from historical aerial photographs using dense image matching and object-based image analysis. *Remote Sensing* 6(9): 8310–8336. DOI:10.3390/rs6098310.
- Pasquale N, Perona P, Schneider P, Shrestha J, Wombacher A, Burlando P. 2011. Modern comprehensive approach to monitor the morphodynamic evolution of a restored river corridor. *Hydrology and Earth System Sciences* 15(4): 1197–1212. DOI:10.5194/hess-15-1197-2011.
- Pérez Álvarez JA, Herrera VM, Martínez del Pozo JÁ, de Tena MT. 2013. Multi-temporal archaeological analyses of alluvial landscapes using the photogrammetric restitution of historical flights: a case study of Medellín (Badajoz, Spain). *Journal of Archaeological Science* 40(1): 349–364. DOI:10.1016/j.jas.2012.08.025.
- Pix4D. 2016. How are the internal and external camera parameters defined? Retrieved 25/04/2016, from <https://support.pix4d.com/hc/en-us/articles/202559089#gsc.tab=0>.
- Pyle C, Richards K, Chandler J. 1997. Digital photogrammetric monitoring of river bank erosion. *The Photogrammetric Record* 15(89): 753–764. DOI:10.1111/0031-868X.00083.
- Regamey B. 2013. *Téledétection des impacts à long terme de l'extraction de l'eau sur un système sédimentaire d'une vallée latérale alpine*. Master's thesis in Geography, University of Lausanne. <http://mesoscaphe.unil.ch/igul/doc.php?id=TIGL-859.pdf>.
- Remondino F, Fraser C. 2006. Digital camera calibration methods: considerations and comparisons. *International Archives of Photogrammetry, Remote Sensing and Spatial Information Sciences* 36(5): 266–272.
- Riegl. 2015. *Riegl laser measurement systems: RiSCAN PRO version: 2.1.1*. Horn, Austria.

- Saint-Geours N, Grelot F, Bailly JS, Lavergne C. 2015. Ranking sources of uncertainty in flood damage modelling: a case study on the cost–benefit analysis of a flood mitigation project in the Orb Delta, France. *Journal of Flood Risk Management* 8(2): 161–176. DOI:10.1111/jfr3.12068.
- Sanyal J, Lu XX. 2004. Application of remote sensing in flood management with special reference to monsoon asia: a review. *Natural Hazards* 33(2): 283–301. DOI:10.1023/b:nhaz.0000037035.65105.95.
- Seitz SM, Curless B, Diebel J, Scharstein D, Szeliski R. 2006. A comparison and evaluation of multi-view stereo reconstruction algorithms. 2006 IEEE Computer Society Conference on Computer Vision and Pattern Recognition (CVPR'06).
- Smith MW, Carrivick JL, Quincey DJ. 2015. Structure from motion photogrammetry in physical geography. *Progress in Physical Geography*. DOI:10.1177/0309133315615805.
- Snively KN. 2008. Scene Reconstruction and Visualization from Internet Photo Collections. Doctoral thesis, University of Washington.
- Stojic M, Chandler J, Ashmore P, Luce J. 1998. The assessment of sediment transport rates by automated digital photogrammetry. *Photogrammetric Engineering and Remote Sensing* 64(5): 387–395.
- Strecha C, Bronstein AM, Bronstein MM, Fua P. 2012. LDAHash: improved matching with smaller descriptors. *Pattern Analysis and Machine Intelligence, IEEE Transactions on* 34(1): 66–78.
- Triggs B, McLauchlan PF, Hartley RI, Fitzgibbon AW. 1999. Bundle adjustment – a modern synthesis. In *Vision Algorithms: Theory and Practice*, Triggs B, Zisserman A, Szeliski R (eds). Springer; 298–372.
- Vallet J, Panissod F, Strecha C, Tracol M. 2011. Photogrammetric performance of an ultra light weight swinglet UAV. *UAV-g 2011-Unmanned Aerial Vehicle in Geomatics*.
- Wackrow R, Chandler JH, Bryan P. 2007. Geometric consistency and stability of consumer-grade digital cameras for accurate spatial measurement. *The Photogrammetric Record* 22(118): 121–134. DOI:10.1111/j.1477-9730.2007.00436.x.
- Wackrow R, Chandler JH. 2008. A convergent image conguration for DEM extraction that minimises the systematic eects caused by an inaccurate lens model. *The Photogrammetric Record* 23(121): 6–18. DOI:10.1111/j.1477-9730.2008.00467.x.
- Wackrow R, Chandler JH. 2011. Minimising systematic error surfaces in digital elevation models using oblique convergent imagery. *The Photogrammetric Record* 26(133): 16–31. DOI:10.1111/j.1477-9730.2011.00623.x.

- Walstra J, Chandler JH, Dixon N, Wackrow R. 2011. Evaluation of the controls affecting the quality of spatial data derived from historical aerial photographs. *Earth Surface Processes and Landforms* 36(7): 853–863. DOI:10.1002/esp.2111.
- Westaway RM, Lane SN, Hicks DM. 2001. Remote sensing of clear-water, shallow, gravel-bed rivers using digital photogrammetry. *Photogrammetric Engineering and Remote Sensing* 67(11): 1271–1282.
- Westaway RM, Lane SN, Hicks DM. 2003. Remote survey of large-scale braided, gravel-bed rivers using digital photogrammetry and image analysis. *International Journal of Remote Sensing* 24(4): 795–815. DOI:10.1080/01431160110113070.
- Westoby MJ, Brasington J, Glasser NF, Hambrey MJ, Reynolds JM. 2012. ‘Structure-from-Motion’ photogrammetry: a low-cost, effective tool for geoscience applications. *Geomorphology* 179: 300–314. DOI:10.1016/j.geomorph.2012.08.021.
- Wheaton JM, Brasington J, Darby SE, Kasprak A, Sear D, Vericat D. 2013. Morphodynamic signatures of braiding mechanisms as expressed through change in sediment storage in a gravel-bed river. *Journal of Geophysical Research. Earth Surface* 118(2): 759–779. DOI:10.1002/jgrf.20060.
- Wheaton JM, Brasington J, Darby SE, Sear DA. 2010. Accounting for uncertainty in DEMs from repeat topographic surveys: improved sediment budgets. *Earth Surface Processes and Landforms* 35(2): 136–156. DOI:10.1002/esp.1886.
- Zhang Z. 1994. Iterative point matching for registration of free-form curves and surfaces. *International Journal of Computer Vision* 13(2): 119–152. DOI:10.1007/BF01427149.



#### **4. ARTICLE 2: COMBINED FLOW ABSTRACTION AND CLIMATE CHANGE IMPACTS ON AN AGGRADING ALPINE RIVER**

This chapter, by Bakker, M., Costa, A., Silva, T.A., Stutenbecker, L., Girardclos, S., Loizeau J.-L., Molnar, P., Schlunegger, F., and Lane, S.N., has been published in *Water Resources Research* 54.

##### *Abstract*

Recent climatic warming and associated glacial retreat may have a large impact on sediment release and transfer in Alpine river basins. Concurrently, the sediment transport capacity of many European Alpine streams is affected by hydropower exploitation, notably where flow is abstracted but the sediment supply downstream is maintained. Here, we investigate the combined effects of climate change and flow abstraction on morphodynamics and sediment transfer in the Borgne River, Switzerland. From photogrammetrically derived historical Digital Elevation Models (DEMs), we find considerable net aggradation of the braided river bed (up to 5 m) since the onset of flow abstraction in 1963. Reaches responded through bed level steepening which was strongest in the upper most reach. Widespread aggradation however did not commence until the onset of glacier retreat in the late 1980s and the dry and warm years of the early 1990s. Upstream flow intake data shows that this aggradation coincided with an increase in sediment supply, although aggradation accounts for no more than 25% of supplied material. The remainder was transferred through the studied reaches. Estimations of bed load transport capacity indicate that flow abstraction reduces transport capacity by 1–2 orders of magnitude. While residual transport rates vary with morphological evolution, they are in the same order of magnitude as the sediment supply rates, which is why significant transport remains. However, the reduction in transport capacity makes the system more sensitive to short-term (annual) changes in climate-driven hydrological variability and climate-induced changes in intake management and sediment delivery rates.

##### *Key points:*

- Hydropower related flow abstraction may drastically reduce sediment transport capacity, but only to rates that are of similar magnitude as sediment supply.
- This causes downstream river bed aggradation and morphodynamics to be very sensitive to external forcing mechanisms related to flow management or climate change.
- Climate-driven sediment supply may propagate through Alpine streams despite large-scale flow abstraction.

## 4.1 Introduction

Many European Alpine glaciated basins are heavily impacted by hydropower exploitation. Besides classical flow impoundment, flow abstraction for within or between valley transfer is a common practice to cumulate hydroelectric capacity from multiple (adjacent) basins (Margot et al., 1992). Whereas reservoir dams tend to trap sediment behind them, leading to downstream sediment starvation (Petts & Gurnell, 2005; Williams & Wolman, 1984), run-of-the-river (e.g., Csiki & Rhoads, 2014) and flow abstraction schemes effectively allow sediment to pass through the river. Although the latter may be of primary relevance in Alpine regions, there are relatively few studies of their impacts upon sediment transport (e.g., Fergus, 1997; Raymond Pralong et al., 2015; Turowski & Rickenmann, 2009; Wold & Østrem, 1979) and very few studies of their downstream morphological impacts (e.g., Gurnell, 1983). As sediment production and delivery rates tend to be high in mountain environments (Hinderer et al., 2013), the volume of sediment that is trapped at flow intakes may be significant such that frequent purges are required to release sediment down the river (e.g., Bezingue et al., 1989). However, due to the reduction in total flow and with it transport capacity, the rate of downstream sediment transfer should be reduced and consequently lead to temporary or even permanent sediment accumulation (Gabbud & Lane, 2016; Lane et al., 2014). River bed aggradation in the affected Alpine streams may have profound impacts on riparian ecosystems (Gabbud & Lane, 2016; Petts & Bickerton, 1994) and infrastructure through increased risk of flooding (Lane et al., 2007), lateral channel instability and bank erosion (Church, 2006; Wheaton et al., 2013), and damage due to high sediment loads (Badoux et al., 2014; Hilker et al., 2009). On a larger scale, the sediment delivery to main rivers and deltas may be affected (Costa et al., 2017).

The direct impacts of human activity on river flow and hence sediment transport that arises from hydropower exploitation may be amplified by the indirect effects of human impacts that are manifest through climate change. Since the little Ice Age, large accumulations of unconsolidated sediment, derived from weathering and glacial erosion, have become available for transport (e.g., Haeberli & Beniston, 1998; Stoffel & Huggel, 2012). In the traditional model of paraglacial response (Ballantyne, 2002; Church & Ryder, 1972), the onset of glacial recession leads to high initial rates of geomorphic activity followed by a process of relaxation as a series of negative feedbacks create progressively greater levels of landscape stability. A critical question then follows as to what happens in such Alpine basins subject to accelerated climatic warming (e.g., Beniston et al., 1994; Gobiet et al., 2014) and associated glacial retreat which has been observed during the last decades (Haeberli & Beniston, 1998; Haeberli et al., 2007; Heckmann et al., 2016; Paul et al., 2004) and is projected in the future. There have been few studies that address the transient state of these environments (Haeberli & Beniston, 1998; Lane et al., 2017). An increase in fluvial sediment supply may be the direct result of

greater access to freshly exposed subglacial sediment (Lane et al., 2017; Warburton, 1990) as well as the effects of increased sediment transport capacity associated with more rapid ice melt (Raymond Pralong et al., 2015). Indirectly, sediment is also derived from hillslope erosion due to glacial debuitressing (Curry et al., 2006; Holm et al., 2004; Norton et al., 2010) and general permafrost degradation (Fischer et al., 2013; Gruber & Haeberli, 2007; Stoffel & Huggel, 2012). The actual system response to increased sediment supply is however complex (Harbor & Warburton, 1993), because the sediment flux through the landscape depends on the interaction between landforms and processes, including feedbacks and conditioned through the connectivity among them (Cossart & Fort, 2008; Geilhausen et al., 2013; Lane et al., 2017).

Thus, both flow abstraction and climate change are likely to have important consequences for sediment transfer and river morphodynamics in Alpine streams and their ecosystems. Yet, despite recognition of the need to factor sediment into water resource management (Wohl et al., 2015), there are very few studies of river response to human forcing of streamflow in combination with indirect human forcing of climate. This can be related to difficulties in quantifying the acting geomorphic processes, typically topographic change and bed load transport, on the relevant annual to decadal timescale, and the complexity and interaction of the processes involved. In this context, we aim to investigate the extent to which flow abstraction slows down the effects of rapid climate warming upon stream flow and sediment supply from propagating downstream through Alpine streams.

We focus on the Arolla Valley, Switzerland, which has long-term discharge records from flow intakes from which it is possible to reconstruct a unique record of reliable coarse sediment supply rates (e.g., Bezingue et al., 1989). Lane et al. (2017) and Micheletti and Lane (2016) used these to investigate the impact of climate change on sediment production and export from basins upstream of flow intakes. In this study, we use the same approach and, in addition, use archival photogrammetry to assess the impact of flow abstraction on the river bed evolution and sediment transfer downstream of hydropower intakes. The objectives of this paper are: (1) to quantify the evolution of river morphology and sediment transfer at the decadal time-scale; and (2) to assess the relative and combined impacts of climate change and hydropower exploitation on this evolution.

## 4.2 Study Area

The Grande Dixence hydropower scheme is located in the Pennine Alps of south-west Switzerland. It produces approximately 2 billion kWh of power per year and accounts for 20% of Switzerland's energy storage capacity. Constructed in the late 1950s, it abstracts water from the headwaters of two Upper Rhône tributaries, the Vispa and Borgne, via 75 flow intakes (Park, 1980). The water is transferred through a network of 100 km of tunnels and four pumping stations to the Lac de Dix (Figure 4-1a), a retaining reservoir in the adjacent Dixence catchment (Tanchev, 2014). From there the water is supplied to four hydropower stations in the Rhône valley (Bezinge *et al.*, 1989; Gurnell, 1983).



Figure 4-1 (a) Overview of Val d'Hérens showing the Borgne River and the downstream part of the Grande Dixence hydropower network; (b) The proglacial river reach of the Borgne d'Arolla is fed by the Bas Glacier d'Arolla (1987 maximum extent indicated) and purges from the Haut Glacier d'Arolla (HGdA), Upper Bertol (UB) and Vuibé (VU) intakes. The Lower Bertol (LB) intake lies just upstream of reach A. The cross-section (CS) is used for bed load transport capacity calculations; (c) Reach B receives flow from reach A that has passed through a narrow, incised reach and from the Tsjiore Nouvelle (TN) tributary. Reaches C and D receive flow from reach B that has passed through another narrow, incised reach. Images are from 2009 (Google Earth); a scale indication is included in (a) but decreases in downstream direction due to oblique imagery.

In this work we focus on the upstream part of the Borgne d'Arolla (Figure 4-1a), where flow has been abstracted since 1963 when the Lower Bertol (LB) intake (Figure 4-1b) and Arolla pumping station became operational. It is largely fed by the Bas Glacier d'Arolla (also known as the Glacier de Mont Collon) but indirectly also receives water and sediment from regulated catchments upstream through purges from three intakes. These are the Upper Bertol (Micheletti & Lane, 2016) and Vuibé tributary catchments, and most notably the Haut Glacier d'Arolla (HGdA) catchment (which has a surface area nearly 1.5 times that of the Lower Bertol). Sediment export from the latter catchment, investigated by Lane *et al.* (2017), enters the LB catchment on the flank of the retreating tongue of the Bas Glacier (Figure 4-1b).

Under normal flow conditions, all water is abstracted by the flow intakes. Downstream, the flow gradually increases due to unregulated tributaries, lateral drainage, and ground water emergence. During a purge from the LB intake, sediment is evacuated from a trap and is transferred downstream into a series of four braided river reaches, A through D (Figures 4-1b and c), which are separated by narrow, incised, semi-alluvial reaches (only reach C and D are more or less directly connected), and so are considered to be transport zones. A major tributary that is also subject to flow abstraction is the Tsijiore Nouve (TN) which has a relatively high sediment yield (as compared to LB; Gurnell *et al.*, 1988) and enters the Borgne d'Arolla between reaches A and B (Figure 4-1c). The studied braided reaches were established before the onset of hydropower activities (SwissTopo, 1946; Appendix A1, reach A, 1959), their presence associated with local valley widenings and reduced stream gradients upstream of tributary alluvial fans (Figures 1b and c). Further downstream, though not directly part of study area, the Borgne alternates between steep, e.g., between reach D and Les Haudères, and channelized sections, e.g., between Les Haudères and Evolène (Figure 4-1a) the latter which have a Post-Glacial history of braiding terraces (Small, 1973).

## **4.3 Methods**

### **4.3.1 Overview**

In this study, we draw upon two main sources of data to analyze the evolution of river bed level and sediment supply. First, we apply an archival photogrammetric method developed by Bakker and Lane (2017) to determine topographic and morphologic change of four braided river reaches since 1959, just before the onset of hydropower exploitation. Second, a record of the flow intake, just upstream of the reaches is used to quantify discharge, both the total “natural” discharge that would have occurred without hydropower exploitation and the residual “purge” discharge associated with intake flushing. This also allows us to determine sediment supply to the studied river reaches as a function

of the number and type of purges associated with emptying the sediment traps. From the determined topographic change and sediment supply, we calculate sediment transfer through the system. Finally, we analyze the forcing mechanisms that have contributed to the system evolution: (1) we quantify the impact of flow abstraction and regulation on transport capacity using a bed load equation; and (2) we compare climatic variability in seasonal temperature and precipitation to the variation in upstream sediment delivery.

#### 4.3.2 Morphologic Change Based on Photogrammetry

##### *SfM Archival Photogrammetry*

Topographic data are acquired using Structure from Motion (SfM) based photogrammetric methods which are described in full in Bakker and Lane (2017) and briefly summarized here. Scanned historical images are provided by the Federal Office of Topography (SwissTopo) for the period 1959–2005, with intervals of 4–12 years. Photographs from a specially commissioned low elevation flight in 2014 are used to extend the record. Pix4D, a commercially available software package, is used to perform photogrammetric reconstruction based on 15–25 ground control points and abundant tie-points generated using computer vision algorithms. This results in a bundle adjustment quality (i.e., reprojection error and control point RMSE), similar to values derived using classical techniques (Bakker & Lane, 2017). An overview of the image and bundle adjustment data is given in Table 1. The resulting densified point clouds are analyzed for potential systematic errors, resulting from random error in the bundle adjustments (Lane *et al.*, 2004), and these errors are minimized through point cloud registration. Stable zones from an additional data set, a 2 m resolution airborne laser scan survey for the year 2010 (ALTI3D data provided by SwissTopo), are used as a reference. The referenced point clouds are used to generate collocated 1 m resolution Digital Elevation Model (DEM) grids (Bakker & Lane, 2017).

In addition to providing DEMs, the photogrammetric analysis also produces orthoimages (provided in Appendix A1) with a ground resolution of 0.09–0.5 m (Table 1). These were used for morphological interpretation where we assess: sedimentation width defined as the active channel width plus overbank deposits, river morphology and channel configuration, riparian vegetation, human impact, and surface grain size.

Year	Scale [1 :x]	Ground resolution [m]	RMSE bundle adjustment [m]
1959	23200	0.49	±0.34
1965	21200	0.45	±0.45
1977	19600	0.27	±0.20
1983	19600	0.27	±0.23
1988	20900	0.29	±0.21
1995	26800	0.38	±0.32
1999	27000	0.38	±0.44
2005	24700	0.35	±0.38
2010*	-	0.50	-
2014	13900	0.09	±0.12

Table 4-1 Summary of Historical Aerial Photographs, Processed Using SfM Photogrammetric Methods, and Derived Bundle Adjustment Quality (From Bakker & Lane, 2017).

### Topographic Change

Local error in the DEMs is assessed based on orthoimage texture which was shown to have a strong impact on the ability of SfM methods to extract and match 3-D tie-points (Bakker & Lane, 2017). We quantify error using an entropy filter (with a  $9 \times 9$  cell running window) and inversely scale the obtained values to 0.5–2 times the theoretical precision which is estimated from the ground resolution. See Appendix A2 for further details. DEMs of difference (DoDs) are generated to quantify net topographic change, using basic error propagation (Brasington *et al.*, 2003; Lane *et al.*, 2004) and probabilistic thresholding (Lane *et al.*, 2003; Wheaton *et al.*, 2010). In this setting, the temporal resolution of the images is insufficient to assess morphological change using spatial coherence (Wheaton *et al.*, 2013, 2010), resulting in multiple noncoherent changes. We did add two basic constraints to filter local outliers from the DoDs: (1) a limit for maximum absolute change in elevation between consecutive DoDs (4 m) and; (2) a limit for maximum opposite changes between consecutive DoDs ( $\pm 1.5$  m), i.e., 1.5 m of erosion may be followed by 1.5 m sedimentation (or *vice versa*). In the latter case we average the consecutive change values as it was likely that there is an error in the common DEM. The resulting DoDs are clipped to the maximum sedimentation width, excluding areas where (temporary) sediment mining and construction took place. We then use the DoDs to determine net volume changes and mean elevational changes for the consecutive periods along the river channel, based on 90% confidence limits (Lane *et al.*, 2003). This provides us with a record of the decadal river bed evolution and gives us some insight (snapshots) in the shorter-term (annual) morphodynamics.

### Channel Gradient and Sediment Grain Size

We determine channel gradient and sediment grain size both to quantify their (relative) downstream trends and as input for further bed load transport capacity calculations. The mean gradient of the river channel is determined from the 2014 DEM (Figure 4-2). Local field measurements of surface

sediment grain size were performed using the Wolman (1954) count, grid-by-number approach (Appendix A3). These values are spatially extrapolated through two-dimensional semivariogram analysis of the 9 cm resolution 2014 orthoimage; for details on this method see Carbonneau *et al.* (2004). We use a  $25 \times 25$  cell running window ( $2.25 \times 2.25$  m) for which we quantify the semivariogram range distance and sill value. Both measured  $D_{50}$  ( $R^2 = 0.77$ ,  $p < 0.001$ ) and  $D_{84}$  ( $R^2 = 0.82$ ,  $p < 0.001$ ) show statistically significant relations with the bilinearly interpolated sill value (Appendix A3), despite the use of a relatively coarse image resolution. Because channel location and grain size vary in time, we derive a value for the regularly inundated section of the channel as the 20th percentile of the sill values within the cross-section (Figure 4-2). These values are in general agreement with a  $D_{50}$  of 18–35 mm found by Warburton (1992) in the proglacial zone, upstream from the intake.

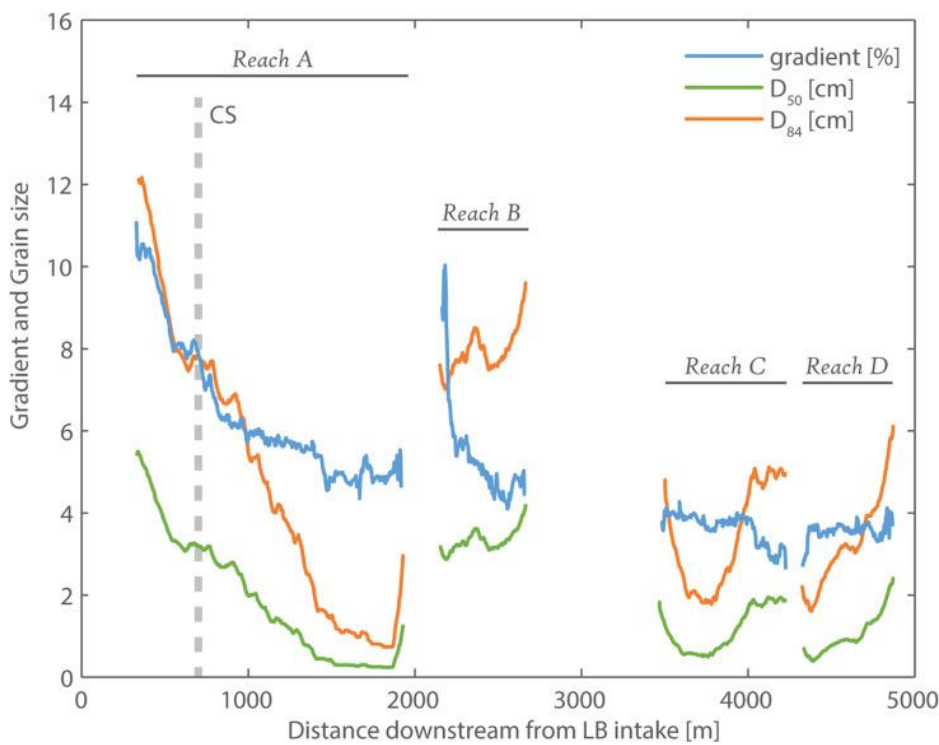


Figure 4-2 Long profile downstream from the Lower Bertol (LB) intake with average gradient and grain size  $D_{50}$  and  $D_{84}$  based on the 2014 DEM and orthoimage (a 200 m averaging window was applied to emphasize reach-scale trends). The cross-section where bed load transport capacity calculations were performed is indicated.

#### 4.3.3 Discharge and Sediment Supply

##### *Flow Intake Record and Purge Identification*

The main flow intake that we consider in this paper is the Lower Bertol (LB), for which we describe: (1) how the system functions and is operated; (2) how we used this to acquire up- and downstream discharge and sediment delivery. In addition we derive data for the TN intake, which functions in a

similar way to LB and is hence treated using the same method (see Appendix A5), and also use data of the HGdA intake from Lane *et al.* (2017).

The LB intake comprises two sediment traps (Bezinge *et al.*, 1989; Gurnell *et al.*, 1988): (1) a gravel and coarser material trap, which is purged using manual controls; and (2) a subsequent sand trap which is purged automatically. Flow enters the intake via the gravel trap, where the coarse bed load (gravel-boulders) is caught, and the water passes through a grill into the underground sand trap designed to allow sediment to settle out of suspension. The remaining flow, which has only wash load, passes over a broad crested weir and enters the hydropower tunnel system. The amount of water abstracted is measured using a stage recorder at the broad crested weir in the intake and logged for regulatory reasons. A 15 min interval time series for the period 1977–2014 is provided by Grande Dixence SA for the LB and TN intakes. During purges, the gates of one of either of the sediment traps are opened and water is allowed to flow down the river, flushing sediment with it (Figure 4-1 photo insert). This causes a rapid drop in water level at the weir and the intake of flow is temporarily stopped for the duration of the purge (Figure 4-3a).

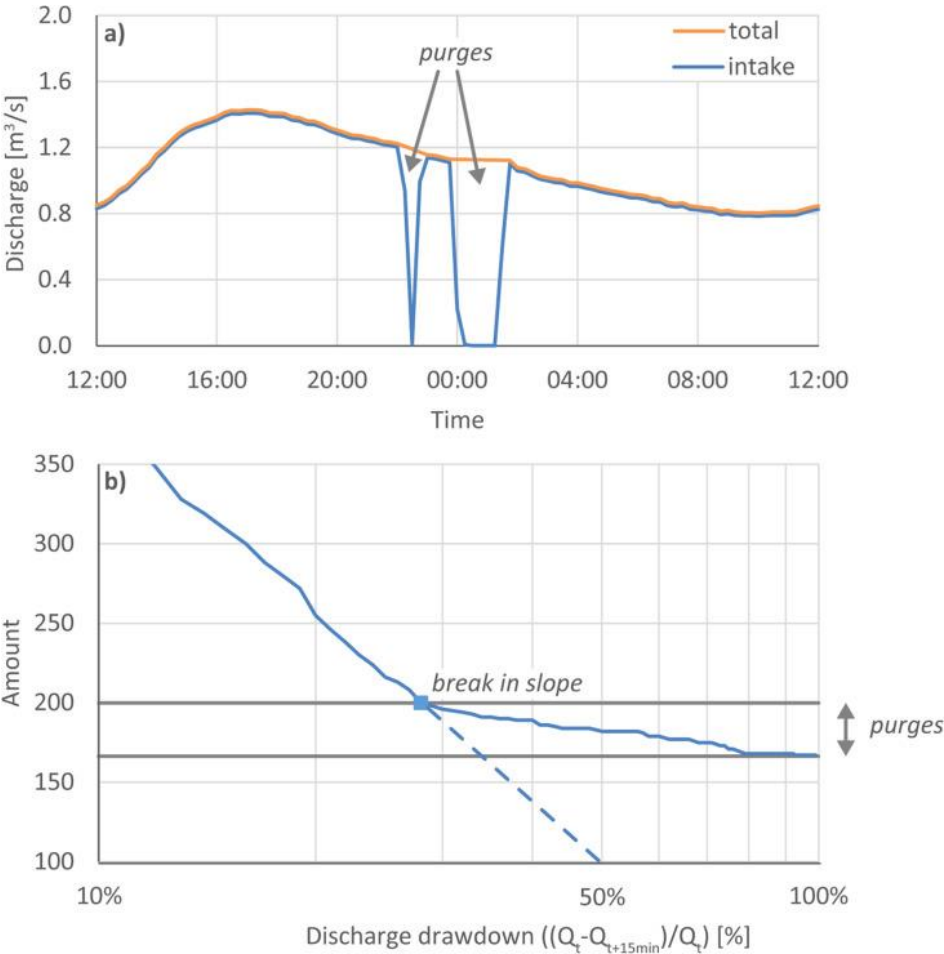


Figure 4-3 (a) Intake discharge and estimated total discharge for two purges; (b) Break in slope in the frequency distribution of discharge drawdowns; year 2006.

To obtain the total upstream discharge, we need to account for the periods of interrupted flow measurement during purges. As a first means of purge identification, we determined all instances where the discharge drops to zero, i.e., a 100% reduction, in a single time step. Where the discharge is averaged on a 15 min basis, the intake time-series may however not always reach zero, depending on the timing and duration of the purge, and therefore anomalously large discharge drawdowns need to be identified. We distinguish these by considering the frequency distribution of the relative changes in discharge per 15 min time step (Figure 4-3b). We note that under normal flow conditions, the occurrence of frequent fluctuations is typically described by a logarithmic distribution. If we extrapolate this, large drawdowns occur very rarely (dotted line). However, in practice, due to flow regulation, large drawdowns occur frequently due to the onset of purges. Where there is a transition in the distributions of the normal and purged flow, we find a break in slope (Figure 4-3b), which we use to identify purges. The purges are visually verified, where the HGdA discharge record (Lane *et al.*, 2017) is used as a reference to aid this process. In addition, we assess purges based on a minimum required flow volume to empty the sediment trap (600 m<sup>3</sup>; Figure 4-5).

Once the purges are identified, we apply linear interpolation to the intake time series over the duration of each purge to estimate both the purge discharge down the river and the upstream total discharge that arrives at the intake, the sum of the intake and purge discharge (Figure 4-3a). When LB purges coincide with those from upstream intakes, notably the HGdA, the discharge interpolation may lead to an underestimate. This is a common practice during night-time purges which were introduced in 2008 for safety reasons (to reduce the frequency of dangerously high flows during the day time) and to enhance sediment throughput. Occasionally, this is also a necessary practice when, during high flow events, the flow intake and transfer system is near or at its maximum capacity and flow abstraction must be stopped (Park, 1980). This results in longer duration, high flows in the river downstream of the intake. From the HGdA and LB time series, we determine the wave propagation time between the intakes as approximately 1 h ( $\pm$  15 min) by considering those purges from the HGdA that can be distinguished in the LB flow intake data (i.e., when the latter is not purging). For these events we perform linear regression analysis to determine the relation between the HG interpolated purge discharge and LB intake discharge, taking into consideration the required propagation time (Figure 4-4). Vice-versa, we also determine the relation between the measured HGdA intake discharge and measured LB interpolated purge discharge. This gives a lower slope due to the absence of the contribution of the HGdA purging (Figure 4-4). Based on the difference between these regression slopes over the period 1988–2013, we can account for an increase in the LB discharge equal to about 35% of the discharge that was released at the HGdA during purging, and

we add this to the LB purges to get a discharge estimate of the coinciding purges. We use this in the evaluation of the impact of flow intake management.

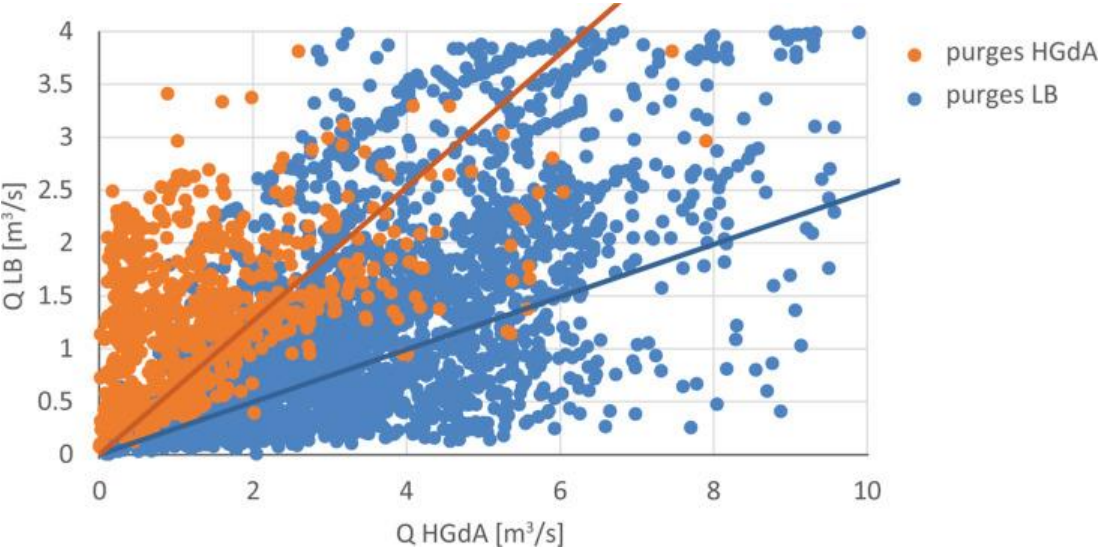


Figure 4-4 Discharge relation between Haut Glacier d'Arolla (HGdA) and Lower Bertol (LB) intakes during coincident purges (purges HGdA) and noncoincident purges (purges LB); period 2008–2013.

*Sediment Supply From Purge Frequency*

Because of the nature of the operating conditions, the intake data can also be used to infer the supply of bed load and suspended load to the intake and sediment delivery to the downstream reach. For the period 1977–1987, we use sediment load quantified by Bezinge *et al.* (1989), based on purge frequency and the dimensions of the LB sediment traps. They estimated the effective volume of purged sediment to be 150 m<sup>3</sup> for the gravel trap and 8 m<sup>3</sup> for the sand trap based on turbidity measurements and sediment height surveys in the gravel trap. Besides loads, it is also possible to obtain an indication of sediment grain size through distinguishing gravel and sand trap purges.

For the period 1988–2014, we use the estimated volume of water that is released per purge to distinguish the type of purge. We base this on a cumulative frequency analysis as shown in Figure 4-5. On the basis of the sand trap dimensions and a typical purge duration of less than 20 min, we estimate that up to 1,500 m<sup>3</sup> of water is required to evacuate the sand, which may be distinguished in the low occurrence frequency around this value (Figure 4-5). Purges of the gravel trap are longer, often more than 30 min, and are characterized by higher water volumes required to remove much larger amounts of sediment with greater resistance to motion. There is also greater variation in the water volume released due to their manual operation. Here, we distinguish night-time (just before midnight) purges which occur since 2008 when the gravel trap is more than half full. For these purges we assign 80% of the full intake capacity with an error of ±20%, following Lane *et al.* (2017). Last, we

identify high water volumes, larger than 17,000 m<sup>3</sup>, which are associated with (near) system surcharge events where flow cannot be abstracted, typically for a few hours, due to capacity limitations of the hydropower system. The sediment load is not easy to quantify where it does not accumulate to a known (sediment trap) volume but passes directly through. Based on the flow volume and typical duration (hours), we assign a sediment volume of  $4 \pm 1$  times the gravel trap capacity as an estimate of the sediment supply. To verify the cumulative frequency analysis we used purges identified from a minute-based time-series for 2015, which shows a similar volume frequency distribution, and for which a number of purges were observed and identified in the field. The same procedure was followed to establish sediment delivery for the TN intake (Appendix A5).

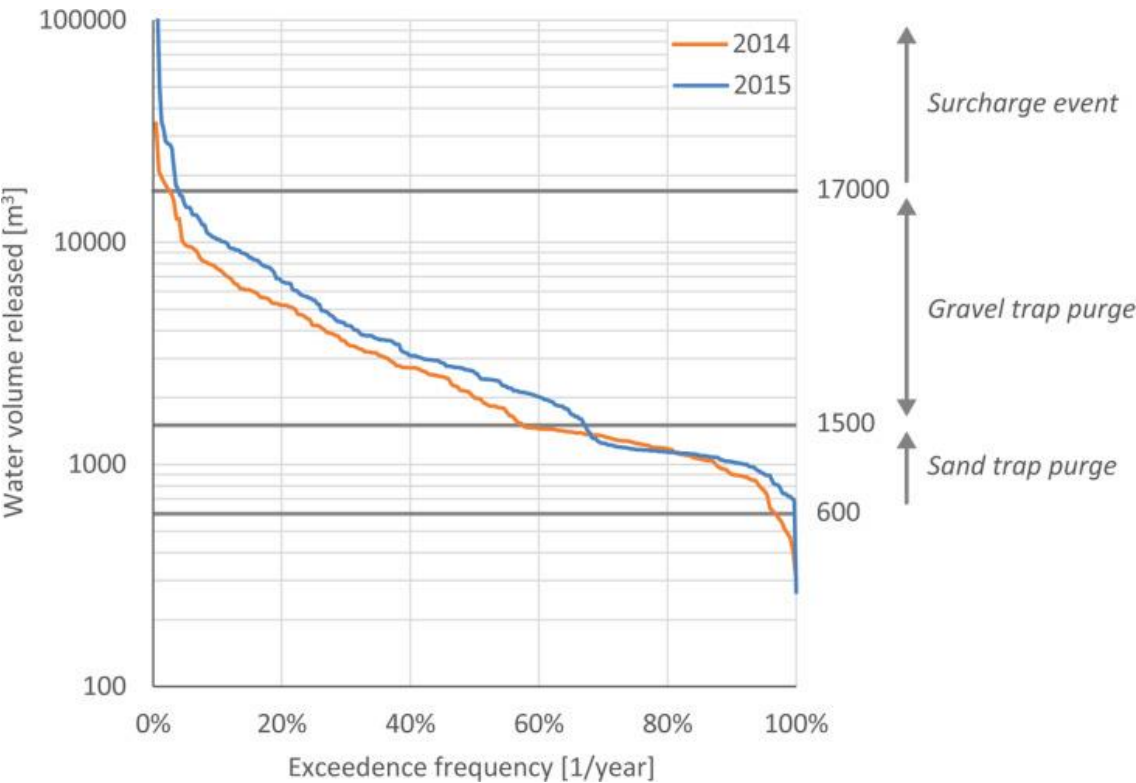


Figure 4-5 Cumulative distribution of the water volume releases as identified from 15 min data in 2014 (197 purges in total) and minute data in 2015 (May–November 2015, 313 purges in total), which forms the basis to distinguish between sand trap purges, gravel trap purges, and (near) system surcharge events.

The process of purge (type) identification and the calculation of sediment volumes contains a number of assumptions and uncertainties. We therefore identified a range in sediment supply where lower and upper limits are defined based on flow reduction for purge identification, 100% flow reduction and large drawdowns, respectively, and sediment supply using  $\pm$  estimates. We would however like to emphasize that the obtained time series of sediment supply may be considered to be fairly unique with regard to its accuracy, given the difficulty of measuring bed load transport rates

directly, and its timespan which covers decades (this was already recognized in the late 1980s by Bezinge *et al.*, 1989; Gurnell *et al.*, 1988).

#### 4.3.4 Sediment Budget and Sediment Transfer

We evaluate net sediment storage and transfer in the river reaches through applying a sediment budget approach (Warburton, 1990), which forms the basis to evaluate the system response to climate and human impacts (e.g., Harbor & Warburton, 1993). Although this approach may underestimate sediment transfer (Lane *et al.*, 1994; Lindsay & Ashmore, 2002), in this case the aggradational nature of the braided reaches and particularly the continuous record of sediment delivery from the LB intake, allow us to quantify sediment transfer more confidently. Since 1977, from which date we have sediment supply, the average annual sediment transfer rate is calculated for periods between the available aerial photographs for reach A individually and the combined reaches B, C, and D. From the intake sediment supply and the net morphological change in reach A, i.e., the change in sediment storage, we estimate the average sediment transfer rate through the reach following the Exner equation (after Ashmore & Church, 1998), assuming constant packing density (that is the packing density in the sediment traps is equal to that of the aggraded river bed). We do not account for sediment input from local bank erosion or sediment lost to gravel mining and river works, where they are difficult to distinguish and the latter largely involves the reworking of sediment within the reaches (rather than its removal) due to legislative constraints. Sediment that is transferred out of reach A is transported through a narrow, incised river section that stores negligible sediment and forms the upstream supply to the combined reaches B, C, and D. Here, we correct for the possible sediment transfer from the TN intake, which ranges between 0 and 100% of the supplied sediment. We do this because we seek to compare the sediment transfer efficiency of sediment that originates from the LB intake between reach A on one hand and reaches B, C, and D on the other hand, and not to analyze the transfer of sediment from the TN intake itself or the total sediment flux. Last, we note that wash load, though potentially significant in amount, is not considered in this context due to its absence in the supply record and its subordinate relevance in the downstream morphodynamics.

#### 4.3.5 Sediment Transport Capacity and Supply Capacity Ratio

Bed load transport capacity is modeled using the same approach as Lane *et al.* (2017) and following (Nitsche *et al.*, 2011), where we: (1) reduce the energy gradient due to flow resistance associated with river-bed macro-roughness based on Ferguson (2007) and Rickenmann and Recking (2011); (2) determine transport capacity using the shear-stress based bed load equation of Rickenmann (1991) that was shown to perform well in Swiss mountain streams (Nitsche *et al.*, 2011); and (3) account for

critical shear stress dependency on gradient (Heimann *et al.*, 2015; Lamb *et al.*, 2008), and transport of finer subsurface material during armor layer breakup (Günter, 1971; Hunziker & Jäggi, 2002), relevant in this setting (Warburton, 1992). See Appendix A4 for details. We quantify bed load transport capacity using discharges measured at the LB intake, and a cross-section 750 m downstream of the intake (CS in Figure 4-1a). This location is chosen to be directly downstream of a narrow (partly channelized) and steep section, just beyond a knick-point in slope (S) and grain size (D50, D84), as shown in Figure 4-2. Here, the channel is at its widest and the largest aggradation is expected (Lane *et al.*, 2014). Flow attenuation between the intake and this location is expected to be minimal. As the morphology is temporally (and spatially) variable, we calculate a range in transport capacity based on the cross-sections from the DEMs in the period 1988–2014 (Appendix A6). To compare the results with purged sediment volumes, we determine the volumetric transport capacity (V) based on the gravel trap packing density  $s = 1,300 \text{ kgm}^{-3}$ , as established by Bezing *et al.* (1989).

The modeling approach provides bed load transport capacity estimates for the period 1977–2014. The results are analyzed using a Supply Capacity Ratio (SCR) where the annual sediment supply that passes the intake is divided by cumulative annual transport capacity, so as to give a relative measure of the variation in sediment surplus that is supplied to the river (Lane *et al.*, 2017). We use this measure gain insight in the evolution of the sediment budget and to evaluate the human impact through comparison with the transport capacity that would have resulted in the absence of flow abstraction.

#### 4.3.6 Climate Change

Widespread temperature increase has been observed in the European Alps (Beniston *et al.*, 1994; Gobiet *et al.*, 2014), being more pronounced at higher elevations (Giorgi *et al.*, 1997). The increase has been particularly strong since the 1980s (Costa *et al.*, 2017) and is projected to continue into the future (Ceppi *et al.*, 2012). In addition to the mean temperature increase, the variability also appears to increase, with more frequently occurring heatwaves (Schar *et al.*, 2004). Precipitation trends are more regional, although here too an increase in variability is expected, associated with enhanced summer convective rainfall (Giorgi *et al.*, 2016).

Such trends, particularly the increase in the 1980s, can also be distinguished in spatially interpolated, daily temperature and precipitation data (MeteoSwiss, 2016a, 2016b) for the Bas Glacier catchment (Figure 4-6), based on Frei (2014); see also Costa *et al.* (2017). We aggregated this data to month-based periods that reflect seasonal changes in hydrology and runoff: summer (July–September) and winter/spring (January–May), which we refer to as “winter” hereafter. Note how these differ to annual averages on a year-to-year basis (Figure 4-6). These data have the necessary uncertainties for

local application, mainly systematic error in absolute values and in the case of precipitation variable error related to underestimation during strong wind (particularly in the case of snow) and high intensity precipitation (MeteoSwiss, 2016b). These however only have a limited effect on our forcing analysis, where we only consider relative changes over a long period of time where temporal weather variability may be expected to average out. Linear regression techniques were used to determine the correlation of summer temperature and winter precipitation on one hand with total annual sediment delivery and water yield at the LB intake on the other hand. Last, we determined the covariation of temperature and precipitation in order to assess their individual or combined forcing of sediment supply.

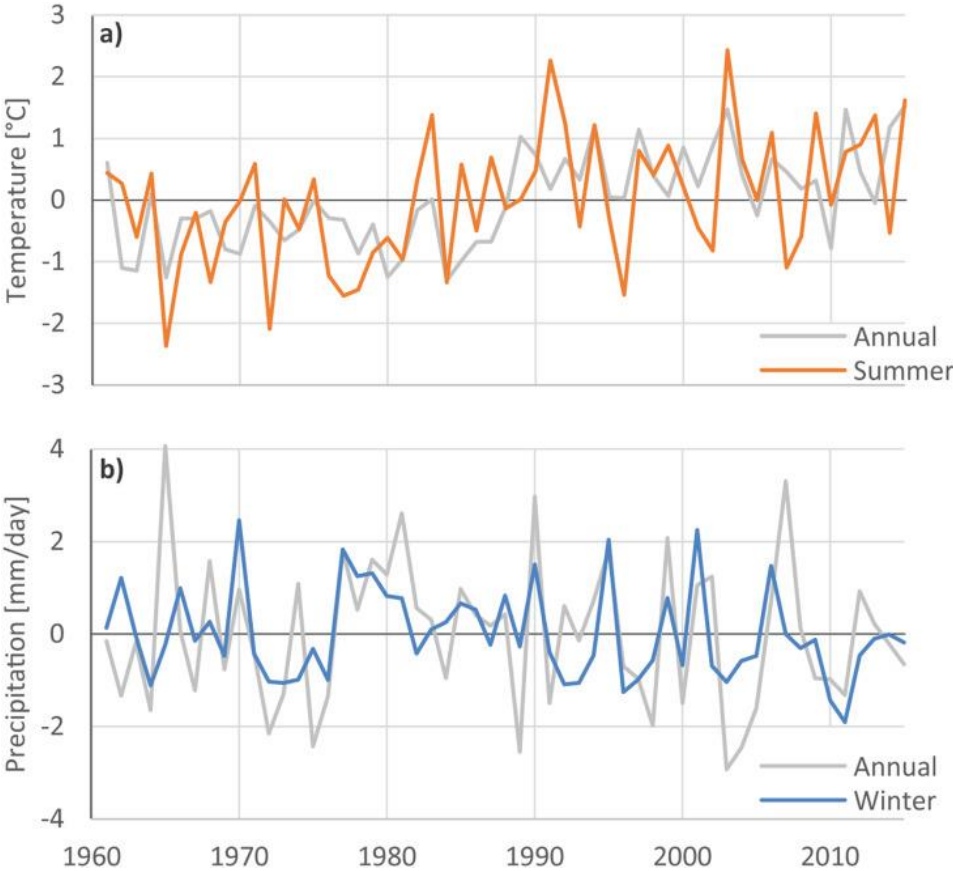


Figure 4-6 (a) Annual and summer (July–September) temperature; (b) annual and winter (January–May) precipitation. Values are spatially interpolated for the Bas Glacier based on Frei (2014) and given as deviation from the mean of the whole period.

## 4.4 Results

### 4.4.1 Evolution of River Bed Aggradation and Sediment Transfer

#### *Morphological Evolution River Bed*

Over the course of the investigated period, from 1959 to 2014, large-scale river bed aggradation took place (Figure 4-7). Sedimentation is widespread and prominent in all reaches, while net erosion is limited to banks in the upper parts of reaches A and particularly B. The largest increase in bed level, up to 5 m, took place near the upstream end of reach A where the channel widens and the gradient decreases (Figure 4-2). Not coincidentally, this is also a site of sediment extraction previously used for the construction of hydropower infrastructure (see also 1959 orthoimage of reach A in Appendix A1). To aid sediment throughput here, a straight channel was constructed on the right bank in 2012, clearly present as a thin zone of erosion in Figure 4-7. Reach D also shows extensive aggradation, but less within channel and more in the form of lateral or overbank deposits (Figure 4-7).

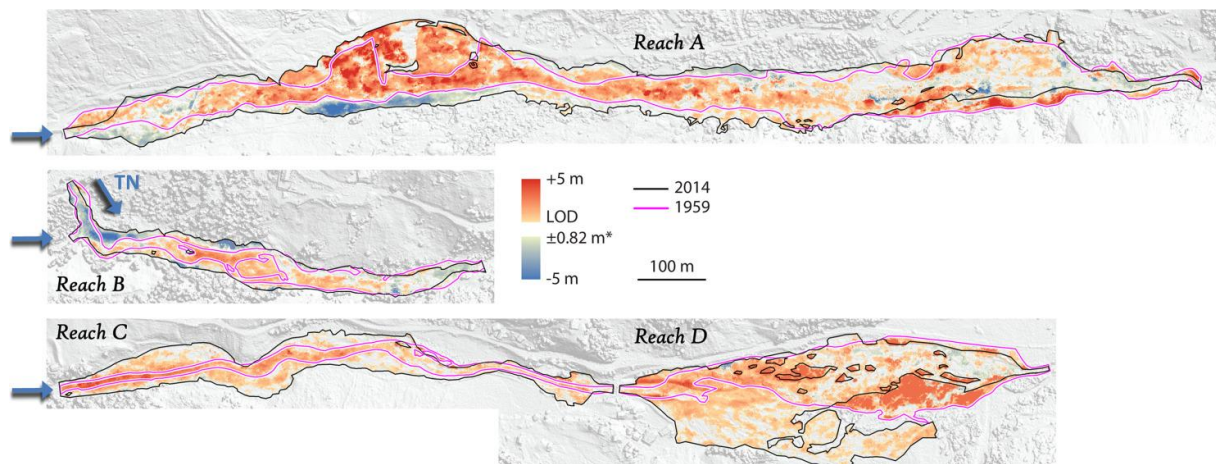


Figure 4-7 DEM of difference and river bed extent for the period 1959–2014 (background is a hillshade of the 2014 DEM). \*The theoretical limit of detection is given but the actual values vary based on the constituent orthoimage entropies. Arrows indicate flow direction.

The temporal evolution of the aggradation is shown in Figure 4-8. Considerable deposition occurred in reach A between 1959 and 1965 (Figure 4-8a), which can at least be partially related to the onset of flow abstraction in 1963. This was followed by a period with very limited net sediment accumulation which lasted until 1983 in the lower part of reach A and 1988 in the upper part of reach A. A phase of major aggradation, which is also reflected in an increase in both channel width and elevation (Figures 4-8b and c), then took place until 1995. A period of less change is then followed by a second phase of major aggradation between 1999 and 2005. In the last period, until 2014, the long-term trend of persistent aggradation is disrupted by substantial net erosion. Note that over the

whole period of net aggradation shorter periods of erosion may have occurred more often, but these cannot be resolved with the temporal resolution of the available topographic data.

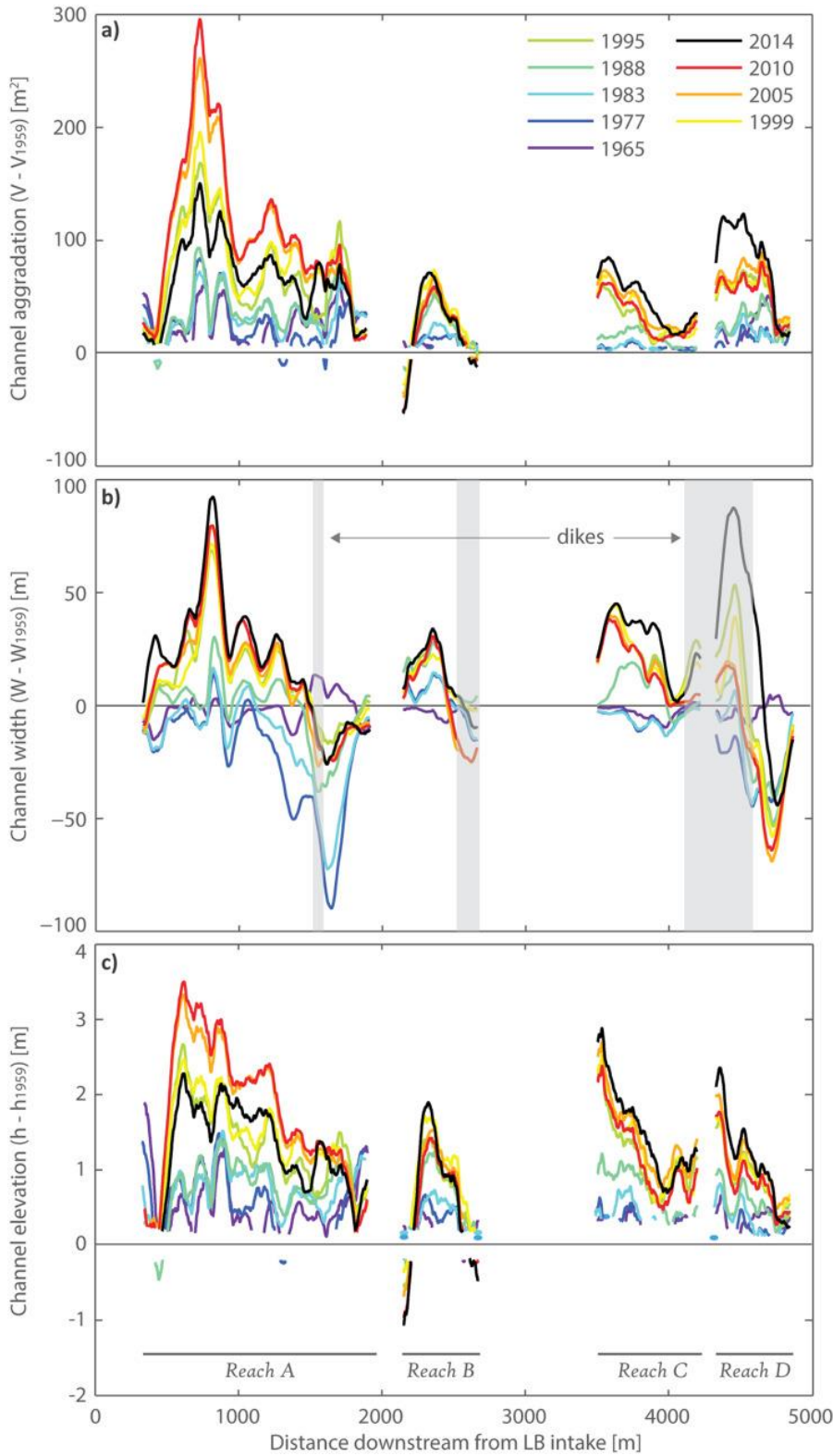


Figure 4-8 Long profiles showing channel change with respect to 1959 in: (a) volume; (b) sedimentation width; (c) elevation. A 200 m averaging window was applied to emphasize reach-scale trends. Note that for Figures 4-8a and c only values that exceed the detection limit are shown.

Until the early 1980s, reaches B, C, and D responded to a lesser degree as compared with reach A, although reach D does show a similar initial response (Figure 4-8a). In reach B, major aggradation occurred in the period 1983–1988, less so in reaches C and D. This prompted extensive river engineering and straightening in the downstream part of reach B (Figure 4-8b), while aggradation intensified in reaches C and D in the period 1988–1995. For reaches B through D, volumes of aggradation until 1995 are not much less than in reach A (Figure 4-8a). Until 2010, there is very limited aggradation and also some local erosion (e.g., between 2005 and 2010). Finally, between 2010 and 2014 sedimentation occurred, particularly in reaches C and D (overbank deposits, Figure 4-7), which appears to correspond to the erosion and release of sediment from reach A in this period.

Although net aggradation was limited, the river channel morphology changed considerably in the period between 1965 and 1988 as reflected in the sedimentation width (Figure 4-8b). Initially the channel contracted, adopting a more wandering or meandering character where bars were stabilized and riparian vegetation developed as shown in 1977 (see also orthoimages of reaches A and D in Appendix A1). Reach C was actually reduced to a low sinuosity single thread channel. These changes may be associated with the low frequency of channel perturbation and bed reworking following from the short and discontinuous nature of purge flows as compared with normal diurnal discharge cycles. After 1977, the channel expanded again to reach its original extent by 1988, in the process burying and removing most of the vegetation that had developed (see also Lane *et al.*, 2014). This corresponds to the increased aggradation in the 1980s (upper part of reach A and reach B). Large flood events in 1987 (Rey & Dayer, 1990; Warburton & Fenn, 1994) may have played a significant role in this morphological change. Later changes in sedimentation width (and also grain size; Figure 4-2) are locally influenced by river works for the protection of the pumping station (reach A), a campsite (reach B), and pastures (reaches C and D) along the river (dikes in Figure 4-8).

Aggradation since 1988 has led to a development of reach-based gradients in the rise of mean channel elevation. In reach A the bed level shows a sharp increase just downstream of the intake where the channel gradient decreases and the river widens, which then progressively decreases along the reach, effectively steepening the reach (Figure 4-8c). Together with the downstream fining trend (Figure 4-2), this illustrates the typical effect of a (maintained) high sediment supply and a significant loss of transport capacity due to flow abstraction and purge attenuation. The lower reaches, which become progressively less steep, mimic this trend although grain size trends are less clear due to TN input, general flow increase and river engineering impacts on channel morphology. These trends in bed level rise suggest that despite the significant (upstream) aggradation, sediment throughput was still sufficient to drive downstream morphological change.

### *Upstream Flow and Sediment Record*

The total annual volume of water arriving at the LB intake is shown in Figure 4-9a. The intake comprises flows from melt of the Bas Glacier, as well as residual flow (mainly purges) from upstream intakes of which the HGdA has by far the largest contribution. The LB inflow increased gradually in the late 1970s and 1980s, reaching its maximum in the early 1990s. This coincides with a transition from a colder and wetter period in the late 1970s (Micheletti *et al.*, 2015) to a warmer and dryer period in the early 1990s (Figure 4-6) and a transition from Bas Glacier advance before 1987 (Glaciological reports, 1881-2016) to retreat after 1987. From 1995 onward the inflow is lower again, but no decreasing trend is observed. Although the Bas Glacier has retreated significantly and lost most of its low altitude ice volume, rising temperature may have increased melt in the higher parts of the basin so sustaining water yield. Since 2003, a rising purge frequency from the HGdA led to an increase in its contribution to the LB flow from approximately 1–6% (Figure 4-9a).

Similar to water yield, the sediment supply to the LB intake shows a steady increase in the 1980s, reaching peak values in the early 1990s (Figure 4-9b). The latter coincides with the onset of rapid sedimentation in the braided reaches, particularly in reach A (Figure 4-8a). After a period of lower sediment supply, the rates increased in 2003 and particularly 2011. The evolution of sediment supply is in broad lines similar to that of the HGdA (Lane *et al.*, 2017), which potentially accounts for about 30% of the sediment availability in the Bas Glacier (sub/)proglacial area and supply to the LB intake. The TN intake, which enters the Borgne downstream of reach A, shows a purging evolution similar to LB (Appendix A5), with the exception that supply rates in the 2000s remain low until 2010 when there is a sharp increase.

The LB purge record may also provide an indication of the sediment composition. We found a relatively low number of sand trap purges when compared to Bezinge *et al.* (1989), who found that the purge frequency was more or less similar to that of the gravel trap in the period 1977–1989. This could be due to an actual decrease in fine sediment supply, although this cannot be verified due to uncertainties in purge identification related to the small size of the sand trap (and therefore small volume of water required to purge it, which is difficult to detect as a drop in the flow intake series; Figure 4-3a). Here we would like to emphasize that whilst the number of gravel trap purges fluctuate, the number of sand trap purges remain fairly constant until a systematic increase around 2005 (only 2009 is an exception).

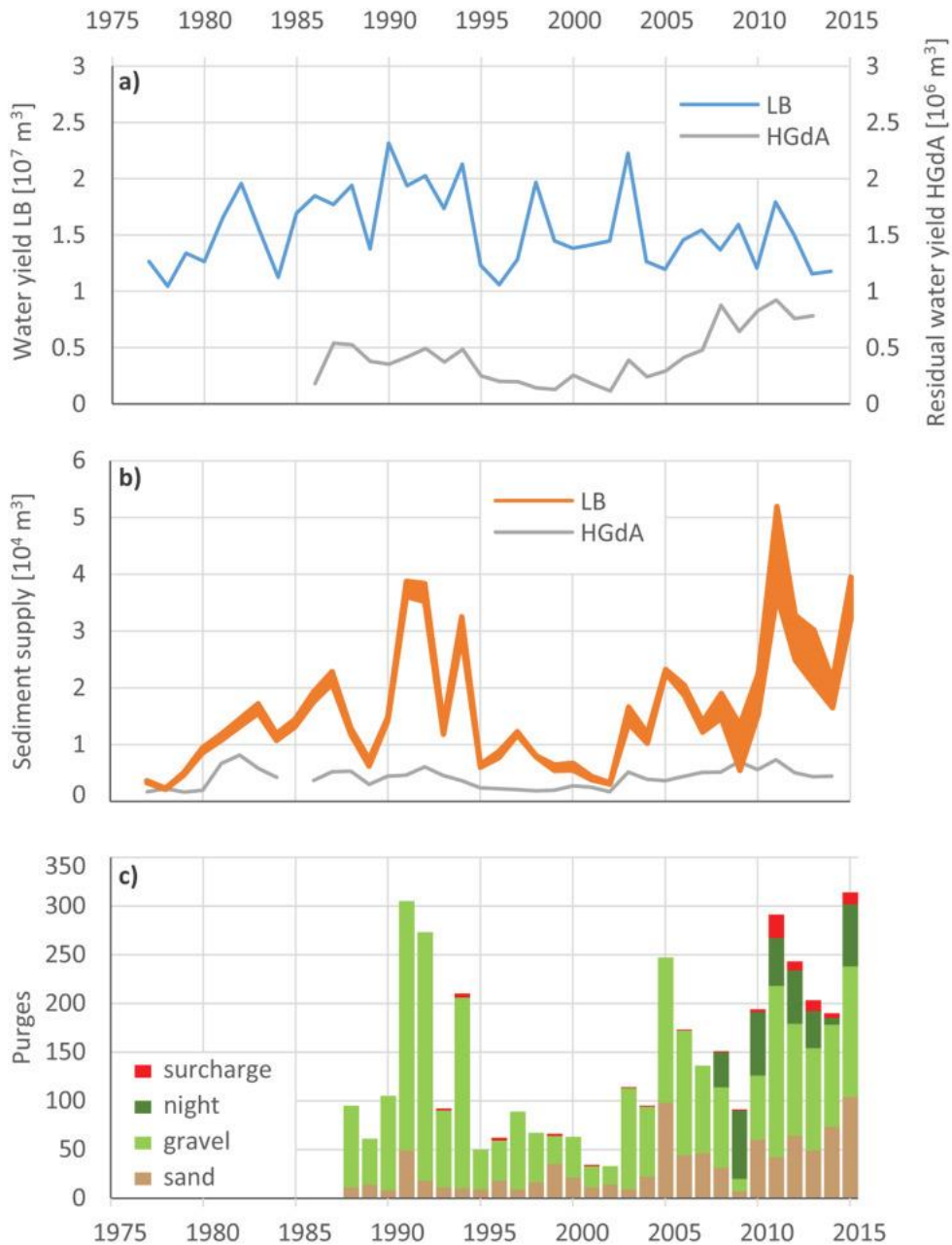


Figure 4-9 (a) Annual water yield at the LB intake and the residual water yield (mainly purges) from the upstream HGdA intake—note that the latter is a factor 10 smaller; (b) calculated (range in) sediment supply at the LB intake and HGdA intake and; (c) identified purges per type at the LB intake: sand trap, gravel trap, night-time purge (gravel trap), and (near) system surcharge events. The uncertainty range in LB water yield due to system surcharge is too small to be visible in Figure 4-9a. The uncertainties in purge identification and sediment volume are reflected in the range in supply values in Figure 4-9b. Data from HGdA is based on Lane et al. (2017).

### Sediment Transfer

Figure 4-10 shows the evolution of sediment input from the LB intake and the subsequent sediment transfer through reach A and reaches B, C, and D since 1977. Although we have no sediment delivery rates from before this period, we can infer that between 1965 and 1977, when net erosion occurred,

all incoming sediment (i.e., > 100%) was transferred through reach A. Between 1977 and 1983 the sediment supply rate was low (Figure 4-9a). This sediment was largely transferred through the reaches (Figure 4-10b) and there was some net aggradation in the lower part of reach A (Figure 4-8a). Between 1983 and 1988, there was a substantial increase in sediment input to reach A (Figure 4-9), but the reaches appear to be able to transfer this increase nearly in its entirety through to the end of reach D. A further increase in supply from the LB intake, (Figure 4-10a) between 1998 and 1995, led to major river bed aggradation in reach A (Figure 4-8), and a drop in the relative amount of sediment transfer through the reach (Figure 4-10b). Reaches B, C, and D also show considerable aggradation (Figure 4-8), but this change could be accounted for by sediment from the TN intake. Between 1995 and 1999, the sediment input to reach A drops markedly (Figure 4-10a), but the low rate of sediment transfer (Figure 4-10b) is maintained. The rate of sediment transfer through reach A falls further between 1999 and 2005, which taken with a slight increase in sediment supply results in rapid aggradation (Figure 4-8a). Given the uncertainty range due to the supply from the TN intake, no significant change could be detected in the transfer of sediment that originates from the LB intake through reaches B, C, and D, which remains around 100% during the period 1977–2005.

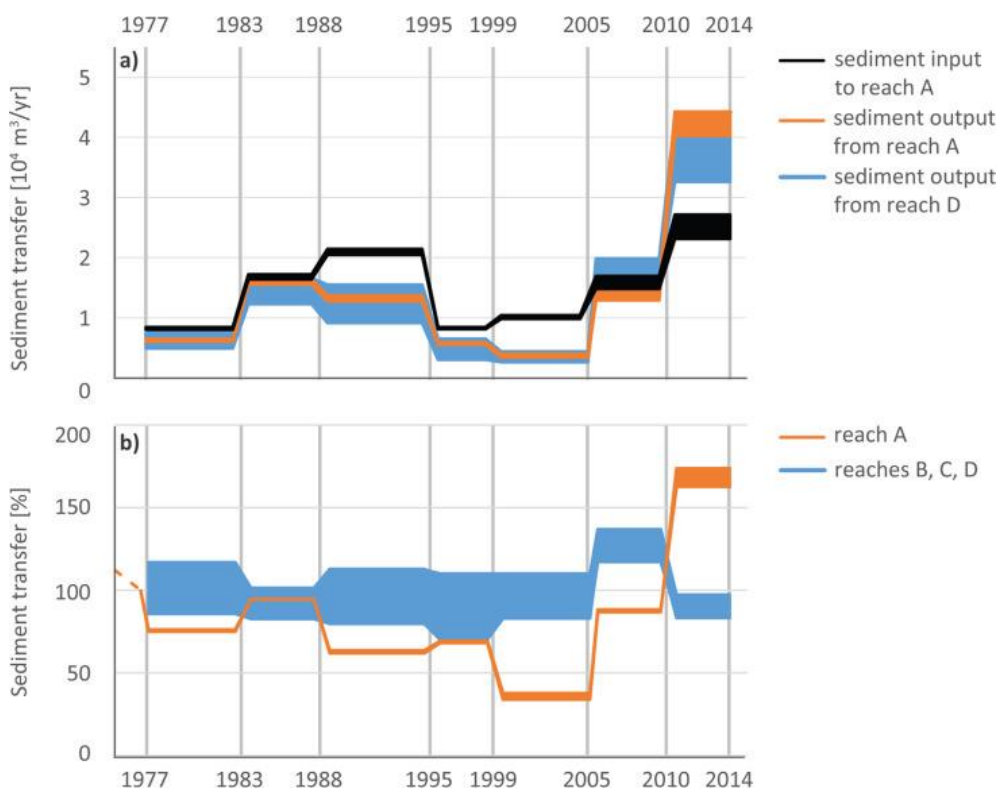


Figure 4-10 (a) Sediment transfer rate as absolute value and; (b) sediment transfer as percentage: sediment exported from the reach divided by sediment supply to the reach. The annual values are averaged for periods between the available aerial photographs. The given ranges reflect uncertainties in sediment supply and, in the case of reaches B, C, D, uncertainties regarding the possible sediment transfer from the TN intake; uncertainties in reach storage are negligible.

There seems to be a marked change in the system after 2005. Sediment supply at the LB intake rises and reaches a maximum in 2010–2014 since the data begin in 1977 (Figure 4-10a). Between 2005 and 2010, there is net aggradation in reach A (Figure 4-8a), with sediment transfer that rises, but remains lower than 100% (Figure 4-10a). However, reaches B through D degrade during this period (Figures 8b and 10b). The inverse then occurs between 2010 and 2014 when despite very high sediment supply to A (Figure 4-10a), reach A shows net degradation (Figure 4-8a) and a high sediment transfer rate (Figure 4-10b). The latter, in turn, appears to lead to net sedimentation in B through D (Figure 4-8a) and a sediment transfer rate slightly lower than 100% (Figure 4-10b).

Over the whole period, more than 75% (76–97%) of the sediment that enters the system is transferred through all reaches. Thus, despite the considerable impacts of flow abstraction and profound morphological changes of the river bed, relatively high rates of sediment transfer downstream are maintained. In addition, it appears that under a system with substantial flow abstraction, relatively small changes in sediment supply can lead to relatively major morphological responses (Figure 4-8). We develop these points further by assessing bed load transport capacity.

#### 4.4.2 Forcing of Sediment Supply and Transport Capacity

##### *Hydrologic Forcing Due to Flow Abstraction*

On annual basis, the total fraction of water that is abstracted is in the range of 85–99% (Figure 4-11a). The water that is not abstracted is largely used to evacuate sediment from the intake during purges, resulting in relatively lower amounts of abstraction when there is high sediment supply in the first half of the 1990s and since the mid-2000s (Figure 4-9b). The capacity of the hydropower intake system to abstract water and at the same time to reduce the residual flow in the river is related to magnitude of the discharge as is shown for different annual exceedance durations in Figure 4-11a. During high discharges (e.g., flows exceeded less than 1 day per year), the hydropower system is typically operating near its maximum capacity due to abstraction of similarly high discharges from catchments higher up in the system. In this case, the intake of water at the LB intake (but similarly for HGdA and TN) has to be temporarily stopped to prevent the surcharge of the system. A trend emerges, where the effect of flow abstraction becomes less with increasing discharge (Figure 4-11a). In addition, a temporal trend may be observed since the mid-2000s, where the effect of flow abstraction decreases (for all exceedance durations) to more or less 0 for the highest flows (1 h per day) since 2010. The latter coincides with a marked increase of (near) system surcharge events (Figure 4-9b) as the limited capacity of the hydropower system is becoming increasingly insufficient to accommodate the increasing peak discharges from the hydropower catchment, and for periods of some hours, all water delivered to the intake is allowed to pass downstream.

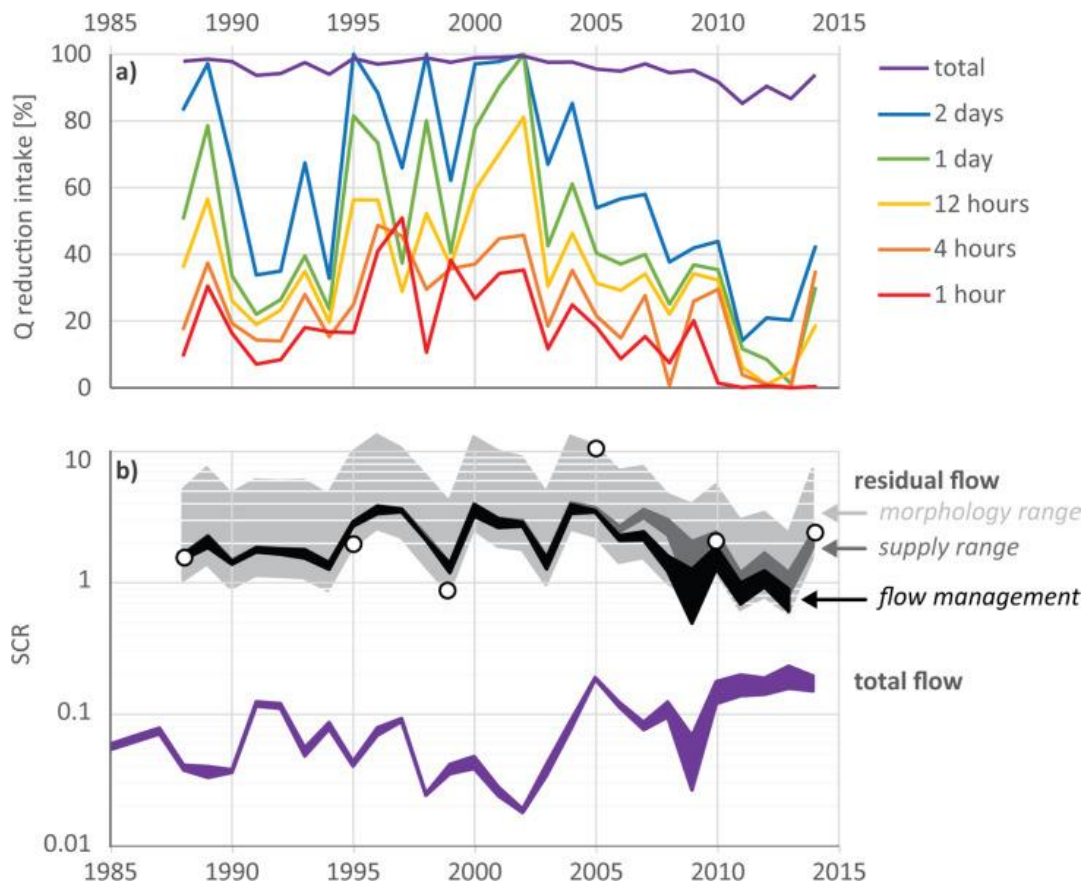


Figure 4-11 (a) Discharge reduction due to flow intake for total discharge and discharges exceeded for durations ranging from 2 days to 1 h per year; (b) Supply Capacity Ratio (SCR) for residual flow and total flow: The “morphology range” reflects the calculated range in transport capacity related to (temporal) changes in cross-section with a constant (maximum) sediment supply (see Appendix A6); where the year and applied cross-section correspond, the SCR values are plotted as a point (temporal changes in grain size are not accounted for). The “supply range” reflects the uncertainty in sediment supply with the transport capacity based on the 2014 cross-section. “Flow management” reflects the effect of coinciding purges from HGdA and LB intakes on transport capacity based on the 2014 cross-section. The SCR for total flow includes the uncertainty in sediment supply and the transport capacity based on the 2014 cross-section.

If we consider the Supply Capacity Ratio (SCR) downstream of the intake under natural conditions (no flow abstraction), values are in the order of 0.02–0.2 (Figure 4-11b). Thus in this case, sediment supply would be substantially lower than transport capacity throughout the period. From 2005 onward, there is a notable increase in SCR (Figure 4-11b) which is associated with an increase in sediment load and fairly constant discharge (Figures 4-9a and b). Note that the calculated bed load transport capacity is only indicative as it is artificial to combine the morphology under a flow abstraction regime with a natural flow regime. In reality, SCR values lower than 1 should lead to erosion, channel geometry changes, grain size sorting, and stream bed armoring to the point at which the transport capacity is reduced and the SCR tends to 1.

Under the actual conditions (with flow abstraction), the SCR is greater than 1 (Figure 4-11b): the transport capacity of the residual flow is ca. 3 times smaller than the supply, which is commensurate with the observed aggradation here (Figure 4-8a). There is a significant band width associated with these calculations due to uncertainties in sediment supply but more notably due to the effect of temporal changes in morphology (see Appendix A6). Morphological change may have led to reinforced transport capacity in periods of relatively low sediment supply, e.g., 1999, or reduced transport capacity in periods of increased sediment supply such as in 2005 (Figure 4-11b), although we must note that in the same period river engineering also took place. Since the mid-2000s, the SCR values have generally decreased and approached the point at which the increase in purge discharges (Figure 4-9a) is sufficient to transfer the increasing rate of sediment supply:  $SCR \approx 1$  (Figure 4-11b). This is reinforced by the effect of coordinated purges and occurrence of (near) system surcharge events; note that this effect is negligible (not visible) for the total discharge. Whereas these calculations are an estimation and do not take into account spatial changes in river morphology, they do indicate a tendency toward reduced sedimentation rates and potential erosion in the last few years, particularly for the finer fractions (e.g. sand).

Even with a substantial reduction in transport capacity due to flow abstraction, there remains sufficient flow to transport a significant proportion of sediment through the system, explaining sediment export between 2005 and 2014 in Figure 4-11b. In addition, the SCR of the natural and purged discharges converge through time, suggesting that the impact of flow abstraction is decreasing. We attribute this change to the changing flow duration (Figure 4-11a) associated with purge management, in the form of a shift toward coordinated night-time purging, and capacity limitations of the hydropower system, resulting in flow intake limitations and consequent high flow events.

#### *Climate Forcing and System Response*

Sediment supply showed the strongest monthly-based correlation with both average daily summer temperature, in the period July–September, and average daily winter precipitation, in the period January–May. Figure 4-12a shows that summer temperature directly forces sediment delivery to the intake through ice melt which both releases sediment and affects the magnitude and duration of competent stream flow, that is sediment transport capacity. No relation was found with summer precipitation, however precipitation in the preceding winter is negatively associated with sediment supply; this reflects snow cover persistence which has a buffering effect on the summer ice melt (Figure 4-12b). Summer temperature and winter precipitation show weak but significant covariation ( $p < 0.05$ , not shown here) and were therefore reduced to a single principal component which

reflects 66% of the common variance. Their combined effect is reflected in the “climate” principal component (Figure 4-12c) which reveals a clear and direct, annual response of sediment delivery to climatic conditions.

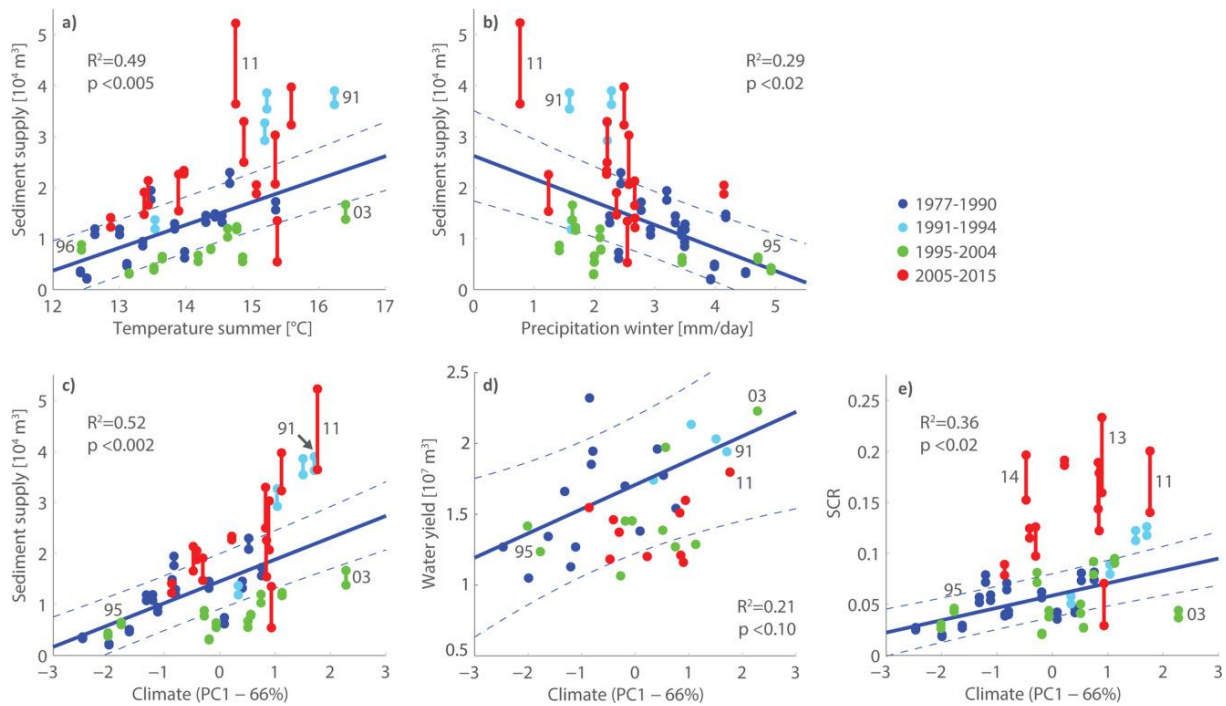


Figure 4-12 Climate forcing of sediment supply and discharge; (a) correlation summer temperature and sediment supply; (b) correlation winter precipitation and sediment supply. Correlation “climate” principal component with: (c) sediment supply; (d) water yield (2015 is not included due to the incomplete discharge series) and; (e) Supply Capacity Ratio (SCR), where the bed load transport capacity of the total discharge downstream of the intake is used. Exceptional years are marked (e.g., 11 is 2011) and the regression line,  $R^2$ ,  $p$  value and 80 percentiles are based on the reference period 1977–1990.

Based on Figure 4-12c we identified four periods with characteristic sediment delivery due to climate forcing and system response. As a reference we used the linear correlation for the period 1977–1990 ( $R^2 = 0.54$ ,  $p < 0.002$ ), which seems to reflect the ice melt and sediment transfer reasonably well. In this period gradual climatic change (Figure 4-6) led to a steady increase in sediment delivery (Figure 4-9b). The particularly warm and dry 1991 marks the beginning of a few years with relatively high sediment delivery rates which may be related to the close-proximity and retreat of the Bas Glacier, with retreat starting not much earlier (since 1987). Following the particularly wet 1995 and cold 1996, sediment delivery rates dropped, remaining relatively low until the early 2000s. Then a transition took place starting in 2003, a dry and the warmest year in the series, when delivery rates are still relatively low, to relatively high values from 2005 onward (only 2009 is markedly lower). A further increase occurs from 2011, the driest year in the series (see also Figure 4-6). This evolution

suggests that climatologically exceptional years, i.e., dry and warm or wet and cold, can lead to an increase or decrease in sediment flux that persists over a longer-than-annual time-scale (Figure 4-12c). These changes can be associated with changes in geomorphic functioning of the catchment system, which may pertain sediment availability, system connectivity, or transport capacity.

Figure 4-12d shows a similar plot of climate forcing on the measured annual water yield for the earlier defined periods. The correlation is less clear and less strong than for sediment supply (for the reference period  $R^2 = 0.21$ ,  $p < 0.02$ ). The periods here are much less distinct, emphasizing that it is probable that the more distinct periods in sediment delivery (Figure 4-12c) relate to differences in sediment access and connectivity. The periods in Figure 4-12d also show a progressive decrease in water yield with respect to the climate reference. If we take this one step further and take into account the evolution of transport capacity in the form of the SCR, the period since 2005 shows an even clearer increase in the effective sediment supply (Figure 4-12e). Interestingly, the differences between the reference period and the periods 1990–1994 and 1995–2004 are less distinct, suggesting a larger role for transport capacity here in the supply of sediment. The observations from Figure 4-12e however need to be taken with care as we determine bed load transport capacity just downstream of the intake and the local morphology is affected by purging as mentioned earlier. In general, the results illustrate the complexity and potentially large response of the proglacial margin in terms of sediment access and transfer. The direct response and sediment transfer here also support the observation of large transfer rates downstream of the intake.

## 4.5 Discussion

### 4.5.1 Morphological Response to Sediment Supply and Transfer

Widespread aggradation of up to 5 m was found in the upstream braided reaches of the studied river since the introduction of flow abstraction and sediment purging in the early 1960s (Figure 4-7). An initial morphologic response was identified (in the period 1959–1965) although modest and short-lived, particularly compared to the aggradation that has occurred since the 1990s (Figure 4-8a). The following phase of morphologic evolution, between 1965 and the mid-1980s, is characterized by relatively low levels of net aggradation (Figure 4-8a). The river does however respond by channel narrowing, bar stabilization, and vegetation encroachment (Figure 4-8b; 1977 orthoimage reach A in Appendix A1; see also Gurnell, 1983), which can be attributed to the reduced frequency of stream perturbing flows since the onset of flow abstraction. These changes appear to reflect the classic model of river response downstream of reservoir dams, where vegetation encroachment often

occurs (Church, 1995; Petts & Gurnell, 2005; Williams & Wolman, 1984) even if in this case there was bed aggradation rather than degradation.

From the mid-1980s, and notably between 1988 and 1995, significant aggradation took place both through lateral channel expansion and an increase in bed level elevation (Figure 4-8). A similar transition in the proglacial channel upstream from the intake was noted by Warburton (1994). The aggradation was widespread, volumes comparable between the reaches studied, with only the upstream part of reach A receiving considerably larger amounts of sediment. The aggradation was accompanied by the steepening of reach-based bed gradients (Figure 4-8c) and to a lesser extent gradients in grain size (Figure 4-2). The greatest aggradation and coarsest sediment is found in the upstream part (or near upstream part in the case of reach A) of each reach. Here, sediment laden purges emerge from steeper and more confined reaches and are attenuated due to a decrease in channel gradient, an increase in flow width and are partially absorbed by the coarse and dry river bed (e.g., Buffington & Tonina, 2009). This morphological signature may be typical for flow abstraction where sediment supply is maintained, most likely preventing the natural morphological evolution following from glacier recession and associated vegetation and ecological succession (Klaar *et al.*, 2015). These results emphasize the observations of Wohl *et al.* (2015) and Gabbud and Lane (2016) that sediment regime needs to be factored into the design of river flows that might improve the ecological status of such streams.

The temporal changes in reach aggradation show little evidence for sequential morphologic response of the reaches (Figures 4-8a and b). A lag in sediment transfer and subsequent downstream propagation of a sediment wave (e.g., Nicholas *et al.*, 1995) may be expected in this setting due to reduced transport conditions (Gabbud & Lane, 2016; Lane *et al.*, 2014), but this is not apparent at the temporal resolution, between 4 and 6 years (with the exception of 1965–1977), of the topographic data. The dynamic river bed and relatively high transfer rates lead to rapid topographic change throughout the reaches in the 1980s (reach B) and more prominently in the early 1990s (reaches A, C, and D). This change occurred in more or less direct response to increased sediment supply from higher up in the catchment relative to the (earlier) hydropower-reduced sediment transport capacity.

Despite there being a major reduction in sediment transport capacity due to flow abstraction (Figure 4-11b), the morphological evolution and downstream extent of aggradation indicate that sediment may still be transported through the river reaches (Figure 4-8a). Indeed, the evolution of the sediment supplied to the upstream reach A mirrors the sediment export from downstream reach D (Figure 4-9a), emphasizing that notwithstanding a substantial amount of sediment that was stored in the reaches since the onset of flow abstraction (Figure 4-7a), significant sediment transfer to

downstream reaches is maintained. This is supported by similar trends in bed level aggradation and lateral expansion of the Borgne near Evolène and confidential gravel mining data from a site downstream. Particularly the finer fractions, if they are not abstracted with the water through the intake system, are expected to be transferred fairly efficiently downstream to the Rhône as flow increases (from tributaries with relatively low sediment loads) and the channel is generally constrained. This would suggest that the introduction of flow abstraction in the 1950s and 1960s (Park, 1980) may have had only a limited impact on decreasing suspended sediment loads in the same period (Loizeau & Dominik, 2000).

In general, our findings show that effects of flow abstraction schemes on downstream morphology and sediment transfer are distinctly different from those of classical reservoir dams. This difference can effectively be explained by the (designed) sediment storage capacity of these systems which leads to different timescales on which sediment flushing may take place: hourly to daily purging, in the case of sediment traps at flow intakes, or infrequent to no flushing at all, in the case of reservoir dams. This difference in sediment purging frequency together with the reduced flow, common to both flow intake and reservoir dam systems, then impacts on the natural channel dynamics and riparian ecology. In flow abstraction systems, we typically find river bed aggradation with sediment throughput and ecological degeneration (Gabbud & Lane, 2016) as compared with downstream of reservoir dams where river bed degradation with sediment starvation and ecosystem stabilization has been observed (e.g., Petts & Gurnell, 2005; Williams & Wolman, 1984).

#### 4.5.2 Climate Forcing of Sediment Delivery

Climate has a strong impact on annual sediment delivery to the upper Borgne d'Arolla (Figures 4-12a to c). High summer temperatures allow for high rates of glacial melt, which simultaneously releases sediment and provides enhanced flow to transport that sediment (Lane *et al.*, 2017). Preceding winter precipitation modulates this effect, where a thick snow cover may delay and shorten the period of summer ice melt. Despite significant flow abstraction, the system downstream of the intake is able to maintain significant sediment transfer (Figure 4-10b), which means that the climate signal is also propagated through the braided river reaches and potentially further through the basin. Indeed, the climate driven increase in glacial sediment export we found in the late 1980s to early 1990s corresponds with an increase in suspended sediment from the Upper Rhône basin as measured near the outlet into Lake Geneva (Costa *et al.*, 2017).

Superimposed on annual variability, climatically exceptional years appear to have an indirect impact on a larger time-scale, of a few years to a decade, through forcing changes in upstream sediment dynamics (Figure 4-12c). The periodic changes shown in Figure 4-12c may relate to systematic

changes in sediment availability and transfer within the proglacial margins of upstream glaciers, as they retreat rapidly. This is a process which initially releases sediment, in the early 1990s, and subsequently feedback processes may reduce that availability (Lane *et al.*, 2017), although this reduction can at least in part be explained through reduced transport capacity (Figure 4-12e). From the mid-2000s there is a marked change in sediment supply, which can be related to supply from the HGdA and the retreating and thinning ice of the Bas Glacier. Initially, HGdA originating sediment that has previously accumulated under the Bas Glacier is released through improved connectivity following glacier recession, which may also explain a possible increase in fine sediment supply (Figure 4-9c). Later, sediment laden purges may more easily pass directly under the remaining ice. The latter coincides with the introduction of coordinated night-time purging of HGdA and LB intakes to enhance sediment output (Figure 4-4). Although these mechanisms and their contributions to sediment delivery can only be inferred here, the system evolution illustrates two important elements that may apply to Alpine systems in general. First, sediment connectivity in expanding proglacial areas is a key factor in the storage and export of sediment in these dynamic environments. Second, climate forcing and proglacial response may have a very large impact on sediment delivery, which in turn affects downstream sediment transfer and river bed morphology. Considering changes in local climate, sediment availability/release and connectivity (e.g., Lane *et al.*, 2017), system evolution may vary strongly (both in time and between systems), making predictions with respect to the impacts of future climate change uncertain. On the long-term however, climate warming and retreating glaciers will inevitably cause the decline of sediment yield from these catchments (e.g., Warburton, 1999).

#### 4.5.3 Human Forcing of System Sensitivity

The introduction of flow abstraction has reduced discharge and bed load transport capacity in the upper Borgne d'Arolla by an estimated 95% (Figure 4-11a). While transport capacity is reduced by 1–2 orders of magnitude, it is only reduced to close to the rates of sediment supply, with resulting SCR values that are not much larger than 1. This is not surprising as both the sediment supply and the residual sediment transport capacity are a function of the number of purges; flow (discharge and duration) are required to empty the sediment traps during purges. SCR values near 1 allow the sediment throughput through the system to be at least partly maintained. This is consistent with the rate and downstream gradient of river bed aggradation (Figure 4-8) and the significant sediment transfer that was maintained (Figure 4-10b).

The tendency for SCR values to be close to 1 due to flow abstraction means that the system has become highly sensitive to small changes in either sediment supply or sediment transport capacity. Due to this sensitivity, phases of external forcing, whether due to flow abstraction/regulation or

climate change, can be distinguished in the morphological evolution of the Borgne. Initially, although little change occurred in the early stages following the onset of flow abstraction, the system dynamics and capacity to respond to external forcing did change. This only became apparent when a climate driven increase in sediment supply in the late 1980s and early 1990s led to an extensive aggradation (although there was still a large sediment transfer component). Similarly, since the early 2000s, there has been a general decrease in the capacity of the flow intake system to abstract high discharges (Figure 4-10a), leading to a sharp increase peak in flows associated with periods of (near) system surcharge (Figure 4-9c) since 2011. These are typically associated with high melt rates from glaciated basins during increasingly warm summers (Birsan *et al.*, 2005) and high amounts of precipitation from convective storms (Giorgi *et al.*, 2016). The resulting high flows from the LB catchment, in exceptional cases combined with flows from upstream catchments, are conveyed down the Borgne as longer duration, peak flow events. They are characterized by a high transport capacity and a relatively low sediment supply as compared to purges due to sediment trap flushing, where the use of water to purge the sediment traps is minimized for economic reasons. Further, the coordination of purges at the basin scale has led to routine night-time purges since 2008, where the LB intake is opened so as to allow purges from the upstream basins to pass through, resulting in elevated purges. Both of these changes are reflected in Figure 4-11a, where since 2003 there is a rising transport capacity, both in absolute and relative sense (with respect to the also increasing sediment supply), and an SCR that evolves toward 1 (Figure 4-11b). These high flow events can entrain sediment deposited downstream of the intake and potentially break armor layers, contributing to the substantial erosion of the upstream section of reach A (Figure 4-8a) and net export of sediment since 2010 (Figure 4-10b). In general, the system has become sensitive to high magnitude events, whether due to climate (e.g., high melt, convective storms), upstream events (e.g., glacial outburst floods), or human flow management (flow releases).

The key point here is that as flow abstraction has generally shifted the SCR toward 1 (Figure 4-11b), the system has become sensitive to relatively small changes in both climatically driven changes in sediment supply and how abstraction is managed, which can have major impacts on sediment transfer and river aggradation/degradation. This is exacerbated by legacy sediment (James, 2013), the accumulation of poorly sorted sediment downstream of the intakes, despite significant sediment throughput. The system sensitivity emphasizes the relevance of purge management, particularly the relative timing of purges from different intakes such that they coincide, optimizing sediment transfer and impacting morphological change. The capacity to which the hydropower system can be used to accommodate climate-driven upstream hydrological variability is however limited to the water intake and transfer capacity of the scheme, which effectively introduces a discharge threshold. The scheme

was designed in a period of markedly cooler climate and lower water yield in the 1950s, which explains why it is now filled to capacity more frequently, leading to the need to reduce or stop water abstraction at the LB intake during peak flows. Thus, generalizing how flow abstraction in mountain environments impacts downstream sediment delivery and river morphodynamics needs to consider not only the direct impacts of abstraction and of climatic variability, but also how the water management system itself is coupled to that climatic variability.

#### **4.6 Conclusions**

In this study, we used decadal scale river bed topographic change and hydropower impacted flow and sediment supply to analyze the evolution of river morphology and sediment transfer of an Alpine stream. The initial morphologic response to the onset of flow abstraction in 1963 was modest, generally associated with channel narrowing and vegetation encroachment. Major, widespread aggradation did not commence until the onset of glacier retreat in the late 1980s and the notably warm (and dry) period in the early 1990s. This aggradation coincided with a phase of increased sediment supply, although aggradation accounts for only circa 25% of supplied material and the remainder was transferred through the reaches downstream. Since the mid-2000s, a second phase of increased sediment supply was accompanied by an increased frequency of (near) system surcharge events due to insufficient intake system capacity, which led to the net export of sediment from the braided reaches. Based on the system evolution, we can summarize the effects of flow abstraction and climate change on Alpine fluvial sediment transfer.

First, flow abstraction schemes for hydropower differ from classical reservoir dam schemes in that they ensure river sediment throughput through intermittent purges. Although flow abstraction may lead to a reduction in bed load transport capacity by 1–2 orders of magnitude, residual transport rates may still be sufficient to maintain significant sediment transfer. However, the sediment transfer rates and system morphological evolution then become much more sensitive both to internal river bed morphodynamics and external forcing mechanisms, whether natural or human induced. Because sediment transfer is largely maintained, the downstream morphological evolution of the stream is distinctly different from that downstream of reservoir dams. With low prevailing sediment supply, river bank stabilization and vegetation development encroachment occurs due to infrequent river perturbations and low flow competence. When this is met by a sufficiently high rate of sediment, aggradation will occur, leading to the removal or burial of vegetation. Maintained sediment supply and loss of transport capacity due to flow abstraction typically lead to a decreasing gradient in bed level rise and grain size.

Second, there is a climate forcing of river morphological response where rapid warming and associated glacial retreat lead to increased sediment availability and an adapting paraglacial landscape in which sediment may be stored and/or transferred. Climatic conditions directly impact annual sediment export not only through elevated summer temperatures, where ice melt leads to sediment release and enhanced transport conditions, but indirectly also through preceding winter snowfall, which may persist into the summer and buffer the effect of ice melt. Climate may also force changes in the proglacial margin, notably through sediment connectivity and access of sediment sources related to glacier retreat.

Third, human forcing and climate forcing may be strongly coupled, where the climate variability experienced by the river is conditioned by design and operation of the hydropower system. The capacity of flow releases from the intake to impact downstream sediment transfer is related to their nature, in this case individual sediment trap purges versus basin-wide coordinated purges and most notably (near) system surcharge events. The increasing occurrence of the latter is directly related to climate warming which leads to higher glacial melt rates while the capacity of the hydropower system, designed in a cooler period with lower water yield, is insufficient to accommodate these. This requires the prolonged opening of intakes (as compared to individual purges), allowing the climate driven peak flows to impact downstream sediment transfer and morphology. Thus besides the direct effect on upstream sediment delivery, climate change may have a profound impact on the operation of the hydropower system and hence also an indirect effect on downstream sediment dynamics. The individual effects of (human induced) climate forcing and direct human forcing through flow abstraction cannot be readily distinguished because the latter evolves continually in response to the former.

Alpine river basins are very sensitive to impacts of climate change. While their response in terms of sediment production and storage dynamics may be complex, we have shown that this may result in both rapid and strong increases in sediment delivery rates from proglacial margins. The sediment transport capacity and dynamics of subsequent mountain streams is such that, even when heavily impacted by flow regulation or even abstraction, they may transfer significant amounts of sediment down to main rivers. This implies that the potential impacts on infrastructure and ecology are not restricted to mountain headwaters but may affect the wider river basin and emphasizes the importance of sediment regime in river management.

### *Acknowledgments*

This paper was written within the context of the SEDFATE project funded by the SNSF Sinergia grant CRSII2\_147689, awarded to Fritz Schlunegger, Stéphanie Girardclos, Stuart Lane, Jean-Luc Loizeau and Peter Molnar. We thank SwissTopo for supplying scanned aerial photographs, Grande Dixence SA, Alpiq, and Hydro Exploitation for providing discharge data, and Christoph Frei (MeteoSwiss) for providing spatially interpolated temperature and precipitation data sets. Additional support came from the students of the University of Lausanne, the Canton Valais, the Fondation Herbette and the Commune of Evolène. We would also like to thank the Associate Editor, David Morche and two anonymous reviewers for their detailed and constructive comments which have led to the improvement of this manuscript. Data concerning reach-based aggradation and annual sediment supply will be made available on <http://ebibalpin.unil.ch/>. For further information on the used data, please contact Maarten Bakker ([maarten.bakker@unil.ch](mailto:maarten.bakker@unil.ch)) or Stuart Lane ([stuart.lane@unil.ch](mailto:stuart.lane@unil.ch)).

### **References**

- Ashmore, P., & Church, M. (1998). Sediment transport and river morphology: A paradigm for study (pp. 115–148). Highlands Ranch, CO: Water Resources Publications LLC.
- Badoux, A., Andres, N., & Turowski, J. (2014). Damage costs due to bedload transport processes in Switzerland. *Natural Hazards and Earth System Science*, 14(2), 279–294. 10.5194/nhess-14-279-2014
- Bakker, M., & Lane, S. N. (2017). Archival photogrammetric analysis of river–floodplain systems using Structure from Motion (SfM) methods. *Earth Surface Processes and Landforms*, 42(8), 1274–1286. 10.1002/esp.4085
- Ballantyne, C. K. (2002). A general model of paraglacial landscape response. *The Holocene*, 12(3), 371–376. 10.1191/0959683602hl553fa
- Beniston, M., Rebetez, M., Giorgi, F., & Marinucci, M. R. (1994). An analysis of regional climate change in Switzerland. *Theoretical and Applied Climatology*, 49(3), 135–159. 10.1007/bf00865530
- Bezinge, A., Clark, M., Gurnell, A., & Warburton, J. (1989). The management of sediment transported by glacial melt-water streams and its significance for the estimation of sediment yield. *Annals of Glaciology*, 13, 1–5. 10.1017/S0260305500007527
- Birsan, M.-V., Molnar, P., Burlando, P., & Pfaundler, M. (2005). Streamflow trends in Switzerland. *Journal of Hydrology*, 314(1–4), 312–329. 10.1016/j.jhydrol.2005.06.008

- Brasington, J., Langham, J., & Rumsby, B. (2003). Methodological sensitivity of morphometric estimates of coarse fluvial sediment transport. *Geomorphology*, 53(3–4), 299–316.  
10.1016/S0169-555X(02)00320-3
- Buffington, J. M., & Tonina, D. (2009). Hyporheic exchange in mountain rivers II: Effects of channel morphology on mechanics, scales, and rates of exchange. *Geography Compass*, 3(3), 1038–1062.  
10.1111/j.1749-8198.2009.00225.x
- Carbonneau, P. E., Lane, S. N., & Bergeron, N. E. (2004). Catchment-scale mapping of surface grain size in gravel bed rivers using airborne digital imagery. *Water Resources Research*, 40, W07202.  
10.1029/2003WR002759
- Ceppi, P., Scherrer, S. C., Fischer, A. M., & Appenzeller, C. (2012). Revisiting Swiss temperature trends 1959–2008. *International Journal of Climatology*, 32(2), 203–213. 10.1002/joc.2260
- Church, M. (1995). Geomorphic response to river flow regulation: Case studies and time-scales. *Regulated Rivers-Research and Management*, 11(1), 3–22. 10.1002/rrr.3450110103
- Church, M. (2006). Bed material transport and the morphology of alluvial river channels. *Annual Review of Earth and Planetary Sciences*, 34, 325–354. 10.1146/annurev.earth.33.092203.122721
- Church, M., & Ryder, J. M. (1972). Paraglacial sedimentation: A consideration of fluvial processes conditioned by glaciation. *Geological Society of America Bulletin*, 83(10), 3059–3072.  
10.1130/0016-7606(1972)83[3059:PSACOF]2.0.CO;2
- Cossart, E., & Fort, M. (2008). Sediment release and storage in early deglaciated areas: Towards an application of the exhaustion model from the case of Massif des Écrins (French Alps) since the Little Ice Age. *Norsk Geografisk Tidsskrift - Norwegian Journal of Geography*, 62(2), 115–131.  
10.1080/00291950802095145
- Costa, A., Molnar, P., Stutenbecker, L., Bakker, M., Silva, T. A., Schlunegger, F., ... Girardclos, S. (2017). Temperature signal in suspended sediment export from an Alpine catchment. *Hydrology and Earth System Sciences Discussions*, 2017, 1–30. 10.5194/hess-2017-2
- Csiki, S. J. C., & Rhoads, B. L. (2014). Influence of four run-of-river dams on channel morphology and sediment characteristics in Illinois, USA. *Geomorphology*, 206(Supplement C), 215–229.  
10.1016/j.geomorph.2013.10.009
- Curry, A. M., Cleasby, V., & Zukowskyj, P. (2006). Paraglacial response of steep, sediment-mantled slopes to post-‘Little Ice Age’ glacier recession in the central Swiss Alps. *Journal of Quaternary Science*, 21(3), 211–225. 10.1002/jqs.954
- Fergus, T. (1997). Geomorphological response of a river regulated for hydropower: River Fortun, Norway. *Regulated Rivers: Research & Management*, 13(5), 449–461. doi:10.1002/(SICI)1099-1646(199709/10)13:5<449::AID-RRR468>3.0.CO;2-#

- Ferguson, R. (2007). Flow resistance equations for gravel- and boulder-bed streams. *Water Resources Research*, 43, W05427. 10.1029/2006wr005422
- Fischer, L., Huggel, C., Kääh, A., & Haerberli, W. (2013). Slope failures and erosion rates on a glacierized high-mountain face under climatic changes. *Earth Surface Processes and Landforms*, 38(8), 836–846. 10.1002/esp.3355
- Frei, C. (2014). Interpolation of temperature in a mountainous region using nonlinear profiles and non-Euclidean distances. *International Journal of Climatology*, 34(5), 1585–1605. 10.1002/joc.3786
- Gabbud, C., & Lane, S. N. (2016). Ecosystem impacts of Alpine water intakes for hydropower: The challenge of sediment management. *Wiley Interdisciplinary Reviews: Water*, 3(1), 41–61. 10.1002/wat2.1124
- Geilhausen, M., Morche, D., Otto, J.-C., & Schrott, L. (2013). Sediment discharge from the proglacial zone of a retreating Alpine glacier. *Zeitschrift für Geomorphologie, Supplementary Issues*, 57(2), 29–53. 10.1127/0372-8854/2012/S-00122
- Giorgi, F., Hurrell, J. W., Marinucci, M. R., & Beniston, M. (1997). Elevation Dependency of the Surface Climate Change Signal: A Model Study. *Journal of Climate*, 10(2), 288–296. 10.1175/1520-0442(1997)010<0288:EDOTSC>2.0.CO;2
- Giorgi, F., Torma, C., Coppola, E., Ban, N., Schar, C., & Somot, S. (2016). Enhanced summer convective rainfall at Alpine high elevations in response to climate warming. *Nature Geoscience*, 9, 584–589. 10.1038/ngeo2761
- Glaciological Reports. (1881-2017). "The Swiss Glaciers," Yearbooks of the Cryospheric Commission of the Swiss Academy of Sciences (SCNAT). Retrieved from <http://www.glamos.ch>
- Gobiet, A., Kotlarski, S., Beniston, M., Heinrich, G., Rajczak, J., & Stoffel, M. (2014). 21st century climate change in the European Alps: A review. *Science of the Total Environment*, 493, 1138–1151. 10.1016/j.scitotenv.2013.07.050
- Gruber, S., & Haerberli, W. (2007). Permafrost in steep bedrock slopes and its temperature-related destabilization following climate change. *Journal of Geophysical Research*, 112, F02S18. 10.1029/2006JF000547
- Günter A. (1971). Die kritische mittlere Sohlenschubspannung bei Geschiebemischungen unter Berücksichtigung der Deckschichtbildung und der turbulenzbedingten Sohlenschubspannungsschwankungen. Diss. Techn.Wiss. ETH Zürich, 4649. 10.3929/ethz-a-000089812

- Gurnell, A. (1983). Downstream channel adjustments in response to water abstraction for hydroelectric power generation from alpine glacial melt-water streams. *The Geographical Journal*, 149(3), 342–354. 10.2307/634009
- Gurnell, A., Warburton, J., & Clark, M. (1988). A comparison of the sediment transport and yield characteristics of two adjacent glacier basins, Val d' Herens, Switzerland. In *Sediment budgets (Proceedings Porto Alegre Symposium December 1988)*, IAHS Publication 174, 431–441.
- Haerberli, W., & Beniston, M. (1998). Climate change and its impacts on glaciers and permafrost in the Alps. *AMBIO*, 27, 258–265.
- Haerberli, W., Hoelzle, M., Paul, F., & Zemp, M. (2007). Integrated monitoring of mountain glaciers as key indicators of global climate change: The European Alps. *Annals of Glaciology*, 46(1), 150–160. 10.3189/172756407782871512
- Harbor, J., & Warburton, J. (1993). Relative rates of glacial and nonglacial erosion in Alpine environments. *Arctic and Alpine Research*, 25(1), 1–7. 10.2307/1551473
- Heckmann, T., McColl, S., & Morche, D. (2016). Retreating ice: Research in pro-glacial areas matters. *Earth Surface Processes and Landforms*, 41(2), 271–276. 10.1002/esp.3858
- Heimann, F. U. M., Rickenmann, D., Turowski, J. M., & Kirchner J. W. (2015). sedFlow—A tool for simulating fractional bedload transport and longitudinal profile evolution in mountain streams. *Earth Surface Dynamics*, 3(1), 15–34. 10.5194/esurf-3-15-2015
- Hilker, N., Badoux, A., & Hegg, C. (2009). The Swiss flood and landslide damage database 1972–2007. *Natural Hazards and Earth System Sciences*, 9(3), 913–925. nhes-9-913-2009\_lq
- Hinderer, M., Kastowski, M., Kamelger, A., Bartolini, C., & Schlunegger, F. (2013). River loads and modern denudation of the Alps—A review. *Earth-Science Reviews*, 118, 11–44. 10.1016/j.earscirev.2013.01.001
- Holm, K., Bovis, M., & Jakob, M. (2004). The landslide response of alpine basins to post-Little Ice Age glacial thinning and retreat in southwestern British Columbia. *Geomorphology*, 57(3–4), 201–216. 10.1016/S0169-555X(03)00103-X
- Hunziker, R. P., & Jäggi, M. N. R. (2002). Grain sorting processes. *Journal of Hydraulic Engineering*, 128(12), 1060–1068. 10.1061/(ASCE)0733-9429(2002)128:12(1060)
- James, L. A. (2013). Legacy sediment: Definitions and processes of episodically produced anthropogenic sediment. *Anthropocene*, 2, 16–26. 10.1016/j.ancene.2013.04.001
- Klaar, M. J., Kidd, C., Malone, E., Bartlett, R., Pinay, G., Chapin, F. S., & Milner, A. (2015). Vegetation succession in deglaciated landscapes: Implications for sediment and landscape stability. *Earth Surface Processes and Landforms*, 40(8), 1088–1100. 10.1002/esp.3691

- Lamb, M. P., Dietrich, W. E., & Venditti, J. G. (2008). Is the critical Shields stress for incipient sediment motion dependent on channel-bed slope? *Journal of Geophysical Research: Earth Surface*, 113(F2). <https://doi.org/10.1029/2007JF000831>
- Lane, S. N., Bakker, M., Balin, D., Lovis, B., & Regamey, B. (2014). Climate and human forcing of Alpine river flow. In A. J. Schleiss *et al.* (Eds.), *River flow* (Vol. 2014, pp. 7–15). London: Taylor & Francis Group.
- Lane, S. N., Bakker, M., Gabbud, C., Micheletti, N., & Saugy, J.-N. (2017). Sediment export, transient landscape response and catchment-scale connectivity following rapid climate warming and Alpine glacier recession. *Geomorphology*, 277, 210–227. [10.1016/j.geomorph.2016.02.015](https://doi.org/10.1016/j.geomorph.2016.02.015)
- Lane, S. N., Reid, S. C., Westaway, R. M., & Hicks, D. M. (2004). Remotely sensed topographic data for river channel research: The identification, explanation and management of error. In R. E. J. Kelly, N. A. Drake, & S. L. Barr (Eds.), *Spatial modelling of the terrestrial environment* (pp. 113–136). Chichester, UK: John Wiley.
- Lane, S. N., Richards, K. S., & Chandler, J. H. (1994). Developments in monitoring and modelling small-scale river bed topography. *Earth Surface Processes and Landforms*, 19(4), 349–368. [10.1002/esp.3290190406](https://doi.org/10.1002/esp.3290190406)
- Lane, S. N., Tayefi, V., Reid, S. C., Yu, D., & Hardy, R. J. (2007). Interactions between sediment delivery, channel change, climate change and flood risk in a temperate upland environment. *Earth Surface Processes and Landforms*, 32(3), 429–446. [10.1002/esp.1404](https://doi.org/10.1002/esp.1404)
- Lane, S. N., Westaway, R. M., & Murray Hicks, D. (2003). Estimation of erosion and deposition volumes in a large, gravel-bed, braided river using synoptic remote sensing. *Earth Surface Processes and Landforms*, 28(3), 249–271. [10.1002/esp.483](https://doi.org/10.1002/esp.483)
- Lindsay, J. B., & Ashmore, P. E. (2002). The effects of survey frequency on estimates of scour and fill in a braided river model. *Earth Surface Processes and Landforms*, 27(1), 27–43. [10.1002/esp.282](https://doi.org/10.1002/esp.282)
- Loizeau, J.-L., & Dominik, J. (2000). Evolution of the Upper Rhone River discharge and suspended sediment load during the last 80 years and some implications for Lake Geneva. *Aquatic Sciences*, 62(1), 54–67. [10.1007/s000270050075](https://doi.org/10.1007/s000270050075)
- Margot, A., Schädler, B., Sigg, R., & Weingartner, R. (1992). Influence on rivers by water power stations (> 300 kW) and the lake control. *Hydrological Atlas of Switzerland*. Plate, 5 Swiss Federal Office of Topography, Bern.
- MeteoSwiss. (2016a). Daily Mean, Minimum and Maximum Temperature: TabsD, TminD, TmaxD. Retrieved from [http://www.meteoswiss.admin.ch/content/dam/meteoswiss/de/service-und-publicationen/produkt/raeumliche-daten-temperatur/doc/ProdDoc\\_TabsD.pdf](http://www.meteoswiss.admin.ch/content/dam/meteoswiss/de/service-und-publicationen/produkt/raeumliche-daten-temperatur/doc/ProdDoc_TabsD.pdf)

- MeteoSwiss. (2016b). Daily Precipitation (final analysis): RhiresD. Retrieved from [http://www.meteoswiss.admin.ch/content/dam/meteoswiss/de/service-und-publikationen/produkt/raeumliche-daten-niederschlag/doc/ProdDoc\\_RhiresD.pdf](http://www.meteoswiss.admin.ch/content/dam/meteoswiss/de/service-und-publikationen/produkt/raeumliche-daten-niederschlag/doc/ProdDoc_RhiresD.pdf)
- Micheletti, N., Lambiel, C., & Lane, S. N. (2015). Investigating decadal-scale geomorphic dynamics in an alpine mountain setting. *Journal of Geophysical Research: Earth Surface*, 120, 2155–2175. 10.1002/2015JF003656
- Micheletti, N., & Lane, S. N. (2016). Water yield and sediment export in small, partially glaciated Alpine watersheds in a warming climate. *Water Resources Research*, 52, 4924–4943. 10.1002/2016WR018774
- Nicholas, A., Ashworth, P., Kirkby, M., Macklin, M., & Murray, T. (1995). Sediment slugs: Large-scale fluctuations in fluvial sediment transport rates and storage volumes. *Progress in Physical Geography*, 19(4), 500–519.
- Nitsche, M., Rickenmann, D., Turowski, J. M., Badoux, A., & Kirchner, J. W. (2011). Evaluation of bedload transport predictions using flow resistance equations to account for macro-roughness in steep mountain streams. *Water Resources Research*, 47, W08513. 10.1029/2011WR010645
- Norton, K. P., Abbühl, L. M., & Schlunegger, F. (2010). Glacial conditioning as an erosional driving force in the Central Alps. *Geology*, 38(7), 655–658. 10.1130/G31102.1
- Park, C. (1980). The Grande Dixence hydro-electric scheme, Switzerland. *Geography*, 65, 317–320.
- Paul, F., Käab, A., Maisch, M., Kellenberger, T., & Haeberli, W. (2004). Rapid disintegration of Alpine glaciers observed with satellite data. *Geophysical Research Letters*, 31, L21402. 10.1029/2004GL020816
- Petts, G. E., & Bickerton, M. A. (1994). Influence of water abstraction on the macroinvertebrate community gradient within a glacial stream system: La Borgne d'Arolla, Valais, Switzerland. *Freshwater Biology*, 32(2), 375–386. 10.1111/j.1365-2427.1994.tb01133.x
- Petts, G. E., & Gurnell, A. M. (2005). Dams and geomorphology: Research progress and future directions. *Geomorphology*, 71(1), 27–47. 10.1016/j.geomorph.2004.02.015
- Raymond Pralong, M., Turowski, J. M., Rickenmann, D., & Zappa, M. (2015). Climate change impacts on bedload transport in alpine drainage basins with hydropower exploitation. *Earth Surface Processes and Landforms*, 40(12), 1587–1599. 10.1002/esp.3737
- Rey, Y., & Dayer, G. (1990). Crues de l'été 1987 dans les bassins versants glaciaires des Alpes Pennines. *Revue de Géographie Alpine*, 78(1), 115–124.
- Rickenmann, D. (1991). Hyperconcentrated flow and sediment transport at steep slopes. *Journal of Hydraulic Engineering*, 117(11), 1419–1439. 10.1061/(ASCE)0733-9429(1991)117:11(1419)

- Rickenmann, D., & Recking, A. (2011). Evaluation of flow resistance in gravel-bed rivers through a large field data set. *Water Resources Research*, 47(7), W07538. 10.1029/2010WR009793
- Schar, C., Vidale, P. L., Luthi, D., Frei, C., Haberli, C., Liniger, M. A., & Appenzeller, C. (2004). The role of increasing temperature variability in European summer heatwaves. *Nature*, 427(6972), 332–336. 10.1038/nature02300
- Small, R. J. (1973). Braiding terraces in the Val d'Herens, Switzerland. *Geography*, 58, 129–135.
- Stoffel, M., & Huggel, C. (2012). Effects of climate change on mass movements in mountain environments. *Progress in Physical Geography*, 36(3), 421–439. 10.1177/0309133312441010
- SwissTopo (1946). Aerial images swisstopo oblique: Picture number: 19461071550811. Retrieved from <https://map.geo.admin.ch>
- Tanchev, L. (2014). Dams and appurtenant hydraulic structures. Boca Raton, FL: CRC Press.
- Turowski, J. M., & Rickenmann, D. (2009). Tools and cover effects in bedload transport observations in the Pitzbach, Austria. *Earth Surface Processes and Landforms*, 34(1), 26–37. 10.1002/esp.1686
- Warburton, J. (1990). An alpine proglacial fluvial sediment budget. *Geografiska Annaler. Series A. Physical Geography*, 72, 261–272. 10.2307/521154
- Warburton, J. (1992). Observations of bed load transport and channel bed changes in a proglacial mountain stream. *Arctic and Alpine Research*, 24(3), 195–203. 10.2307/1551657
- Warburton, J. (1994). Channel change in relation to meltwater flooding, Bas Glacier d'Arolla, Switzerland. *Geomorphology*, 11(2), 141–149. 10.1016/0169-555X(94)90078-7
- Warburton, J. (1999). Environmental change and sediment yield from glacierised basins: The role of fluvial processes and sediment storage (Chapter 19). In A. G. Brown & T. A. Quine (Eds.), *Fluvial processes and environmental change* (pp. 363–384). Chichester, UK: Wiley.
- Warburton, J., & Fenn, C. (1994). Unusual flood events from an Alpine glacier: Observations and deductions on generating mechanism. *Journal of Glaciology*, 40(134), 176–186. 10.1017/S0022143000003956
- Wheaton, J. M., Brasington, J., Darby, S. E., Kasprak, A., Sear, D., & Vericat, D. (2013). Morphodynamic signatures of braiding mechanisms as expressed through change in sediment storage in a gravel-bed river. *Journal of Geophysical Research: Earth Surface*, 118, 759–779. 10.1002/jgrf.20060
- Wheaton, J. M., Brasington, J., Darby, S. E., & Sear, D. A. (2010). Accounting for uncertainty in DEMs from repeat topographic surveys: Improved sediment budgets. *Earth Surface Processes and Landforms*, 35(2), 136–156. 10.1002/esp.1886

- Williams, G. P., & Wolman, M. G. (1984). Downstream effects of dams on alluvial rivers. Washington, DC: US Government Printing Office.
- Wohl, E., Bledsoe, B. P., Jacobson, R. B., Poff, N. L., Rathburn, S. L., Walters, D. M., & Wilcox, A. C. (2015). The natural sediment regime in rivers: Broadening the foundation for ecosystem management. *BioScience*, 65(4), 358–371. [10.1093/biosci/biv002](https://doi.org/10.1093/biosci/biv002)
- Wold, B., & Østrem, G. (1979). Morphological activity of a diverted glacier stream in Western Norway. *GeoJournal*, 3(4), 345–349.
- Wolman, M. G. (1954). A method of sampling coarse river-bed material. *Eos, Transactions American Geophysical Union*, 35(6), 951–956.

## 5. ARTICLE 3: MORPHOLOGICAL RESPONSE OF AN ALPINE BRAIDED REACH TO SEDIMENT-LADEN FLOW EVENTS

This chapter, by Bakker, M., Antoniazza, G., Odermatt, E. and Lane, S.N., was submitted to *Journal of Geophysical Research – Earth Surface* in July 2018.

### *Abstract*

Braided gravel-bed rivers show characteristic temporal and spatial variability in morphological change and bed load transport under steady flow and sediment supply rates. Their morphodynamic behavior and long term evolution in response to non-stationary external forcing is less well known. We studied daily morphological changes in a well-constrained reach of an Alpine braided river that is subject to regulated sediment-laden flows associated with hydro-electric power exploitation, and occasional floods. Based on two-dimensional patterns of morphological change and modelled sediment routing, we inferred the spatially distributed, mean sediment transport rates needed to conserve mass. Although net reach erosion and deposition are forced by upstream sediment supply, in a non-linear fashion, the spatial distribution of morphological change and sediment transport varies strongly along the braided reach and between successive sequences of flushing. Local morphological change is driven by two effects: 1) local relief, leading to the preferential filling of lows and erosion of highs, particularly during longer duration floods; and 2) system memory, leading to a negative feedback in bed level changes where erosion is followed by deposition of similar magnitude and vice versa. This effect is associated with the temporary storage of high sediment loads from flushing due to the abrupt 'on-off' nature of these flows, and reveals the relatively efficient transport of sediment in a river that is heavily impacted upon by flow abstraction. In general, the internal morphodynamics of the braided river condition their own response to external forcing events and thus sediment transfer.

### *Key points:*

- Braided river response to longer duration floods reveals the effects of local relief, 'filling of lows and erosion of highs'.
- Morphodynamic response to short and abrupt sediment-laden flows reveals 'system memory' with alternating local erosion and sedimentation.
- The internal morphodynamics of the braided river condition their own response to external forcing events and thus sediment transfer.

## 5.1 Introduction

Braided river reaches form an important link in the storage and transfer of sediment in Alpine systems. Their beds can accommodate and release large amounts of sediment through erosion and deposition within channel and bar complexes (Ashmore, 1991; Ferguson, 1993). The result is high spatial and temporal variability in sediment storage and associated sediment transport across multiple scales (Hoey, 1992). It is therefore crucial to understand the internal functioning of these braided reaches if we want to gain insight in their response to external forcing mechanisms including impacts of flow management or climate change.

The complexity of braided gravel bed streams has long been investigated in controlled flume experiments where cyclical variability was found at various temporal and spatial scales in bed load transport, e.g. Gomez et al. (1989), and bed morphology, e.g. Ashmore (1982). These experiments have shown braiding can occur under steady flow and sediment supply rates, and it is therefore a fundamental instability arising from the interaction between flowing water and a mobile bed provided river banks remain erodible (Murray & Paola, 1994). In natural systems, the detailed functioning of braided gravel bed streams may be more complex because they respond to continuously changing upstream conditions at varying rates and intensities. The general question that then arises is how do braided rivers respond to non-stationary external forcing in terms of their morphodynamic behavior and longer term evolution? To answer this, the extent to which river bed morphodynamics respond to upstream forcing events, particularly higher magnitude flow events (e.g. Bertoldi et al., 2009; Warburton, 1994), needs to be investigated, including the spatial and temporal scales associated with such a response. This is not an easy task, because braided systems in general and Alpine mountain systems in particular typically have large temporal fluctuations in both flow and sediment supply (quantity and caliber). In addition, there are time-dependent feedback mechanisms that originate from the location and organization of sediment during deposition and low flow which may affect subsequent entrainment, e.g. through bed surface stabilization (e.g. Reid et al., 1985; Turowski et al., 2011), which we refer to as 'memory' effects. Combined with the spatial variability in braided river bed morphology, this may lead to an ensemble of feedback processes and associated temporal lags in morphological response and sediment transfer. Such continuous dynamic adjustment and persistent memory effects, make it challenging to investigate internal morphological processes and to couple these to external forcing mechanisms.

In this study, we investigate the morphodynamics and sediment transport in a well-constrained, 1.7 km long Alpine braided river reach of the Borgne d'Arolla in Switzerland. The reach is more or less dry for most of the time due to flow abstraction for hydroelectric power generation (hereafter

‘hydropower’), with the exception of frequent sediment-laden flows which are used to flush sediment from flow intakes and occasional, non-regulated floods (Bakker et al., 2018). Our aim is to quantify the effect of these flow events and to assess the spatio-temporal extent to which they affect the braided river reach morphodynamics. We do this by combining event-based flow and sediment records (Bezinge et al., 1989) with high-frequency, remote sensing (e.g. Milan et al., 2007; Williams et al., 2013). These data allow us to characterize river bed morphology as well as upstream flow and sediment supply drivers, and to quantify flow and sediment routing and storage that are crucial in downstream sediment transfer. The analyses are used not only to quantify and to interpret change, but also to determine spatially distributed mean sediment transport rates, which may be inferred from observed morphological change and sediment routing based on the ‘two-dimensional morphological method’ (Antoniazza et al., in revision). We will show that this approach gives additional insight into the spatial structure of braided river bed morphodynamics and, in particular, the distinct morphodynamic signature and sediment transfer associated with flow events and sediment supply in this system.

## 5.2 Study area

The Borgne is a left bank tributary of the Rhône River that drains glaciated basins of the Pennine Alps in south-west Switzerland. In this study, we investigate a braided headwater reach of the Borgne d’Arolla (Figure 5-1), whose upstream end lies c. 1 km downstream from the terminus of the Bas Glacier d’Arolla.

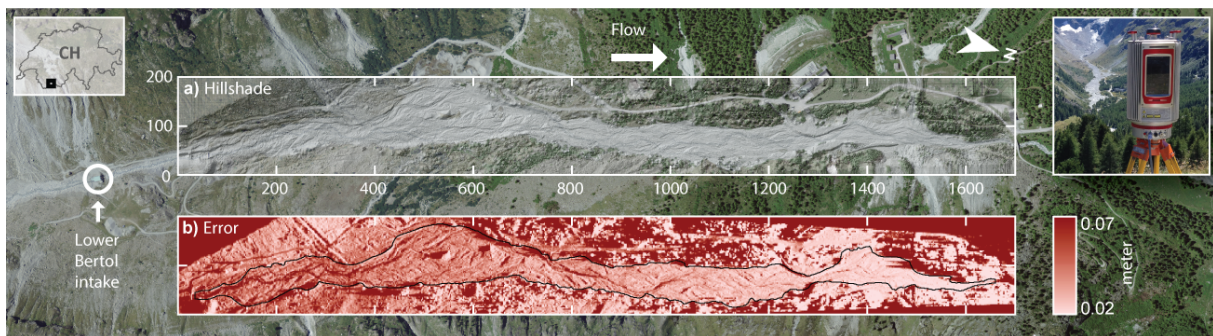


*Figure 5-1 a) Aerial photo and hillshade map of the Borgne d’Arolla headwater reach and upstream hydropower flow intake; a photo insert of the laser scanner overseeing the investigated reach from the vantage point; b) local error in elevation measurements due to point cloud density from the laser scanner survey and the channel bed outline used in the analysis.*

Nearly all of the water (c. 90%) from the glacier and upstream tributaries is intercepted by the Lower Bertol intake (Bakker et al., 2018) that lies 225 m from the upstream end of the reach. The intake is one of 75 intakes that make up a wider hydropower scheme that abstracts water from the Matter

and Hérens valleys and transfers this via 100 km of pipes and 4 pumping stations to the Lac de Dix reservoir in the Héréme valley (Park, 1980). Sediment delivered to the intake is trapped in a gravel and subsequent sand trap, which are flushed (sometimes referred to as ‘purged’) when they are full, i.e. abstraction is temporarily stopped and flow is used to evacuate sediment from the traps into the braided reach (Bezinge et al., 1989; Gurnell et al., 1988). There are two important exceptions to this (semi-)automatic operation which are related to the flow management of the hydropower system. First, precautionary night-time flushing is performed for safety and sediment transfer purposes (Bakker et al., 2018). In this case longer duration flushing is designed to coincide with flushing of upstream intakes, most notably the Haut Glacier d’Arolla intake (Lane et al., 2017). Second, under exceptionally high flow conditions, water cannot always be abstracted due to the limited capacity of the flow transfer system and water intake is stopped at the Lower Bertol intake to prevent system surcharge. These events and in particular the longer duration floods in combination with flushing of upstream intakes have a strong impact on morphological change in the investigated reach (Bakker et al., 2018; Gurnell, 1983).

Table 1 shows the basic characteristics of the braided reach. Nearly all sediment that is supplied to the reach passes through the Lower Bertol intake. There are a few small, unregulated tributaries that enter the reach and 2 regulated (flow abstraction) tributaries: Douves Blanches, which enters the reach at 500 m on the right bank and is very rarely active (unpublished data indicate that during 2015, it supplied less than 1% of the total sediment supplied to the reach); and Pièce, which has a higher sediment supply (nearly 10% of the total sediment supply), but enters the reach almost at its downstream end, 1500 m downstream, on the left bank (Figure 5-1).

Length	Width	Elevation	Gradient	Grain size	Vegetation
1600 m	20-120 m	2090-1985 m	11-5% (concave profile)	D50: 55-2 mm D84: 120-5 mm (fining downstream)	none

Table 5-1 Reach dimensions and hydraulic parameters; gradient and grain size are based on Bakker et al. (2018).

### 5.3 Methods

#### 5.3.1 Overview

To study the morphological change and associated sediment transport in the braided reach we benefit from the presence of flow abstraction in two ways. First, we use intake data provided by the hydropower company Grande Dixence SA to determine discharge and, indirectly through identifying flushing events, to estimate the sediment supply to the reach during flow events (Bakker et al.,

2018). Second, because the riverbed is more or less dry between flushing events, we could readily use a terrestrial laser scanner to survey the entire river bed topography and to quantify morphological change on a daily basis. We then combine upstream sediment supply and morphological change data to determine reach-based sediment budgets and to infer spatially distributed mean bed load transport rates, combining hydraulic flow simulations with topographic forcing in a two-dimensional application of the Exner equation (Antoniazza et al., in revision). Finally, we analyze the spatial distribution and temporal dynamics of morphological change and sediment transport as a function of upstream forcing, flow and sediment input, river bed morphology and preceding morphological change.

### 5.3.2 Flow events: upstream discharge and sediment supply

Fieldwork was performed in the exceptionally warm summer of 2015. The average temperature in July at Sion (where the Borgne enters the Rhône) was 24 °C, 0.7 °C warmer than the previous recorded maximum (MeteoSuisse measurements since the year 1864). The warm conditions led to generally high flow conditions and sediment loads that were observed during frequent flushing events, typically 3-6 per day, and 3 longer flood events related to (near) system surcharge on 24 July (evening), 10 August (morning) and 14 August (morning).

Daily laser scanner surveys of the braided river reach were performed between 27 July and 13 August, with the exception of 1 and 9 August (we will refer to this as 'daily'). In addition, surveys were performed on 6 June and 2 September to capture the longer-term change in river bed topography. For the whole period, river flow data was derived based on the identification of distinct flow events from 1-minute flow intake data provided by Grande Dixence SA, accounting for potential flow contribution from the upstream Haut Glacier d'Arolla intake (Bakker et al., 2018); see Figure 5-2a and 5-2b. Based on the characteristic timing and estimated water yield of different types of events we could attribute associated sediment loads: sand trap flushing, 8 m<sup>3</sup>; gravel trap flushing, 150 m<sup>3</sup>, gravel trap flushing during precautionary night-time events, 120 ± 20 m<sup>3</sup> (Figure 5-2c). Although, the longer duration floods are inherently uncertain due to their non-regulated nature and continuous throughput of sediment, we attributed a load of 600 m<sup>3</sup> to close the longer term sediment budget. The obtained flow and sediment yield for the investigated period is given in Figure 5-2d and for full details on the approach we refer to Bakker et al. (2018).

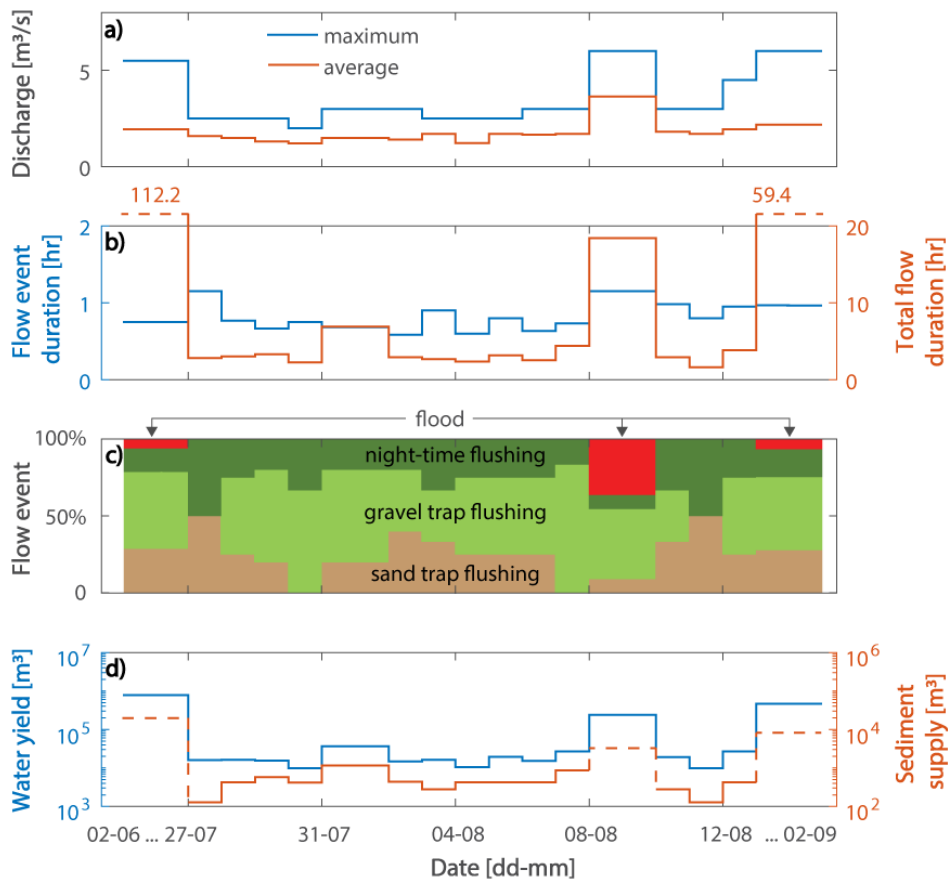


Figure 5-2 Flow events: a) maximum and average river discharge estimated from flow intake data; b) average flow event duration (flushing) and total flow duration, c) flow events classified by event type, d) water yield and sediment supply to the investigated reach (dashed line due to uncertainty in upstream sediment input due to floods).

### 5.3.3 Morphological change

#### *Lidar point cloud acquisition*

We used a Riegl VZ 6000 terrestrial laser scanner (or lidar) to survey the braided river reach. The scans were taken from a well-accessible vantage point, at an elevation of approximately 2170 m, on the valley slope just above the village of Arolla. This site is in line with the braided reach at a distance of 1200 m from the bridge at the downstream end of the reach (Figure 5-1 photo insert). We acquired a 10 to 30 cm resolution point cloud, depending on distance, with a scan time of approximately 7 minutes.

We processed the obtained point clouds with Riscan PRO software and registered them to a reference scan (27 July). Here, we adopted the same general procedure as Gabbud et al. (2015), which consists of: (1) the removal of erroneous points, due to atmospheric reflection and power lines that cross the river; (2) manual coarse registration using fixed points including buildings,

(hydropower) infrastructure and stationary boulders; and (3) the application of automatic multi-station adjustment to optimize the alignment of so-called plane patches that were generated from the points clouds (Rieggl, 2015) using an inverse distance weighted algorithm (Zhang, 1994). The alignment was based on the area surrounding the river channel, which is assumed to be stable on the timescale of the surveys.

#### *DEM generation*

From the point cloud data, we generated 0.2 m resolution Digital Elevation Models (DEMs) (e.g. see the hillshade in Figure 5-1a). We did this using (default) linear point kriging (slope and anisotropy equal to 1) in Surfer 10 software. Heritage et al. (2009) found that this interpolation method gave the best results in a comparable setting, using aerial lidar to map a gravel bar.

To quantify the local uncertainty due to interpolation, we evaluated the spatial distribution of lidar point density (Figure 5-1b). This allows us to directly address the source of the uncertainty, as opposed to combining factors including distance from scanner, aspect of the surface, reflectance of the surface etc. through e.g. a fuzzy inference system (Wheaton et al., 2013). The uncertainty associated with the point density was assessed using a sub-area (size 50 x 50 m) with a high point density, i.e. negligible occlusions and at a relative short distance from the lidar (1400 m distance in Figure 5-1). We computed a reference DEM at 2.2 m resolution, reflecting the general scale of morphological features in the river and limiting the number of cells with no points. For the same sub-area we computed DEMs with lower point densities ( $\rho_p$ ) through consecutively removing random points. This allowed the quantification of the standard deviation of error ( $\sigma_E$ ) of these DEMs with respect to the reference grid as a function of point density. We found a clear logarithmic trend with the point density (p value < 0.001,  $R^2 = 0.99$ ) which is described by:

$$\sigma_E = 10^{a \cdot \rho_p + b} \pm c$$

where  $a = -0.08$  and  $b = -1.3$  were derived from the regression. This trend was consistent for different DEM resolutions and DEMs of different dates (see Appendix B1). Additionally  $c = \pm 0.02$  m was added to the local error function to represent the inherent uncertainty in the equipment itself.

#### *Morphological change*

To verify residual systematic error in the lidar registration, DEMs of Differences (DoDs) were generated for all dates with respect to the reference date, 27 July (Figure 5-3a). This revealed a residual systematic error, visible as banding in the direction of the laser beams that diverge with increased distance from the laser scanner. We attribute this error to the instrument operation, potentially related to the mechanics of instrument components which set the vertical angle and

which becomes evident at the applied long range. The result is that the error may vary with the horizontal scanning angle and significant changes may occur between scan lines. To correct for this error we assessed changes smaller than 0.20 m, with respect to the reference date for both the river bed and banks. This limit was chosen to account for the largest systematic errors, whilst minimizing the inclusion of actual morphological change, although this cannot be entirely excluded. We applied linear regression to these changes along the distance axis from the lidar (x-axis) for 2.2 m wide bands in the y-axis. The regression function was then used to generate a correction grid (Figure 5-3b; note the error increases with distance from the lidar in upstream direction) which was applied to correct the DEM that was compared with the reference DEM.

The corrected set of DEMs were used to determine consecutive DoDs that were thresholded with a limit of detection using a 95%-confidence student t-test (Lane et al., 2003); Figure 5-3d gives the corresponding example for a non-consecutive grid.

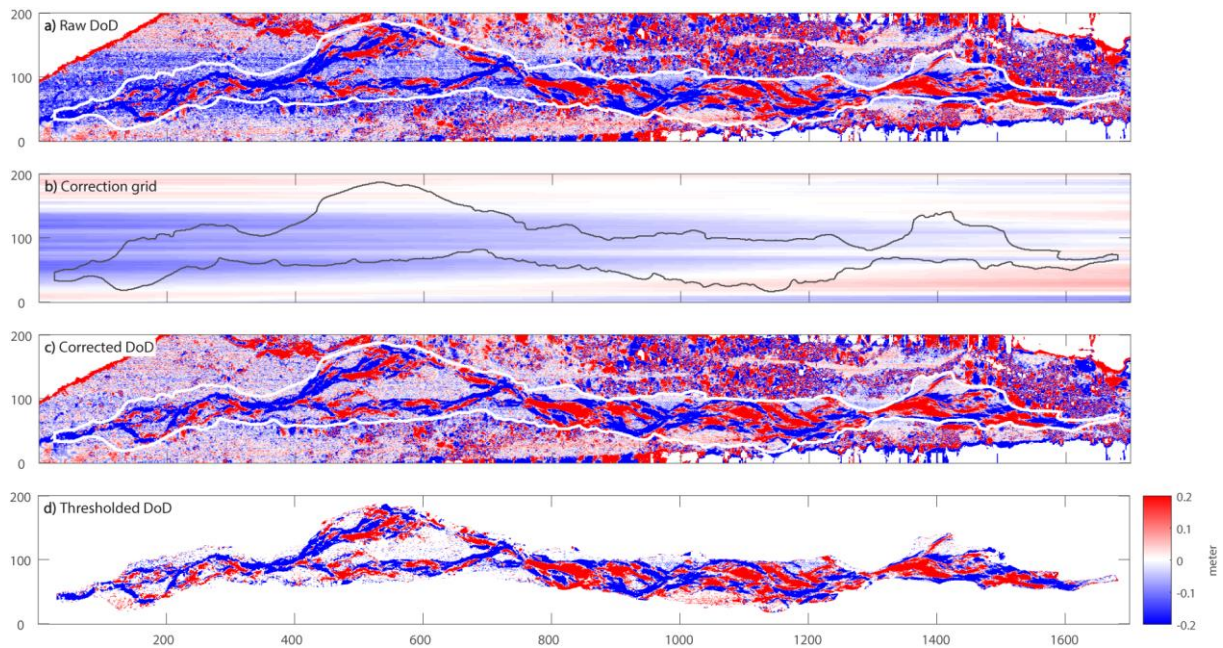


Figure 5-3 a) DoD showing morphological change smaller than 0.2 m in the river bed (channel bed outline indicated) and the surrounding area; b) correction grid for systematic error or 'banding' based on regression analysis; c) DoD corrected for systematic error; d) DoD with 95% probability thresholding.

Although a single scan position and relatively long distance scanning are not ideal considering errors related to shadowing and (potential) systematic error, these have been limited with the applied methodology and allow us to readily obtain data at a high temporal frequency.

#### 5.3.4 2D Sediment transport rates

##### *Morphological method*

The morphological method (Ashmore & Church, 1998) provides a sediment budget approach to infer the minimum sediment transport rates that are required to account for total morphological change along a river section (Vericat et al., 2017). Here we apply the two-dimensional (2D) morphological method based on a framework first proposed by Lane et al. (1995) and described in detail by Antoniazza et al. (in revision). This method gives additional insight into sediment origin and bed load routing within the river bed, allowing for more comprehensive sediment budgeting and the assessment of cross channel morphological forcing.

We determine the local, grid cell based sediment transport rates through considering bed load influx from adjacent cells and local topographic change as detected with consecutive lidar topographic surveys. For any grid cell  $x, y$ , the two-dimensional volumetric form of the Exner equation is given by (Antoniazza et al., in revision):

$$\left(\frac{\partial q_b^x}{\partial x}\right) + \left(\frac{\partial q_b^y}{\partial y}\right) + (1 - \varepsilon) * \frac{\partial z_{xy}}{\partial t} + \frac{\partial c_b}{\partial t} = 0 \quad [1]$$

where  $q_b$  is the bed material transport in the  $x$  and  $y$  downstream and cross-stream directions respectively,  $\varepsilon$  is the sediment porosity,  $z$  is elevation,  $t$  is time and  $c_b$  is the concentration per unit bed area of sediment in transport. Volumetric transport rates were integrated across the duration of effective flow and converted to mass transport rates by assuming a sediment density of 2680 kg/m<sup>3</sup> and a porosity of 0.18 was taken as typical for unsorted gravel and sediment (Carling & Reader, 1982). At the upstream boundary, the sediment load that passes the sediment traps per unit time (Figure 5-2d) is assumed to be supplied to the reach at a constant rate and evenly divided over the wetted width. We assume that the impact of sediment input from tributaries on the morphological change is negligible; Douves Blanches has a very low supply (Micheletti & Lane, 2016) and Pièce enters the reach at the downstream end of the study reach and has little impact upon the study area.

### *2D Hydraulic modelling*

To assess the 2D extent of the river bed where sediment transport occurs and to quantify the 2D bed load transport direction, 2D hydraulic simulations are performed. We used the open-source software BASEMENT v2.7 (<http://www.basement.ethz.ch/>) to perform two-dimensional hydrodynamic simulations. The finite volume method is applied based on the integral form of the shallow water equations (Vetsch et al., 2014) and a formulation for partially wetted cells (Begnudelli & Sanders, 2006) to reconcile these where flow depth is close to zero, such as at the wetting front during flow rise and the drying front during flow recession. The use of an explicit Euler scheme and an exact Riemann solver to integrate over time allow for the stable and accurate application in near-critical and super-critical flow conditions that are prominent in steep Alpine streams (Perona et al., 2009).

For each lidar scan we derived a 1m resolution elevation grid (coarser than the 0.2 m DEM resolution for computational reasons) using the kriging approach mentioned earlier. This was the basis for the generation of a structured 2D mesh with the BASEmesh (v 1.4) plugin in QGIS. A spatially constant bed friction was used for model calibration of the reference grid (27 July), based on the propagation velocity of flushing events with different magnitudes over a dry river bed. We could relate these to a large number of events that were measured in the same period with in-stream stage measurements (unpublished data). A Manning's  $n$  value of 0.04 was found, which is lower than the value obtained by Antoniazza et al. (in revision) for the same reach, yet commensurate given the higher resolution of the computational grid that was used in this case and therefore lower contribution of macro-roughness. The calculated wetted area for each period was used to delimit the morphological changes, due to sediment transport in the river, used in the morphological analysis.

### *2D Bed load routing*

Sediment routing for the 2D morphological method (Antoniazza et al., in revision) is determined using the shear stress ( $\tau$ ) in the x and y direction resulting from local flow and the component of gravity along the local slope following Nelson and Smith (1989):

$$\tau_x = \rho_w g \frac{|u|u_x n^2}{d^{1/3}} + \tau_c \frac{\sin \alpha s_x}{\sin \phi |s|} \quad [2a]$$

$$\tau_y = \rho_w g \frac{|u|u_y n^2}{d^{1/3}} + \tau_c \frac{\sin \alpha s_y}{\sin \phi |s|} \quad [2b]$$

The first term of the right-hand side of [2a] and [2b] represents the bed shear stress due to the flow velocity magnitude ( $|u|$ ) and direction ( $u_{x,y}$ ), based on a Manning's  $n$  roughness formulation, where  $d$  is water depth in meters, water density  $\rho_w$  is 1000 kg/m<sup>3</sup> and gravity  $g$  is 9.81 m/s<sup>2</sup>; this approach is in accordance with the abovementioned BASEMENT numerical simulations. The second part of the equation describes the gravitational or topographic forcing of sediment routing, where  $\tau_c$  is the critical shear stress to motion based on Shields criterion,  $\alpha$  is the arctan of slope  $|s|$  which can be resolved into  $s_x$  and  $s_y$ , and  $\phi$  is the bulk angle of repose of the sediment.

Similar to Antoniazza et al. (in revision), we used a generalised likelihood approach (Beven & Binley, 1992) to calibrate the sediment routing through minimizing total negative transport (sum of all grid cells); here we implicitly assume that the error in transport results entirely from the error in bed load transport direction (and not from topographic measurements). We based this on 2000 simulations with randomly selected, plausible values of critical shear stress, bulk angle of repose and Manning's  $n$ , which address the relative contributions of the flow and gravity component of bed shear stress

(see also Antoniazza et al. in revision). For all periods, values of  $\tau_c = 150 \text{ N/m}^2$ ,  $\phi = 30^\circ$  and  $n=0.04$  were found to be suitable, which may be expected in this setting and where the latter is also conform the hydraulic simulations.

### 5.3.5 Spatial forcing and response

Repeat, high frequency surveys of topographic change have been previously used to assess braided river morphodynamics (e.g. Lane et al., 2003; Milan et al., 2007; Williams et al., 2013). Here, we also use spatially distributed, daily-based sediment transport rates to infer changes that are not recorded in the local geomorphology, but can be deduced from the spatial distribution of changes. Besides quantifying the reach-based sediment budget from spatial changes in the river bed, we also: 1) consider cumulative absolute change and change frequency (number of periods with change) on a daily basis; noting that both are survey frequency dependent and do not consider intermittent changes of scour and fill that lead to non-detectable change; and 2) quantify the spatial distribution of morphological age, that is the time since last reworking (Lane & Richards, 1997). Similarly, we assess the temporal dynamics of bed load transport rates through transport frequency (number of periods with transport) and transport age (time since last transport).

To investigate the mechanisms that drive morphological change and sediment transport, we trace the transfer of sediment from the intake downstream through the reach to investigate the extent of the impact that the upstream flow and sediment supply has on river bed changes and sediment transport. On a reach-based scale, we quantify the impacts of local relief on the subsequent morphological change, through correlating local, grid cell based morphological change with a normalized height index, which we refer to as the topographic index ( $TI$ ). For this measure, the inundated topography is scaled per cross-section  $y$  between 0, the deepest point, and 1, the highest point:  $TI_{x,y} = (z_{x,y} - \min(z_y)) / (\max(z_y) - \min(z_y))$ . Similarly, we assess the memory of the reach, through correlating local morphological change in one period with that in the following period. We cumulate changes over larger periods combining the effects of successive periods to assess the general persistence of the forcing of change.

### 5.4 Results

#### 5.4.1 Sediment budget

Over the whole period of investigation, from 6 June until 2 September, net erosion of the river bed took place, amounting to c. 2880 m<sup>3</sup>. Erosion was dominant in June and July (-590 m<sup>3</sup>) and in the second half of August (-3230 m<sup>3</sup>). During the daily lidar surveys, between 27 July and 13 August, there was net aggradation of +940 m<sup>3</sup> (Figure 5-4a).

On a daily basis, the total amounts of either erosion or deposition observed through river bed changes are on average a factor 3 larger than the net change, although this factor may be less than 2 and as much as 10, the latter for the flood of 10 August (Figure 5-4a). Despite the large scale erosion and sedimentation that took place throughout the river bed during the flood, the net effect was limited, amounting to not much more deposition than in the days preceding it. The 10<sup>th</sup> of August flood caused a marked shift from net sedimentation to net erosion in the days directly after the flood and later in August during which another flood occurred on the 14<sup>th</sup>. Similarly, a temporary response in terms of erosion may be observed on 27 July, shortly after the flood of 24 July. Therefore, although the flood events may not necessarily be erosive, there are indications that they may impact the river morphology such that it is susceptible to subsequent erosion during smaller flow events.

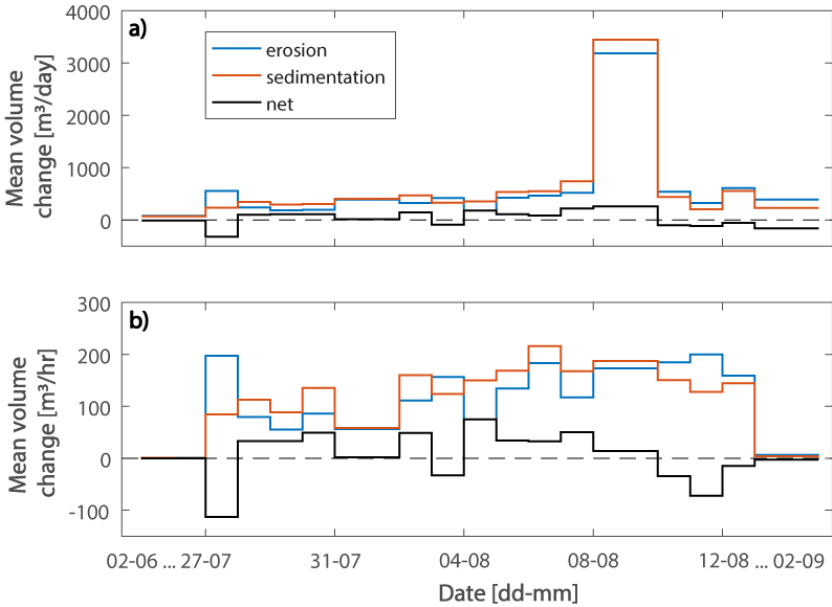


Figure 5-4 a) Sediment budget on daily basis: net sedimentation, net erosion and net change in the braided reach and b) associated mean rates of change during effective flow (that is the total duration without flow intake).

The mean rates of sedimentation and erosion during the period vary much less than the associated volumes (Figure 5-4b). Most notably, the period with the 10<sup>th</sup> of August flood has similar rates as the

days that precede it, indicating the importance of the long flood duration and not necessarily high flow conditions in changing the river bed topography (Figure 5-2). However, we have to note that net changes are recorded in morphological change and that the actual, instantaneous rates may be much higher as intermittent erosion and sedimentation occurs.

The mean rate at which net daily morphological change occurs in the reach is related to the relative amount of upstream sediment supply and water yield (Figure 5-5; periods longer than 1 day are excluded to allow for comparable net changes). When relative sediment input rates (sediment supply/water yield) drop below 0.02, this causes strongly increasing river bed degradation rates; typically when there are few normal gravel trap flushing events which are most efficient in terms of the water used to evacuate a volume of sediment. Here, there is no evidence that these erosion rates approach a maximum or are reduced due to river bed sorting and stabilization. On the other hand, increasing relative sediment input rates above 0.02 (generally a larger contribution of gravel trap flushing events) leads to sedimentation, but the sedimentation rates increase more slowly as a function of supply to yield ratio. This non-continuous response to upstream forcing indicates changes in the efficiency with which sediment-laden flushing events are transferred and hence changes in the river morphodynamic behaviour.

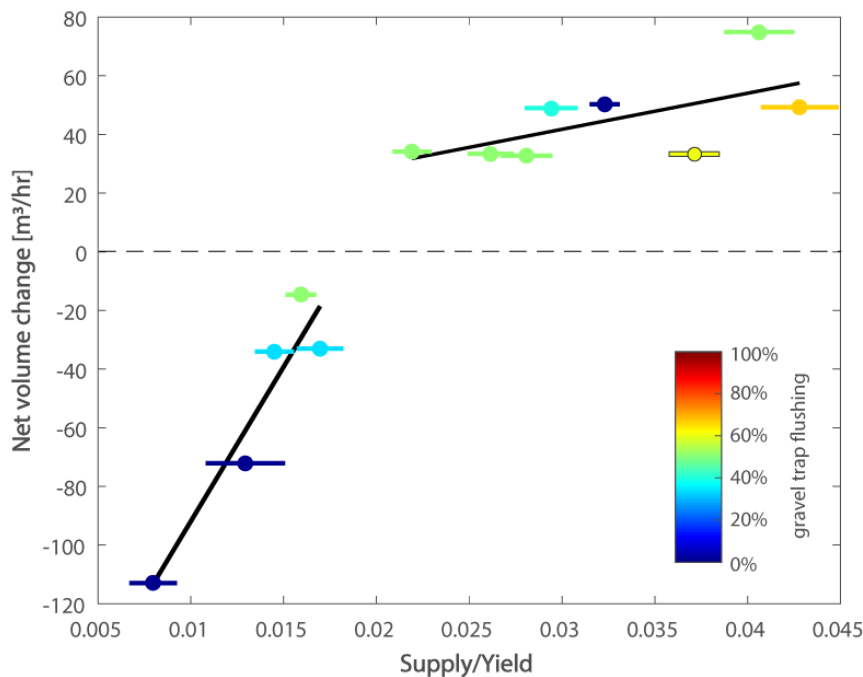


Figure 5-5 Mean rate of net volume change in the river bed as a function of the upstream input of sediment and water, supply/yield (including uncertainties in sediment load) and the fraction of gravel trap flushing events with respect to the total amount flow events (colour); regression lines are given for negative and positive net volume changes.

### 5.4.2 Morphological change

Along the reach, the variability in width-averaged bed level change is large both at a specific location between different events, particularly in the narrower stretches of the channel (upstream and downstream end), and for individual events in the downstream direction (Figure 5-6). There is no apparent large scale morphological forcing that leads to systematic bed changes along the river channel. We may distinguish a downstream recurring trend of net erosion and sedimentation in the period with the 10th of August flood, which has a large impact on the total change.

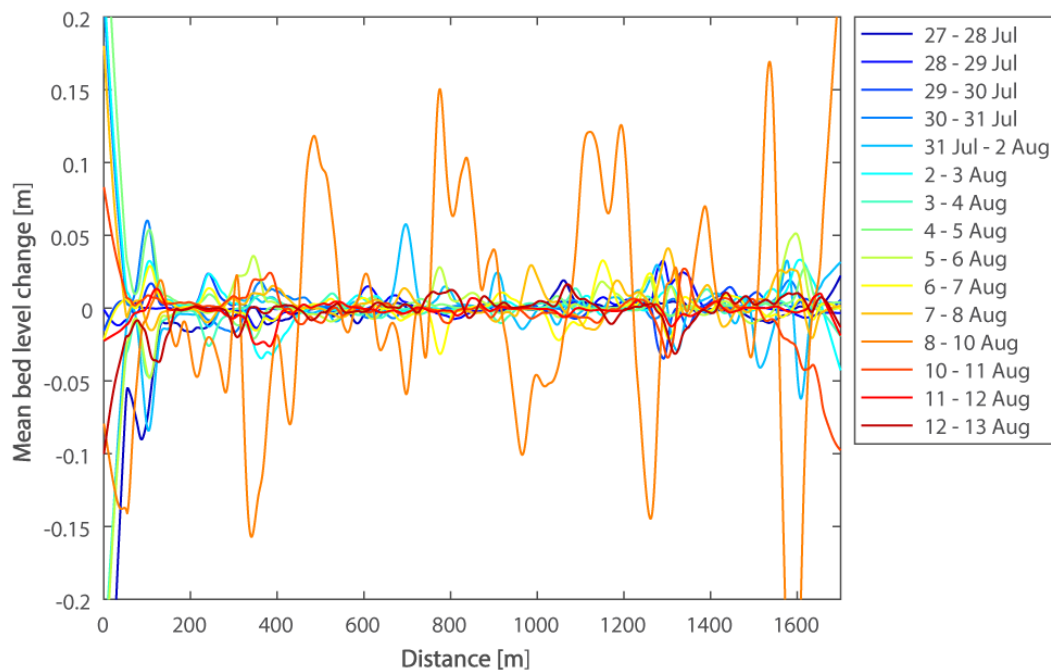


Figure 5-6 Width-averaged channel bed level change (greater than the limit of detection), smoothed with a 50 m running filter along the braided reach on a daily basis for the period 27 July - 13 August.

The cumulative morphological change for the period 27 July - 13 August is characterised by a spatially distributed pattern of patches with net sedimentation and net erosion (Figure 5-7a). Local changes in both erosion and sedimentation range up to c. 2 m. The percentage of the bed that has been reworked ranges from 25% upstream to nearly 75% of the active width downstream. The area of change comprises 48% net erosion with an average erosion depth of 0.35 m and 52% net sedimentation with an average height of 0.31 m. This indicates that erosional and deposition processes may lead to very similar yet opposite net changes, which may be expected in a bed load dominated braided river system. Where the system is close to competence, it follows that these are strongly coupled in space and related to the river bed morphology (see also Figure 5-6).

Temporal fluctuations in bed level may locally be very large as shown in the cumulative absolute change (Figure 5-7b). Although the absolute amounts depend strongly on survey frequency (the

same applies for the change frequency in Figure 5-7c), it reveals local ‘hot-spots’ of temporal change whereas net change may be much smaller. In the upstream half of the reach these are local sites of temporary sediment storage which are repeatedly emptied and refilled (Figure 5-7b and 5-7c). In the downstream half of the reach these areas become less patchy and are more spread out over the width of the active river bed. A relatively large area of river bed was altered during the 10<sup>th</sup> of August flood (Figure 5-7d) which reworked earlier areas of erosion and sedimentation due to flushing events which were more local and channel-bound. There is therefore no spatial gradient in change or morphological age, but rather two main types of morphodynamic events which shape the river bed: high frequency smaller magnitude flushing events and intermittent higher magnitude floods.

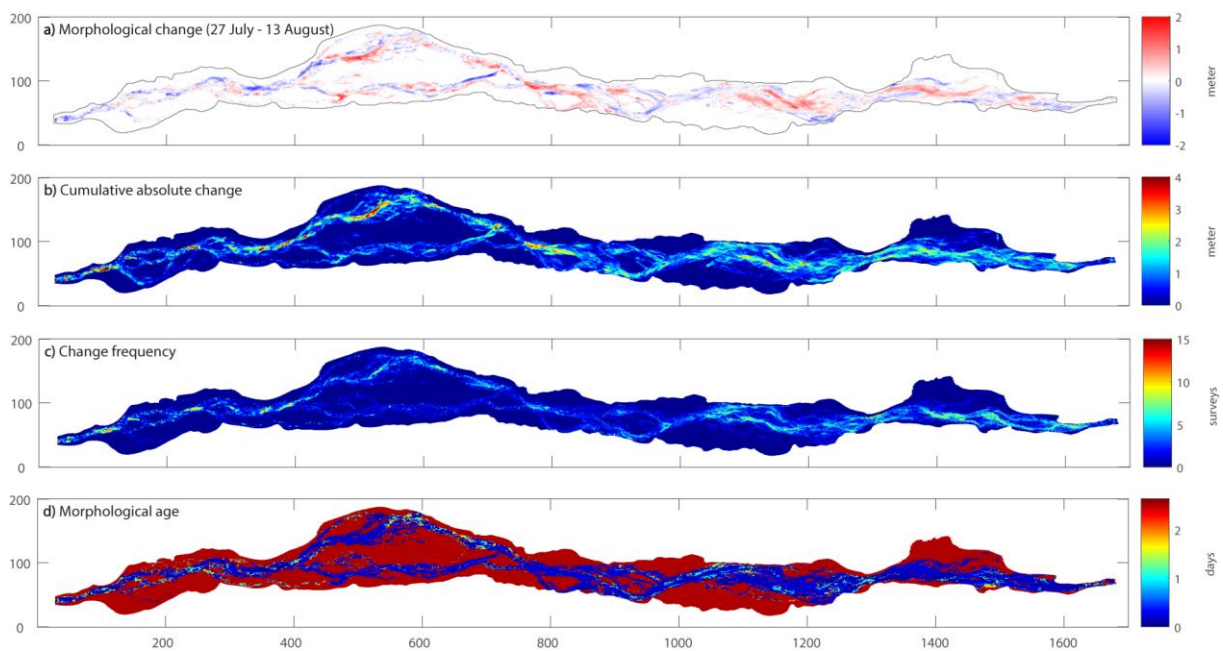


Figure 5-7 a) Morphological change in the period 27 July - 13 August (greater than the limit of detection); b) the cumulative absolute change measured on daily basis; c) the surveyed frequency of significant change; and d) morphological age of the river bed in terms of flow duration (not actual time because flow is intermittent).

#### 5.4.3 Sediment transport

Daily mean sediment transport rates in the period 27 July - 13 August are shown in Figure 5-8. On average, transport rates increase until the widening of the channel at c. 450 m distance, which is the result of the net erosion in this part of the reach (Figure 5-7a). At this location there is also a general decrease in slope and grain size in the reach (Bakker et al., 2018), from where there is gradual deposition in downstream direction (Figure 5-4).

In general, the sediment input rates are larger than the fluctuations in transport rate down the reach which indicates the importance of upstream supply, which is for the most part transported through

the reach. As with observations in Figure 5-5, low input rates tend to be associated with sediment transport increase along the reach (indicating erosion) and vice-versa, although this is not necessarily the case, and downstream fluctuations may be relatively large and local. The 10<sup>th</sup> of August flood appears to play an important contribution to mean transport down the reach. Here we must note that there is a significant uncertainty in magnitude of the sediment supply and transport rates during this long, continuous flow period. Similar to width-averaged bed level change (Figure 5-6), sediment transport shows a large variability between different periods and in downstream direction (Figure 5-8). There appears to be no systematic upstream forcing on the local downstream sediment transport dynamics.

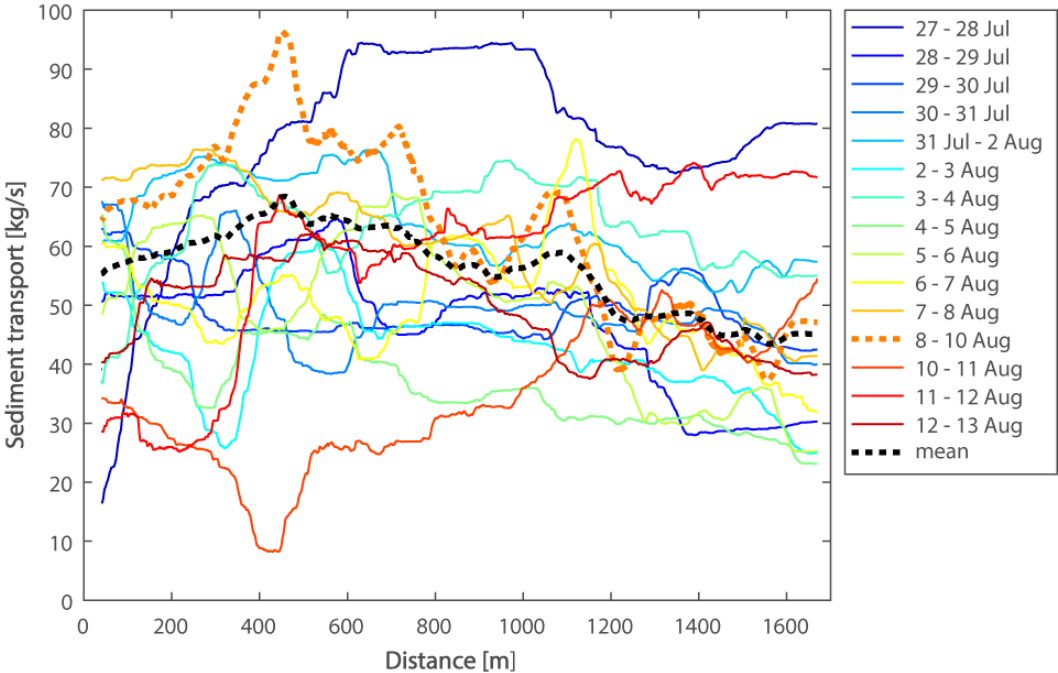


Figure 5-8 Width-averaged sediment transport along the braided reach on a daily basis in the period 27 July - 13 August; the transport during the flood period 8-10 August (orange) and average transport (black) are shown with a dashed line due to uncertainties in upstream sediment input.

A significant proportion of the total estimated amount of sediment transport for the period 27 July - 13 August is transferred through a main transfer channel (Figure 5-9a; note the logarithmic scale). The main transport follows the right bank channel between 400 and 800 m in the downstream direction. This is reflected in the observation that the largest morphological changes occur in the left channel which is gradually abandoned (Figure 5-7b). Further downstream, from 1000 m, the sediment transport follows a remarkably straight path (Figure 5-9a). We quantified total sediment transfer here as a volume, so it can be directly compared to the morphological change (Figure 5-7b), which reveals that transport may locally be orders of magnitude larger. Similarly, there are areas that frequently transfer sediment (Figure 5-9b) which appear to be inactive in terms of morphological

change (Figure 5-7c). The age since last transport (Figure 5-9c) does not differ much from the morphological age (Figure 5-7d) due to the large-scale ‘resetting’ of the age near the end of the surveyed period, during the 10<sup>th</sup> of August flood.

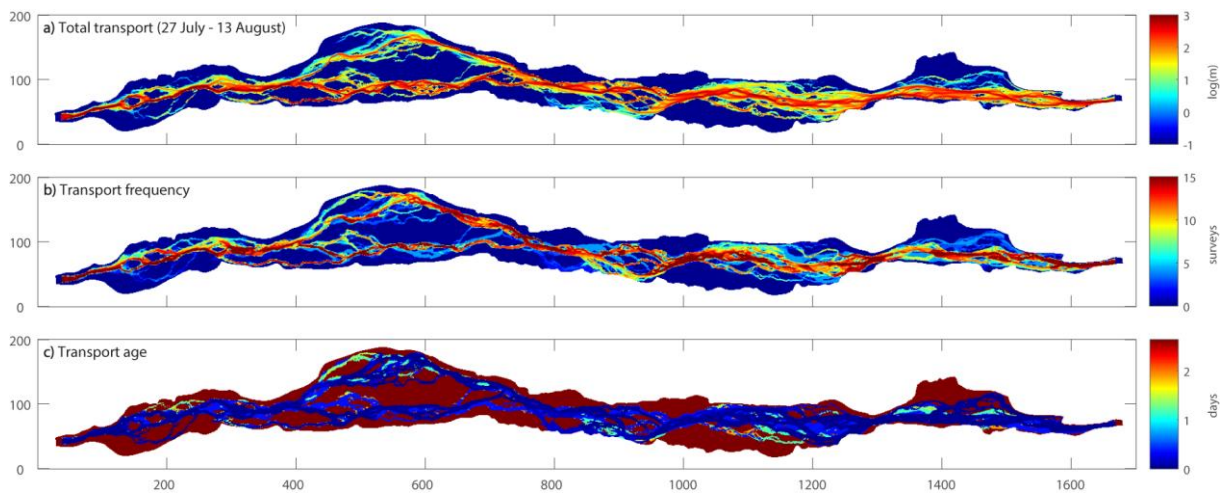


Figure 5-9 Sediment transport in the period 27 July - 13 August expressed as a) total transported volumetric load (log-scale); b) transport frequency; and c) transport age, i.e. flow duration since last recorded transport phase.

#### 5.4.4 Morphological forcing of change

##### *Local relief*

We found that local relief has an impact on river bed change throughout the reach, where (net) sedimentation dominates change in the channel bottom and erosion dominates change at higher elevations within the wetted profile. This effect is particularly clear in the period with the 10<sup>th</sup> of August flood (Figure 5-10a). The influence of local relief upon morphological change is also present during intervals with sequences of flushing events, although the effect is minor (e.g. Figure 5-10b). Two observations can be made here which may not be directly evident. First, the range of (potential) morphological change is much higher for the flood than for the sequence of flushing events (and the maximum frequency values are lower). However, this does not yield a more scattered and weaker response, but rather a more distinct (gradient steepness) and significant (r-value) forcing trend. Second, the duration of the flood event over which the channel bed evolves is also much longer than for the sequence of flushing events, the difference is nearly a factor 10 (Figure 5-2b). The influence of local relief is still stronger over the longer period, despite intermittent topographic change which may alter the forcing.

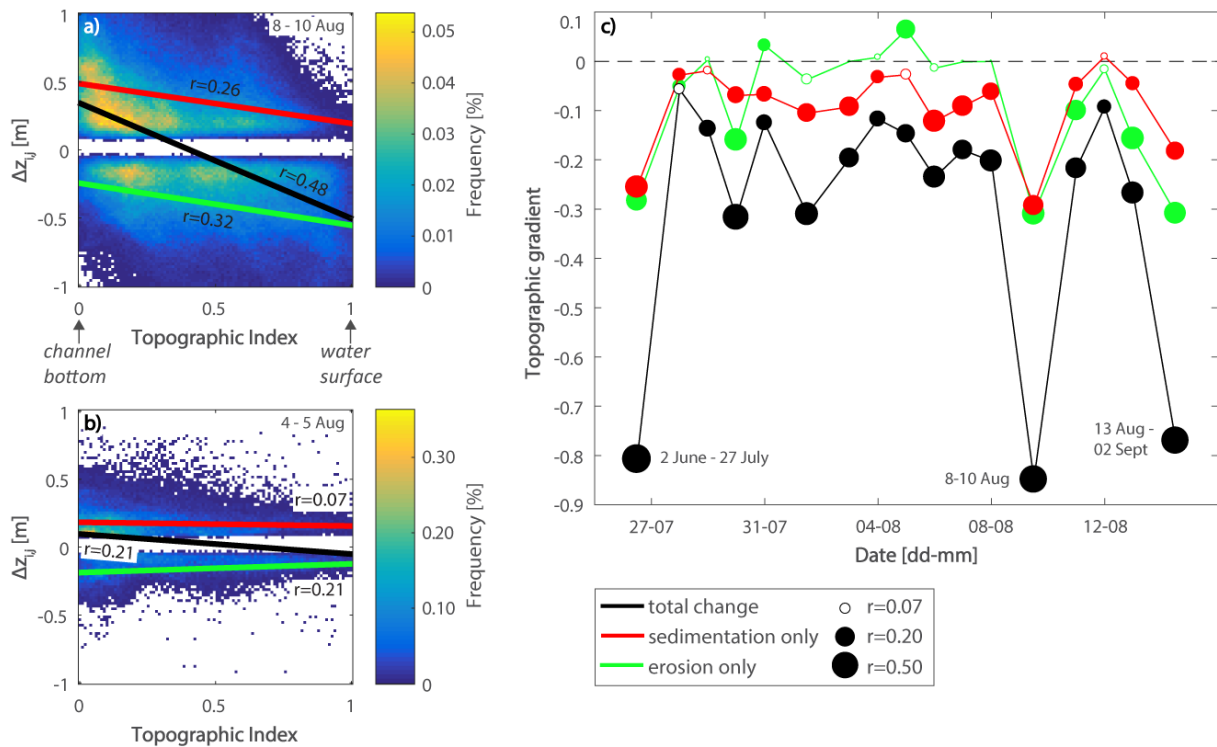


Figure 5-10 Local relief: occurrence frequency of morphological change (greater than the limit of detection) along the relative depth of the wetted profile (Topographic Index) for the periods a) 8 - 10 August flood and b) 4 - 5 August flushing event sequence; regression lines describe total change, and deposition and erosion separately; c) Topographic gradient, corresponding to the gradient of regression lines in e.g. a) and b), representing the influence of local relief on morphological change in the investigated period; the significance and strength of the relation is depicted as point fill (filled points are significant) and size (the larger the point the stronger the correlation), the r-value in e.g. a) and b).

Figure 5-10c summarizes the influence of local relief, showing that the effect occurs throughout the investigated period. Negative topographic gradients (gradients of regression lines in plots a, b) indicate the tendency to fill the lows and to erode the highs and are significant in nearly all cases (filled points). This provides a mechanism that drives the instability that is characteristic of braided channel dynamics. It is observed both in periods with net sedimentation and erosion (Figure 5-4a), although the contributions of sedimentation differ somewhat (Figure 5-10c), where before the 10<sup>th</sup> of August flood channel sedimentation dominates the forcing signal, and after the flood, it is largely the erosion of higher parts within the channel. In addition, the longer periods of change of 2 June until 27 July and 13 August until 2 September (both net erosion) show an effect very similar to the period with the 10<sup>th</sup> of August flood. This indicates that floods, despite their infrequent nature, may have a dominant impact on the longer term, seasonal dynamics and may override daily effects from flushing events.

## System memory

Besides being conditioned by channel bed topography, there is evidence that morphological change is also forced by earlier changes. The period including the 10<sup>th</sup> of August flood shows a weak dependency on earlier morphological change in the form of a negative feedback (Figure 5-11a); higher frequency values (> 0.08%) coincide to a certain extent with the negative feedback axis, the dashed line with equal quantities of opposite change. In an earlier flushing dominated period this effect strongly dominates the morphological response (Figure 5-11b). The observed memory effect during flushing event sequences can be attributed to temporary sediment storage in the river channel, due to the high sediment loads and the abrupt 'on-off' nature of these flows, which can be easily entrained during the next flushing event sequence. This illustrates the dynamic character of the braided reach with ample morphological change, but with a very small net change in sediment storage (see also Figure 5-4a).

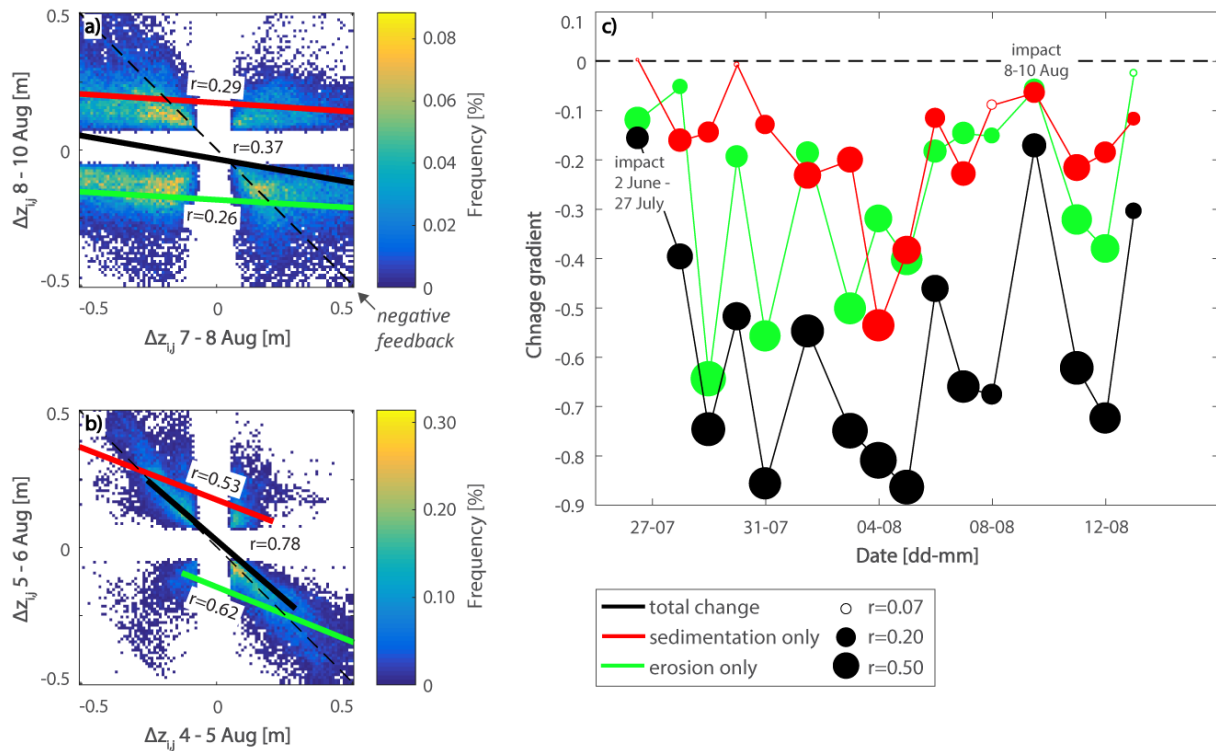


Figure 5-11 Memory effect: occurrence frequency of morphological change (greater than the limit of detection) for the periods a) 8 - 10 August change (y-axis) in response to the change in 7 - 8 August (x-axis) and b) 5 - 6 August change in response to the change in 4 - 5 August; regression lines describe total change, and deposition and erosion separately; the dashed line indicates perfect negative feedback; c) change gradient, corresponding to the gradient of regression lines in e.g. a) and b), representing the impact of changes on subsequent changes for all consecutive periods in the investigated period; the significance and strength of the relation is depicted as point fill (filled points are significant) and size (the larger the point the stronger the correlation), the r-value in e.g. a) and b).

Figure 5-11c generalises the results shown in Figures 5-11a and 5-11b. Over the total investigated period, in nearly all consecutive events, significant negative feedback is observed where a period of sedimentation is followed by erosion and vice versa. The memory effect of earlier morphological changes is smallest, though present, during periods with floods that largely respond to local relief (Figure 5-10c; 2 June - 27 July and 8 - 10 August). The change gradient is negative throughout, despite variable upstream forcing (Figure 5-5), signifying a general autogenic mechanism that slows the rate of river bed aggradation or degradation.

When we determine the change gradient for all combinations of survey intervals (not only period 1 vs period 2 as in Figure 5-11c, but also period 1 + period 2 vs. period 3 etc.) and relate these to the corresponding effective flow period, the longer timescale over which the memory effect forces cumulative morphological change emerges (Figure 5-12). The effect of perturbations lasts for approximately 6 days of effective flow although there may be longer exceptions. Considering the average daily flow duration in the investigated period this corresponds to nearly 60 days, although it must be noted that high flows are overrepresented in the flow record when compared to ‘natural’ conditions without flow abstraction. The duration or persistence of the memory effect is related to 1) the cumulative effects in the main channel which leads to progressive change which conditions 2) the effect of single large floods that rework large sections of the braided reach (Figure 5-7c).

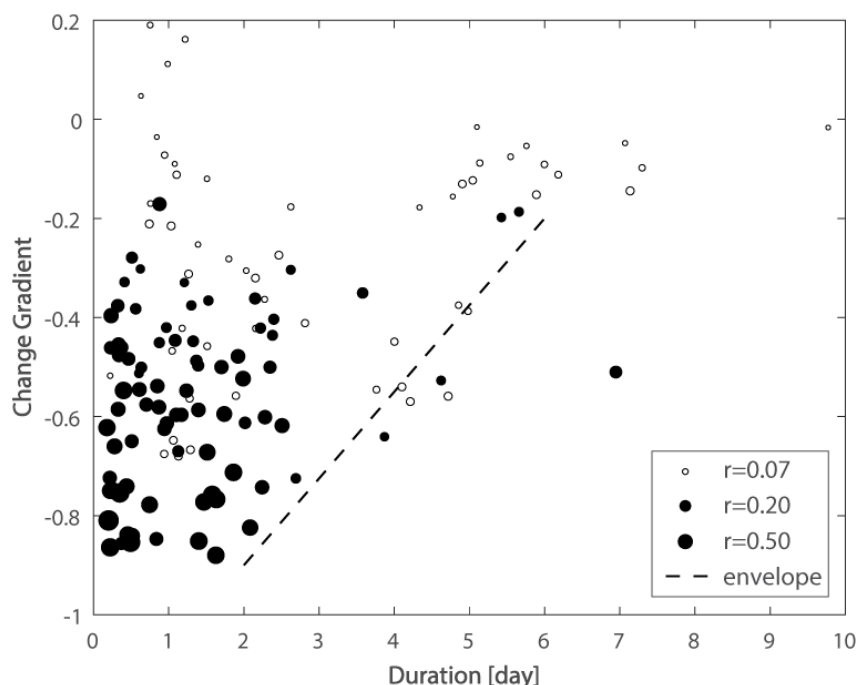


Figure 5-12 Duration of memory effect in the system, based on the change gradient for all combinations of survey intervals (see Figure 5-11); the strength of the relation is depicted as point fill (filled points are significant) and size (the larger the point the stronger the correlation); an envelope line is drawn to depict the maximum duration and associated change gradient.

## 5.5 Discussion

### 5.5.1 Spatial and temporal morphodynamics

In this study, we quantified the spatial and temporal morphodynamics of a braided Alpine river reach over different spatio-temporal scales and using a number of different metrics. When addressing the spatial scale of the analysis, we found that net reach-based changes in the Borgne may be up to one order of magnitude smaller than total erosion and deposition which are spatially distributed throughout the braided reach (Figure 5-4a). Similarly, when increasing the temporal resolution from three week period (27 July - 13 August) to daily surveys, the variability of morphological change increases by as much as a factor two if we total absolute daily changes (Figure 5-7a vs. 5-7b). If we assume a typical inverse decay of change as a function of time (Lindsay & Ashmore, 2002), we may expect much higher rates of change over even shorter time scales. This decay may break down when the survey frequency captures individual flow events and the unaccounted morphological change relates to the temporal distribution of transport within events. Comparison of the total transported load and its spatial distribution (Figure 5-9a) to the cumulative morphological change during the three week period (Figure 5-7a) does suggest that integrated transport volumes may be orders of magnitude higher than net morphological change. Data suggest the relatively concentrated and efficient nature of bed load transport within individual reaches (Figure 5-9a), while a much wider section of the studied reach is morphologically reworked. Interestingly, just upstream in the unregulated pro-glacial reach of the Borgne, Warburton (1992) found similar narrow bands of transport using contemporary bed load sampling, estimating up to an order magnitude change per meter cross-section.

The observations above illustrate the limitations of survey frequency and ordinary change detection approaches (Lane et al., 1994; Lindsay & Ashmore, 2002; Milan et al., 2007). Spatially, it emphasizes the importance of distributing transport rates using the 2D morphological approach (Antoniazza et al., in revision). To determine absolute amounts, a well constrained upstream boundary, in our case known volumes of flushed sediment, is of importance, particularly where there is relatively high throughput of sediment. Using a similar routing approach, Kasprak et al. (2018) apply particle path length modelling to simulate transport loads. The combination of repeat remote sensing and conceptual sediment transfer modelling may provide an effective way to handle limitations of process-based 2D modelling approaches in braided systems (Haff, 1996) and to study braided river dynamics and processes.

The temporal dynamics of the Borgne are directly impacted upon by the short duration of flow events associated with the large-scale abstraction of water. A large part of the riverbed is either old

or not morphologically active (Figure 5-7), even though it is not actively integrated into the floodplain. The part of the river bed that is directly affected by the relatively short duration flows is reworked through a combination of high-frequency flushing events and low-frequency floods. This leads to a largely bimodal distribution in age and perturbation frequency as reflected in both morphological change and sediment transport (Figures 5-7c, 5-7d and Figures 5-9b and 5-9c). Flow management through flushing can be associated with laterally relatively stable channel morphology that is eroded into flood deposits (Figure 5-4) and efficiently transfers sediment (Figure 5-9a). This is occasionally disrupted by floods that redistribute large amounts of sediment in the reach which may lead to channel migration and avulsion. The key point here is that upstream flow management does not only have an impact on the local magnitude and frequency of braided channel dynamics, but also on its spatial distribution. This will have important implications for morphodynamics, in terms of bed forms, grain size sorting, and for vegetation and ecological succession (Gabbud & Lane, 2016).

Where relatively distinct surface extents are affected by flushing and flooding, the question arises whether in more natural systems a continuum in surface reworking may be expected? Based on steady-state flume experiments, Wickert et al. (2013) found that unworked surface area decays exponentially in time. Under natural, unsteady forcing of flow and sediment input however, thresholds in the system functioning, such as pavement breakup (Vericat et al., 2006) or above/below bankfull discharge (Bertoldi et al., 2010), may lead to a non-continuous reworking of the channel bed in both space and time. This is what Warburton (1992, 1994) found in the reach upstream of the investigated Lower Bertol flow intake, where meltwater floods cause 'dramatic channel shifts', but what has also been observed elsewhere, typically in proglacial braid plains, e.g. Nicholas and Sambrook Smith (2003). This indicates the importance of unsteady forcing of braided river morphodynamics and that this may have impacts that are not revealed in steady-state experiments.

#### 5.5.2 Upstream and local forcing of morphodynamics

The Borgne river bed response to upstream sediment and water input during flushing events (external forcing) leads to different rates of reach-scale morphological change (Figure 5-5). Flushing event sequences with relatively high sediment loads (gravel trap flushing) lead to net aggradation at relatively low rates. On the other hand, flushing event sequences with relatively low sediment loads (sand trap flushing and night-time flushing) cause degradation at higher rates but occurred less frequently. Within the reach, there appears no systematic trend in the deposition and erosion along the length of the braided channel that indicates systematic morphological forcing of the bed level change (Figure 5-6) or a related adjustment in sediment transport loads (Figure 5-8). The spatial

distribution of morphological change varies considerably in magnitude and direction throughout the braided channel of the Borgne (Figure 5-7a).

Although no large-scale spatial morphological forcing was evident, there is a notable reach-wide trend in the effects of local relief which is found throughout the investigated period (Figure 5-10). This is characterized by channel bottom deposition and erosion higher up in the channel or on the bars. The strongest effect is found during floods which may be supported by two mechanisms. First, the longer duration flow of flood events allows for coherent morphological change to occur. In contrast, during flushing sequences, multiple relatively short phases of entrainment, transport and deposition lead to a less apparent effect of local relief. Second, the filling of lows and eroding of highs effectively widens channels to accommodate the higher flow and particularly sediment loads that largely remain within the channel (Figure 5-9a). The erosive effect at higher elevations within the wetted profile may lead to an increase in sediment loads in the channel bottom providing a positive feedback mechanism. The filling of lows and eroding of highs is a key characteristic that drives braided river dynamics and a necessary condition to maintain the braided state.

The morphodynamics of the river bed also shows negative auto-correlation, where morphological changes in one period are partly compensated in the next period (Figure 5-11). This memory effect is most prominent in the short duration sequences of flushing events, where deposition at one location in one time period is largely balanced by erosion in the next period and vice-versa. In this case, local channel deposition is related to the temporal dynamics of sediment availability, which is a direct consequence of the timing and abrupt cessation of flushing events, and not so much forced by the local topography (although there are preferential 'hot-spots' of temporal change; Figure 5-7b). The sediment that is temporarily stored in the channel can subsequently easily be entrained by the flushing wave front in the following period. Mechanisms that affect changes in the bed surface and associated critical bed shear stress (Kirchner et al., 1990) may strengthen such a memory effect. A deposition sequence of graded sediment typically consists of the initial deposition of coarse material in topographic lows and subsequent deposition of finer material which preferentially fills the voids between the coarser grains, leading to a decrease in bed roughness and critical shear stress (Ferguson et al., 1989; Venditti et al., 2010), and hence facilitating erosion in a subsequent event (Johnson, 2016). Differences in flow conditions under which deposition in one event and entrainment in the following event occurs (Turowski et al., 2011) are not likely to play a role due to the consistently highly competent flows. In addition, due to the flow abstraction in this case, there are low flows which may stabilize the river bed over time between higher flow events (Masteller & Finnegan, 2017; Reid et al., 1985).

Field-based studies have shown memory effects on a local scale and at high temporal resolution, e.g. Turowski et al. (2011). In this study, we complement such work through showing the spatial extent and coherence of memory effects throughout a braided reach on a low, daily temporal resolution. In fact, this effect persists for days of effective flow (Figure 5-12) and potentially considerably longer if it were not for occasional flood events. In space, it appears that there is a decreasing impact of flushing (memory effect) and increasing lateral dynamics (effect of local relief) in downstream direction, where change is less concentrated in channel pockets and more widespread throughout the braided channel cross-section (Figure 5-7b).

### 5.5.3 System dynamics driving morphological evolution

Over the whole period of investigation, June - September 2015, net river bed degradation occurs, which corresponds to the trend for the period 2010-2014 (Bakker et al., 2018). In 2015, erosion was observed in the beginning of the study period (June - July), but also in the second half of August (Figure 5-4). In both periods, larger magnitude floods occurred. It may be expected that these floods are important for river bed degradation, considering their relatively high flow competence and low sediment loads. Here, relative is defined as to flushing which is designed to evacuate sediment traps while using a minimal amount of water.

Based on the daily topographic surveys, however, we found sedimentation in the period with the 10<sup>th</sup> of August flood and erosion in the days after the event (Figure 5-4). A similar response was found in 2013 (Antoniazza, 2015). This could be caused by the relatively lower rates of sediment supply (Figure 5-2d), related to a relatively low frequency in efficient gravel trap flushing (Figure 5-5). It may also be related to the morphological changes in the river following the flood; i.e. channel bottom deposits that formed during floods (Figure 5-10a) are entrained by subsequent flushing event sequences (Figure 5-4). This could be supported by grain size related mechanisms: 1) high water levels and potential pavement break-up during the flood may allow the access to finer sediment that is more readily eroded in subsequent events, e.g. Hoey and Sutherland (1991); Lenzi et al. (2004), and 2) the relative input of fine sediment in the reach, both from the within reach sources accessed by the flood and deposited during the falling limb and the sand trap flushing, which may decrease bed roughness and facilitate erosion. Therefore, besides the sediment load, there is an element of grain size control on flushing type and frequency and downstream morphological change. Concerning the role of floods, the point we want to make here is that they may have a phased impact on morphology and morphodynamics, which lasts longer than the duration of the event, which may be considered as a longer-term memory effect. In the short term, they may cause either net erosion or deposition, largely depending on how much sediment is supplied with them, as has been observed in

upstream pro-glacial reaches (Lane et al., 1996; Warburton, 1994). On the longer term, these floods may cause critical changes in morphology that lead to subsequent river bed reworking and potential erosion.

Besides the highly competent floods, series of flushing events have been shown to be effective in the transfer of sediment. Similarly, Ashworth and Ferguson (1986) found that transport rates could be very efficient, even at low discharges, as a function of previous sediment delivery events. During flushing, the sediment-laden flow remains within the channels, limiting the inundation area where sediment may be deposited. Sediment that is deposited may be entrained in subsequent events, leading to a pulsed kinematic effect where sediment is transferred fairly efficiently through the system (Figure 5-9a). This is reflected in low aggradation rates, e.g. Figure 5-5, and may explain longer term observations in the period 1959-2014 that, whilst there is large scale flow abstraction (c. 90%), flow capacity is still sufficient to export a very significant proportion (> 75%) of the sediment delivered to the reach (Bakker et al., 2018). High sediment loads maintain the high turnover rates that prevent either the development of river bed armouring or the encroachment of vegetation, allowing the persistence of braiding processes (Harvey, 1991).

## **5.6 Conclusions**

In this study, we investigated the morphodynamics of a well-constrained Alpine braided river reach through frequent (daily) lidar topographic surveys. We further used these to determine spatially distributed mean sediment transport rates to infer changes that are not recorded in the local geomorphology, but can be deduced from the spatial distribution of changes. This approach allowed us to characterize the spatial and temporal signature of the system dynamics. We found that, although a relatively wide section of the river bed is reworked, bed load transport is highly concentrated and efficiently transported through a narrow channel thread. The temporal variation of discrete flow events, in the form of frequent flushing events and occasional floods, translates into a bimodal distribution in spatial reworking of the river bed corresponding to these types of events, with the necessary implications for morphological and ecological development. Although the impact of the regulated nature of this setting is evident, we argue that similar effects may result in more natural settings as a result of non-linear response to external forcing, due to system thresholds which may be exceeded during floods, such as pavement breakup.

Reach-scale morphological change is driven by upstream sediment supply during flushing events, but in a non-linear fashion, where flushing events with low sediment loads lead to erosion with relatively high rates of change, but are less frequent than flushing events with high sediment loads that show

lower rates of change. The spatial distribution of sediment transport and local morphological change varies strongly within the braided reach and between successive flushing event sequences. Local morphological change is driven to a large extent by two effects that are found throughout the investigated period, regardless whether there was net aggradation or degradation. First, local relief leads to the preferential filling of low areas within the channel cross-section and eroding of higher areas. The effect was most prominent in the response to longer duration floods and is regarded as a necessary condition to maintain a braided river. Second, system memory was present in the form of a negative feedback in bed level change: erosion in one period is followed by aggradation of a similar magnitude in the following period and vice-versa. This effect is most prominent in the flushing event sequences and can be attributed to the temporary storage of high sediment loads and the abrupt 'on-off' nature of flushing flows. Deposited sediment is readily entrained during subsequent events, which may be enhanced through temporal bed surface changes that facilitate erosion. Despite their high sediment loads, flushing events may therefore still efficiently evacuate sediment through sequential transport and play an important role in maintaining relatively low aggradation rates in a river that is heavily impacted upon by flow abstraction.

In general, the data reveals a crucial point for how we conceptualize braided river dynamics. The internal morphodynamics of the system (that is morphological variability in space and time as reflected in respectively the effects of local relief and system memory) condition their own response to external forcing by, in this case, sediment-laden flows. Thus, events with similar external forcing may lead to a different morphodynamic response and consequently sediment transfer. This point challenges simplistic notions regarding the equilibrium morphology that forms after adjustment to a flood event and emphasizes the need to factor in historic evolution and morphodynamics in order to quantify and predict future system response.

#### *Acknowledgments*

Maarten Bakker is supported by the Swiss National Science Foundation, Synergia grant CRSII2\_147689, awarded to Fritz Schlunegger, Stéphanie Girardclos, Stuart Lane, Jean-Luc Loizeau and Peter Molnar. We would like to thank Grande Dixence SA, Alpiq, and Hydro Exploitation for providing discharge data and Chrystelle Gabbud for field support with the lidar surveys.

## References

- Antoniazza, G. (2015). Morphological forcing of erosion and deposition patterns in a braided river revealed through an Alpine field laboratory. Master's thesis in Geography, University of Lausanne.
- Antoniazza, G., Bakker, M., & Lane, S. N. (in revision). Revisiting the morphological method in two-dimensions to quantify bed material transport in braided rivers. Submitted to *Earth Surface Processes and Landforms* Special Issue.
- Ashmore, P., & Church, M. (1998). Sediment transport and river morphology: a paradigm for study. Water Resources Publications LLC, Highlands Ranch, Colorado, 115-148.
- Ashmore, P. E. (1982). Laboratory modelling of gravel braided stream morphology. *Earth Surface Processes and Landforms*, 7(3), 201-225.
- Ashmore, P. E. (1991). How do gravel-bed rivers braid? *Canadian Journal of Earth Sciences*, 28(3), 326-341. doi:10.1139/e91-030
- Bakker, M., Costa, A., Silva, T. A., Stutenbecker, L., Girardclos, S., Loizeau, J. L., . . . Lane, S. N. (2018). Combined Flow Abstraction and Climate Change Impacts on an Aggrading Alpine River. *Water Resources Research*, 54(1), 223-242. doi:10.1002/2017WR021775
- Begnudelli, L., & Sanders, B. F. (2006). Unstructured Grid Finite-Volume Algorithm for Shallow-Water Flow and Scalar Transport with Wetting and Drying. *Journal of Hydraulic Engineering*, 132(4), 371-384. doi:10.1061/(ASCE)0733-9429(2006)132:4(371)
- Bertoldi, W., Zanoni, L., & Tubino, M. (2009). Planform dynamics of braided streams. *Earth Surface Processes and Landforms*, 34(4), 547-557. doi:10.1002/esp.1755
- Bertoldi, W., Zanoni, L., & Tubino, M. (2010). Assessment of morphological changes induced by flow and flood pulses in a gravel bed braided river: The Tagliamento River (Italy). *Geomorphology*, 114(3), 348-360. doi:10.1016/j.geomorph.2009.07.017
- Beven, K., & Binley, A. (1992). The future of distributed models: Model calibration and uncertainty prediction. *Hydrological Processes*, 6(3), 279-298. doi:10.1002/hyp.3360060305
- Bezinge, A., Clark, M., Gurnell, A., & Warburton, J. (1989). The management of sediment transported by glacial melt -water streams and its significance for the estimation of sediment yield. *Annals of Glaciology*, 13, 1-5. doi:10.1017/S0260305500007527
- Carling, P. A., & Reader, N. A. (1982). Structure, composition and bulk properties of upland stream gravels. *Earth Surface Processes and Landforms*, 7(4), 349-365. doi:10.1002/esp.3290070407
- Ferguson, R. (1993). Understanding braiding processes in gravel-bed rivers: progress and unsolved problems. Geological Society, London, Special Publications, 75(1), 73-87. doi:10.1144/GSL.SP.1993.075.01.03

- Ferguson, R. I., Prestegard, K. L., & Ashworth, P. J. (1989). Influence of sand on hydraulics and gravel transport in a braided gravel bed river. *Water Resources Research*, 25(4), 635-643.  
doi:10.1029/WR025i004p00635
- Gabbud, C., & Lane, S. N. (2016). Ecosystem impacts of Alpine water intakes for hydropower: the challenge of sediment management. *Wiley Interdisciplinary Reviews: Water*, 3(1), 41-61.  
doi:10.1002/wat2.1124
- Gabbud, C., Micheletti, N., & Lane, S. N. (2015). Lidar measurement of surface melt for a temperate Alpine glacier at the seasonal and hourly scales. *Journal of Glaciology*, 61(229), 963-974.  
doi:10.3189/2015JoG14J226
- Gomez, B., Naff, R. L., & Hubbell, D. W. (1989). Temporal variations in bedload transport rates associated with the migration of bedforms. *Earth Surface Processes and Landforms*, 14(2), 135-156. doi:10.1002/esp.3290140205
- Gurnell, A. (1983). Downstream channel adjustments in response to water abstraction for hydro-electric power generation from alpine glacial melt-water streams. *The Geographical Journal*, 149(3), 342-354. doi:10.2307/634009
- Gurnell, A., Warburton, J., & Clark, M. (1988). A Comparison of the Sediment Transport and Yield Characteristics of Two Adjacent Glacier Basins, Val d' Herens, Switzerland. IN: *Sediment Budgets*. IAHS Publication (174).
- Haff, P. K. (1996). 14 Limitations on Predictive Modeling in Geomorphology. Paper presented at the *The Scientific Nature of Geomorphology: Proceedings of the 27th Binghamton Symposium in Geomorphology*, Held 27-29 September, 1996.
- Harvey, A. M. (1991). The influence of sediment supply on the channel morphology of upland streams: Howgill Fells, Northwest England. *Earth Surface Processes and Landforms*, 16(7), 675-684. doi:10.1002/esp.3290160711
- Heritage, G. L., Milan, D. J., Large, A. R. G., & Fuller, I. C. (2009). Influence of survey strategy and interpolation model on DEM quality. *Geomorphology*, 112(3-4), 334-344. doi:10.1016/j.geomorph.2009.06.024
- Hoey, T. (1992). Temporal variations in bedload transport rates and sediment storage in gravel-bed rivers. *Progress in Physical Geography: Earth and Environment*, 16(3), 319-338.  
doi:10.1177/030913339201600303
- Hoey, T. B., & Sutherland, A. J. (1991). Channel morphology and bedload pulses in braided rivers: a laboratory study. *Earth Surface Processes and Landforms*, 16(5), 447-462.  
doi:10.1002/esp.3290160506

- Johnson, J. P. L. (2016). Gravel threshold of motion: a state function of sediment transport disequilibrium? *Earth Surf. Dynam.*, 4(3), 685-703. doi:10.5194/esurf-4-685-2016
- Kasprak, A., Brasington, J., Hafen, K., Williams, R. D., & Wheaton, J. M. (2018). Modelling braided river morphodynamics using a particle travel length framework. *Earth Surf. Dynam. Discuss.*, 2018, 1-53. doi:10.5194/esurf-2018-17
- Kirchner, J. W., Dietrich, W. E., Iseya, F., & Ikeda, H. (1990). The variability of critical shear stress, friction angle, and grain protrusion in water-worked sediments. *Sedimentology*, 37(4), 647-672. doi:10.1111/j.1365-3091.1990.tb00627.x
- Lane, S. N., Bakker, M., Gabbud, C., Micheletti, N., & Saugy, J.-N. (2017). Sediment export, transient landscape response and catchment-scale connectivity following rapid climate warming and Alpine glacier recession. *Geomorphology*, 277, 210-227. doi:10.1016/j.geomorph.2016.02.015
- Lane, S. N., & Richards, K. S. (1997). Linking river channel form and process: time, space and causality revisited. *Earth Surface Processes and Landforms*, 22(3), 249-260. doi:10.1002/(SICI)1096-9837(199703)22:3<249::AID-ESP752>3.0.CO;2-7
- Lane, S. N., Richards, K. S., & Chandler, J. H. (1994). Developments in monitoring and modelling small-scale river bed topography. *Earth Surface Processes and Landforms*, 19(4), 349-368. doi:10.1002/esp.3290190406
- Lane, S. N., Richards, K. S., & Chandler, J. H. (1995). Morphological Estimation of the Time-Integrated Bed Load Transport Rate. *Water Resources Research*, 31(3), 761-772. doi:10.1029/94WR01726
- Lane, S. N., Richards, K. S., & Chandler, J. H. (1996). Discharge and sediment supply controls on erosion and deposition in a dynamic alluvial channel. *Geomorphology*, 15(1), 1-15. doi:10.1016/0169-555X(95)00113-J
- Lane, S. N., Westaway, R. M., & Murray Hicks, D. (2003). Estimation of erosion and deposition volumes in a large, gravel-bed, braided river using synoptic remote sensing. *Earth Surface Processes and Landforms*, 28(3), 249-271. doi:10.1002/esp.483
- Lenzi, M., Mao, L., & Comiti, F. (2004). Magnitude-frequency analysis of bed load data in an Alpine boulder bed stream. *Water Resources Research*, 40(7). doi:10.1029/2003WR002961
- Lindsay, J. B., & Ashmore, P. E. (2002). The effects of survey frequency on estimates of scour and fill in a braided river model. *Earth Surface Processes and Landforms*, 27(1), 27-43. doi:10.1002/esp.282
- Masteller, C., & Finnegan, N. J. (2017). Interplay between grain protrusion and sediment entrainment in an experimental flume. *Journal of Geophysical Research: Earth Surface*, 122(1), 274-289. doi:10.1002/2016JF003943

- Micheletti, N., & Lane, S. N. (2016). Water yield and sediment export in small, partially glaciated Alpine watersheds in a warming climate. *Water Resources Research*, 52(6), 4924-4943. doi:10.1002/2016WR018774
- Milan, D. J., Heritage, G. L., & Hetherington, D. (2007). Application of a 3D laser scanner in the assessment of erosion and deposition volumes and channel change in a proglacial river. *Earth Surface Processes and Landforms*, 32(11), 1657-1674. doi:10.1002/esp.1592
- Murray, A. B., & Paola, C. (1994). A cellular model of braided rivers. *Nature*, 371, 54. doi:10.1038/371054a0
- Nelson, J. M., & Smith, J. D. (1989). Evolution and stability of erodible channel beds. *River meandering*, 321-377.
- Nicholas, A. P., & Sambrook Smith, G. H. (2003). Relationships Between Flow Hydraulics, Sediment Supply, Bedload Transport and Channel Stability in the Proglacial Virkisa River, Iceland. *Geografiska Annaler: Series A, Physical Geography*, 80(2), 111-122. doi:10.1111/j.0435-3676.1998.00030.x
- Park, C. (1980). The Grande Dixence hydro-electric scheme, Switzerland. *Geography*, 317-320.
- Perona, P., Molnar, P., Savina, M., & Burlando, P. (2009). An observation-based stochastic model for sediment and vegetation dynamics in the floodplain of an Alpine braided river. *Water Resources Research*, 45(9), n/a-n/a. doi:10.1029/2008WR007550
- Reid, I., Frostick, L. E., & Layman, J. T. (1985). The incidence and nature of bedload transport during flood flows in coarse-grained alluvial channels. *Earth Surface Processes and Landforms*, 10(1), 33-44. doi:10.1002/esp.3290100107
- Riegl. (2015). Riegel Laser Measurement Systems: RiSCAN PRO version: 2.1.1. Horn, Austria.
- Turowski, J. M., Badoux, A., & Rickenmann, D. (2011). Start and end of bedload transport in gravel-bed streams. *Geophysical Research Letters*, 38(4). doi: 10.1029/2010GL046558
- Venditti, J. G., Dietrich, W. E., Nelson, P. A., Wydzga, M. A., Fadde, J., & Sklar, L. (2010). Mobilization of coarse surface layers in gravel-bedded rivers by finer gravel bed load. *Water Resources Research*, 46(7), W07506. doi:10.1029/2009WR008329
- Vericat, D., Batalla, R. J., & Garcia, C. (2006). Breakup and reestablishment of the armour layer in a large gravel-bed river below dams: The lower Ebro. *Geomorphology*, 76(1), 122-136. doi:10.1016/j.geomorph.2005.10.005
- Vericat, D., Wheaton, J. M., & Brasington, J. (2017). Revisiting the Morphological Approach Gravel-Bed Rivers (pp. 121-158): John Wiley & Sons, Ltd. doi: 10.1002/9781118971437.ch5

- Vetsch, D., Rousselot, P., Volz, C., Vonwiller, L., Peter, S., Ehrbar, D., . . . Veprek, R. (2014). System Manuals of BASEMENT, Version 2.4. Laboratory of Hydraulics, Glaciology and Hydrology (VAW). ETH Zurich. <http://www.basement.ethz.ch>
- Warburton, J. (1992). Observations of bed load transport and channel bed changes in a proglacial mountain stream. *Arctic and Alpine Research*, 24(3), 195-203. doi:10.2307/1551657
- Warburton, J. (1994). Channel change in relation to meltwater flooding, Bas Glacier d'Arolla, Switzerland. *Geomorphology*, 11(2), 141-149. doi:10.1016/0169-555X(94)90078-7
- Wheaton, J. M., Brasington, J., Darby, S. E., Kasprak, A., Sear, D., & Vericat, D. (2013). Morphodynamic signatures of braiding mechanisms as expressed through change in sediment storage in a gravel-bed river. *Journal of Geophysical Research: Earth Surface*, 118(2), 759-779. doi:10.1002/jgrf.20060
- Wickert, A. D., Martin, J. M., Tal, M., Kim, W., Sheets, B., & Paola, C. (2013). River channel lateral mobility: metrics, time scales, and controls. *Journal of Geophysical Research: Earth Surface*, 118(2), 396-412. doi:10.1029/2012JF002386
- Williams, R. D., Brasington, J., Vericat, D., & Hicks, D. M. (2013). Hyperscale terrain modelling of braided rivers: fusing mobile terrestrial laser scanning and optical bathymetric mapping. *Earth Surface Processes and Landforms*, 39(2), 167-183. doi:10.1002/esp.3437
- Zhang, Z. (1994). Iterative point matching for registration of free-form curves and surfaces. *International journal of computer vision*, 13(2), 119-152. doi:10.1007/BF01427149



## 6. CONCLUSIONS

The Conclusions address three aims. First, Section 6.1 provides a synthesis of the three main Chapters of the thesis and their wider relevance. Second, Section 6.2 aims to situate these within the context of the Swiss Upper Rhône basin, the focus of the SEDFATE project. Third, Section 6.3 considers opportunities to investigate further the fundamental questions that need to be addressed in order for research in this field to be taken forward.

### 6.1 Synthesis

#### 6.1.1 Quantifying river morphodynamics at the decadal scale

Chapter 3 presented an SfM-based methodology which allowed accurate quantification of historic topographic change, demonstrated for river-floodplain systems. Through benefitting from modern computer vision techniques the efficient nature of the methodology may help unlock larger archives of historical imagery. Image scale, texture and overlap were shown to be important factors in the quality of the photogrammetric analysis and so influence the quality of the data acquired. The work demonstrated that careful consideration of photogrammetric principles is necessary as systematic errors may significantly impact morphological change calculations (Figure 3-5), particularly where changes are small, near the limit of detection. Such methodological developments may contribute to the wider analysis of morphological changes at the decadal time-scale. This is the scale at which climate change and human activities have impacted Alpine fluvial landscapes, or for that matter any type of landscape, and therefore the scale at which changes need to be addressed (e.g. Lane *et al.* 1993; Micheletti *et al.* 2015; Rainato *et al.* 2018). Such long term records are therefore crucial to understand the extent and timing of changes forced by external drivers.

This work may stimulate the quantification of river and floodplain topographic change as complimentary to more widely used sedimentation records in proglacial lakes (e.g. Leemann and Niessen 1994) or hydropower reservoirs (Anselmetti *et al.* 2009) and stratigraphic records in river floodplain deposits (e.g. Laute and Beylich 2010) or moraine deposits (e.g. Karlén 1973; Burki *et al.* 2010). The combination of long-term records, sediment storage and sediment flux as in this thesis or consecutive sediment fluxes, may provide further information on the transfer of sediment in proglacial and fluvial systems. Sediment budgets are crucial to understanding sediment fluxes in these environments (Warburton 1990; Beylich *et al.* 2011; Carrivick *et al.* 2013; Rascher *et al.* 2018). These are however also challenging to construct because multiple sediment sources and sinks need to be constrained and/or quantified and addressed on a longer time-scale (e.g. Carrivick and Heckman 2017).

## 6.1.2 External forcing of Alpine river evolution

### *Paraglacial response to climate change*

Chapter 4 showed that an increase in the frequency of intake flushing and sediment delivery to the intakes could be related to annual variations in climate and glacial melt rates. Although temperature is the driving factor here, the buffering effect of winter precipitation in the form of snow was apparent. This confirms the importance of climate warming and glacial retreat in driving increases in sediment flux through proglacial streams and also shows the rapid and direct nature with which this may occur.

Lane *et al.* (2017), who studied the Haut Glacier d'Arolla proglacial margin located upstream of the reaches studied in this thesis, showed that although glacial recession increases sediment connectivity in the proglacial area, it is also accompanied by negative feedback processes which serve to reduce erosion and also slow sediment flux. Most notably is proglacial river bed reworking which may lead to armouring (Orwin and Smart 2004). Further, whilst it was possible to identify increased sediment input from newly developing sidewall gullies (Curry *et al.* 2006), coarse sediment accumulation at the base of these gullies formed alluvial fans which, following their diffusive nature, inhibit delivery to the proglacial stream (Lane *et al.* 2017; Figure 6-1). In addition to sediment supply and the degree of connectivity, the effect of glacial melt on stream discharge and transport capacity may be critical for the downstream transfer of sediment. Perolo *et al.* (in review) found the importance of flow competence as a control on the transport bed load sediment from under the Haut Glacier d'Arolla. This competence was related to the intensity of the melt-driven diurnal discharge cycles, with sediment transport capacity greater when the intensity was higher, and the development of a more efficient subglacial drainage network (Swift *et al.* 2005). Under accelerated glacial retreat there are continuous forcing mechanisms and various spatio-temporal responses, such that the net effect does not necessarily result in the progressive stabilization of the landscape.



Figure 6-1 Processes and feedback mechanisms before, during and after the transition to glacial recession that impact sediment delivery to the fluvial system; taken from Lane *et al.* (2017).

Whereas in the studied system there was a clear climate signal, generated near the glacier terminus, and this signal was rapidly transferred through the proglacial zone to the Borgne River, in other basins this may not be the case. There are considerable differences in glacial sediment yield and proglacial response between regions (Hallet *et al.* 1996) and individual basins (e.g. Kirkbride and Deline 2018). First, climate impact is manifest where the glacier surface lies within the elevation window of ice melt and glacial retreat; high altitude glaciers or parts of glaciers may not (yet) be susceptible. Where a climate signal may be generated, the strength of the signal depends on subglacial sediment production and availability, with respect to 'background' sediment production in the basin. This strongly depends on the nature of the glacial base: bedrock or unconsolidated sediment (Cuffey and Alley 1996; Alley *et al.* 1997). For instance, Burki *et al.* (2010) found basin erosion rates at the glacial margin may be up to an order of magnitude larger for a Norwegian glacier that was associated with bed accumulated sediment as compared to other glaciers in Norway that eroded bedrock. Second, sediment transfer in the proglacial margin then strongly depends on the extent to which processes are capable of connecting different landforms. Large amounts of sediment may not be transferred but are stored behind moraines (Cossart and Fort 2008), in proglacial lakes

(Geilhausen *et al.* 2013; Bogen *et al.* 2015) or in hanging valleys (Otto *et al.* 2009). In contrast to the transfer in the proglacial system of the Borgne, the presence of a proglacial lake may lead to a system where hillslopes, tributaries and bank erosion providing the largest contribution to sediment supply (e.g. Beylich and Laute 2015). These sources may be less affected by climate change or otherwise carry a different climate signal. Sediment connectivity may be (re-)instated with the filling of these sediment sinks, leading to potential thresholds in system response; similar to the hypothesized improved sediment connectivity of the Borgne with the Haut Glacier d’Arolla following glacier recession of the Bas Glacier d’Arolla (Section 4.5.2).

#### *River response to flow abstraction*

Flow abstraction has major impacts on downstream river bed morphology (Chapter 3) and sediment transfer (Chapter 3, 4). In the studied river c. 90% of the flow is abstracted, and it therefore may be expected that this should lead to a significant decrease in downstream sediment flux, given that sediment supply is maintained. In practice, c. 25% of the delivered sediment load is deposited, which whilst sufficient to create significant deposition downstream of the intakes, indicates that significant volumes of sediment are still transferred downstream. Similar results were found for different flow abstraction scheme in Austria, where ‘in spite of the low downstream flow volumes, bed load capacity - although considerably reduced - was still sufficient to transport the flushed bed load’ (Tschada and Hofer 1990). Calculations showed that sediment transport in the Borgne without flow abstraction would have been significantly greater than the rate of sediment supply, even given the increases in sediment supply described above in response to rapid climate warming. Under natural conditions, the river would have eroded and consequently armoured its bed, as found directly upstream (Warburton 1992), such that critical discharge needed to transport sediment would have increased and the sediment transport capacity would have fallen. With flow abstraction, sediment transport capacity falls to levels close to or just below sediment supply rates.

The supply-capacity relationship explains why only c. 25% of delivered sediment is deposited but also shows that flow abstraction makes the system particularly sensitive to small changes that can flip the system from supply limited to capacity limited (or *vice versa*) and degradation to aggradation (or *vice versa*). The sensitivity of these schemes was shown in the decadal scale record of sediment deposition in the Borgne (Chapter 4). It was also shown that the management of flow abstraction schemes has limitations (e.g. transfer tunnel capacity) and that consequent changes in the management may be driven by changing climate. This resulted in a recent increase in flood events that led to a differential response along the reach; degradation in the upstream reaches and aggradation in downstream reaches. Similar morphological changes have been observed in a

'natural', more stable proglacial river system, but were related to more extreme flooding, potentially related to the rupture of a glacial water pocket (Baewert and Morche 2014).

In the analysis of long-term sediment fluxes (Chapter 4) and spatially distributed sediment transport (Chapter 5), suspended bed material and washload are not specifically addressed, although these concentrations are typically high in these Alpine systems (Fenn and Gomez 1989). Flow and turbidity measurements that were taken during the summer of 2015 give an indication of the 'fate' of the suspended bed material in the headwater reach (Bakker *et al.* in prep.). First, the total amount of suspended sediment that is intercepted at the intake under normal flow conditions is low, of the order of 10%, and in line with values found by Bezingue *et al.* (1989). This is mostly suspended bed material that is caught in the sand trap (Figure 1-6). The washload that is not trapped enters the hydropower system and is transferred to the Lac de Dix (Figure 1-4). Second, the total suspended sediment load during commonly occurring night time flushing event is so high, that for the duration of these events (typically 1 hour), c. 50% of the daily load is passed by the intake and the investigated upstream reach (shown in Figure 5-1). The high suspended bed material loads of these flushing events is due to their coincidence with the flushing events of upstream intakes; sediment passes upstream intakes and flow conditions are considerably higher than during regular flushing events. This confirms the importance of the wider hydropower system operations for the general throughput of sediment (Chapter 4). It is important to consider here that operation is a function of the design of sediment traps and the transfer system and it is these that indirectly define the magnitude and frequency of non-regulated events under changing climate. For the morphological evolution of the system, the effects of non-regulated events are critical, whether caused by system capacity limitations (Chapter 4), system malfunctioning, etc.

### 6.1.3 Alpine river morphodynamics

The impacts of climate change and hydropower exploitation may have a large impact on river evolution, although this requires good connectivity in the proglacial system to deliver sediment and limitations in the capacity and operation of flow abstraction systems to reduce sediment transport capacity. The braided river bed subsequently responds to the external forcing through storing and transferring sediment and accordingly adjusting its braided morphology and associated dynamics (Chapter 5). Daily net change observed within the investigated reach was directly affected by upstream sediment supply during regulated intake flushing, but in a non-linear way. This indicates changes in the efficiency with which sediment-laden flushing events are transferred and hence changes in river morphodynamics. High sediment loads seem to be evacuated relatively efficiently through phases of transport and temporary storage within a relatively confined channel, which is

generally registered as a system memory effect. The demonstrated spatial distribution and extent of this effect can be related to similar short-term temporal effects in bed load transport found by Turowski *et al.* (2011). Over the longer term, the efficiency in transport allows for relatively low aggradation rates despite the large impact of flow abstraction (Chapter 4). The river bed shows a slightly different response to floods that when flow intake is ceased due to (near) system surcharge. The longer duration and relatively lower sediment load of these events allow for coherent morphological change to occur through the filling of lows and erosion of highs. Although these flood events may cause net erosion or deposition, depending on the sediment supply from upstream, they may also cause critical changes in morphology that lead to subsequent river bed reworking and potential erosion. This supports the notion that the increase in unregulated flood events, observed in Chapter 4, played an important role in the transition to net degradation and sediment export in the upstream reach studied here, after 2010. In general, the impact of flow abstraction on braided river morphodynamics and sediment transfer rates appears to be limited and cannot inhibit large scale transfer and export of sediment during climate driven flood events.

## **6.2 Implications for sediment transfer from glacier to delta**

The above results have provided information on the morphodynamics of a reach of braided stream on the left bank of the River Rhône, and assessed how these are being driven by climate change and human forcing related to hydropower at the scale of days to decades. This Section aims to situate these results in the context of the wider SEDFATE project.

Two elements of the SEDFATE project suggested substantial changes in sediment loading to Lake Geneva. First, Costa *et al.* (2018b) analyzed the effects of basin-wide forcing of hydro-climatic variables on the suspended sediment load at the outlet of the Rhône into Lake Geneva. Based on a spatially distributed temperature index method (Hock 2003), they focused on the changes before and after 1987, which saw a step-wise increase in temperature (Figure 2-1) and corresponding suspended sediment concentrations (Figure 1-2; here only the onset of this change is visible). Temperature increases were found throughout spring and summer, reducing snow-cover fractions in these periods (Figure 6-2), enabling hillslope erosion by rainfall on snow-free surfaces and, most notably, increased meltwater production from snow-free glacier surfaces (Figure 6-3) which cover c. 10% of the basin area. The latter was thought to lead to the 'activation' of proglacial sediment sources and a marked increase in suspended sediment supply in mid to late summer, and hence higher concentrations.

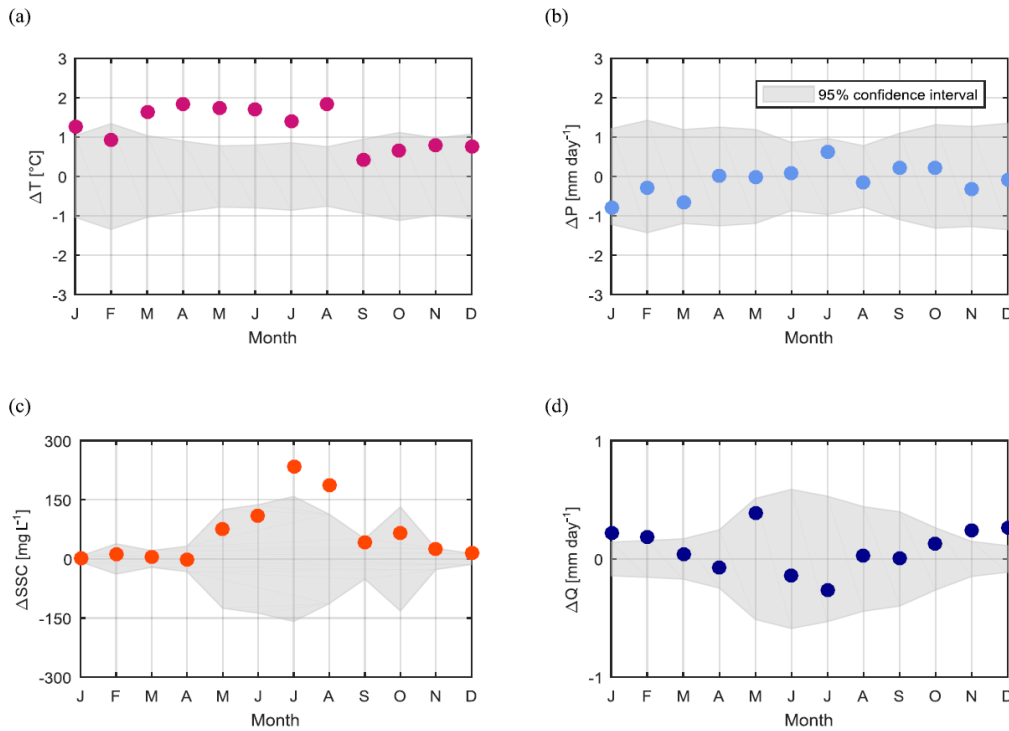


Figure 6-2 Differences in a) temperature and b) precipitation in Swiss Rhône basin before and after 1987 (1965-1986 and 1987-2015), and c) suspended sediment concentration and d) discharge at the Rhône outlet into Lake Geneva; taken from Costa et al. (2018b).

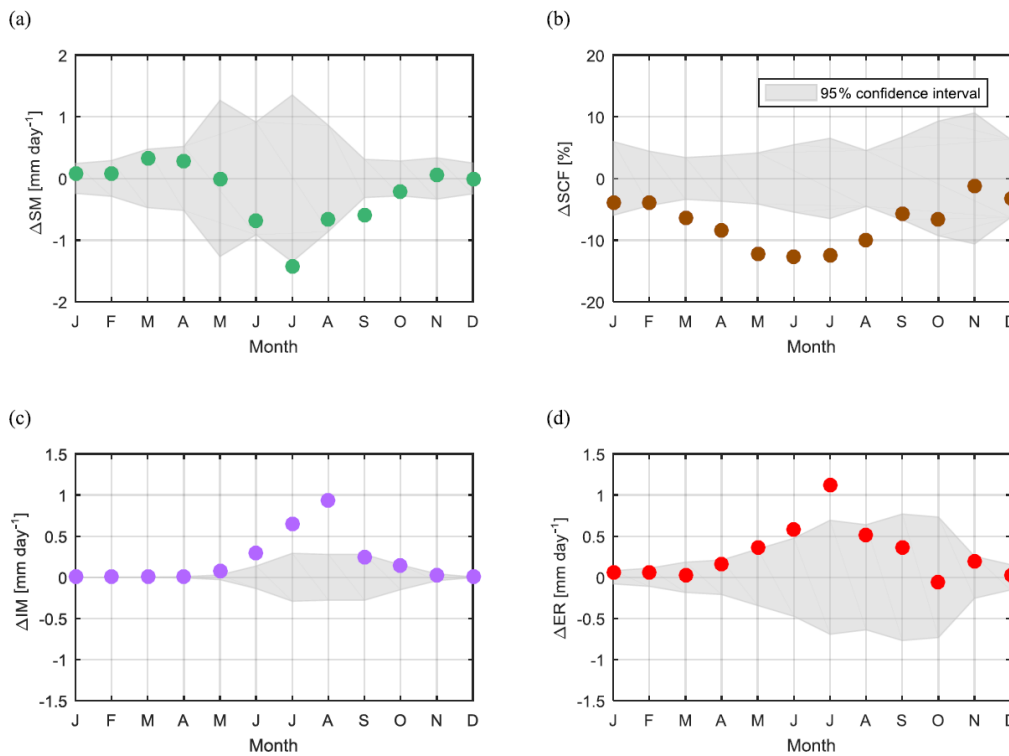


Figure 6-3 Differences in modelled a) snow-melt, b) snow-cover fraction, c) ice melt, and d) effective rainfall (liquid precipitation over snow-free areas) for the Swiss Rhône before and after 1987 (1965-1986 and 1987-2015); basin taken from Costa et al. (2018b).

Similar observations were made for sedimentation in Lake Geneva. Sediment at the mouth of the Swiss Rhône is transferred and deposited in a dynamic canyon-lobe system in Lake Geneva (T.A. Silva pers. comm.). By using this information to select carefully where to take sediment cores, a relative decrease in sediment accumulation rates was observed after 1964. Initial analysis might suggest that this is due to hydropower expansion and sediment retention behind dams. However, sedimentation rates, reflecting the Costa *et al.* (2018b) records of sediment loading, increase after 1984 (the dates are related to Cs isotope horizons), changes which also seem to reflect the general temperature trend (Figure 2-1). In the latter warming period, a general increase in grain size is detected.

The work presented in Chapter 4 goes some way to explaining these results. It showed that with the increased frequency of intake flushing more sediment was delivered to the Borgne. At the same time, and notwithstanding substantial deposition downstream of the intakes, significant sediment flux downstream was maintained. Thus, even though this is a basin with extensive hydropower impacts, and these include some important dams, the widespread presence of intakes whose operation is itself a function of climate change (i.e. climate warming produces more frequent flushing) make it possible for the upstream signature of warming climate on glacial melt and sediment transport to propagate through to Lake Geneva. Of course, the actual sedimentation rates in Lake Geneva may still be affected by other processes, but it is interesting that the Lake Geneva cores also report sediment coarsening from the 1980s which would also reflect an increase in the frequency of intake flushing and supply of suspended bed material whilst washload, the finer fraction, is transferred to dam reservoirs where it is retained as these reservoirs are not normally flushed.

This thesis has not reported on one important element of the system which is the way in which sediment waves propagate through the Borgne system and then the main Rhône itself. Suspended sediment waves were to be detected with turbidity measurements throughout the Borgne down to the confluence with the Rhône, but a series of operational challenges meant that no basin-wide sediment budget has yet been determined for the Val d'Hérens basin. This is also due to additional complexities in the system, including other hydropower installations and gravel mining sites further downstream in the Val d'Hérens (Lane *et al.* 2014). Under the SEDFATE project, however, it was possible to investigate these processes through an alternative approach. Stutenbecker *et al.* (in review) used a geochemical fingerprinting and compositional mixing approach to investigate sediment (sand) provenance at the outlet of the Borgne (Figure 6-4). This revealed high sediment yield (c. 80%) from glacial ice melt in the uppermost part of the basin (c. 30% of the total area) that persisted throughout the year. Based on a conceptual model of sediment production and transfer (Costa *et al.* 2018a), they showed that although sediment transfer from areas impacted by flow

abstraction is delayed, the uppermost part of the Val d'Hérens basin provided the largest contribution of sediment.

In the wider Swiss Rhône catchment, Stutenbecker *et al.* (2017) used a similar fingerprinting approach in combination with  $^{10}\text{Be}$  cosmogenic nuclide analysis to assess the relative contributions of tributary basins as a function of sediment production and transfer (Figure 6-4). The largest contribution to Rhône sediment comes from tributaries located in the North and the East (in the Helvetic nappes and External massifs), while the tributaries from the South (in the Penninic nappes) are relatively underrepresented (Figure 6-4), particularly considering the relatively high denudation rates. This can at least be partly attributed to the storage of sediment in reservoirs (Hinderer *et al.* 2013). Interestingly, similar results were found in the adjacent Aosta valley, Italy (Vezzoli 2004). The Mt. Blanc External massif with extreme relief and heavy glaciation encompasses only 3% of total basin area but produces 50% of total bed load output from the basin. Here too hydropower exploitation is most prominent in the Penninic Alps, north of Aosta. In the Swiss Rhône, however, the effects of sediment mining may perhaps be even larger (Kündig 1997; Stutenbecker *et al.* 2017). In the case of sediment mining, we see that, as identified in Section 4.5.1, there is a supply-demand relation where the extracted amount depends on the sediment supply from upstream. In this sense the direct human impact functions as a negative feedback and this confirms the observation above: whilst the nature of hydropower in the Rhône allows climate signals to be propagated through the basin to the downstream outlet, these signals are strongly modified by other processes. Changes in sedimentation rates are detectable, but the actual rates do not only reflect the effects of climate warming upon glacial sediment production.

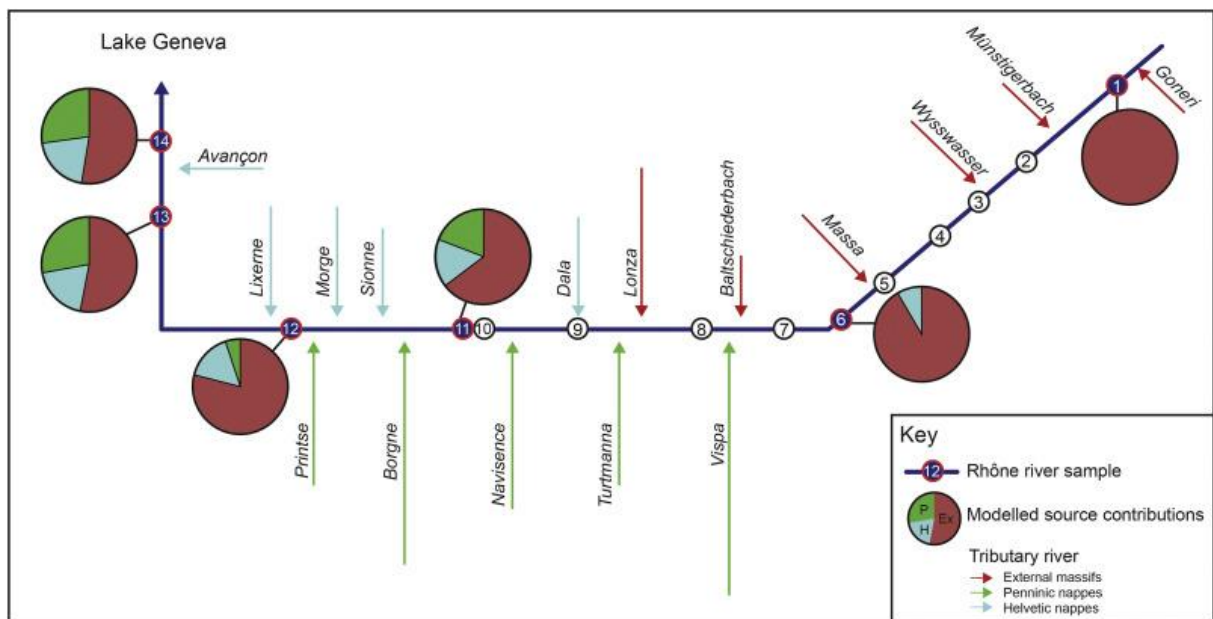
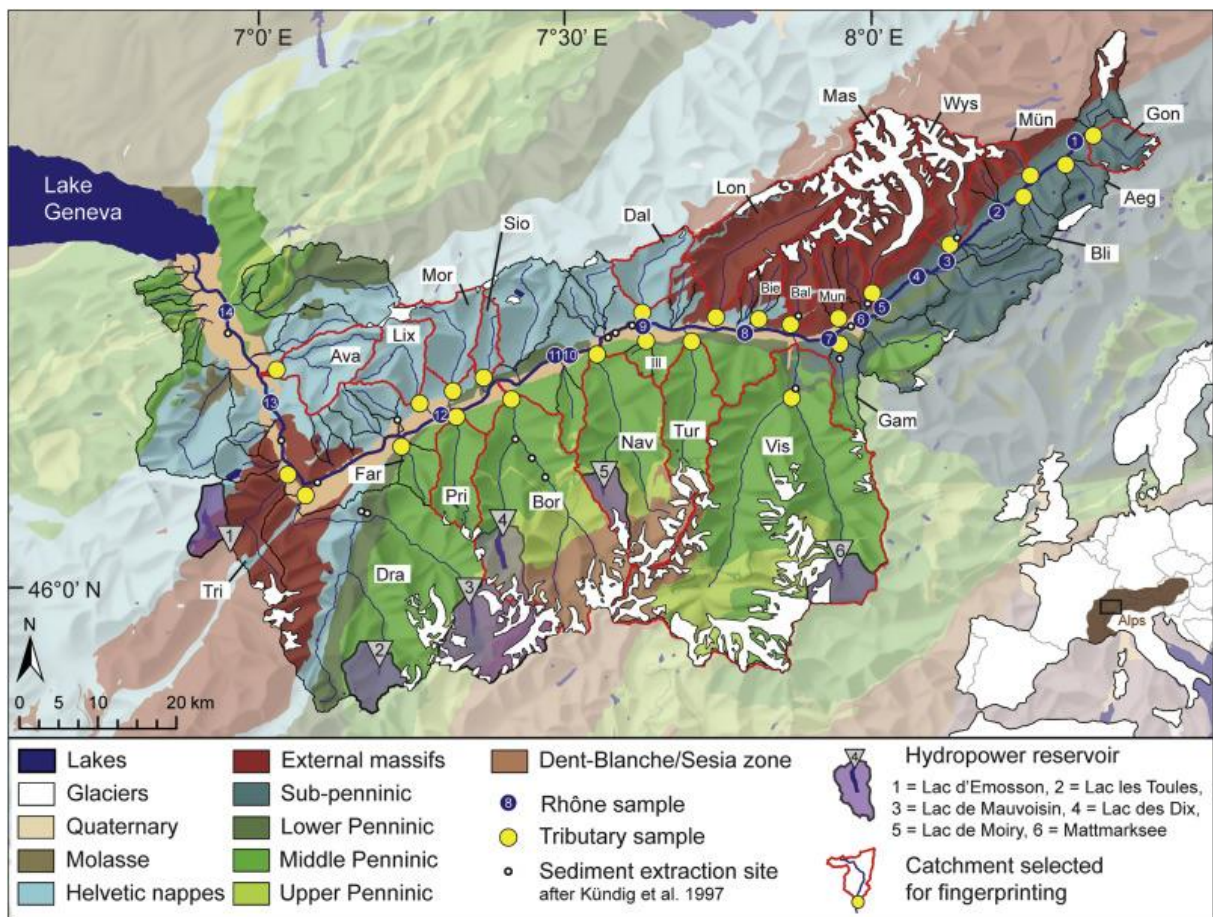


Figure 6-4 Lithological map of the Swiss Rhône basin, with the Val d'Hérens marked in the rectangle (top), and the associated modelled source contributions to the Rhône (bottom); taken from Stutenbecker et al. (2017).

### 6.3 Perspectives

This thesis has demonstrated the large impact that combined climate change and flow abstraction may have on Alpine river morphology and sediment transfer. For this, long term records were essential; historic topographic data was quantified using a novel application of SfM methods to archival imagery (Chapter 3) and sediment delivery to the investigated reaches was quantified based on the analysis of flow intake data (Bezinge *et al.* 1989). The observed river response to upstream forcing was rapid and widespread, occurring throughout the investigated reaches (Chapter 4), which may have important consequences for downstream river dynamics and river management in these systems. The understanding of the system response is however limited to the temporal resolution of topographic measurements, c. 5 years, and the spatial extent of the investigated reaches, c. 5 km.

An important question that remains is how increased sediment flux, notably the increase in the late 1980s, propagates through the system? Studies performed on the controls of dispersion and translation of sediment waves in gravel bed rivers have been largely based on theoretical and experimental work (Lisle *et al.* 2001; Cui *et al.* 2003) and field investigations are relatively rare; the few examples include river response to widespread logging in a basin (Madej and Ozaki 1996) and sediment supply by a large landslide (Sutherland *et al.* 2002). Such studies are however very important in the larger context of human-impacts on increased sediment delivery in Alpine regions. To increase the temporal resolution of morphological change in the Borgne there are opportunities for the application of dendrochronological techniques on riparian trees. This may provide information on an annual resolution where growth rings may be impacted upon by water availability, related to river bed level elevation, and most importantly sediment burial (Friedman *et al.* 2005). Similarly, stratigraphic techniques may be applied on channel banks that have incised into earlier deposits over recent years (e.g. Laute and Beylich 2010). Further downstream, photogrammetric analysis may provide additional insight in the extent of change. A combination of such techniques may be used to resolve the relatively rapid historic changes and sediment throughput rates in the Borgne or similar systems.

This thesis has also demonstrated the variable morphological response amongst regulated flushing events and between intermittent flushing events and longer flood events (Chapter 5). Sequences of controlled flushing events with known sediment loads (released from sediment traps) were routed through the river bed using a novel application of the 2D morphological method which allows event-based transfer rates to be inferred (Antoniazza *et al.* in revision). These showed highly concentrated and efficient sediment transfer, giving a process-based insight into long term river bed evolution (Chapter 3 and 4), where despite flow abstraction aggradation rates are low. Although net river bed

changes and mean transfer rates were identified, the temporal and spatial dynamics of sediment transport during events could not be revealed. Such data may provide detailed information on the rates and dynamics of braiding processes.

Observations in the highly turbulent, sediment-laden flows are challenging both in terms of visibility and in terms of damage to measurement equipment at the river bed. Indirect methods to measure bed load transport (dynamics), including in-stream acoustic techniques (Geay *et al.* 2017) or remote (out of the water) seismic techniques (Burtin *et al.* 2016), may therefore be useful. These have the additional advantage that locally measured bed load processes are not disrupted, although they do require calibration with (conventional) in-stream measurements and sampling techniques, and may be easily deployed; they don't require large-scale structures such as the Swiss impact plate geophones (e.g. Rickenmann *et al.* 2014). Additionally, the use of seismic measurements is not limited to fluvial systems, but they may cover a range of processes including mass movements and sub-glacial transport, allowing the interface and therefore connectivity between systems to be studied.

The well regulated nature of flow abstraction schemes may be exploited through monitoring upstream sediment supply and downstream flushing events (with a known volume of sediment) with only a single seismometer next to the intake. Temporally continuous and spatially distributed measures of bed load dynamics, may also be realized through the use of an extensive network of seismometers (Schmandt *et al.* 2017). This would allow the distribution of sediment rates to be observed as flushed sediment from the intake propagates through the braided channel. Practical insights may be gained regarding the morphodynamic impacts of sediment flushing operations, particularly the effects of timing and duration on sediment travel distance. More fundamentally, the dynamics of flushing and flood events can be investigated, i.e. the local onset of motion, transport phases and deposition. Indirect information may be derived regarding the transported sediment fractions and river bed grain size dynamics, which play an important role in the characterization of sediment loads and the dynamic response of the river bed. As such, additional insights and evidence may be provided for the mechanisms of morphological change that were observed throughout the braided reach (Chapter 5), particularly effects of local relief and system memory, and their coupling with temporal fluctuations in bed load transport (Turowski *et al.* 2011).

## References

- Alley, R. B., Cuffey, K. M., Evenson, E. B., Strasser, J. C., Lawson, D. E., Larson, G. J. 1997. How glaciers entrain and transport basal sediment: Physical constraints. *Quaternary Science Reviews* 16(9): 1017-1038. DOI: 10.1016/S0277-3791(97)00034-6.
- Anselmetti, F. S., Bühler, R., Finger, D., Girardclos, S., Lancini, A., Rellstab, C., Sturm, M. 2007. Effects of Alpine hydropower dams on particle transport and lacustrine sedimentation. *Aquatic Sciences* 69(2): 179-198.
- Antoniazza, G., Bakker, M., Lane, S. N. in revision. Revisiting the morphological method in two-dimensions to quantify bed material transport in braided rivers. *Earth Surface Processes and Landforms* Special edition.
- Baewert, H., Morche, D. 2014. Coarse sediment dynamics in a proglacial fluvial system (Fagge River, Tyrol). *Geomorphology* 218: 88-97. DOI: 10.1016/j.geomorph.2013.10.021.
- Bakker, M., Boillat, M., Lane, S. N. in prep. Sediment flux in a hydropower impacted Alpine catchment.
- Beylich, A., Lamoureux, S., Decaulne, A. 2011. Developing frameworks for studies on sedimentary fluxes and budgets in changing cold environments. *Quaestiones Geographicae* 30(1): 5-18.
- Beylich, A. A., Laute, K. 2015. Sediment sources, spatiotemporal variability and rates of fluvial bedload transport in glacier-connected steep mountain valleys in western Norway (Erdalen and Bødalen drainage basins). *Geomorphology* 228: 552-567. DOI: 10.1016/j.geomorph.2014.10.018.
- Bezinge, A., Clark, M., Gurnell, A., & Warburton, J. (1989). The management of sediment transported by glacial melt-water streams and its significance for the estimation of sediment yield. *Annals of Glaciology*, 13, 1–5. 10.1017/S0260305500007527
- Bogen, J., Xu, M., Kennie, P. 2015. The impact of pro-glacial lakes on downstream sediment delivery in Norway. *Earth Surface Processes and Landforms* 40(7): 942-952. DOI: 10.1002/esp.3669.
- Burki, V., Hansen, L., Fredin, O. L. A., Andersen, T.A., Beylich, A.A., Jaboyedoff, M., Larsen, E., Tønnesen, J.-F. 2010. Little Ice Age advance and retreat sediment budgets for an outlet glacier in western Norway. *Boreas* 39(3): 551-566. DOI: 10.1111/j.1502-3885.2009.00133.x.
- Burtin, A., Hovius, N., Turowski, J. M. 2016. Seismic monitoring of torrential and fluvial processes. *Earth Surf. Dynam.* 4(2): 285-307. DOI: 10.5194/esurf-4-285-2016.
- Carrivick, J. L., Geilhausen, M., Warburton, J., Dickson, N. E., Carver, S. J., Evans, A. J., Brown, L. E. 2013. Contemporary geomorphological activity throughout the proglacial area of an alpine catchment. *Geomorphology* 188: 83-95. DOI: 10.1016/j.geomorph.2012.03.029.

- Carrivick, J. L., Heckmann, T. 2017. Short-term geomorphological evolution of proglacial systems. *Geomorphology* 287: 3-28. DOI: 10.1016/j.geomorph.2017.01.037.
- Cossart, E., Fort, M. 2008. Sediment release and storage in early deglaciated areas: Towards an application of the exhaustion model from the case of Massif des Écrins (French Alps) since the Little Ice Age. *Norsk Geografisk Tidsskrift - Norwegian Journal of Geography* 62(2): 115-131. DOI: 10.1080/00291950802095145.
- Costa, A., Anghileri, D., Molnar, P. 2018a. Hydroclimatic control on suspended sediment dynamics of a regulated Alpine catchment: a conceptual approach. *Hydrol. Earth Syst. Sci. Discuss.* 2018: 1-23. DOI: 10.5194/hess-2018-5.
- Costa, A., Molnar, P., Stutenbecker, L., Bakker, M., Silva, T. A., Schlunegger, F., Lane, S. N., Loizeau, J. L., Girardclos, S. 2018b. Temperature signal in suspended sediment export from an Alpine catchment. *Hydrol. Earth Syst. Sci. Discuss.* 2018: 1-30. DOI: 10.5194/hess-22-509-2018.
- Cuffey, K., Alley, R. B. 1996. Is erosion by deforming subglacial sediments significant? (Toward till continuity). *Annals of Glaciology* 22: 17-24. DOI: 10.3189/1996AoG22-1-17-24.
- Cui, Y., Parker, G., Lisle, T. E., Gott, J., Hansler-Ball, M. E., Pizzuto, J. E., Allmendinger, N. E., Reed, J. M. 2003. Sediment pulses in mountain rivers: 1. Experiments. *Water Resources Research* 39(9).
- Curry, A. M., Cleasby, V., Zukowskyj, P. 2006. Paraglacial response of steep, sediment-mantled slopes to post-'Little Ice Age' glacier recession in the central Swiss Alps. *Journal of Quaternary Science* 21(3): 211-225. DOI: 10.1002/jqs.954.
- Delaney, I., Bauder, A., Huss, M., Weidmann, Y. 2017. Proglacial erosion rates and processes in a glacierized catchment in the Swiss Alps. *Earth Surface Processes and Landforms* 43(4): 765-778. DOI: 10.1002/esp.4239.
- Eltner, A., Kaiser, A., Abellan, A., Schindewolf, M. 2017. Time lapse structure-from-motion photogrammetry for continuous geomorphic monitoring. *Earth Surface Processes and Landforms* 42(14): 2240-2253. DOI: 10.1002/esp.4178.
- Fenn, C., Gomez, B. 1989. Particle size analysis of the sediment suspended in a proglacial stream: Glacier de Tsidjiore Neue, Switzerland. *Hydrological processes* 3(2): 123-135.
- Geay, T., Belleudy, P., Gervaise, C., Habersack, H., Aigner, J., Kreisler, A., Seitz, H., Laronne, J. B. 2017. Passive acoustic monitoring of bed load discharge in a large gravel bed river. *Journal of Geophysical Research: Earth Surface* 122(2): 528-545. DOI: 10.1002/2016JF004112.
- Geilhausen, M., Morche, D., Otto, J.-C., Schrott, L. 2013. Sediment discharge from the proglacial zone of a retreating Alpine glacier. *Zeitschrift für Geomorphologie, Supplementary Issues* 57(2): 29-53.

- Hallet, B., Hunter, L., Bogen, J. 1996. Rates of erosion and sediment evacuation by glaciers: A review of field data and their implications. *Global and Planetary Change* 12(1–4): 213-235. DOI: 10.1016/0921-8181(95)00021-6.
- Hinderer, M., Kastowski, M., Kamelger, A., Bartolini, C., Schlunegger, F. 2013. River loads and modern denudation of the Alps — A review. *Earth-Science Reviews* 118(0): 11-44. DOI: 10.1016/j.earscirev.2013.01.001.
- Hock, R. 2003. Temperature index melt modelling in mountain areas. *Journal of Hydrology* 282(1): 104-115. DOI: 10.1016/S0022-1694(03)00257-9.
- Karlén, W. 1973. Holocene glacier and climatic variations, Kebnekaise mountains, Swedish Lapland. *Geografiska Annaler: Series A, Physical Geography* 55(1): 29-63.
- Kirkbride, M. P., Deline, P. 2018. Spatial heterogeneity in the paraglacial response to post-Little Ice Age deglaciation of four headwater cirques in the Western Alps. *Land Degradation & Development* 0(0). DOI: 10.1002/ldr.2975.
- Kündig, R. 1997. Die mineralischen Rohstoffe der Schweiz, Schweizerische Geotechnische Kommission.
- Lane, S., Richards, K., Chandler, J. 1993. Developments in photogrammetry; the geomorphological potential. *Progress in Physical Geography* 17(3): 306-328.
- Lane, S. N., Bakker, M., Balin, D., Lovis, B., Regamey, B. 2014. Climate and human forcing of Alpine river flow. In *River Flow 2014*. Schleiss, A. J., de Cesare, G., Franca, M. J., Pfister, M. (eds): 7-15.
- Lane, S. N., Bakker, M., Gabbud, C., Micheletti, N., Saugy, J.-N. 2017. Sediment export, transient landscape response and catchment-scale connectivity following rapid climate warming and Alpine glacier recession. *Geomorphology* 277: 210-227. DOI: 10.1016/j.geomorph.2016.02.015.
- Laute, K., Beylich, A.A. 2010. Characteristics of floodplain deposits within a braided sandur system in upper Erdalen (Nordfjord, western Norway). *Geografiska Annaler: Series A, Physical Geography* 92(2): 211-223.
- Leemann, A., Niessen, F. 1994. Holocene glacial activity and climatic variations in the Swiss Alps: reconstructing a continuous record from proglacial lake sediments. *The Holocene* 4(3): 259-268. DOI: 10.1177/095968369400400305.
- Lisle, T. E., Cui, Y., Parker, G., Pizzuto, J. E., Dodd, A. M. 2001. The dominance of dispersion in the evolution of bed material waves in gravel-bed rivers. *Earth Surface Processes and Landforms* 26(13): 1409-1420.
- Madej, M. A., Ozaki, V. 1996. Channel response to sediment wave propagation and movement, Redwood Creek, California, USA. *Earth Surface Processes and Landforms* 21(10): 911-927.

- Micheletti, N., Lane, S. N., Chandler, J. H. 2015. Application of archival aerial photogrammetry to quantify climate forcing of alpine landscapes. *The Photogrammetric Record* 30(150): 143-165. DOI: 10.1111/phor.12099.
- Otto, J.-C., Schrott, L., Jaboyedoff, M., Dikau, R. 2009. Quantifying sediment storage in a high alpine valley (Turtmanntal, Switzerland). *Earth Surface Processes and Landforms* 34(13): 1726-1742. DOI: 10.1002/esp.1856.
- Orwin, J. F., Smart, C. C. 2004. The evidence for paraglacial sedimentation and its temporal scale in the deglaciating basin of Small River Glacier, Canada. *Geomorphology* 58(1): 175-202. DOI: 10.1016/j.geomorph.2003.07.005.
- Perolo, P., Bakker, M., Gabbud, C., Moradi, G., Rennie, C., Lane, S. N. in review. Subglacial sediment production and snout marginal ice uplift during the late ablation season of a temperate valley glacier. *Earth Surface Processes and Landforms*.
- Rascher, E., Rindler, R., Habersack, H., Sass, O. 2018. Impacts of gravel mining and renaturation measures on the sediment flux and budget in an alpine catchment (Johnsbach Valley, Austria). *Geomorphology* 318: 404-420. DOI: <https://doi.org/10.1016/j.geomorph.2018.07.009>.
- Rainato, R., Picco, L., Cavalli, M., Mao, L., Neverman Andrew, J., Tarolli, P. 2017. Coupling Climate Conditions, Sediment Sources and Sediment Transport in an Alpine Basin. *Land Degradation & Development* 29(4): 1154-1166. DOI: 10.1002/ldr.2813.
- Rickenmann, D., Turowski, J. M., Fritschi, B., Wyss, C., Laronne, J., Barzilai, R., Reid, I., Kreisler, A., Aigner, J., Seitz, H., Habersack, H. 2014. Bedload transport measurements with impact plate geophones: comparison of sensor calibration in different gravel-bed streams. *Earth Surface Processes and Landforms* 39(7): 928-942. DOI: 10.1002/esp.3499.
- Schmandt, B., Gaeuman, D., Stewart, R., Hansen, S. M., Tsai, V. C., Smith, J. 2017. Seismic array constraints on reach-scale bedload transport. *Geology* 45(4): 299-302. DOI: 10.1130/G38639.1.
- Stott, T. 2002. Bedload Transport and Channel Bed Changes in the Proglacial Skeldal River, Northeast Greenland. *Arctic, Antarctic, and Alpine Research* 34(3): 334-344. DOI: 10.2307/1552492.
- Stutenbecker, L., Costa, A., Bakker, M., Anghileri, D., Molnar, P., Lane, S. N., Schlunegger, F. in review. Disentangling the influence of human impact from natural controls of the sediment dynamics of an Alpine catchment. *Earth Surface Processes and Landforms*.
- Stutenbecker, L., Delunel, R., Schlunegger, F., Silva, T. A., Šegvić, B., Girardclos, S., Bakker, M., Costa, A., Lane, S. N., Loizeau, J.-L., Molnar, P., Akçar, N., Christl, M. 2017. Reduced sediment supply in a fast eroding landscape? A multi-proxy sediment budget of the upper Rhône basin, Central Alps. *Sedimentary Geology*. DOI: 10.1016/j.sedgeo.2017.12.013.

- Sutherland, D. G., Ball, M. H., Hilton, S. J., Lisle, T. E. 2002. Evolution of a landslide-induced sediment wave in the Navarro River, California. *Geological Society of America Bulletin* 114(8): 1036-1048. DOI: 10.1130/0016-7606(2002)114<1036:eoalis>2.0.co;2.
- Swift, D. A., Nienow, P. W., Hoey, T. B., Mair, D. W. F. 2005. Seasonal evolution of runoff from Haut Glacier d'Arolla, Switzerland and implications for glacial geomorphic processes. *Journal of Hydrology* 309(1): 133-148. DOI: 10.1016/j.jhydrol.2004.11.016.
- Tschada, H., Hofer, B. 1990. Total solids load from the catchment area of the Kauter hydroelectric power station: the results of 25 years of operation.
- Turowski, J. M., Badoux, A., Rickenmann, D. 2011. Start and end of bedload transport in gravel-bed streams. *Geophysical Research Letters* 38(4). DOI: 10.1029/2010GL046558.
- Vezzoli, G. 2004. Erosion in the Western Alps (Dora Baltea Basin): 2. Quantifying sediment yield. *Sedimentary Geology* 171(1): 247-259. DOI: 10.1016/j.sedgeo.2004.05.018.
- Warburton, J. 1990. An alpine proglacial fluvial sediment budget. *Geografiska Annaler. Series A. Physical Geography*: 261-272.
- Warburton, J. 1992. Observations of bed load transport and channel bed changes in a proglacial mountain stream. *Arctic and Alpine Research* 24(3): 195-203. DOI: 10.2307/1551657.



## **APPENDICES**

Appendix A contains the Supplementary Information that was provided with Article 2: 'Combined flow abstraction and climate change impacts on an aggrading Alpine river', which was published in *Water Resources Research* 54.

Appendix B contains the Supplementary Information that was submitted with Article 3: 'Morphological response of an alpine braided reach to sediment-laden flow events' to *Journal of Geophysical Research – Earth Surface*.

**A1: Orthoimages for reaches A-D, for the years 1959-2014**

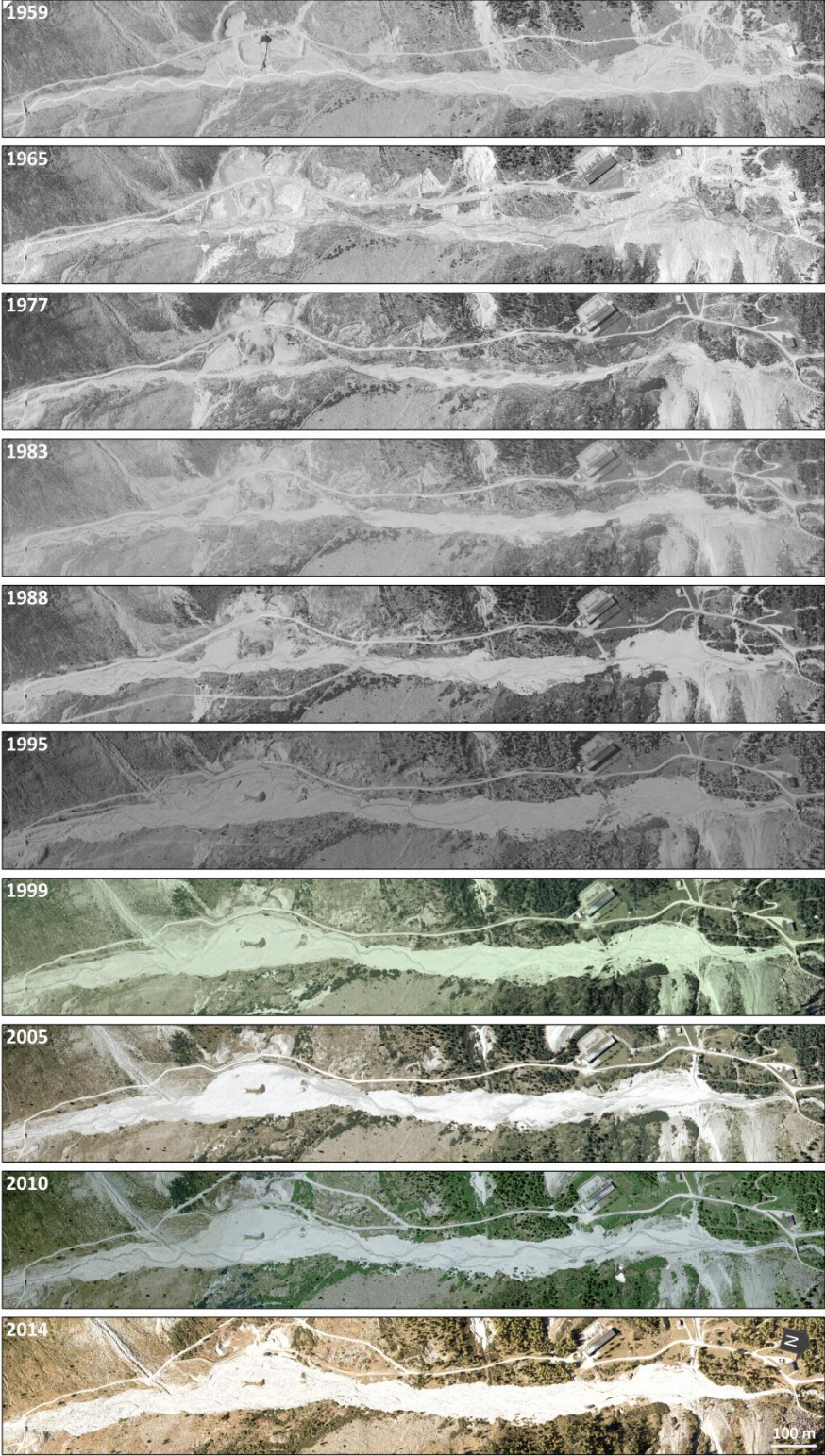


*Figure A1-1 Orthoimage series of reach A.*

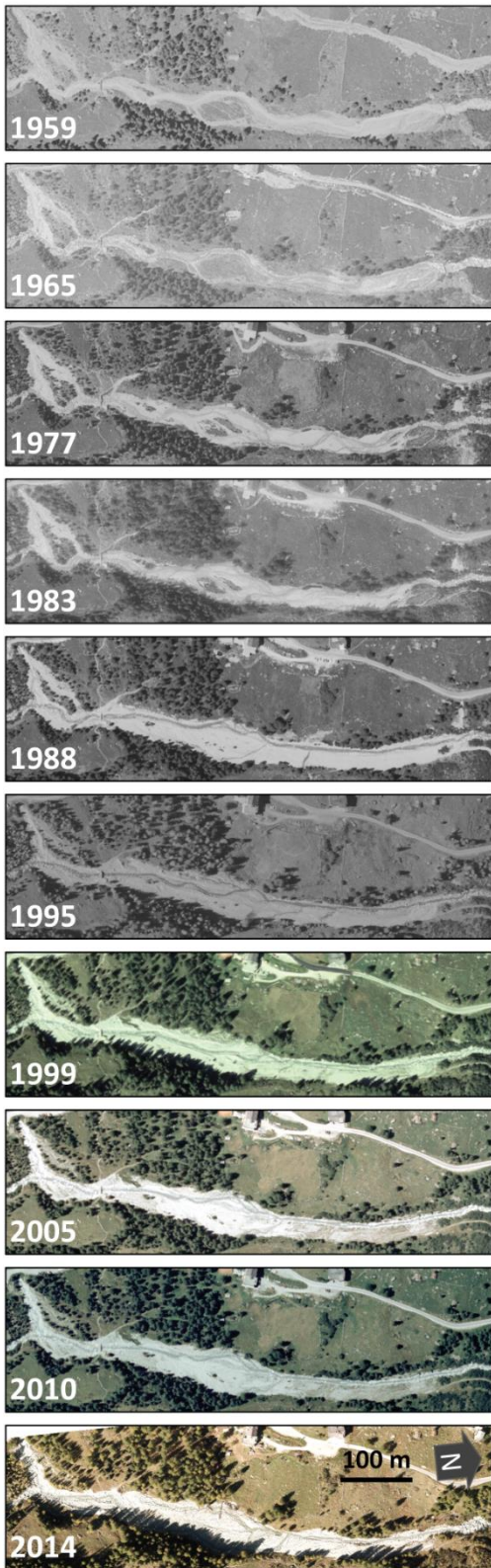


Figure A1-2 Orthoimage series of reach B.

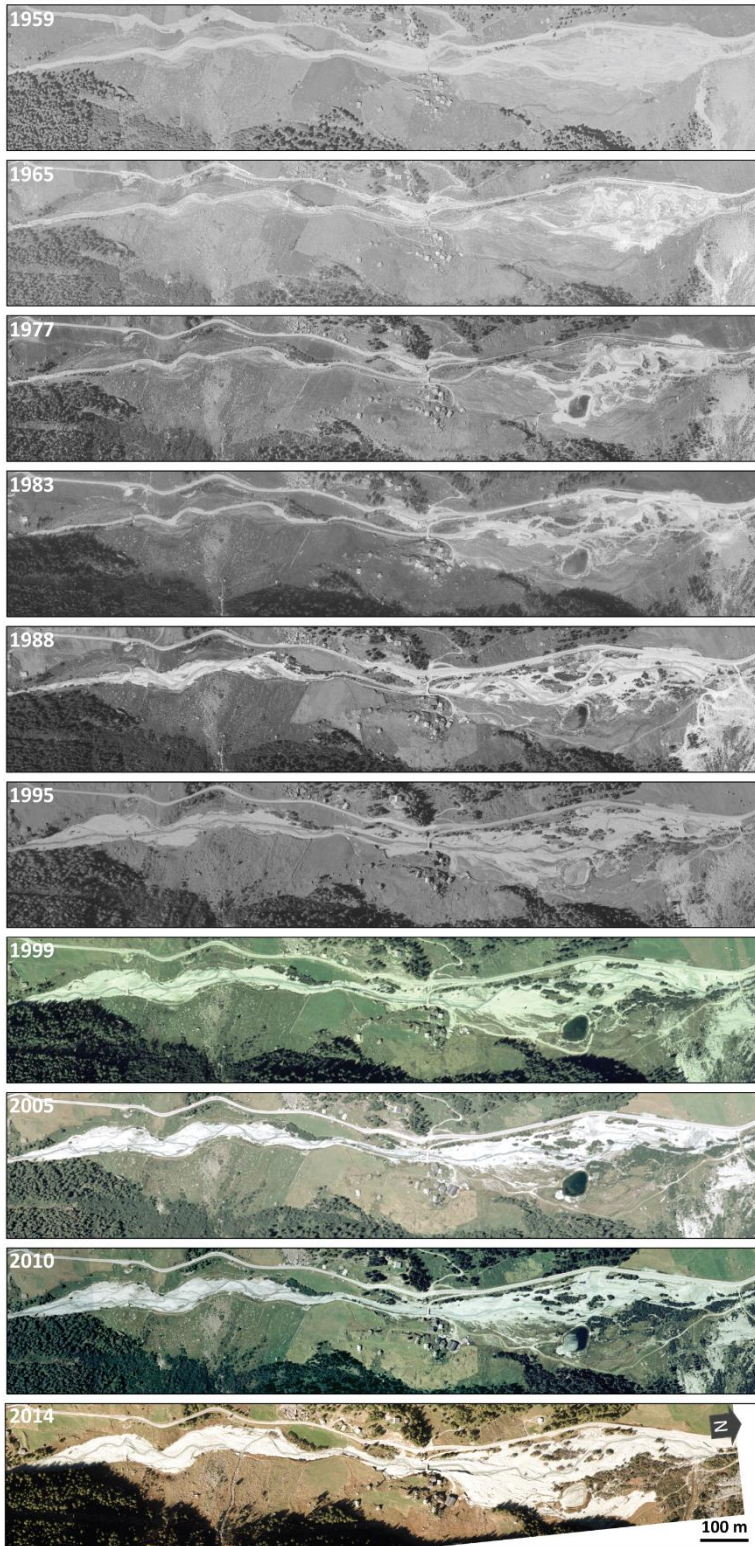


Figure A1-3 Orthoimage series of reach C and D.

## A2: DEM local error estimation based on orthoimage texture

Local errors may occur in DEMs as a result of difficulties in automatic feature matching, either through inaccurate/imprecise matching or the absence of matched features which leads to interpolation error. We assessed local error in the DEMs based on image texture which was shown to have a strong impact on the ability of SfM methods to extract and match 3D tie-points (Bakker & Lane, 2017). Here, we use an entropy filter with a 9x9 cell running window as a measure for both the photogrammetric point density and quality. The entropy values were inversely scaled to the theoretical precision (i.e. the object space pixel size derived from the image scale and scanning resolution; see Table 3 in Bakker & Lane, 2017), covering a range of half to double the theoretical precision (Figure A2-1b). In general the riverbed has low entropy values, with the exception of (pioneer) vegetation and the edges of wetted areas.

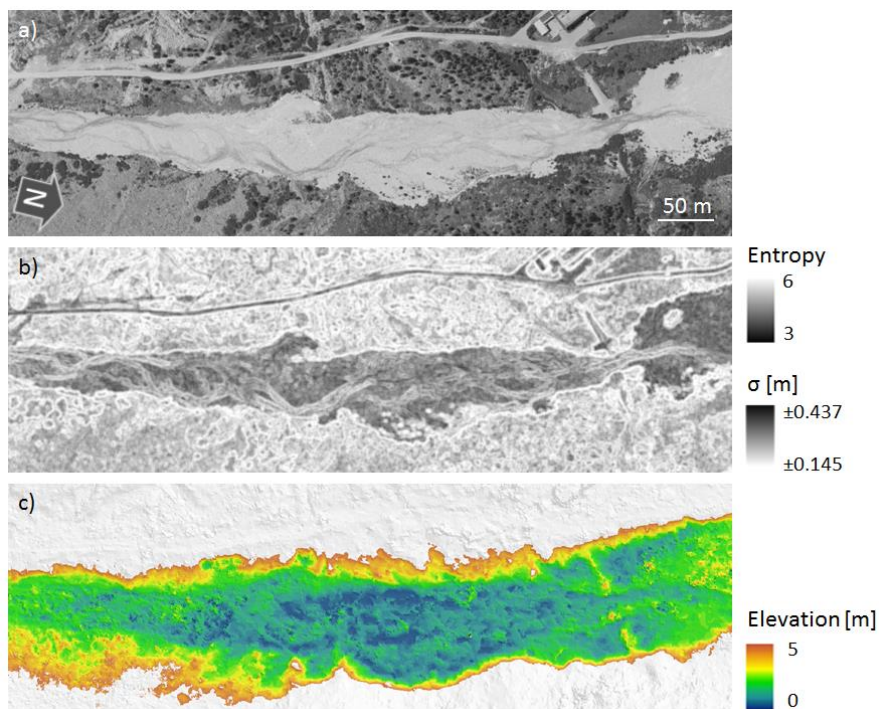


Figure A2-1 a) Orthophotograph of a section of reach A in 1988; b) local entropy and associated precision; c) de-trended DEM with hillshade overlay.

### A3: Grain size sampling and orthoimage semivariogram analysis

Surface sediment grain size was determined using the Wolman (1954) count, grid-by-number approach at 12 sample locations in Reach D (Figure A3-1a). In addition, samples were taken in Reach A: c. 150 m upstream from the intake (4 samples) and c. 500 m downstream from the intake (4 samples), the latter being the 4 coarsest samples that were obtained. Other samples that have been taken were discarded due to changes in river topography between the moment of the aerial photography and sediment sampling and due to edge effects of vegetation and shadows in the aerial image. Figure A3-1b shows the obtained sill values from two-dimensional semivariogram analysis of the orthoimage. Figure A3-1c shows the (statistically significant) rating curves that were used to determine spatially distributed values for D50 and D84 based on the measured samples.

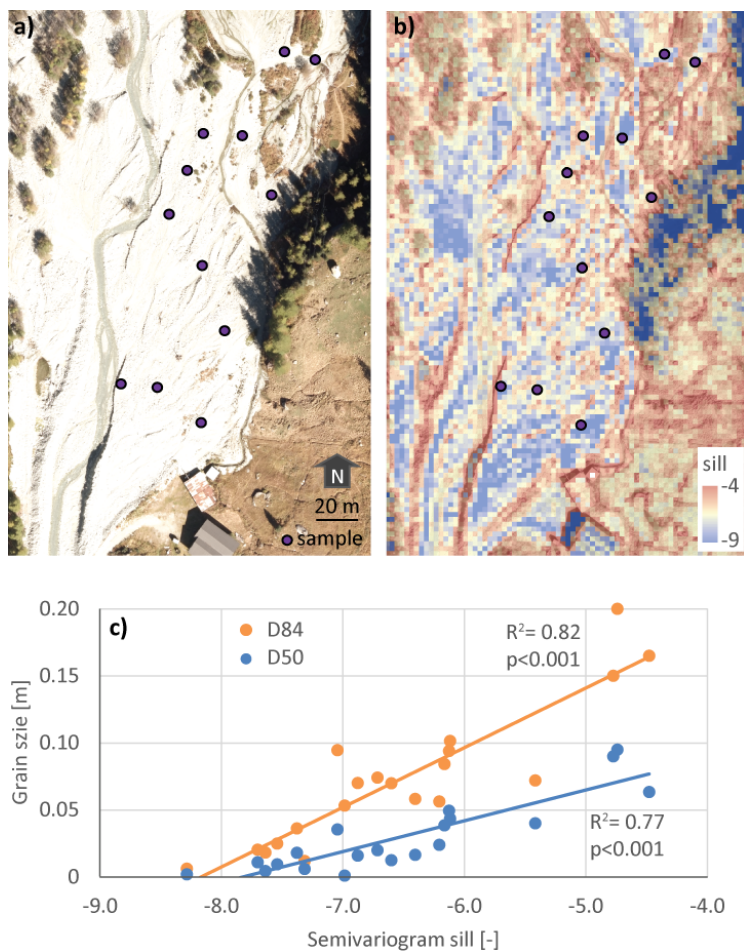


Figure A3-1 a) 2014 orthoimage of the upstream section of reach D, including grain-size sampling locations; b) semivariogram sill values derived from the orthoimage using a 2.25 x 2.25 m window size; c) resulting sediment grain-size rating curves.

#### A4: Sediment transport capacity calculation

Flow resistance partitioning, using a Variable Power Equation (Ferguson, 2007), is applied to adequately represent the macro-roughness in the river bed. Taking all energy losses into account, the flow velocity ( $v_t$ ) is predicted as [1]:

$$v_t = \frac{6.5\sqrt{gRS} \ 2.5 \left(\frac{R}{D_{84}}\right)}{\sqrt{6.5^2 + 2.5^2 \left(\frac{R}{D_{84}}\right)^{5/3}}} \quad [1]$$

Where  $g$  is the acceleration due to gravity;  $R$  is the hydraulic radius of the river bed;  $S$  is the energy gradient (which may be approximated with the bed gradient); and  $D_{84}$  is the 84<sup>th</sup> percentile of the grain size distribution. This is used to quantify the reduced energy gradient ( $S_r$ ) that is available for sediment transport [2] following Rickenmann & Recking (2011):

$$S_r = S \left( \frac{f}{f_t} \right)^e = S \left( \frac{v_t}{v} \right)^{1.5} \quad [2]$$

Where  $f$  is a general friction coefficient and  $v$  is mean flow velocity ( $v$ ). Nitsche et al. (2011) found that the empirical approach by Rickenmann (1991) to determine bed load, accounting for macro roughness through a non-explicit, shear-stress based equation, produced the best results for a large number of Swiss mountain streams. We applied the reduced energy gradient to this transport equation to calculate volumetric transport capacity ( $V$ ) [3]:

$$V = 2.5w \sqrt{sgD_{50}^3 \theta_r (\theta_r - \theta_{rc}) Fr} \quad [3]$$

$$\theta_r = \frac{RS_r}{(s-1)D_{50}} \quad , \quad \theta_{rc} = \frac{0.15R_c S^{0.25}}{(s-1)D_{50}} \quad [4]$$

Where  $w$  is the flow width;  $s$  is the specific density of sediment;  $D_{50}$  is the median diameter of the bed sediment;  $\theta$  is the dimensionless shear stress,  $r$  denoting reduced and  $c$  denoting critical; and  $Fr$  is the Froude number defined as  $\frac{v_t}{\sqrt{gd}}$  where  $d$  is the mean flow depth.

Where the critical shear stress is independent of discharge we used the non-reduced gradient similar to Heimann et al. (2015) and corrected for the gradient dependency according to (Lamb et al., 2008). We distinguished between surface-layer transport and finer sub-surface layer transport which comes into effect when the critical shear stress of the armour layer ( $\theta_a$ ) is exceeded (Günter,1971; Hunziker & Jäggi, 2002) [5]:

$$\theta_a = \theta_c \left( \frac{D_a}{D} \right)^{2/3} \quad [5]$$

## A5: Tsijore Nouve water yield and sediment supply

The effective volume of the Tsijore Nouve sediment traps are 20 m<sup>3</sup> and 7 m<sup>3</sup> for the gravel and sand trap respectively (Bezinge et al., 1989). Based on a cumulative frequency analysis of water volumes released during purges, we distinguished purges from the sand trap, between 500 and 750 m<sup>3</sup>, gravel trap, between 750 and 4700 m<sup>3</sup> and (near) system surcharge events, larger than 4700 m<sup>3</sup>. The resulting annual water yield and sediment supply are shown in Figure A5-1.

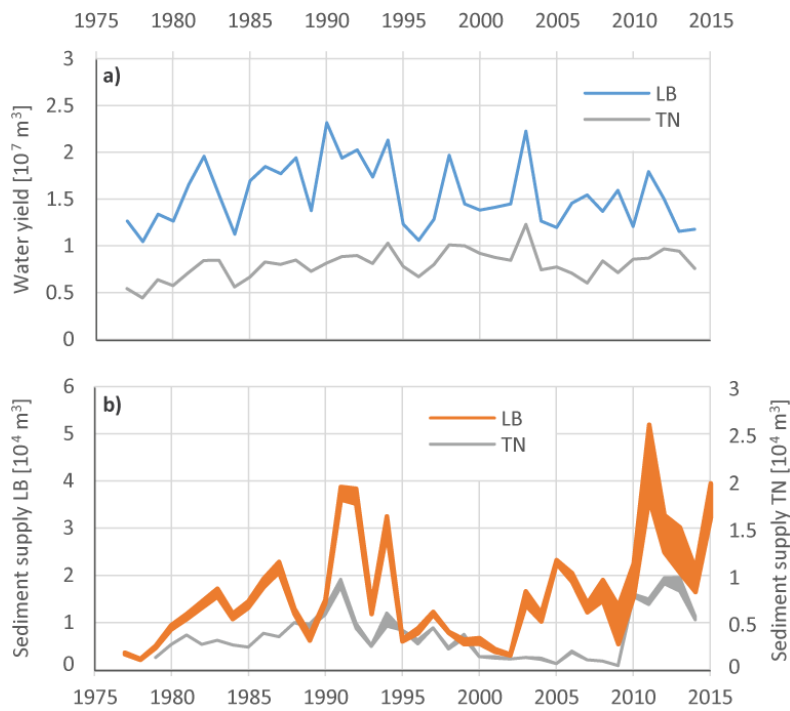


Figure A5-1 a) Annual water yield at the LB and TN intake; b) calculated (range in) sediment supply at the LB intake and TN intake - note that the latter is a factor 2 smaller. The uncertainties in purge identification and sediment volume are reflected in the range in supply values in b).

## **A6: Cross section evolution and effect on SCR**

The cross section (CS in Figure 1a) where bed load transport capacity calculations were performed has evolved considerably in the period 1988-2014 (Figure A6-1a, b). In this period, net aggradation was largest on the true right bank, which was stimulated by engineering measures, channelizing the flow near the right bank; in 1999 and 2014 the channels are visible. These measures were taken to mitigate lateral river bed expansion and potential flooding on the left bank, which would threaten the road (which was rerouted in this period) and downstream power station (Figure A1-1).

The transport capacity calculations based on the evolving cross section give insight in the range of SCR values that may be expected due to temporal changes in morphology (Figure A6-1c). Here we must however consider that although we can quantify the cross section from the DEMs, we lack information on changes in grain size (based on orthoimage inspection, particularly the sediment in 2005 appears to be finer) and flow partitioning over multiple channels (which largely depends on upstream flow routing). Therefore these calculations must be regarded as indicative of temporal variations and that transport capacity in general may vary within an order of magnitude.

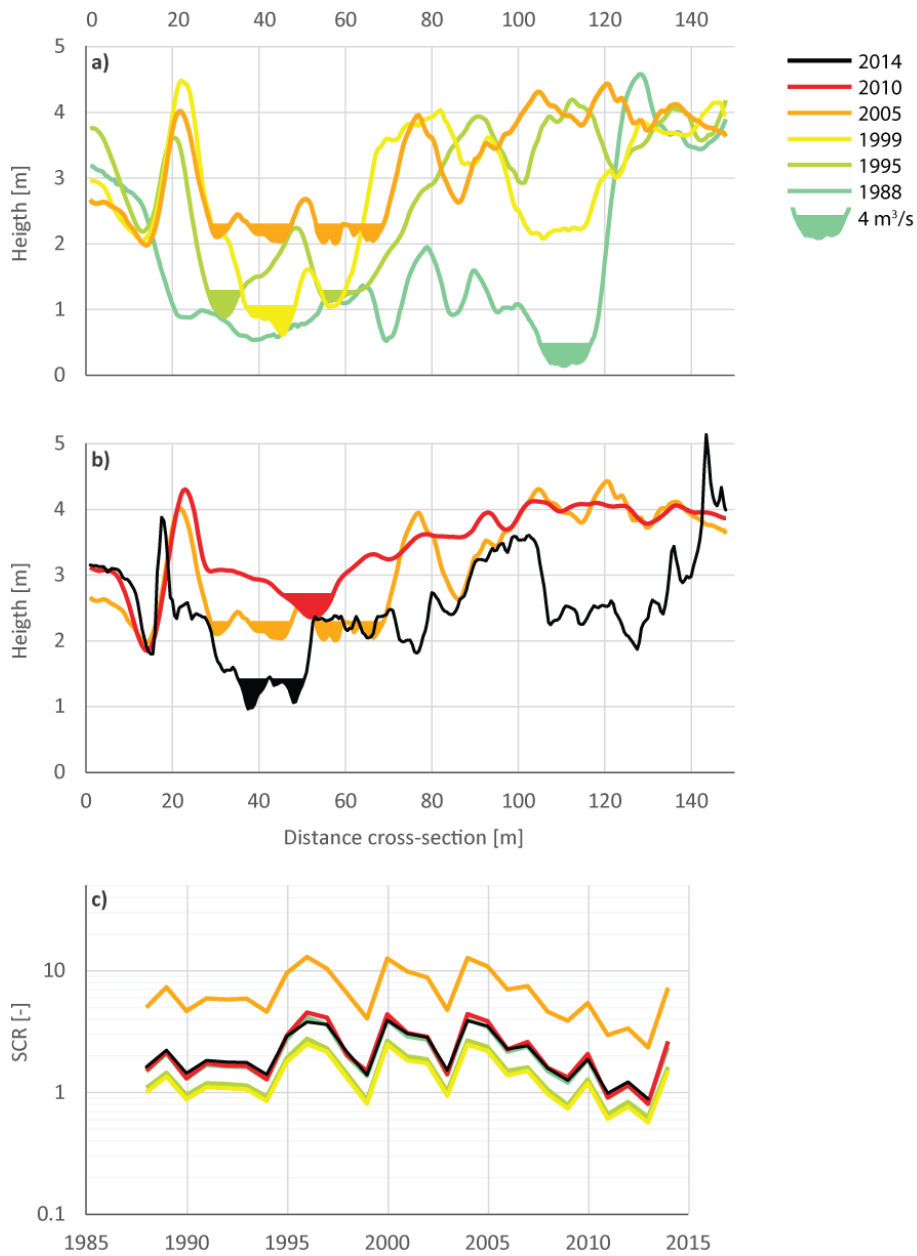


Figure A6-1 a), b) Cross section profiles for the period 1988-2014 (see location in Figure 4-1); c) variation in temporal SCR, assuming maximum sediment supply, with varying cross section (note that temporal changes in grain size are not accounted for).

## References

- Bakker, M. & Lane, S. N. (2017). Archival photogrammetric analysis of river–floodplain systems using Structure from Motion (SfM) methods. *Earth Surface Processes and Landforms*, 42(8), 1274-1286. doi:10.1002/esp.4085
- Bezinge, A., Clark, M., Gurnell, A. & Warburton, J. (1989). The management of sediment transported by glacial melt -water streams and its significance for the estimation of sediment yield. *Annals of Glaciology*, 13, 1-5. doi:10.1017/S0260305500007527
- Ferguson, R. (2007). Flow resistance equations for gravel- and boulder-bed streams. *Water Resources Research*, 43(5), W05427. doi:10.1029/2006wr005422
- Günter, A. (1971). Die kritische mittlere Sohlenschubspannung bei Geschiebemischungen unter Berücksichtigung der Deckschichtbildung und der turbulenzbedingten Sohlenschubspannungsschwankungen. Diss. Techn.Wiss. ETH Zürich, 4649. doi:10.3929/ethz-a-000089812
- Heimann, F. U. M., Rickenmann, D., Turowski, J. M., & Kirchner, J. W. (2015). sedFlow - a tool for simulating fractional bedload transport and longitudinal profile evolution in mountain streams. *Earth Surf. Dynam.*, 3(1), 15-34. doi:10.5194/esurf-3-15-2015
- Hunziker, R. P. & Jaeggi, M. N. R. (2002). Grain Sorting Processes. *Journal of Hydraulic Engineering* 128(12), 1060-1068. doi:10.1061/(ASCE)0733-9429(2002)128:12(1060)
- Lamb, M. P., Dietrich, W. E., & Venditti, J. G. (2008). Is the critical Shields stress for incipient sediment motion dependent on channel-bed slope? *Journal of Geophysical Research: Earth Surface*, 113(F2). doi:10.1029/2007JF000831
- Nitsche, M., Rickenmann, D., Turowski, J. M., Badoux, A. & Kirchner, J. W. (2011). Evaluation of bedload transport predictions using flow resistance equations to account for macro-roughness in steep mountain streams. *Water Resources Research*, 47(8), W08513. doi:10.1029/2011WR010645
- Rickenmann, D. (1991). Hyperconcentrated flow and sediment transport at steep slopes. *Journal of Hydraulic Engineering*, 117(11), 1419-1439. doi: 10.1061/(ASCE)0733-9429(1991)117:11(1419)
- Rickenmann, D., & Recking, A. (2011). Evaluation of flow resistance in gravel-bed rivers through a large field data set. *Water Resources Research*, 47(7), W07538. doi:10.1029/2010WR009793
- Wolman, M. G. (1954). A method of sampling coarse river-bed material. *Eos, Transactions American Geophysical Union*, 35(6), 951-956.

## B1: Local uncertainty assessment based on lidar point density

Local uncertainty due to lidar point density was quantified based on an area of 50 x 50 m (Figure B1-1). Based on this data set, additional DEMs at grid resolutions of 0.5, 1, 2.2 and 5 m were computed.

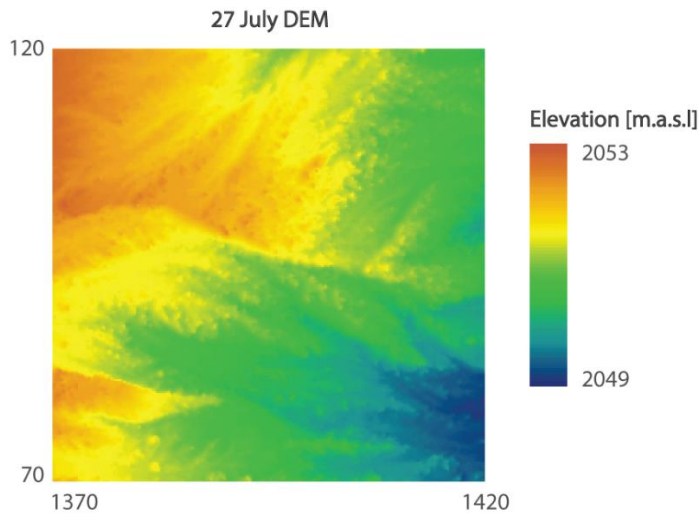


Figure B1-1 Sub-area of original 27 July DEM (0.2 m resolution) used for the local error analysis.

We recomputed the DEM for the coarser grids after randomly removing lidar points, keeping 80%, 60%, 40%, 20% and 10% of the original amount of points. For each recomputed DEM the cell-based standard deviation of error was computed with respect to the reference DEM of the same resolution (the DEM with 100% of the points). The results are given in Figure B1-2, where the standard deviation of error follows a logarithmic trend when plotted against point density.

The error function of the different resolutions is more or less parallel (with the exception of 0.5 m). The error decreases with increased grid resolution due to loss in small-scale river bed topography, which is also reflected in the error plots derived for the different resolutions (Figure B1-3). We chose a 2.2 m resolution error grid to account for the general scale of the channel morphology (Figure 1b in the paper). At higher spatial resolutions the topographic detail as reflected in the point density is lost, e.g. at 5 m resolution in Figure B1-3. At lower spatial resolutions, frequently occurring grid cells with little or no lidar points, particularly in the upstream part of the reach, introduce local noise, e.g. at 0.5 m resolution in Figure B1-3.

The error function that was applied to all DEMs in the paper is based on the 2.2 m grid regression with the addition of 0.02 m to account for inherent uncertainty in the equipment and preventing values to approach zero; see Figure B1-2.

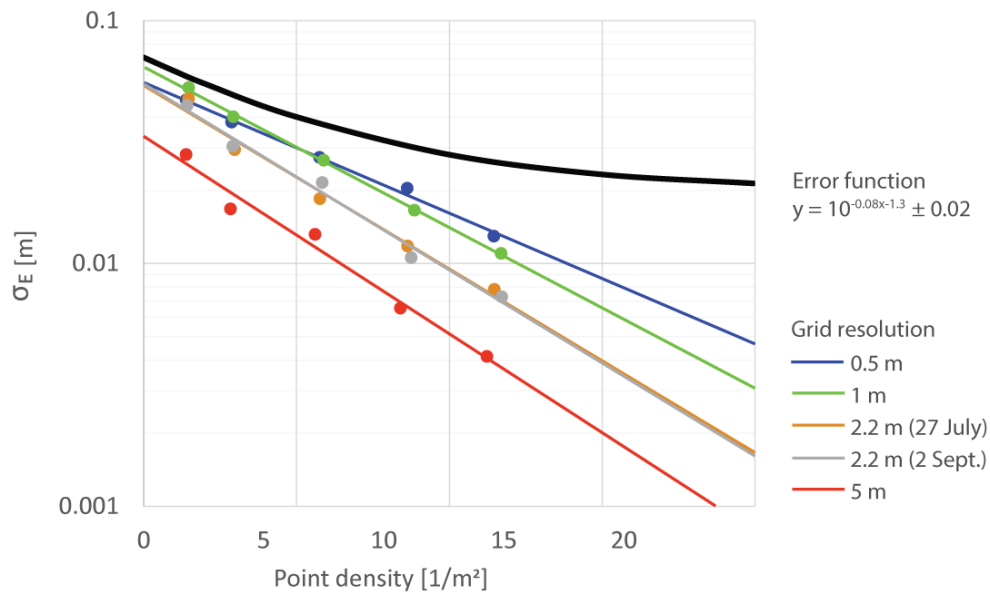


Figure B1-2 Standard deviation of error as a function of point density for different grid resolutions. Data and regression lines are derived using the 27 July DEM, with the addition of data from 2.2 m resolution grid based on the 2 September DEM. The error function used to quantify local error in the paper is also given.

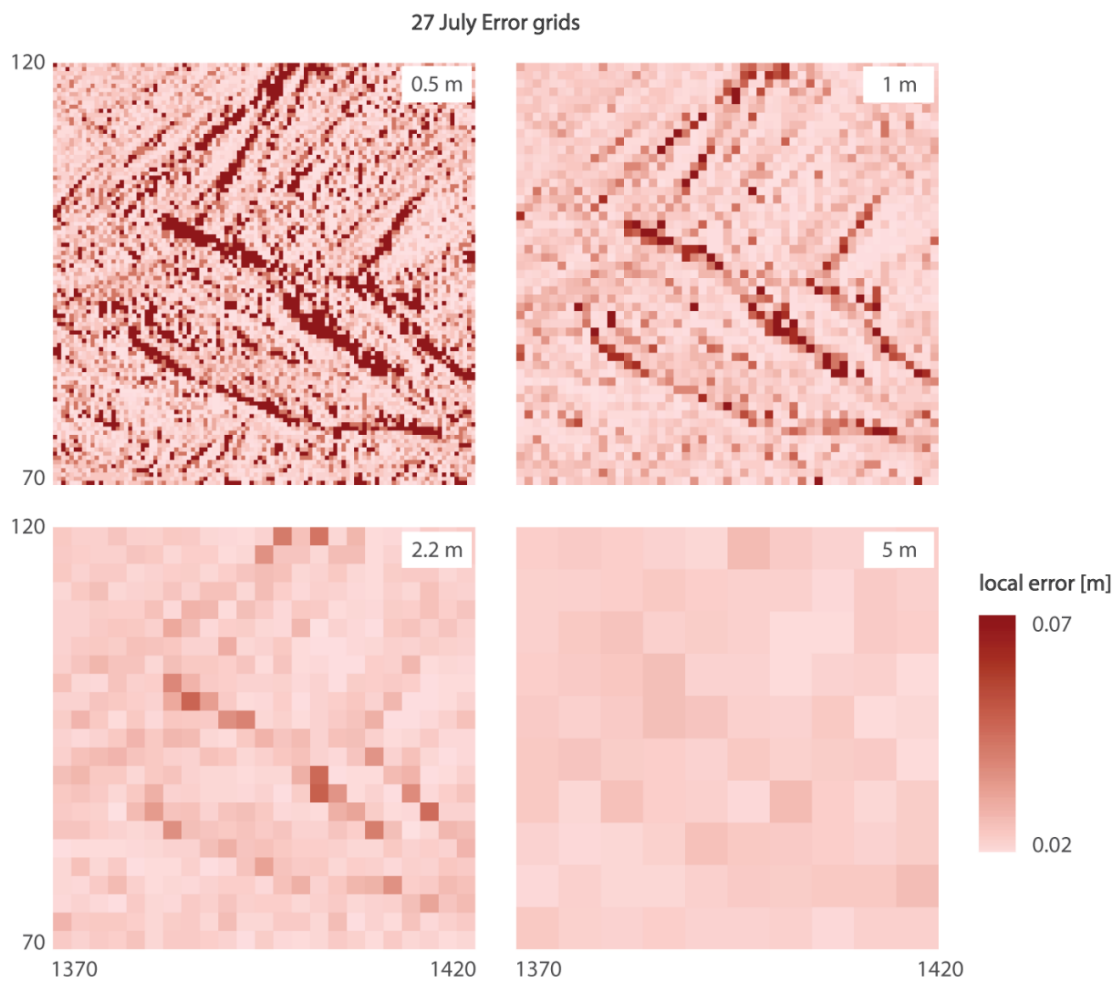


Figure B1-3 Error grids 3 derived for the 27 July DEM with 0.5, 1, 2.2 and 5 m resolution.